UNIVERISITY OF WATERLOO
WATERLOO RESEARCH INSTITUTE

2 THERMAL ANALYSIS OF TRAPEZOIDAL GROOVED HEAT PIPE WALLS

BY: Schneider, G.E. and Yovanovich, M.M.

DSS. Contract No. OSU4-0178

Scientific Authority: V. Wehrle DSM

UNIVERSITY OF WATERLOO

WATERLOO RESEARCH INSTITUTE

THERMAL ANALYSIS OF TRAPEZOIDAL GROOVED HEAT PIPE WALLS

by

G. E. Schneider and M. M. Yovanovich

Thermal Engineering Group
Department of Mechanical Engineering
University of Waterloo
Waterloo, Ontario

Prepared for

Communications Research Centre

CRC 6656-1 (SCS) Program

Supported by

The Department of Communications

under Department of Supply and Services Contract Number OSU4-0178

WRI Project 3061-2

August, 1975

ACKNOWLEDGEMENT

The authors wish to express their sincere appreciation to the Communications Research Centre for their financial support under Research Grant CRC 6656-1 (SCS) program.

During the course of the investigation the authors had on several occasions the privilege of discussing various aspects of the problem with Professors J. C. Thompson and G. M. McNeice of the Department of Civil Engineering, University of Waterloo. Conversations with Dr. R. Kosson, Grumman Aerospace Corporation, New York, N.Y. and with Dr. C. C. Roberts, Bell Laboratories, Naperville, Illinois, were also helpful.

Abstract

It has been the purpose of this report to examine the thermal characteristics of heat transfer through a heat pipe wall whose inner surface is grooved with grooves of trapezoidal cross-section. An understanding of the heat transfer characteristics of such a wall is fundamental to the accurate prediction of heat pipe performance characteristics. The cases considered in this report degenerate to grooves of V-shaped cross-section in one limit and to rectangular grooves in the other limit. While results are presented for symmetric groove cross-sections only, the analysis and prediction program maintain the flexibility of considering the non-symmetric situation.

It is established that conduction heat transfer is the dominant mode of energy transport within the composite metal/working fluid section of the grooved pipe wall. The composite conduction problem is mathematically formulated and the analytic solution to the governing differential equations is examined. While the functional form of the solution is easily obtained, the many constraints which must simultaneously be satisfied leave the complete analytic solution intractable. It is concluded that a numerical solution procedure must be used to effect the solution and that due to the geometric irregularity of the solution domain, the finite element method will be most appropriate.

A limit study is performed to provide upper and lower bounds for the equivalent groove Nusselt number. The two theorems of Elrod are used to provide these limiting values. Although the limits resulting from such a study can often be used to provide acceptable engineering predictions, this is not the case here. As a result the limit study

here serves to provide a check on the values determined from the finite element prediction program.

A finite element formulation of the heat conduction equation is derived for application to any general orthogonal curvilinear co-ordinate system. The generalized formulation presented herein bears a strong resemblance to the cartesian form in common usage with only minor modifications required to a cartesian program to reflect the co-ordinate system generalization. Reduction of the general form is made to the cartesian coordinate system for application to the trapezoidal groove problem.

Although the finite element method maintains the flexibility of considering irregular geometries, application of the method to the trapezoidal groove heat transfer prediction is not direct. Difficulties were experienced in generating a discretization mesh which could adequately describe both the severe local thermal behavior near the meniscus/metal contact and the conductive region in the remainder of the fin. Description of the above thermal field is subject to the further constraint that the prediction program storage requirement does not exceed that available on current computing facilities. After two unsuccessful mesh generators were discarded, a third, acceptable, mesh generation scheme was adopted. The difficulties encountered here reflect the difficulty involved in solving the complete, composite, thermal problem.

With the finite element program functioning correctly, a parametric study was conducted to determine fully the thermal characteristics of the equivalent Nusselt number. Symmetric groove cross-sections only are explicitly considered in this work thus restricting the dependence to four parameters. These are the liquid/metal conductivity ratio, the groove depth, the metal fin tip land area ratio, and the normalized apparent meniscus contact angle. The dependence of the equivalent groove Nusselt number is fully discussed in the text. A correlation equation, applicable over the range of parameters investigated in this work, is presented and interpolates the numerical data with a maximum error of correlation of seven per cent.

Application of the results of this work is made to the prediction of heat pipe surface temperature variations. It is found that in cases where substantial variations exist in the groove equivalent heat transfer coefficient, the variations exhibited by the pipe surface temperatures can be considerably less severe, but that the degree of insensitivity will be application dependent.

Nomenclature

A_i	heat pipe internal surface area evaluated at the groove root diameter
A_f	working fluid flow cross-sectional area
A_1, A_2	constants (defined in text)
B_1, B_2	constants (defined in text)
[B]	coefficient matrix in effective curvilinear field vector
c	geometric constant (defined in text)
c_p	specific heat at constant pressure
C_1, C_2, C_3, C_4	constants (defined in text)
d	depth of groove section
D_h	hydraulic diameter
D_1, D_2, D_3, D_4	correlation constants (defined in text)
f	friction factor
f_1, f_2, f_3	elements of effective curvilinear property matrix, equation (5-13)
[f]	constant vector in finite element equations
g	metric coefficient, $g = g_1 \cdot g_2 \cdot g_3$
g_1, g_2, g_3	metric coefficients, equation (5-3)
[G]	curvilinear field vector
h_a	pipe to ambient film or attachment heat transfer coefficient
h_{eq}	equivalent heat transfer coefficient
h_{fg}	latent heat of vaporization
H	total wall thickness of typical cell
HLSD	H-d
J	Jacobian of local-global coordinate transformation
k	thermal conductivity

K	friction factor coefficient or conductance (defined in text)
$K(\lambda)$	complete elliptic integral of the first kind with modulus λ
$K'(\lambda)$	complementary complete elliptic integral of the first kind, $K'(\lambda) = K(\sqrt{1-\lambda^2})$
$[K]$	coefficient matrix in finite element equations
ℓ_1, ℓ_2, ℓ_3	direction cosines of surface with the three principal coordinates
L, L_a, L_c, L_e	length of heat pipe; total, adiabatic, condenser, and evaporator lengths
$\dot{m}$	mass flow rate
n	normal to surface
N	groove pitch (number of grooves/lineal distance)
N_i	element shape functions for use in finite element analysis
Nu	Nusselt number (defined in text)
per	wetted flow perimeter
P	pressure or heat generation rate per unit volume (defined in text)
Pr	Prandtl number
P_s	saturation pressure
q	heat flux
q_e	applied evaporator heat flux
r	radial coordinate
r_{in}	inner pipe radius
r_o	liquid level in V-groove measured along the groove wall
r_{out}	outer pipe radius
r_p	mean inner (groove) pipe radius
R	universal gas constant or thermal resistance (defined in text)
Re	Reynold's number

R_o	groove side wall length for V-groove
$[K]$	effective curvilinear property matrix
s	groove coordinate, curvilinear distance, or finite element local coordinate (defined in text)
S	surface
t	time or local finite element coordinate (defined in text)
T	temperature
T_a	heat pipe ambient temperature
T_v	vapor temperature
T_{fi}	interface liquid temperature
T_{si}	interior pipe surface temperature
T_{so}	exterior pipe surface temperature
T_{vi}	interface vapor temperature
u_1, u_2, u_3	general orthogonal curvilinear coordinates
v	argument of Jacobian elliptic sine amplitude function
V	volume
w	width of typical groove cell
x	cartesian coordinate
x_α	non-dimensional apparent contact angle, $x_\alpha = \alpha/(\pi/2 - \theta_o)$
X	separated component of analytic solution in the x-direction
y	cartesian coordinate
y_i	ordinate for interface geometric description
Y	separated component of analytic solution in the y-direction
z	longitudinal coordinate

Greek Letters

α	apparent liquid/metal contact angle
α_o	groove entrance apparent contact angle
α_{ba}	minimum break-away contact angle
β	radius of curvature of liquid free surface
γ	ratio of specific heats, $\gamma = c_p/c_v$, or included angle of liquid or metal section in limit study (defined in text)
γ_E	coupling coefficient, $0 < \gamma_E < 1$
δ	variational operator
Δ	increment in accompanying argument
$\varepsilon_1, \varepsilon_2$	groove tip and root area ratio
η	oblate spheroidal coordinate
θ	circumferential or oblate spheroidal coordinate (defined in text)
κ	geometric parameter or modulus of complete elliptic integral of first kind (defined in text)
λ	separation constant or modulus of complete elliptic integral of first kind (defined in text)
μ	viscosity
ν	kinematic viscosity, $\nu = \mu/p$
ρ	mass density or radial coordinate in limit study (defined in text)
σ	surface tension
ψ	circumferential or oblate spheroidal coordinate (defined in text)
ω	circulation flow velocity in V-grooves
$\bar{\omega}$	average groove section velocity
ω_o	reference velocity for normalization, $\omega_o = (r_o^2/\mu r_p) \frac{\partial P}{\partial \psi}$

Subscripts

a	ambient
f	liquid
i	interface
m	metal
o	outer
s	surface
T	total
I	sub-region I in limit study
II	sub-region II in limit study
III	sub-region III in limit study

Table of Contents

Chapter 1

Introduction

In recent years it has become increasingly important to develop methods for the efficient transport of thermal energy from one location to another. The use of high component-density electronic circuitry and the operational, inefficiencies of the components used may impose heat transfer requirements on the design which conventional heat transfer devices are unable to maintain. In such applications, the heat pipe may often offer the only practical solution to the thermal problem under consideration.

In addition the realization of a limited world supply of conventional forms of energy has led to a search for more efficient methods of energy conversion. Here, heat pipes may find a role in reducing extraneous temperature drops not directly related to the conversion of thermal energy to, say, electrical energy, thus allowing a closer approach of the system conversion efficiency to the limiting Carnot efficiency for the conversion cycle.

Perhaps the most demanding heat transfer requirement at present is the thermal control of spacecraft [1 - 8]. Due to the large thermal gradients which are commonly experienced in spacecraft applications and the associated high thermal stresses, a device is sought which would serve to 'isothermalize' the spacecraft structure. This is an important consideration in the design of the telemetry, guidance, and orbit stabilization systems of a spacecraft. A second problem of spacecraft thermal control is related to the efficient utilization of the available space within the spacecraft for the experimental, control, and communications equipment packages. If the heat generated within the spacecraft due to the operational inefficiencies of the onboard equipment is not effectively dissipated from the spacecraft, the resultant temperature rise of the electronic equipment above tolerable operational limits may lead to performance degradiation and/or complete system failure. In view of the consequences of a complete system failure in spacecraft applications, these thermal problems warrant considerable attention and here, again, the use of heat pipes may provide the only practical solution. In addition to its favorable thermal characteristics, heat pipes in spacecraft applications also present a low weight penalty to the spacecraft design as a result of their hollow construction. Since the heat pipe can offer substantial advantages over conventional heat transfer devices in its application to thermal control, its appearance in spacecraft designs is becoming increasingly prevalent.

A definition of a heat pipe has been given in the comprehensive review article by Winter and Barsch [9] as, "A heat pipe is defined as a closed structure containing some working fluid which transfers thermal energy from one part of the structure to another by means of vaporization of a liquid, transport and condensation of the vapor, and the subsequent return of the condensate from the condenser by capillary action to the evaporator". If the working fluid of such a device is free of contaminants, then the temperature within the structure will be very nearly isothermal throughout the region of vapor transport by virtue of the two phases present within the pipe existing simultaneously in equilibrium with one another. While the vapor/liquid interaction leads to isothermal behavioral, characteristics, significant overall temperature drops may often occur due to heat transfer within the wicking mechanism and pipe walls. Since the thermal conductivity of typical working fluids for moderate temperature heat pipes is low, considerable effort has been directed towards the development of high conductance wicking mechanisms [7, 10-14]. The present generation of high capacity, high conductance heat pipes is a direct result of this development.

The wide variety of heat pipe designs currently in use can be broadly categorized according to the maximum heat transfer rate they will afford the designer. This heat transfer rate is directly proportional to the mass flow of the working fluid which can be circulated within the pipe through the proportionality factor, the latent heat of vaporization. For moderate temperature applications (150-750^{o}K) the maximum rate of circulation is determined primarily by the viscous losses within the liquid which must be overcome by the capillary pumping action of the wicking mechanism.

The most primitive wick design consists of simply lining the smooth inner diameter of a pipe with a porous material [15]. Wire mesh screening is commonly used in these designs with the maximum available pumping capability determined by the 'pore size' of the mesh. Due to the small spacing between the screen and pipe inner wall, however, viscous shear stresses arising from this configuration will be large resulting in a relatively low liquid re-circulation capability.

Since this necessarily dictates a relatively low heat transfer capability, such designs are characterized as low capacity heat pipes. Indeed, not only do these designs have a low heat transfer capacity, but also, since the heat addition and extraction must occur through a relatively low conductance liquid/wick matrix, these designs also have a relatively low overall thermal conductance. This is an unavoidable consequence of these designs since the wick mechanism serves not only as a liquid return path but also to wet the inner pipe wall of the evaporator to maximize the evaporative heat transfer.

In recognition of the disadvantages of the low capacity heat pipes, subsequent efforts were directed at increasing the ratio of flow area to flow perimeter in the liquid return passages. One means of achieving this result is by machining (extruding) longitudinal grooves in the pipe wall. Not only does this reduce the viscous flow losses of the return path but, due to the fin-like behaviour of the remaining extended portions of the original pipe wall, the heat transfer characteristics of this design are also improved. Since the passage size is restricted by capillarity considerations, however, the available gains from this design are also limited. Heat pipe designs typified by that described above are characterized as moderate capacity designs and also have moderate performance characteristics.

Attempts to alleviate the limitations associated with the previous two designs have led to the conception of the present generation of high capacity heat pipe designs, with which this work is primarily concerned, although the results may also be applied to certain moderate

It is the object of this study to examine in greater detail the heat transfer processes occurring in the liquid/metal composite region of grooved heat pipe walls. In addition, this work will extend consideration to grooves of an arbitrary trapezoidal cross-section including as limiting cases the V-groove section discussed above as well as the rectangular groove section. In the prediction of heat pipe performance, the accurate prediction of the pipe wall and groove conductance is paramount to accurate prediction of the overall pipe conductance since by virtue of its operation, the vapor core of the heat pipe will exhibit near isothermal behaviour. Thus, since the majority of the temperature drop encountered in high capacity, moderate temperature heat pipes will occur in the groove region, accurate prediction of the groove thermal behaviour is fundamental to the accurate prediction of the overall performance of heat pipes of this design.

Chapter 2

Background

2.1 Introduction

In a previous report [16], the present authors examined the three-dimensional thermal analysis of a high capacity heat pipe operating in the steady-state. The heat pipe of interest consisted of a circular tube having circumferential grooves of V-shaped cross-section wound in a tight helix along the length of the pipe. Liquid return transport is afforded by three longitudinal arteries aligned across the diameter of the pipe. The cross-section of the pipe of interest is illustrated schematically in figure 2-1.

The pipe shown in figure 2-1 is a high capacity heat pipe having the mechanisms of liquid return transport and wall wetting distribution decoupled from each other. The larger diameter artery passages are used to minimize the re-circulation viscous pressure losses in order to obtain a high thermal transport capability while the grooves, used for distribution of the working fluid over the pipe inner wall, can be designed to minimize the temperature drop between the pipe exterior surface and the vapor core over both the evaporator and condenser regions of the pipe. A complete thermal analysis must include, then, the variation of the temperature distribution within the pipe which results from changes in the liquid flow cross-section. These liquid flow cross-sectional changes in turn are the result of the viscous pressure losses associated with the hydrodynamic return path taken by the working fluid as it flows from the condenser back to the evaporator. It is the influence of changes in the liquid flow cross-section on the local heat transfer characteristics of a grooved heat pipe wall which is under investigation in this work.

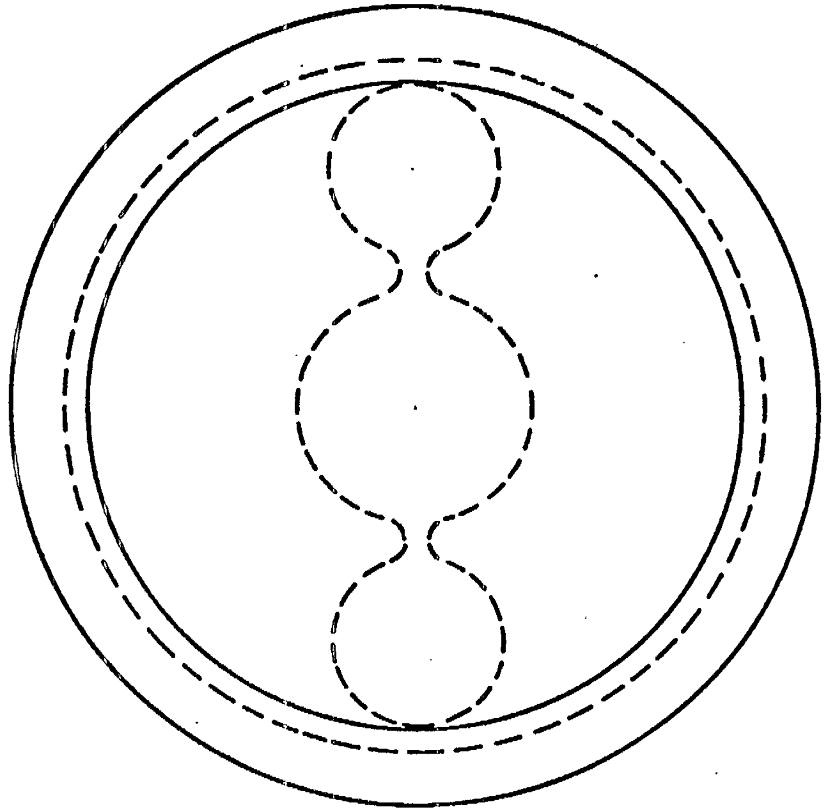

Figure 2-1

The purpose of the present chapter is to briefly review the work performed in the previous report. This brief review will serve both as an introduction to and as motivation for the present work.

2.2 Thermal Analysis

Figure 2-2 illustrates schematically a typical heat pipe shell. Due to the tubular nature of the pipe design under consideration the coordinate system best able to describe the temperature field within the pipe will be the circular cylinder coordinate system. The origin of this system and the coordinate directions are indicated in the figure.

The region of heat input on the exterior surface of the pipe, L_e, is given the name 'apparent evaporator section' while by a similar definition the region of heat extraction on the exterior surface, L_c, is given the name 'apparent condenser section'. The remaining exterior surface area will be adiabatic and is given the name 'apparent adiabatic section', denoted by L_a. The regions of actual evaporation and condensation, however, are not restricted to the physical confines of the apparent evaporator and condenser sections respectively. Under suitable conditions [17] there may be no appreciable effective adiabatic section on the inner surface even if there exists an adiabatic section of considerable length on the exterior surface.

In the absence of internal heat generation and in consideration of steady state operation, the differential equation governing the heat transfer within the pipe shell will be Laplace's equation in circular cylinder coordinates,

$$\frac{\partial^2 T}{\partial r^2} + \frac{1}{r}\frac{\partial T}{\partial r} + \frac{1}{r^2}\frac{\partial^2 T}{\partial \psi^2} + \frac{\partial^2 T}{\partial z^2} = 0 \qquad (2\text{-}1)$$

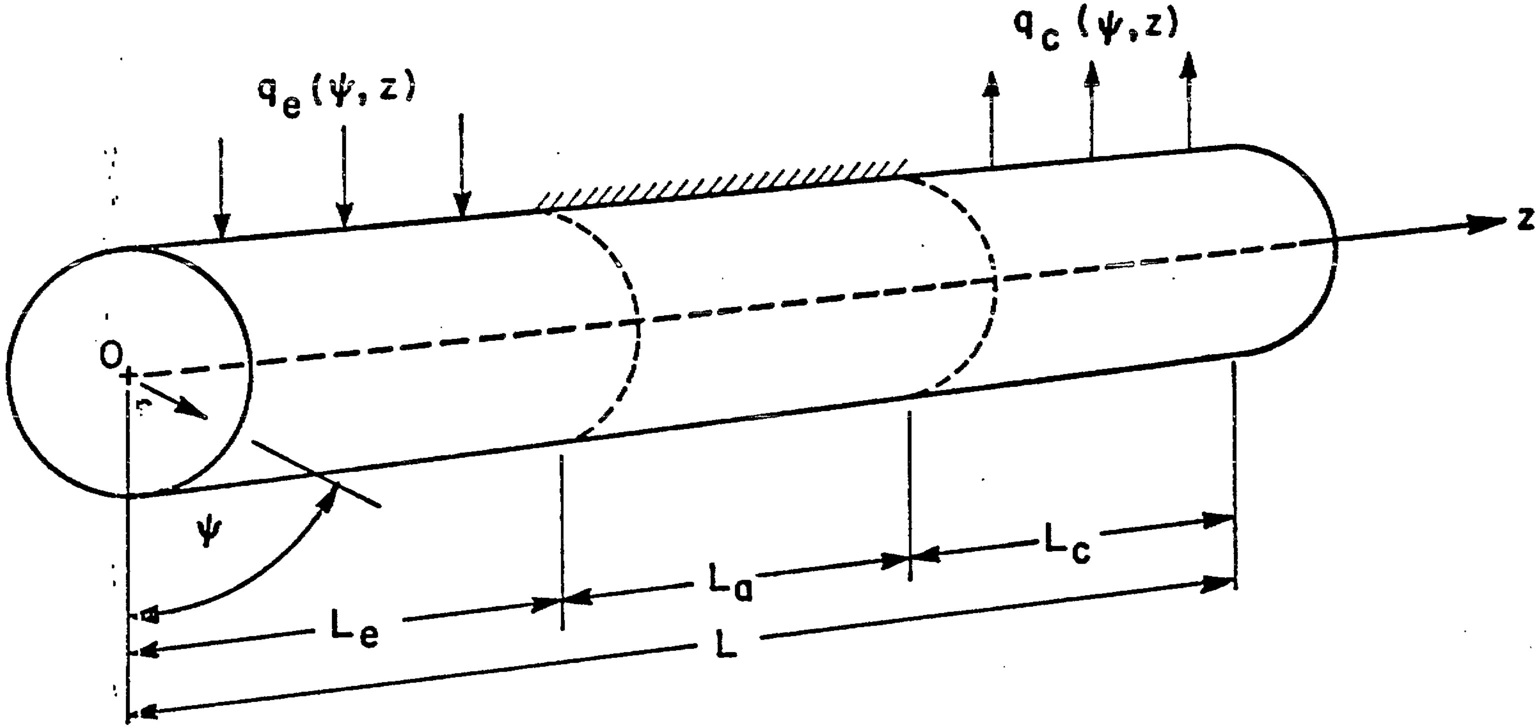

Figure 2-2

The inclusion of all three coordinates, r, ψ, and z, has been made since in general the temperature field must be allowed to vary independently in each of the three principal directions.

The boundary conditions which apply to the solution of equation (2-1) are all well defined with one exception. The exception is the specification of the inner pipe surface thermal interaction with the vapor core.

As shown by the cross-section as illustrated in figure 2-3(a), even the geometric description of the inner pipe boundary will be a tedious and difficult task. To apply the conditions existing at this boundary directly would lead to an unnecessarily complicated analytic solution or require an extremely high degree of detail if numerical methods are used. It becomes apparent, then, that a simplification of this boundary condition is desired to avoid an unduly complicated solution. In addition to the above geometric complications, the heat transfer mechanism at the pipe inner surface may also vary in both the circumferential and longitudinal directions.

To avoid an unduly complicated solution, an equivalent heat transfer coefficient, h_{eq}, has been defined to characterize the thermal behavior in the region extending from a hypothetical surface located at the groove root diameter, through the metal 'fin' and the fin/liquid interface, and finally through the liquid within the groove to the vapor core. This is illustrated in figure 2-3(b) for the case of triangular or V-shaped grooves. Once this equivalent heat transfer coefficient has been determined, the inner surface boundary condition application becomes that of a hypothetical inner surface interacting with an environment at the vapor temperature, T_v, through a heat transfer coefficient, h_{eq}.

The complete set of boundary conditions assumed for this analysis can then be written as

$$
\begin{array}{lll}
1) & z = 0 & \dfrac{\partial T}{\partial z} = 0 \\[2ex]
2) & z = L & \dfrac{\partial T}{\partial z} = 0 \\[2ex]
3) & \psi = 0 & \dfrac{1}{r}\dfrac{\partial T}{\partial \psi} = 0 \\[2ex]
4) & \psi = \pi & \dfrac{1}{r}\dfrac{\partial T}{\partial \psi} = 0 \\[2ex]
5) & r = r_{in} & \dfrac{\partial T}{\partial r} = \dfrac{h_{eq}(\psi,z)}{k}\left(T_{si}(\psi,z) - T_v\right) \\[2ex]
6) & r = r_{out} & \text{(a)}\quad 0 \leq z \leq L_e;\ k\dfrac{\partial T}{\partial r} = q_e(\psi,z) \\[2ex]
 & & \text{(b)}\quad L_e \leq z \leq (L_e + L_c);\ \dfrac{\partial T}{\partial r} = 0 \\[2ex]
 & & \text{(c)}\quad (L_e + L_c) \leq z \leq L;\ \dfrac{\partial T}{\partial r} = \dfrac{-h_a(\psi,z)}{k}\left(T_{so} - T_a\right)
\end{array}
\qquad (2\text{-}2)
$$

As can be seen from these conditions, a condition of symmetry about the plane defined by $\psi = 0$ and $\psi = \pi$ is assumed, insulated end caps are assumed, and a specified flux distribution is prescribed over the evaporator surface while the condenser interacts with the environment at T_a through an attachment coefficient, h_a.

The vapor temperature, not known a priori, must further satisfy the relation

$$
T_v = \frac{\int_{A_i} h_{eq}(\psi\ z)\ T_{si}(\psi,z)\ dA_i}{\int_{A_i} h_{eq}(\psi,z)\ dA_i} \qquad (2\text{-}3)
$$

where $T_{si}(\psi,z)$ is the temperature distribution over the hypothetical inner surface, A_i, located at the groove root diameter.

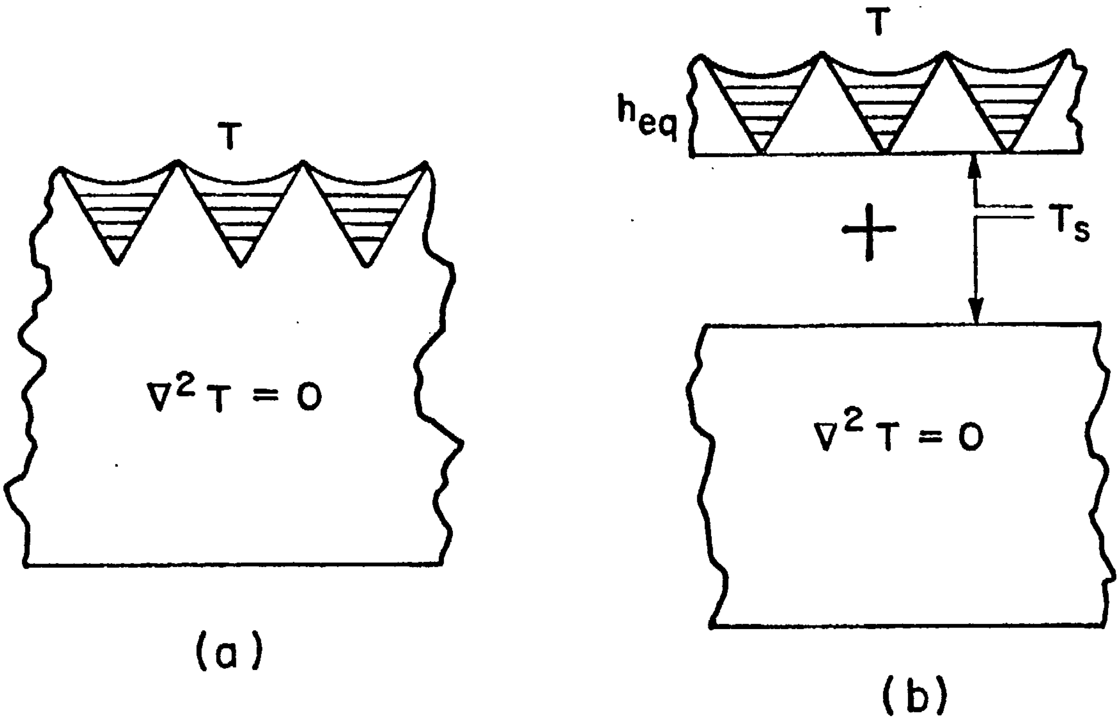

Figure 2-3

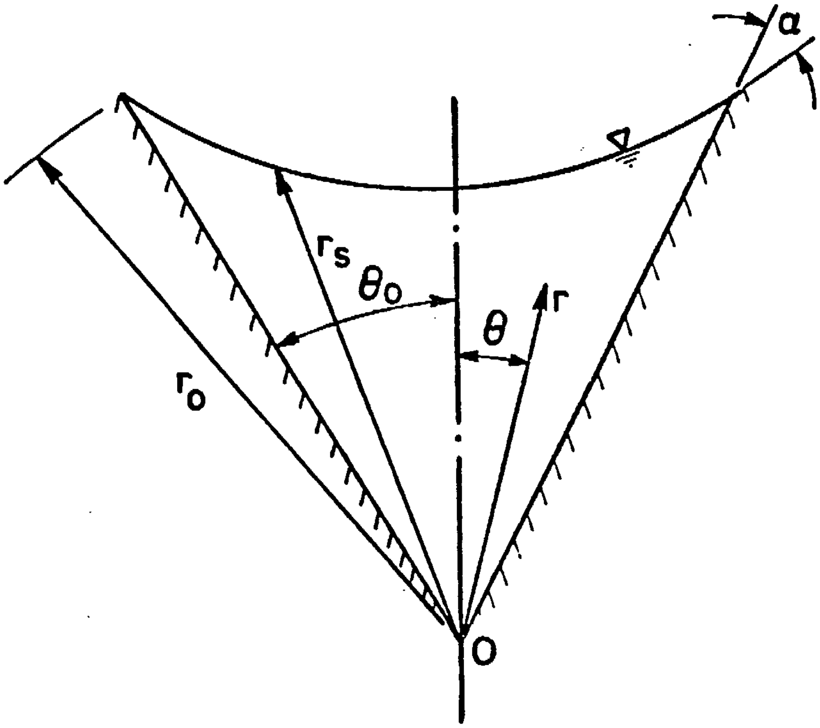

Figure 2-4

In the previous report [16] a finite difference solution to equation (2-1) subject to the boundary conditions (2-2) and the constraint equation (2-3) was presented. In applying the solution to heat pipe situations, however, the distribution of the equivalent heat transfer coefficient over the pipe inner surface, must be known. Determination of h_{eq} is not direct, though, since it will depend on the local liquid flow cross-section, which in turn depends on the pipe operating conditions. It was therefore necessary to examine the hydrodynamics of the heat pipe liquid flow as the condensate returns from the condenser to the evaporator.

2.3 Liquid Re-circulation Hydrodynamics

There are two separate regions of hydrodynamic consideration in the operation of the high capacity heat pipe. The first of these is the liquid return flow within the arteries and for this case, it was assumed that the viscous pressure drops locally can be determined from friction factor results for flow in a pipe where the mass flow rate is the local arterial one. This analysis, then, and the requirement that the pressure at any given longitudinal position be unique, provides an input to the second hydrodynamic region, the liquid flow within the circumferential grooves. While correlations already exist for the first region above, the second region had not been previously examined and required analysis.

Under the assumption that the groove flow is quasi-fully-developed at any circumferential station, an analysis was performed to determine the friction factor for laminar flow in a V-groove. With the origin of a circular cylinder coordinate system located as indicated in figure 2-4 the normalized equation and boundary conditions are

$$\frac{\partial^2\omega^*}{\partial r^{*2}} + \frac{1}{r^*}\frac{\partial\omega^*}{\partial r^*} + \frac{1}{r^{*2}}\frac{\partial^2\omega^*}{\partial\theta^2} = 1 \tag{2-4}$$

and

$$\begin{aligned}
&1)\quad \omega^*(0,\theta) = 0\\
&2)\quad \omega^*(r^*,\theta_o) = 0\\
&3)\quad \left[\frac{1}{r^*}\frac{\partial\omega^*}{\partial\theta}\right]_{\theta=0} = 0\\
&4)\quad \left[\frac{\partial\omega^*}{\partial n}\right]_{r^*=r_s^*(\theta)}
\end{aligned} \tag{2-5}$$

where in the above

$$r^* = r/r_o$$

$$\omega^* = \omega/\omega_o \tag{2-6}$$

and $$\omega_o = \left(\frac{r_o^2}{\mu r_p}\right)\frac{\partial P}{\partial\psi}$$

In their normalized form, the above equation and boundary conditions are identical to the system solved by Ayyaswamy, Catton, and Edwards [18] for a slightly different problem. Nevertheless, their solution is directly applicable here.

By defining a groove friction factor, f, by the relation

$$\frac{1}{r_p}\frac{\partial P}{\partial\psi} = \frac{f}{D_h}\left(\frac{1}{2}\rho\bar{\omega}^2\right) \tag{2-7}$$

with D_h the hydraulic diameter, r_p the groove mean radius from the pipe centerline, ψ, the angular coordinate around the pipe, and $\bar{\omega}$ the average section velocity. By further defining a friction factor coefficient, K, by the equation

$$f = \frac{K}{Re} \tag{2-8}$$

with $$\mathrm{Re} = \frac{D_h \bar{\omega}}{\nu} \tag{2-9}$$

the friction factor was found to be

$$K = \frac{2D_h^{*2}}{\bar{\omega}^*} \tag{2-10}$$

After completing the analysis to determine $\bar{\omega}^*$, the results were correlated by the correlation equation

$$K = 46.222 - 14.905\ \theta_o + 26.699 \tan(1.014\ \theta_o)\alpha$$

$$+ 4.592 \sqrt{\sin(1.8\ \theta_o)} \sin\left(\frac{\pi\alpha}{\pi/2 - \theta_o}\right) \tag{2-11}$$

with an error of $\pm$ 2% for all reported values.

After having determined the friction factor for quasi-fully-developed, laminar flow, the results were applied in a one-dimensional analysis along the groove in which the pressure forces due to surface tension are balanced by the viscous, groove wall shear stresses. The flow situation is depicted in figures 2-5(a) and (b). The differential equation governing the contact angle and liquid level recession was derived to be

$$\frac{\sigma \cos(\alpha+\theta_o)}{r_o^2 \sin\theta_o} \frac{dr_o}{ds} + \frac{\sigma \sin(\alpha+\theta_o)}{r_o \sin\theta_o} \frac{d\alpha}{ds} = \frac{-K\mu\dot{m}}{\rho D_h^{*3} r_o^4} \tag{2-12}$$

Equation (2-12) indicates, in its present form, that both a liquid level recession and a contact angle recession may occur simultaneously. In practice, however, there will be two distinct regions of flow in a V-groove: the first consisting of contact angle recession to a minimum 'break-away' angle and the second consisting of liquid level recession. The basis for arriving at this conclusion is illustrated in figure 2-6.

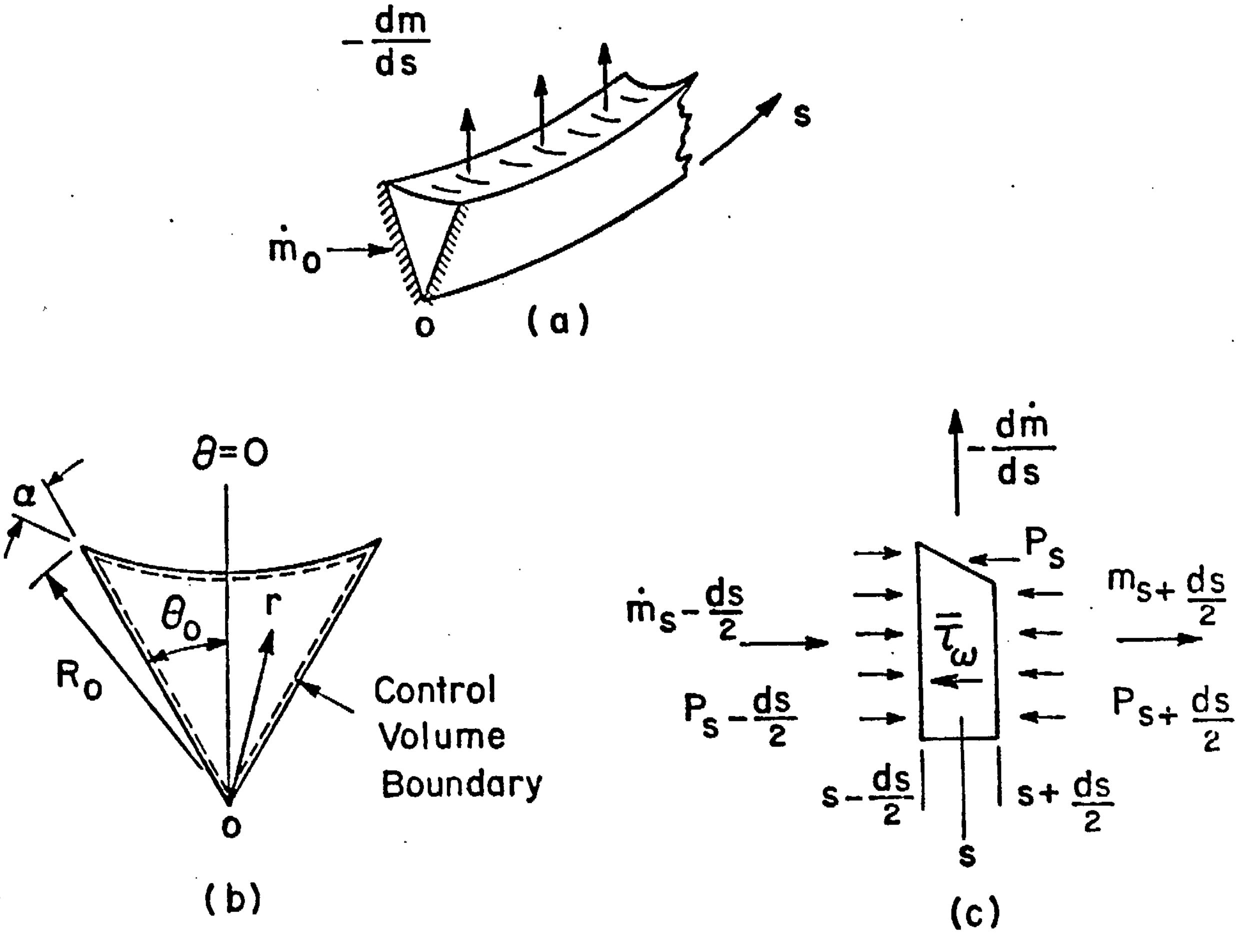

Figure 2-5

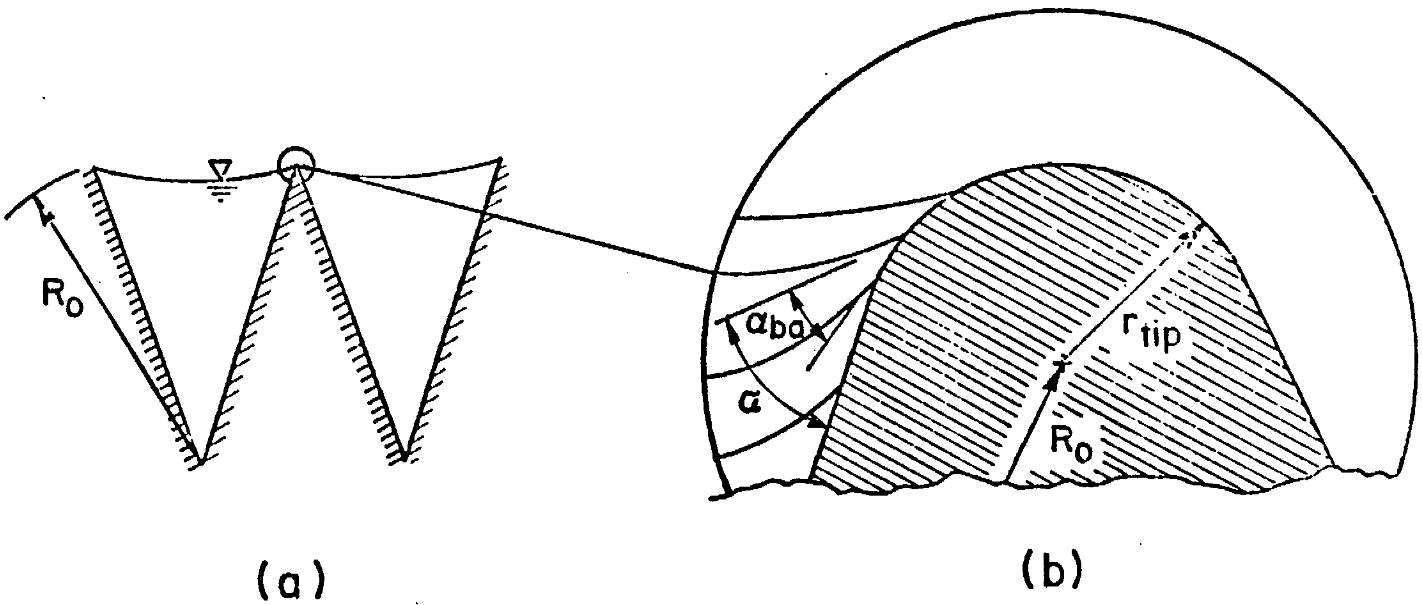

Figure 2-6

Ideally the contact angle exhibited by a solid/liquid/vapor interface will take on a unique value, and when operating under design conditions, the liquid level at the groove inlet will be R_o, the maximum value. However, as shown in the figure, due to the practical impossibility of obtaining perfectly sharp groove tips, a rounded edge will occur in actuality. (Note that since the radius of the rounded edge is small relative to the dimension of R_o, any location on the rounded surface can be characterized by R_o).

It becomes apparent, then, that for a fixed actual solid/liquid/vapor contact angle or 'break-away' angle, α_{ba}, an infinite number of apparent contact angles can be imagined without appreciable change in R_o. Upon recession to the location where the round meets the flat groove side, the apparent and actual contact angles take on the same value, α_{ba}. A further pressure drop must then be exhibited by a recession in liquid level with fixed contact angle.

The single differential equation in two unknowns, equation (2-12), can then be reduced to two differential equations, each valid over a single flow region. These are

$$\frac{\sigma \sin(\alpha+\theta_o)}{R_o \sin\theta_o} \frac{d\alpha}{ds} = \frac{-K\mu \dot{m}}{\rho D_h^{*3} R_o^4} \qquad (2-13)$$

for $(\pi/2 - \theta_o) > \alpha > \alpha_{ba}$, and

$$\frac{\sigma \cos(\alpha+\theta_o)}{r_o^2 \sin\theta_o} \frac{dr_o}{ds} = \frac{-K\mu \dot{m}}{\rho D_h^{*3} r_o^4} \qquad (2-14)$$

for $\alpha = \alpha_{ba}$.

It was found that under moderate thermal loading, the contact angle recession is not severe. In consideration of an evaporator groove, whose contact angle at groove entrance is α_o, the variation of the apparent contact angle is given by

$$\alpha = \frac{-D_4}{D_3} + \sqrt{(\alpha_o + \frac{D_4}{D_3})^2 - \frac{2D_1}{D_3}(s^* - \frac{s^{*2}}{2})} \qquad (2\text{-}15)$$

where $$D_1 \equiv (\frac{2\nu}{\sigma\, h_{fg}}) \cdot (q) \cdot (\frac{s_o}{R_o})^2 \qquad (2\text{-}16)$$

and D_3 and D_4 are obtained from Table 2-1.

For the condenser grooves the contact angle variation is given by

$$\alpha = \frac{-D_4}{D_3} + \sqrt{(\alpha_o + \frac{D_4}{D_3})^2 - \frac{D_1}{D_3}(s^* - 1)^2 + \frac{D_1}{D_3}} \qquad (2\text{-}17)$$

where D_1, D_3, and D_4 are obtained as previously indicated.

Although only angle recession has been considered here, the case of level recession is fully considered in the previous report [16] and will not be presented here. Let it suffice, for the purpose intended here, to say that, for grooves of V-shaped cross-section, the variation of the contact angle throughout the pipe may be determined. It remains, therefore, in the thermal analysis to determine the influence that the groove geometric details have on the thermal behavior at the pipe inner surface, and thus on h_{eq}.

2.4 The Equivalent Heat Transfer Coefficient

Determination of the equivalent heat transfer coefficient is the final link in the thermal analysis of the heat pipe. Having determined the variation of the liquid cross-section throughout the pipe, if the variation of h_{eq} on this geometry is known, then the final boundary condition for the thermal analysis can be applied.

In the previous report [16], an analysis was presented, for the case of grooves of V-shaped cross-section, which determined the equivalent heat transfer coefficient. This analysis was performed on the assumption that the metal fin, due to its large thermal conductivity relative to the liquid conductivity, was nearly isothermal. The temperature field determined in this work, when applied to the V-groove situation, indicates that this condition of isothermality of the metal fin is not true, in particular near the meniscus contact with the metal groove side.

The remaining chapters of this report are concerned with a more detailed investigation of the equivalent heat transfer coefficient. In particular, the complete, composite metal/fluid thermal, interaction at their common interface is fully considered. In addition, the investigations are extended to grooves of general trapezoidal cross-section, reducing in one limit to the V-shaped grooves and in the other limit to the rectangular channel grooves. A detailed problem description is presented in the following chapter of this report.

Table 2-1

Correlation Parameters D_3 and D_4

θ_o (degrees)	α (degrees)	D_3	D_4	Max. Expected Error (per cent)
5	0 - 45	.01109	.00091	2.1
	45 - 80	.00689	.00441	3.3
10	0 - 60	.01903	.00245	4.9
	60 - 80	.01342	.00782	0.6
20	0 - 15	.02485	.00463	2.0
	15 - 45	.03218	.00258	2.3
	45 - 70	.03397	.00145	0.3
30	0 - 15	.02738	.00485	2.6
	15 - 35	.03871	.00179	2.2
	35 - 60	.04982	-.00500	1.0
40	0 - 10	.0246	.00388	2.2
	10 - 25	.03556	.00184	2.4
	25 - 50	.05462	-.00693	3.7
50	0 - 10	.02064	.00246	3.3
	10 - 20	.03083	.00067	1.9
	20 - 40	.04982	-.00642	4.8
60	0 - 10	.01513	.00120	5.5
	10 - 20	.02607	-.00074	3.3
	20 - 30	.04000	-.00558	1.6

Chapter 3

The Groove Heat Transfer Problem

3.1 Introduction

The mechanism of thermal energy transport across a grooved surface, whose grooves are supplied with a volatile liquid by means of surface tension forces, is an important consideration in the design and analysis of moderate and high capacity heat pipes. This importance arises since the groove surface will in general form part of a direct link between the vapor core of the heat pipe and the heat source or heat sink, depending upon whether it is an evaporator or condenser section of the heat pipe.

Since this thermal link is a direct one, inaccuracies in the estimation of its heat transfer characterisitics are directly reflected as uncertainties in the evaluation of the overall heat pipe temperature drop for a given total heat flow rate through the pipe. Prediction of the heat transfer characteristics for a heat pipe design being a principal goal of heat pipe analysis, it is imperative that the phenomena involved in heat transfer from these grooved surfaces be fully understood and the dependencies of the heat transfer explored.

In the steady-state operation of a heat pipe, the return flow of the condensate from the condenser region to the evaporator region will establish a pressure distribution in the liquid phase throughout the pipe. Since the condensate return flow is governed by surface tension forces, particularly in the case of a zero gravitational environment, the pressure distribution within the liquid throughout the pipe will be manifested as a variation in the liquid free surface radius of curvature. Further, since changes in heat flow geometry will undoubtedly influence the heat transfer characteristics of any system, it becomes clear that the heat transfer characteristics of a heat pipe may be expected to vary, in general, both longitudinally and circumferentially throughout the pipe.

The hydrodynamic considerations leading to this variation in the liquid phase cross-section throughout the pipe have been considered elsewhere [16] and will not be repeated here. The present work is directed at examinining the dependence of the equivalent heat transfer coefficient, h_{eq}, on the liquid phase cross-section and on the groove geometry.

3.2 General Considerations

The cross-section of a portion of a grooved heat pipe wall is shown in figure 3-1. The vapor within the vapor core is at a temperature T_v and over the external surface a uniform heat flux distribution is applied. For the case shown in the figure heat is flowing from an external supply through the pipe wall and fin/liquid matrix to the vapor core for transport along the pipe. Arguments similar to those which follow also apply to the condenser section with the exception that the additional heat transfer mode of condensation

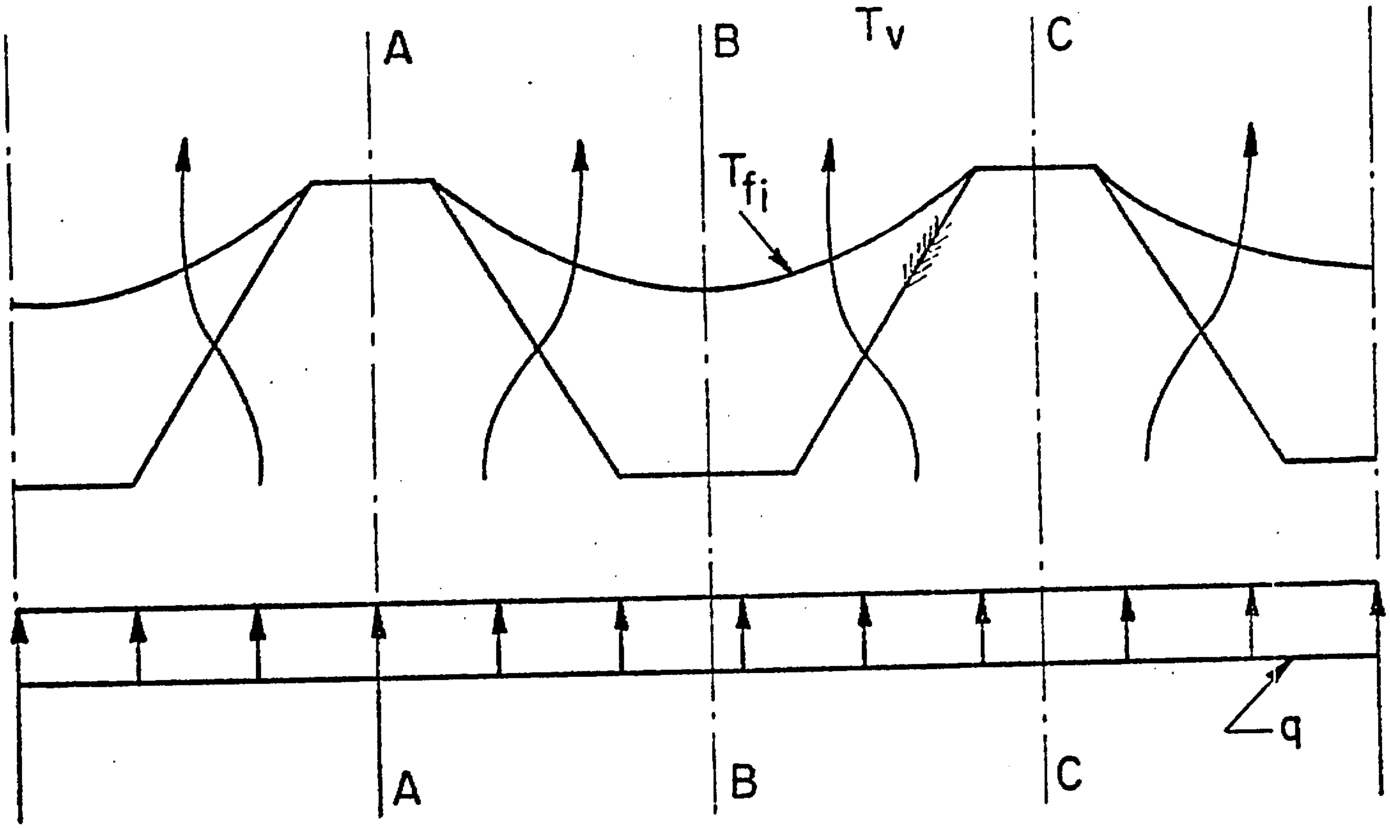

Figure 3-1

on the exposed land area must be considered. The condensation problem, however, is extremely complex and is beyound the scope of this examination. Consequently the contribution to the heat transfer due to condensation on the exposed land area of the condenser regions will not be considered in this work.

Returning to the problem as illustrated in figure 3-1, in the thermal analysis of grooved heat pipe walls consideration must be given to heat conduction within the pipe wall, heat conduction as well possible convective heat transfer in the liquid contained within the grooves, and the mechanism for heat transfer at the liquid/vapor interface. These considerations follow.

3.2.1 Vapor/Liquid Interface

The behavior of the vapor/liquid interface in heat pipe operation is important when examining the heat transfer through grooved heat pipe walls since the mechanisms occurring at this interface are directly responsible for the phase change that is fundamental to heat pipe operation. Examination of the interfacial phenomenon, however, is not direct since the process of continued net evaporation or condensation is a non-equilibrium one and the conventional heat and mass transfer equations as well as the constitutive relations no longer apply.

The phase change problem has been previously examined by several authors [19, 20, 21]. Bornhorst [22, 23] used the theory of irreversible thermodynamics and the Onsager reciprocal law to establish the appropriate governing equations for the phase change problem. These same results can also be obtained from kinetic theory as shown by Kucherov and Rikenglaz [24], and Labunstov [25]. A result of these analyses relates the surface vapor temperature to the liquid temperature at the surface. The relation is given by

$$T_{vi} = T_{fi} \left[1 - \frac{\dot{m} \;{}_{E}}{2\left(\frac{\gamma+1}{\gamma-1}\right) \frac{P_s}{\sqrt{2\pi R T_{fi}}}}\right] \qquad (3\text{-}1)$$

where T_{vi} is the vapor temperature at the interface, P_s is the saturation pressure, T_{fi}, the interface liquid temperature, γ is the ratio of specific heats, $\dot{m}$ is the steady-state evaporative mass flux, and ${}_E$ is a coupling coefficient which lies in the interval $0 < \gamma_E \leq 1$. Clearly the difference between the vapor and liquid temperatures at the interface will be a maximum for the case of $\gamma_E = 1$. Feldman and Berger [26] evaluated equation (3-1) for the case where water is the working fluid, assuming a value of unity for γ_E. They assumed a steady-state evaporative mass flux of $1 kw/in^2$. The results of their evaluation are presented in figure 3-2. It is seen that the temperature difference between the liquid and the vapor phases at the interface is negligible for operating conditions of practical concern. Similar results are obtained for the other fluids commonly used in moderate temperature heat pipe applications. As a consequence of the above, it will be assumed that the boundary condition at the liquid/vapor interface is

$$T_{fi} = T_v \qquad (3\text{-}2)$$

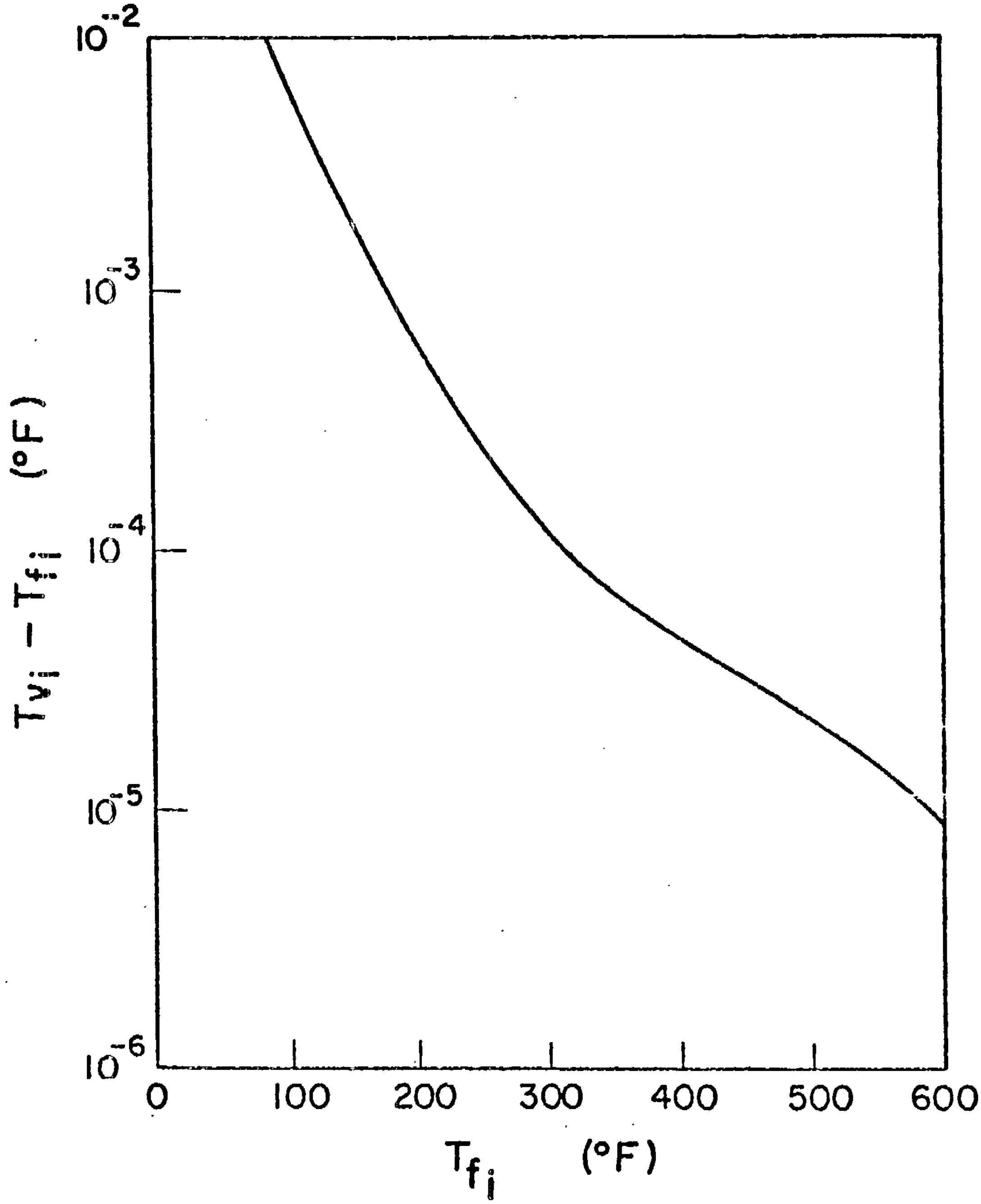

Figure 3-2

3.2.2 Convective Energy Transport

There are two basic mechanisms within a single groove of a grooved heat pipe wall by which thermal energy transport by convection may occur.

The first of these is the convection of thermal energy along the groove as a result of the velocity field which supplies liquid to the evaporation sites along the length of the groove. This will be recognized as a conventional convective energy transport mechanism. The second mechanism for convection within the groove is a direct result of the phase change process itself. If, for example, evaporation is occurring at the free surface, then this surface appears to the groove as a sink for fluid mass. Consequently, for steady-state operation, liquid must continuously be supplied to the sink location. This necessarily establishes flows within the plane of the groove cross-section which terminate at the free surface. If these flows originate with a significantly different specific internal energy than that at the vapor temperature and if their velocities are sufficiently large, then a substantial contribution to the heat transfer may result from this convective motion.

The following two sections provide an assessment of the importance of these two effects.

i) Convection along the groove length

Along the length of a single groove, the temperature variation within the working fluid will be very small. This is the direct consequence of the saturation condition existing at the liquid/vapor interface, with small variations occurring due to changes in the meniscus radius of curvature and the corresponding effect of pressure on temperature for the working fluid. In any case the energy convected along a groove will be small when compared to the evaporation or condensation exchanges occurring at the free surface. This allows a decoupling of the equations of motion from the energy equation.

In support of the neglect of convective energy transport, we consider the energy equation, disregarding expansion work and viscous dissipation, given in cartesian coordinates:

$$\frac{\partial^2 T}{\partial x^{*2}} + \frac{\partial^2 T}{\partial y^{*2}} + \frac{\partial^2 T}{\partial z^{*2}} = Pe\left[u^* \frac{\partial T}{\partial x^*} + v^* \frac{\partial T}{\partial y^*} + w^* \frac{\partial T}{\partial z^*}\right] \qquad (3\text{-}3)$$

where normalization of the velocity is made with respect to the groove entrance mean longitudinal velocity and that of the length scale is made with respect to the cross-sectional hydraulic diameter. The Peclet number is then defined by

$$Pe \equiv Re\ Pr = \left(\frac{\bar{w}\ d_h}{\nu}\right)\left(\frac{k_f}{\mu\ c_p}\right) \qquad (3\text{-}4)$$

with Re, the Reynold's number, Pr, the Prandtl number, and d_h, the hydraulic diameter. Under the quasi-fully-developed flow assumption, we can set the normalized velocities $u^* = v^* \approx 0$, where z is the coordinate along the groove length. Further, utilizing the isothermality of the free surface in the flow direction permits the specification of $\frac{\partial^2 T}{\partial z^{*2}} = \frac{\partial T}{\partial z^*} \approx 0$. Using these results, the governing equation

(3-3) becomes

$$\frac{\partial^2 T}{\partial x^{*2}} + \frac{\partial^2 T}{\partial y^{*2}} = 0 \qquad (3-5)$$

the heat conduction equation within the groove cross-section.

ii) Convection within the groove cross-section

Determination of the convective energy transport within the groove cross-section resulting from the replenishment of evaporated fluid is performed using the results presented later in this report which are based upon a pure conductive model. The liquid is assumed to be flowing from the groove root to the free surface with an average velocity equal to that required to supply the appropriate evaporative mass flow. Using typical temperature data from the conductive results, the cross-sectional convective energy transport contributes an estimated 0.38 per cent of the conductive transport.

It is therefore concluded that conduction heat transfer is the dominant heat transfer mechanism within the liquid.

3.2.3 Typical Cell for Analysis

In the geometry of figure 3-1, we are considering as a thermal boundary condition the application of a uniform heat flux distribution on the external surface of the pipe wall. In general the thermal interaction of the portion of the pipe wall shown in the figure with the total heat pipe environment may result in a net conduction of heat along the wall within the metal. Through the use of a grooved surface, however, this effect is minimized since the lateral conductance will be large compared to that along the wall. Further, a net conduction along the wall will in general result from the variation of the equivalent heat transfer coefficient in this direction providing preferential conductive paths to the evaporation sites. Due to the close proximity of adjacent grooves in typical heat pipes, however, the local liquid cross-sectional variation from groove to groove will indeed be small. It is therefore assumed that for purposes of evaluating the equivalent heat transfer coefficient, there is no thermal interaction between adjacent grooves. Referring to the geometry of figure 3-1, then, this implies that the sections A-A and C-C will be adiabatic surfaces. Thus the typical cell bounded by sections A-A and C-C in the one direction and by the pipe external surface and the vapor/liquid interface in the other can be extracted from the overall geometry for analysis purposes.

A closer examination of this typical cell reveals that a further reduction of the analysis geometry is possible. Due to the geometric symmetry of the groove and liquid about the groove centreline, there is no cause for preferential heat flow on either side of this centerline. Consequently, not only are the bounding surfaces A-A and C-C adiabatic planes, but in addition the groove centerline, surface B-B, will represent a zero net heat flux surface. The net result is that the typical cell for consideration in the thermal analysis is the one shown in figure 3-3.

3.3 Problem Description

Using the analysis geometry of figure 3-3, a cartesian coordinate system is set up with the origin located at the intersection of the groove centerline and the pipe wall external surface. The pipe wall external surface is defined by the line $y = 0$ and the groove centerline by the line $x = 0$. The coordinate system is presented in the figure.

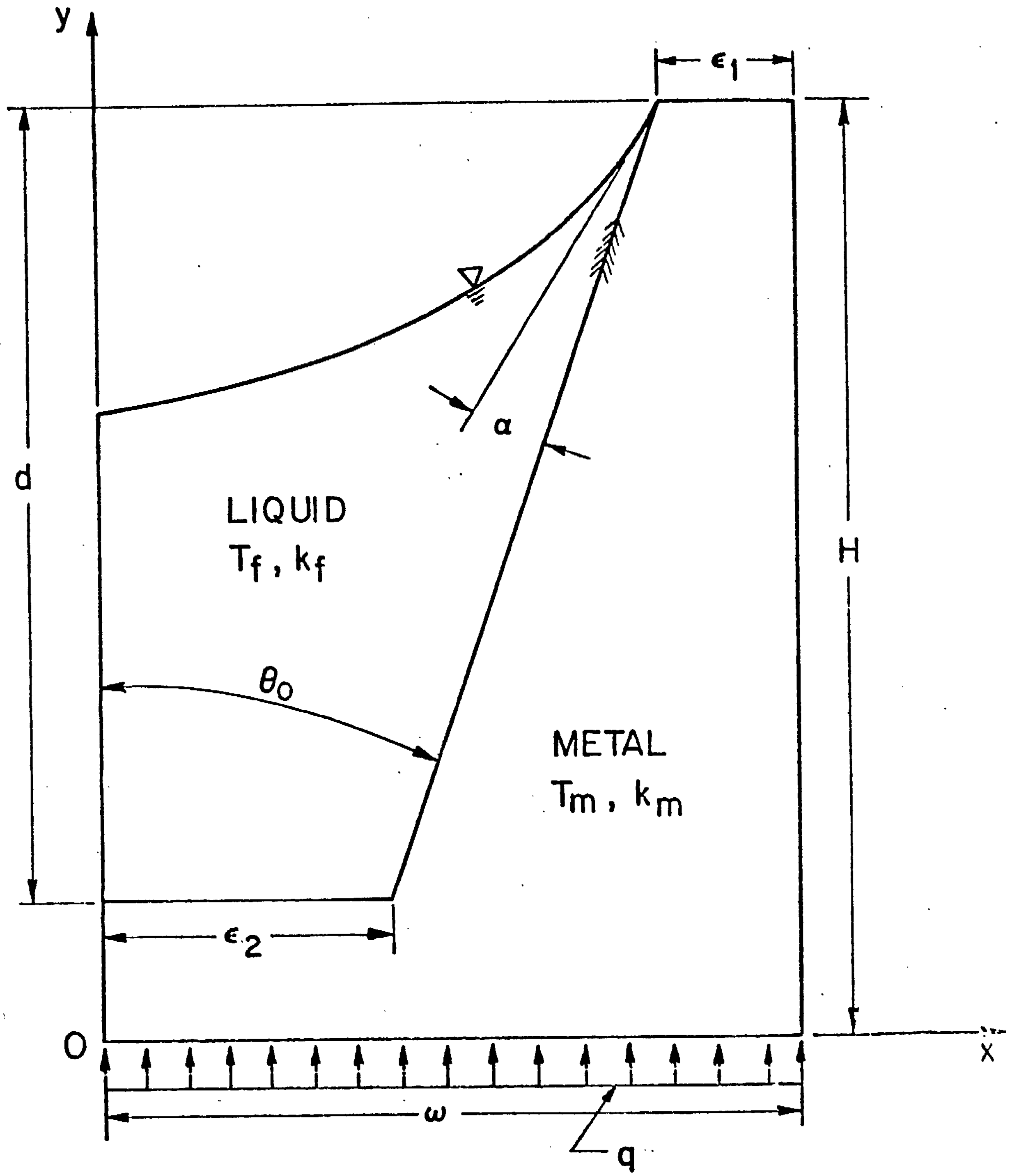

y
ϵ_1
d
α
LIQUID
T_f , k_f
H
θ_0
METAL
T_m , k_m
ϵ_2
O
X
ω
q

Figure 3-3

The geometry presented is representative of a general trapezoidal groove. The exposed land area of the groove section is denoted by ε_1 while the flat groove root half-width is denoted by ε_2. The groove included half-angle is θ_o and the liquid free surface meets the groove wall with an apparent contact angle of α. The groove depth available for fill by the working fluid is d with the total thickness of the wall, extending from the pipe external surface to the innermost portion of the groove sidewall, denoted by H.

The general trapezoidal shape of figure 3-3 readily degenerates to the two limiting cases commonly employed in heat pipe designs. For the case where $\varepsilon_1 = \varepsilon_2 = 0$, the resulting geometry becomes the sharp V-groove situation commonly employed in high capacity arterial pipes as a mechanism for circumferential wetting of the pipe inner wall. In the other extreme, when $\varepsilon_1 = \varepsilon_2 = 0.5$, the rectangular channel-like shape results which is a common configuration for moderate capacity pipes where the grooves serve both as an evaporative agent and as a longitudinal liquid transport mechanism.

Steady-state heat transfer is considered in this work with the liquid and metal components of the composite problem having thermal conductivities k_f and k_m respectively. Heat is supplied to or removed from the outer surface of the pipe, $y=0$, at a uniform rate q with the lateral normal gradients of temperature at $x = 0$ and $x = w$ being zero. The heat flow is transferred to/from the vapor core through the liquid free surface where the temperature is uniform at T_v. Over the land area exposed to the vapor, it is assumed that an insignificant amount of energy is being transferred in comparison with that transferred at the liquid free surface, so that over this region a zero normal temperature gradient condition is applied. This results from the very low vapor thermal conductivity and of course does not consider the contribution to the heat transfer due to condensation on the land area in the condenser regions. At the liquid/metal interface both the temperature and the normal surface heat flux must be continuous in passing from the metal region to the liquid region.

3.4 Mathematical Statement of the Problem

Denoting the temperature distribution within the fluid and metal by T_f and T_m respectively, and considering steady-state heat transfer, the governing differential equations are Laplace's equation for both regions respectively. In terms of the cartesian coordinates of figure 3-3 these are written as

$$\frac{\partial^2 T_f}{\partial x^2} + \frac{\partial^2 T_f}{\partial y^2} = 0 \tag{3-6}$$

and

$$\frac{\partial^2 T_m}{\partial x^2} + \frac{\partial^2 T_m}{\partial y^2} = 0 \tag{3-7}$$

The boundary conditions which the solution to equations (3-6) and (3-7) must satisfy are

1. $y=0,\ 0\leq x\leq w,\ \dfrac{\partial T_m}{\partial y} = \dfrac{-q}{k_m}$ (3-8)

2. $y=H-d,\ 0\leq x\leq \varepsilon_2,\ k_m \dfrac{\partial T_m}{\partial y} = k_f \dfrac{\partial T_f}{\partial y}$ (3-9)

3. $y=(H-d) + \dfrac{d(x-\varepsilon_2)}{w-\varepsilon_1-\varepsilon_2},\ \varepsilon_2 < x < w-\varepsilon_1,$

$$k_m \frac{\partial T_m}{\partial n} = k_f \frac{\partial T_f}{\partial n} \tag{3-10}$$

where n is a vector normal to the liquid/metal interface.

4. $y=H, \; w-\varepsilon_1 \leq x \leq w, \; \frac{\partial T_m}{\partial y} = 0$ (3-11)

5. $x=0, \; 0 \leq y \leq H-d, \; \frac{\partial T_m}{\partial x} = 0$ (3-12)

6. $x=0, \; H-d \leq y \leq y_i(0), \; \frac{\partial T_f}{\partial x} = 0$ (3-13)

where $y_i(x)$ is used to denote the description of the liquid free surface.

7. $y=y_i(x), \; 0 \leq x \leq w-\varepsilon_1, T_f(x, y_i(x)) = T_v$ (3-14)

8. $x=w, \; 0 \leq y \leq H, \; \frac{\partial T_m}{\partial x} = 0$ (3-15)

To provide greater utility to the results of this heat transfer problem, the equations and boundary conditions above can be non-dimensionalized by introducing suitable non-dimensional parameters. This also has the effect of reducing by one the number of nonhomogeneous boundary conditions in equations (3-8)-(3-15).

Defining a temperature excess by the definitions

$$T_f^* = T_f - T_v$$

and (3-16)

$$T_m^* = T_m - T_v$$

and normalizing the spatial coordinates by the groove half-width, w, the governing equations become

$$\frac{\partial^2 T_f^*}{\partial x^{*2}} + \frac{\partial^2 T_f^*}{\partial y^{*2}} = 0 \qquad (3\text{-}17)$$

and

$$\frac{\partial^2 T_m^*}{\partial x^{*2}} + \frac{\partial^2 T_m^*}{\partial y^{*2}} = 0 \tag{3-18}$$

where

$$x^* \equiv x/w, \quad y^* \equiv y/w \tag{3-19}$$

The boundary condition statements for use with equations (3-17) and (3-18) are

1. $y^* = 0,\ 0 \leq x^* \leq 1,\ \dfrac{\partial T_m^*}{\partial y^*} = \dfrac{-qw}{k_m}$ (3-20)

2. $y^* = H^*-d^*,\ 0 \leq x^* \leq \varepsilon_2^*,\ k_m \dfrac{\partial T_m^*}{\partial y^*} = k_f \dfrac{\partial T_f^*}{\partial y^*}$ (3-21)

3. $y^* = (H^*-d^*) + \dfrac{d^*(x^*-\varepsilon_2^*)}{1-\varepsilon_1^*-\varepsilon_2^*},\ \varepsilon_2^* < x^* < 1-\varepsilon_1^*,$

$$k_m \frac{\partial T_m^*}{\partial n^*} = k_f \frac{\partial T_f^*}{\partial n^*} \tag{3-22}$$

4. $y^* - H^*,\ 1-\varepsilon_1^* \leq x^* \leq 1,\ \dfrac{\partial T_m^*}{\partial y^*} = 0$ (3-23)

5. $x^* = 0,\ 0 \leq y^* \leq H^*-d^*,\ \dfrac{\partial T_m^*}{\partial x^*} = 0$ (3-24)

6. $x^* = 0,\ H^*-d^* \leq y^* \leq y_i^*(0),\ \dfrac{\partial T_f^*}{\partial x^*} = 0$ (3-25)

7. $y^* = y_i^*(x),\ 0 \leq x^* \leq 1-\varepsilon_1^*,\ T_f^*(x^*, y_i^*(x)) = 0$ (3-26)

8. $x^* = 1,\ 0 \leq y^* \leq H^*,\ \dfrac{\partial T_m^*}{\partial x^*} = 0$ (3-27)

The equations (3-17) and (3-18) together with the boundary conditions (3-19) -(3-27) completely define the mathematical problem whose solution is required.

3.5 Analytic Solution

If an analytic solution to the problem specified above is pursued, we can follow the classical method of separation of variables [ ]. According to the method, we assume a solution of the form

$$T^* = X(x^*) \cdot Y(y^*) \tag{3-28}$$

for both the liquid and metal temperature distributions. Using equation (3-28) in either of equations (3-17) or (3-18) leads to an equation of the form

$$\frac{1}{X}\frac{\partial^2 X}{\partial x^{*2}} + \frac{1}{Y}\frac{\partial^2 Y}{\partial y^{*2}} = 0 \tag{3-29}$$

again for both the liquid and the metal temperature distributions. Separating the x^* and y^* dependence in such an equation then leads to the separated equations

$$\frac{\partial^2 x}{\partial x^{*2}} + \lambda^2 X = 0 \tag{3-30}$$

and

$$\frac{\partial^2 Y}{\partial y^{*2}} - \lambda^2 Y = 0 \tag{3-31}$$

where the separation constant was taken as λ^2.

The solutions to equations (3-20) and (3-31) are respectively

$$X(x^*) = C_1\sin(\lambda x^*) + C_2\cos(\lambda x^*) \qquad (3\text{-}32)$$

$$Y(y^*) = C_3\sinh(\lambda y^*) + C_4\cosh(\lambda y^*) \qquad (3\text{-}33)$$

The general solution can then be written as

$$T_f^* = [C_{1f}\sin(\lambda_f x^*) + C_{2f}\cos(\lambda_f x^*)][C_{3f}\sinh(\lambda_f y^*) + C_{4f}\cosh(\lambda_f y^*)] \qquad (3\text{-}34)$$

and

$$T_m^* = [C_{1m}\sin(\lambda_m x^*) + C_{2m}\cos(\lambda_m x^*)]\ ]C_{3m}\sinh(\lambda_m y^*) + C_{4m}\cosh(\lambda_m y^*)] \qquad (3\text{-}35)$$

Applying boundary conditions (3-24) and (3-25) simplifies the solution by the requirement that $C_{1f} = C_{1m} = 0$. The temperature distributions then become

$$T_f^* = \sum_{n=1}^{\infty} \cos\ (\lambda_f x^*)\ [C_{3f}\sinh(\lambda_f y^*) + C_{4f}\cosh(\lambda_f y^*)] \qquad (3\text{-}36)$$

and

$$T_m^* = \sum_{n=1}^{\infty} \cos\ (\lambda_m x^*)\ [C_{3m}\sinh(\lambda_m y^*) + C_{4m}\cosh(\lambda_m y^*)] \qquad (3\text{-}37)$$

where further using the condition (3-27) the λ_m's can be determined to be

$$\lambda_m = n\pi,\ n = 1,2,3,\ldots \qquad (3\text{-}38)$$

while the values for the λ_f remain unresolved.

Unfortunately, the development of the solution for either temperature field beyond that presented in equations (3-36) and (3-37) becomes extremely complex as a result of the irregular geometry of each solution domain and the inherent coupling of the two temperature fields through the condition of equation (3-21) and (3-22). Indeed, it is not clear whether an exact analytical solution to the complete composite problem can be achieved using present mathematical methods. On the basis of the difficulties involved in overcoming the mathematical barriers presented by the analytic solution, it was decided to use a numerical method of solution to solve the system of equations and boundary conditions of (3-17) - (3-27).

3.6 Numerical Solution

Having decided to forego further analytical efforts in favor of a numerical method of solution it remains to select an appropriate numerical method for this problem. The two most common numerical methods in current usage are the finite difference and the finite element method. Both methods involve discretizing the spatial domain into discrete regions of finite size, and as a consequence the solution is available in the form of values for the dependent variable at discrete locations throughout space rather than as a continuous analytic solution. In addition, both methods lead to a system of simultaneous algebraic equations which must be solved to yield the corresponding values at the discretized locations.

The finite difference method has as its basis the same basic principles as does the differential formulation leading to the differential equation.* That is, an energy balance is applied to each control volume of the discretized continuum [31]. The first law of thermodynamics then provides a relation between the transfer of heat by conduction across the control volume surfaces, the rate of generation of internal energy within the control volume, and the rate of change of the control volume internal energy. Since the control volume dimensions are not of infinitesimal size, however, the concept of a derivative is no longer of direct use for application of Fourier's law of heat conduction since the surface area segments are finite and the gradient will in general vary over the surface. The approximation is usually introduced that for purposes of evaluating the heat conduction terms, a first central different quotient can be used to describe the local gradient. It is usually further assumed that this gradient is uniform over each of the control volume surfaces.

Because of the control volume formulation forming the basis of the method, the grid network usually follows the contours of an orthogonal coordinate system. Although the finite difference coefficients have been derived for any orthogonal curvilinear coordinate system [31, 32], the complex geometric description of the analysis geometry of figure 3-3 does not lend itself readily to any of the available coordinate systems. On this basis, then, and particularly

---

*Alternatively, some investigators prefer to use as a basis for the method, a Taylor series expansion approximation to the original differential equation. While there are subtle differences between the two approaches, either can be used.

in consideration that the finite element method is readily adopted to irregular geometries, the finite difference method was discarded for use in this analysis in favor of the finite element method.

The method of finite elements entails employing a variational principle to minimize a certain functional over the solution domain of interest [33]. Alternatively, where a variational principle does not exist, the method of weighted residuals applied to the governing differential equation can also be used [34]. In the former case the functional can be obtained by application of the calculus of variations to the governing differential equation. In this case the associated Euler equation resulting from the minimization of the appropriate functional is identically the governing differential equation. The steady-state conduction of heat has a governing variational principle.

In the method of finite elements it is the governing functional equation, an integral equation, which is approximated in the discretized continuum rather than the governing differential equation as is the case in using finite differences. Through an appropriate choice of the local approximation to the temperature field, the required integration over volume in the functional equation can readily accommodate both irregular solution domain geometries as well as irregular, non-orthogonal 'finite elements'. It is the flexibility of the finite element method in its ability to readily describe irregular geometries that has led to its selection as the method for use in this analysis. The method and its application will be discussed in greater detail in Chapter 5 of this work where the numerical solution is presented.

Chapter 4

Bounds on the Groove Heat Transfer

4.1 Introduction

In this chapter, limits will be established which provide upper and lower bounds for the equivalent heat transfer coefficient associated with the typical cell presented in the previous chapter of this report. The bounds will be established using the theorems of Elrod [35]. Although its introduction to the heat transfer community by Elrod is recent, the basis of his theorems is not new and has received considerable attention in other disciplines [36]. The theorems and their proofs are valid whenever the pertinent unknown quantity can be expressed in terms of a dependent variable which obeys the equation for a potential field. The two theorems as put forward by Elrod [35] are presented below.

> Theorem 1 Consider a solid body composed of material which may be both inhomogeneous and anisotropic, but whose properties are independent of temperature. Let the body be isolated from its surroundings except for exposure through space-variable heat-transfer coefficients to two distinct ambient temperatures. If, within some region of this body, the heat conductivity is increased (decreased), then the total heat flow from one exposed surface to the other will either increase (decrease), or remain the same.

> Theorem 2 The actual heat flow taking place under the circumstances described in theorem 1 will be no greater than that calculated when the shapes of the isothermal surfaces within the body are arbitrarily

assumed, and no less than that calculated when the adiabatic surfaces within the body are assumed.

Use will be made in this chapter primarily of the second of the above theorems in order to establish limits on the groove heat transfer characteristics. The reasons for examining limits on the groove heat transfer are twofold and are presented in the following paragraphs.

Firstly, in establishing a system's upper and lower heat transfer limits, it is possible in certain cases that the limiting values obtained by such an analysis may be sufficiently close that acceptable accuracy is obtained for the required application. That is, by employing the arithmetic average value of the two extreme values, the error or uncertainty band of the obtained value may be sufficiently small to suffice for use in engineering calculations. This possibility was suggested in the paper by Elrod [35] and was demonstrated in the application considered by Yovanovich, Schneider, and Strong [37] in their examination of the effective thermal conductivity of a composite having square fibers embedded as a square array within a second matrix material. If this objective cannot be achieved for the system under consideration, however, the second motivation for examining the limiting behavior becomes important.

The second motivation for examining limiting values for the groove heat transfer is to provide a check, although it may be crude, on the results of a numerical solution to the problem at hand. Since the application of either of the two theorems leads to maximum and minimum values for the heat transfer associated with a given system, any numerical results must as a consequence lie in the range bounded by the two limits. Numerical results outside this range can then be immediately discarded and a study initiated to determine the causes for the unreliable numerical results. Unfortunately, however, if the numerical results lie within the range of values allowed by the limit study, and if the objective of the first reason stated for examining the limits is not achieved, the limit study will be of little further value. Its use as a check on the numerical results will still warrant its consideration in this report.

4.2 Maximum Groove Heat Transfer

As was stated in Theorem 2 above, the heat transfer through the typical cell cannot be greater than that for the case where the shapes of the isotherms are arbitrarily assumed. The result of such an assumption is to yield an upper limit for the groove heat transfer.

To facilitate the computation of this upper limit the typical cell was subdivided into three distinct sub-regions, each of which is bounded on both sides by a thin layer of infinitely conducting material; i.e. the bounding surfaces of the sub-regions are assumed isothermal. The sub-division scheme, designed partly for ease of later computation, is illustrated in figure 4-1. The shaded region seen in the figure is constructed by replacing that portion of the original cell with a material of infinite thermal conductivity. As a result, this portion does not contribute to the thermal resistance of the cell and need not be considered. This is consistent with Theorem 1 in establishing an upper bound for the heat transfer. Consideration of each of the three regions follows.

4.2.1 Sub-Region I

An expanded and detailed view of sub-region I is shown in figure 4-2 where the pertinent geometric parameters are also presented. A circular cylinder coordinate system is set up in the figure with its origin at the free surface center of curvature with the angular coordinate, γ, measured counterclockwise from a line extending from the origin, along the groove

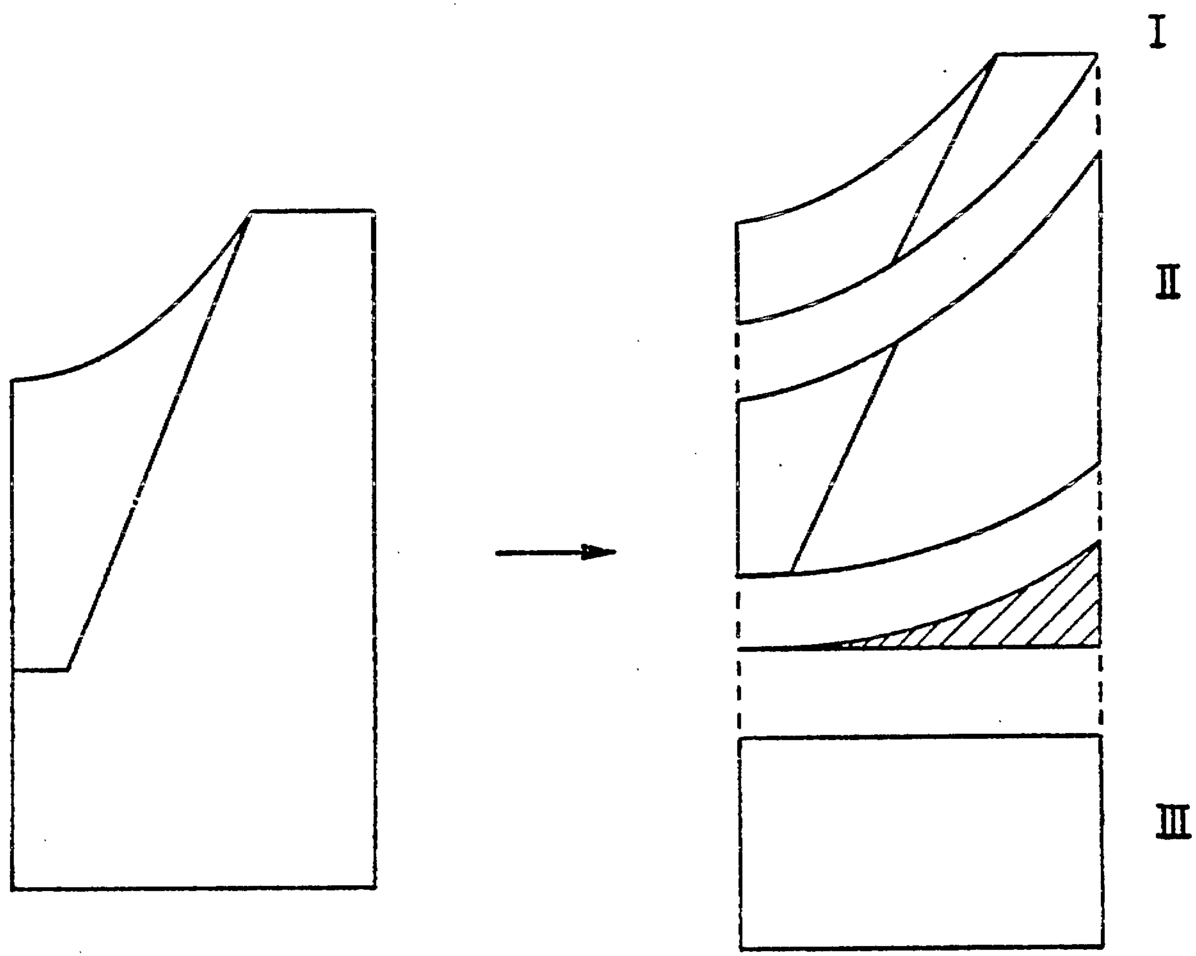

Figure 4-1

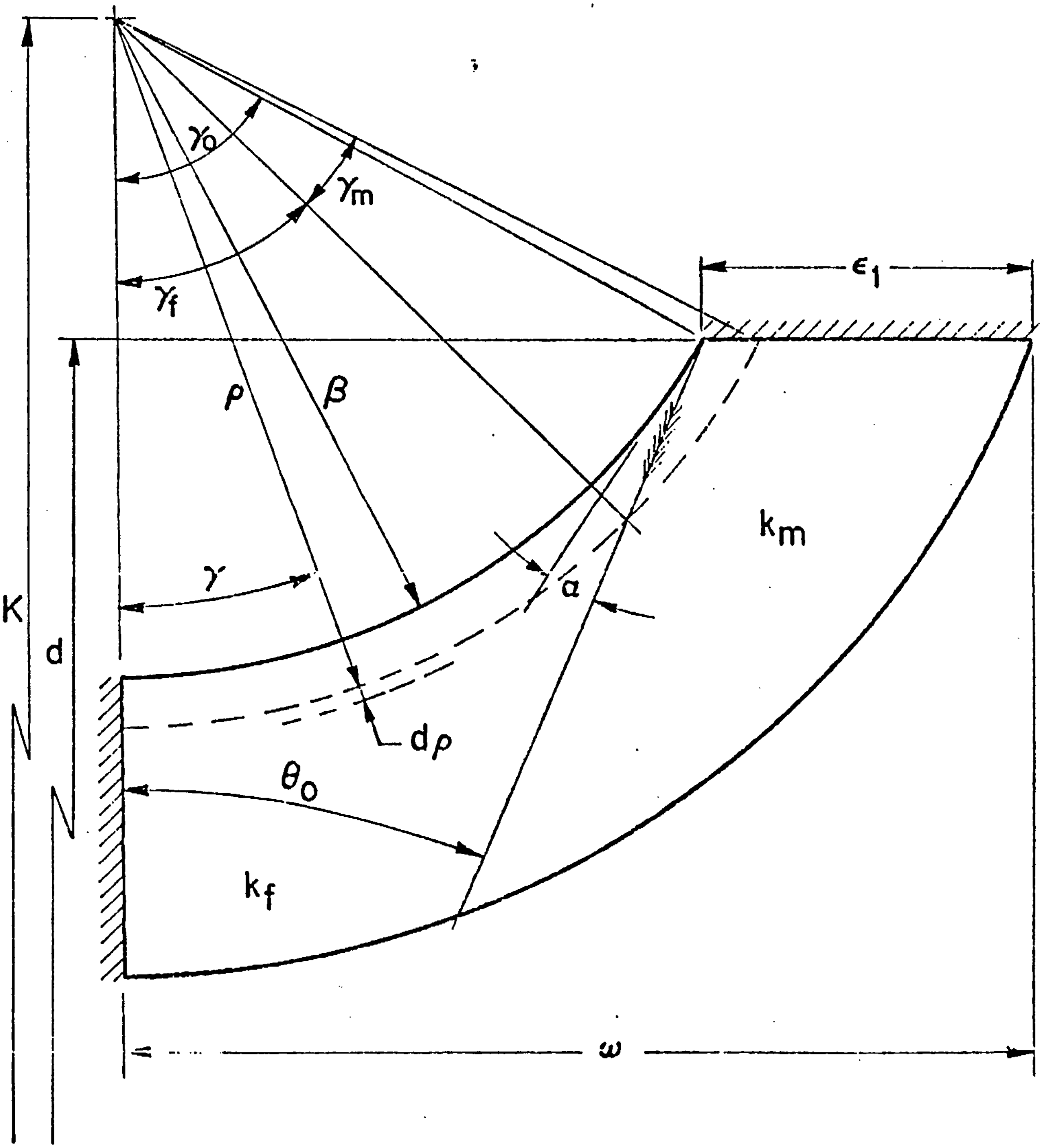

γ_o
γ_m
γ_f
ϵ_1
ρ
β
k_m
γ
a
K
d
$d\rho$
θ_o
k_f
ω

Figure 4-2

centerline, through the composite.

In accordance with Theorem 2 of Elrod, the shapes of the isotherms will be assumed for sub-region I. For convenience they are assumed here to be circumferential lines about the origin and extending through the cross-section of this sub-region. The quantities γ_f and γ_m are the subtended angles within the liquid and metal parts of the cell respectively. The situation shown is seen to represent radial flow through the composite section with for each differential thickness, a parallel system of the liquid path with the metal path.

Considering a typical strip of differential thickness, $d\rho$, the associated resistance, dR_I, is given by

$$dR_I = \left[\frac{1}{k_f\gamma_f + k_m\gamma_m}\right] \frac{d\rho}{\rho} \tag{4-1}$$

where γ_f and γ_m are the angles subtended by the liquid and metal regions respectively. For aid in the evaluation of γ_f and γ_m, figure 4-3 is constructed. Applying the sine law [38] to the triangle having vertices A,B, and C, we find

$$\frac{\kappa \tan \theta_o}{\sin(\gamma_f+\theta_o)} = \frac{\rho}{\sin(\frac{\pi}{2} - \theta_o)} \tag{4-2}$$

Using (4-2), γ_f can be evaluated as a function of its radial position, ρ, and is given by

$$\gamma_f = \sin^{-1}\left[\frac{\kappa \sin\theta_o}{\rho}\right] - \theta_o \tag{4-3}$$

from which γ_m is determined to be

$$\gamma_m = \cos^{-1}\left[\frac{\kappa - r_o \cos \theta_o}{\rho}\right] - \gamma_f \tag{4-4}$$

The resistance for sub-region I is then found by integration of (4-1) over

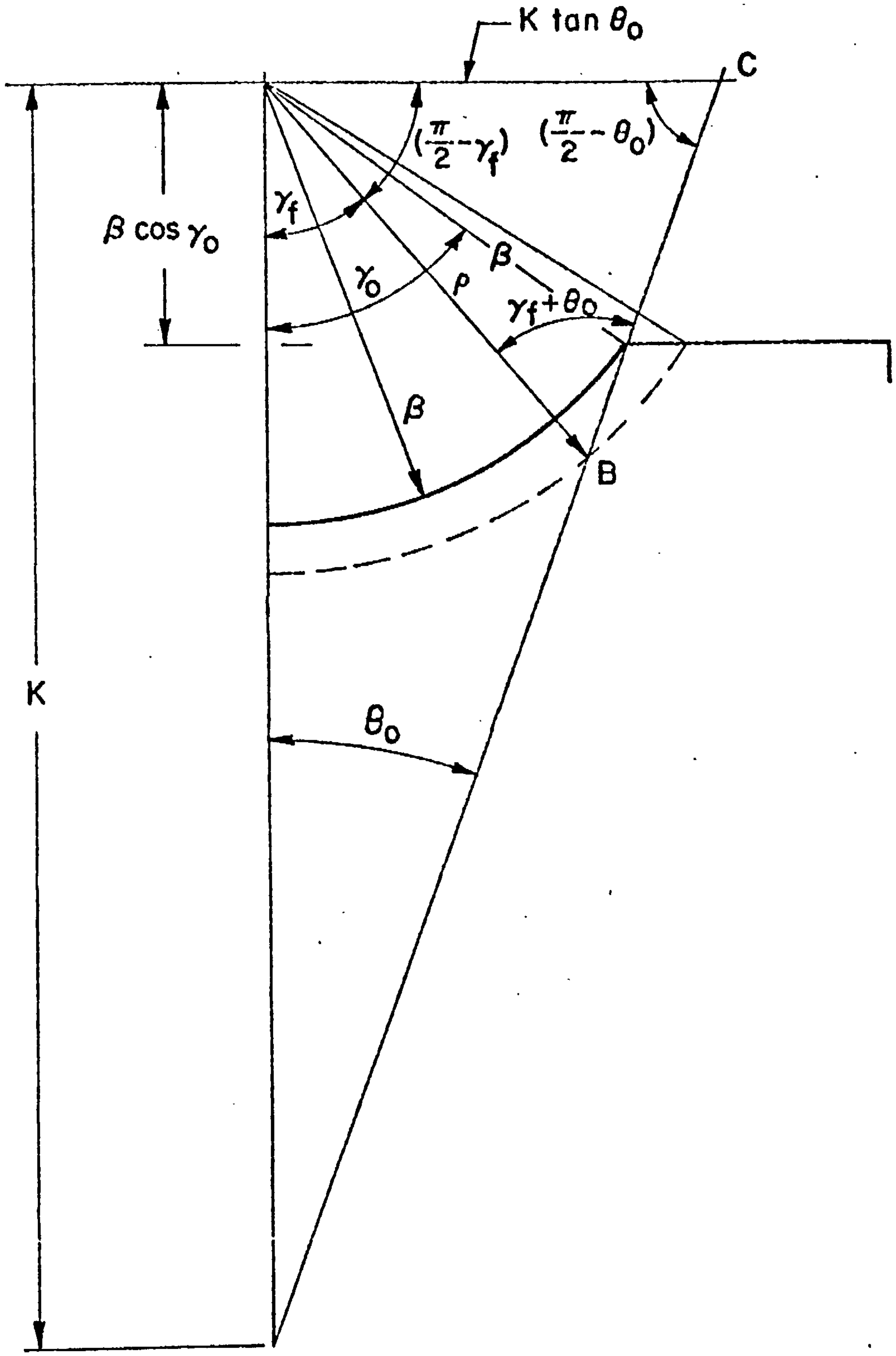

Figure 4-3

this region,

$$R_I = \int_{\rho_1}^{\rho_2} \left[\frac{1}{k_f\gamma_f + k_m\gamma_m}\right] \frac{d\rho}{\rho} \tag{4-5}$$

where $\rho_1 = \beta$

$$\rho_2 = \sqrt{\omega^2 + (\kappa - r_o \cos \theta_o)^2} \tag{4-6}$$

and from Appendix A,

$$\beta = \frac{r_o \sin \theta_o}{\cos(\alpha+\theta_o)}$$

$$\kappa = \frac{r_o \cos \alpha}{\cos(\alpha+\theta_o)} \tag{4-7}$$

and $\quad r_o = (\omega - \varepsilon_1)/\tan \theta_o$

Integration of (4-5) will be reserved until the three regions are assembled to reform the overall geometry.

4.2.2 Sub-Region II

A detailed view of sub-region II is illustrated in figure 4-4. The coordinate system here is the same as that used for sub-region I and the resistance for a differential strip, $d\rho$, is given as before by

$$dR = \left[\frac{1}{k_f\gamma_f + k_m\gamma_m}\right] \frac{d\rho}{\rho} \tag{4-8}$$

where now the contained angles for the liquid and metal portions are given by

$$\gamma_f = \sin^{-1}\left[\frac{\kappa \sin \theta_o}{\rho}\right] - \theta_o \tag{4-9}$$

and $\quad \gamma_m = \sin^{-1} (\frac{\omega}{\rho}) - \gamma_f$

The total resistance for sub-region II is again given by integration as

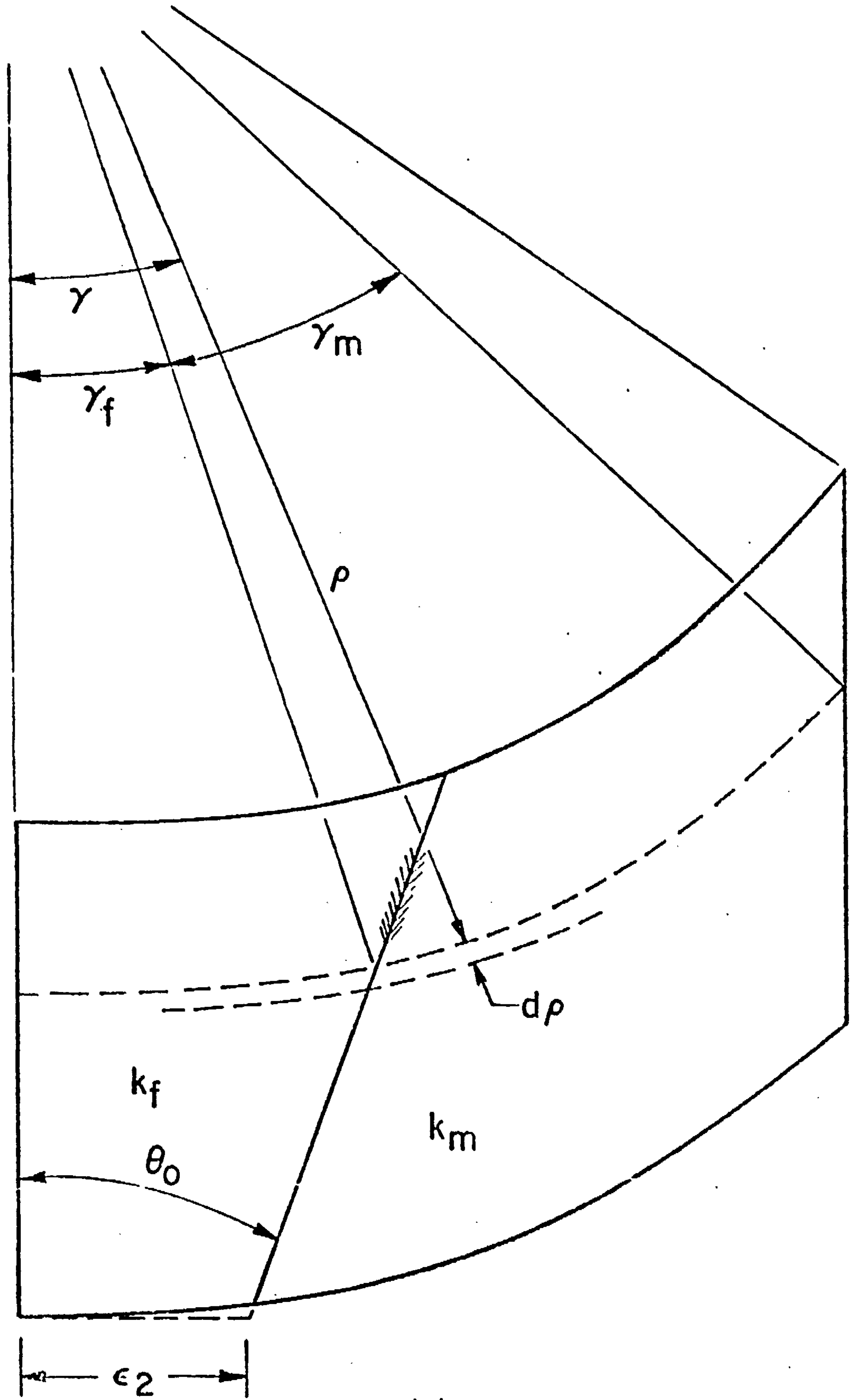

Figure 4-4

$$R_{II} = \int_{\rho_2}^{\rho_3} \left[\frac{1}{k_f\gamma_f + k_m\gamma_m}\right] \frac{d\rho}{\rho} \tag{4-10}$$

where ρ_2 is that determined for the consideration of sub-region I and ρ_3 is given by

$$\rho_3 = \kappa - \frac{\varepsilon_2}{\tan\theta_o} \tag{4-11}$$

Again, integration is reserved for the assembly of the sub-regions.

4.2.3 Sub-Region III

With the cross-hatched region of figure 4-1 constructed of a material having infinite thermal conductivity, its thermal resistance will be zero. The final region then, sub-region III, is simply a slab of thickness (H-d) and having width w. Consequently, the thermal resistance of sub-region III is simply

$$R_{III} = \frac{(H-d)}{k_m w} \tag{4-12}$$

4.2.4 Overall Heat Transfer

The three sub-regions examined in the preceding section form a series thermal circuit for heat transfer between the exterior pipe wall and the vapor core of the heat pipe. As a result the total resistance for this maximum heat transfer case is given by the sum of the individual resistances

$$R_T = R_I + R_{II} + R_{III} \tag{4-13}$$

The heat transfer through the typical cell can be given by

$$Q = \frac{\overline{T}(y = H-d) - T_v}{(R_T - R_{III})} = h_{eq}\, w[\overline{T}(y = H-d) - T_v] \tag{4-14}$$

where $\overline{T}$ $(y = H-d)$ is the average temperature of the groove root surface. Using equation (4-14) it follows that

$$h_{eq} = \frac{1}{(R_T - R_{III})w} \tag{4-15}$$

Further, for a lateral pitch of N grooves per unit length, the dimensionless group can be formed

$$Nu_f \frac{k_f}{k_m} \equiv \frac{h_{eq}}{Nk_f} \frac{k_f}{k_m} \tag{4-16}$$

Using equation (4-15) in (4-16) leads to the result

$$Nu_f \frac{k_f}{k_m} = \frac{2}{(R_T - R_{III})k_m} \tag{4-17}$$

This equation together with (4-13) and the component resistance definitions (4-5), (4-10), and (4-12) will be used to determine the maximum value for the groove Nusselt number.

The component integrations appearing in equations (4-5) and (4-10) are not readily integrable to obtain the required results. As a result, numerical integration was performed using a modified Simpson's rule algorithm. The program listing is presented in detail in Appendix B with only the results presented here. The results are presented in Table 4-1 for the material combinations and geometries considered here.

4.3 Minimum Groove Heat Transfer

Returning to Theorem 2, the heat transfer through the typical cell cannot be less than that for which the shape of the adiabatic surfaces are arbitrarily assumed. By assuming the shape of the adiabats, then, a lower limit for the groove heat transfer can be established.

To facilitate the computation of this lower limit, the typical cell

Table 4-1

Groove Nusselt Number Upper Limit

$Nu_f \cdot k_f/k_m$

			x_α			
d	k_f/k_m	$\varepsilon_1 = \varepsilon_2$	0.05	0.25	0.50	1.00
1.0	0.1	0.01	2.0638	1.5260	1.5166	0.7996
		0.25	2.1379	1.5584	1.2295	1.0356
		0.49	1.8631	1.2767	1.0068	1.0987
	.01156	0.01	1.7178	1.1148	.7754	.5058
		0.25	1.7100	1.1003	.8582	.9244
		0.49	1.4080	0.8371	.6502	1.0088
	.001	0.01	1.5574	0.9053	0.6208	0.4352
		0.25	1.5012	0.8400	0.6468	0.9096
		0.49	1.2067	0.6137	0.4670	0.9964
1.5	0.1	0.01	1.2684	0.9631	0.7412	0.5330
		0.25	1.2886	0.9975	0.8125	0.6904
		0.49	1.1190	0.8561	0.7124	0.7327
	0.01156	0.01	1.0727	0.7180	0.5044	0.3372
		0.25	1.0814	0.7513	0.6000	0.6164
		0.49	0.9151	0.6210	0.5040	0.6731
	0.001	0.01	0.9892	0.5993	0.4119	0.2901
		0.25	0.98104	0.6026	0.4730	0.6067
		0.49	0.8230	0.4874	0.3853	0.6652
2.0	0.1	0.01	0.8757	0.6841	0.5391	0.3997
		0.25	0.8824	0.7165	0.6014	0.5178
		0.49	0.7675	0.6304	0.5458	0.5497
	0.01156	0.01	0.7474	0.5173	0.3693	0.2529
		0.25	0.7610	0.5632	0.4616	0.4624
		0.49	0.6516	0.4846	0.4082	0.5050
	0.001	0.01	0.6982	0.4417	0.3065	0.2176
		0.25	0.7053	0.4688	0.3765	0.4552
		0.49	0.6019	0.3984	0.3260	0.4993

is subdivided into two separate sub-regions as illustrated in figure 4-5. An adiabat will be located along the common boundary of the two sub-regions in accordance with the establishment of a lower limit for the heat transfer. Each of the two regions are examined in greater detail in the following two sub-sections of this report.

4.3.1 Sub-Region I

An expanded view of sub-region I is shown in Figure 4-6. The origin of a cartesian coordinate system is located at the intersection of the groove centerline and the extension of the groove sidewall. Within sub-region I, a strip of width dx_1, emanating from the liquid free surface is examined. This strip is extended as shown in the figure, terminating at the lower surface with width dx_4. The subscripts used in the above refer to the location in figure 4-6 where evaluation is made.That is, in general $dx_4 \neq dx_1$ but a relationship between the two can be derived.

Considering first the section of this strip from points 1 to 1a, the liquid free surface can be described by the equation

$$x_1^2 + (y_1-\kappa)^2 = \beta^2 \tag{4-18}$$

from which the vertical coordinate of the free surface can be found. This is given by

$$y_1 = \kappa - \sqrt{\beta^2 - x_1^2} \tag{4-19}$$

with κ and β as previously defined. The location of point 1a is given by

$$y_{1a} = \varepsilon_2 \cot \theta_o \tag{4-20}$$

and so the component resistance can be determined from

$$dR_{1-1a} = \frac{\kappa - \sqrt{\beta 2 - x_1^2} - \varepsilon_2 \cot \theta_o}{k_f \, dx_1} \tag{4-21}$$

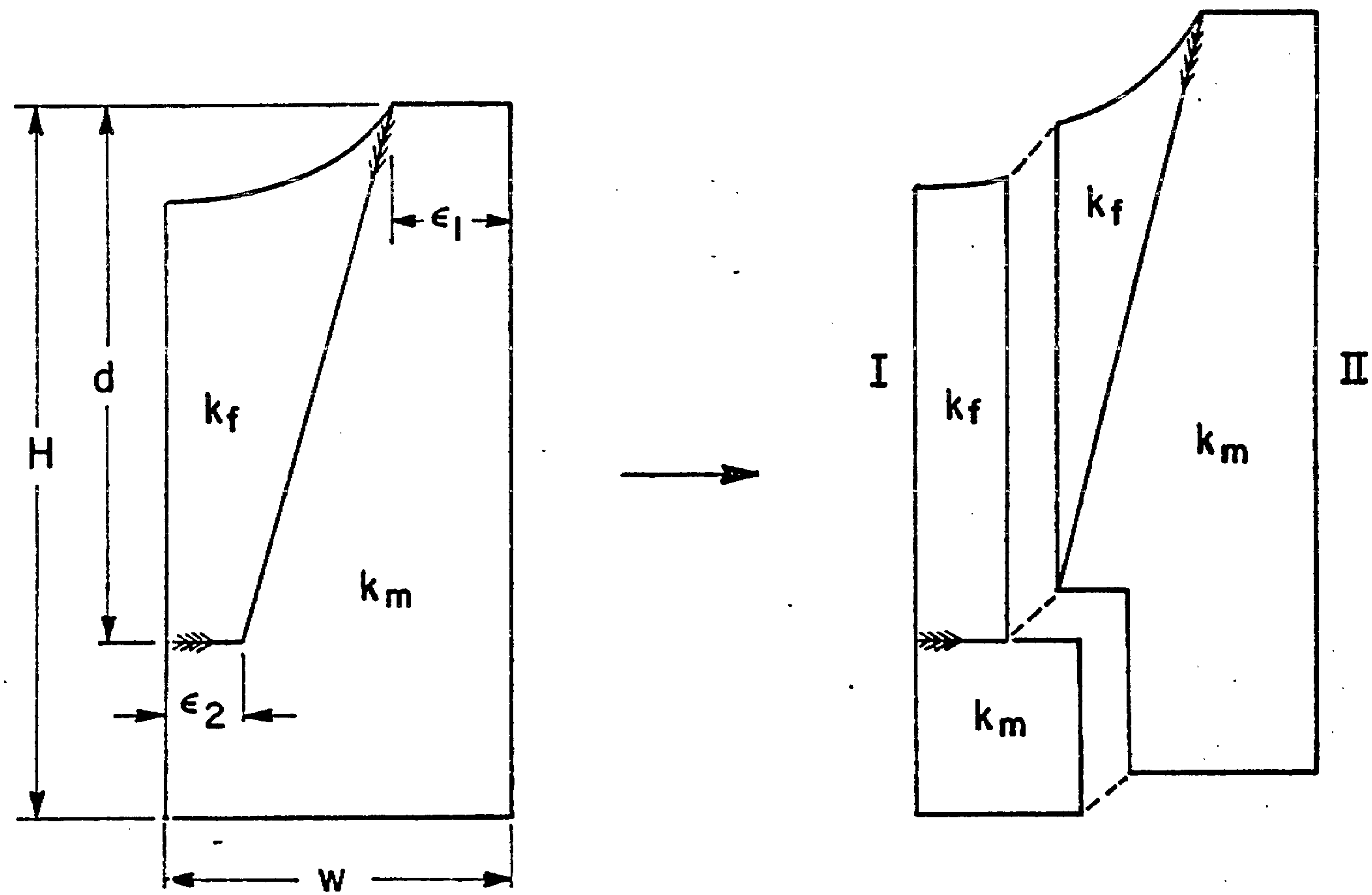

Figure 4-5

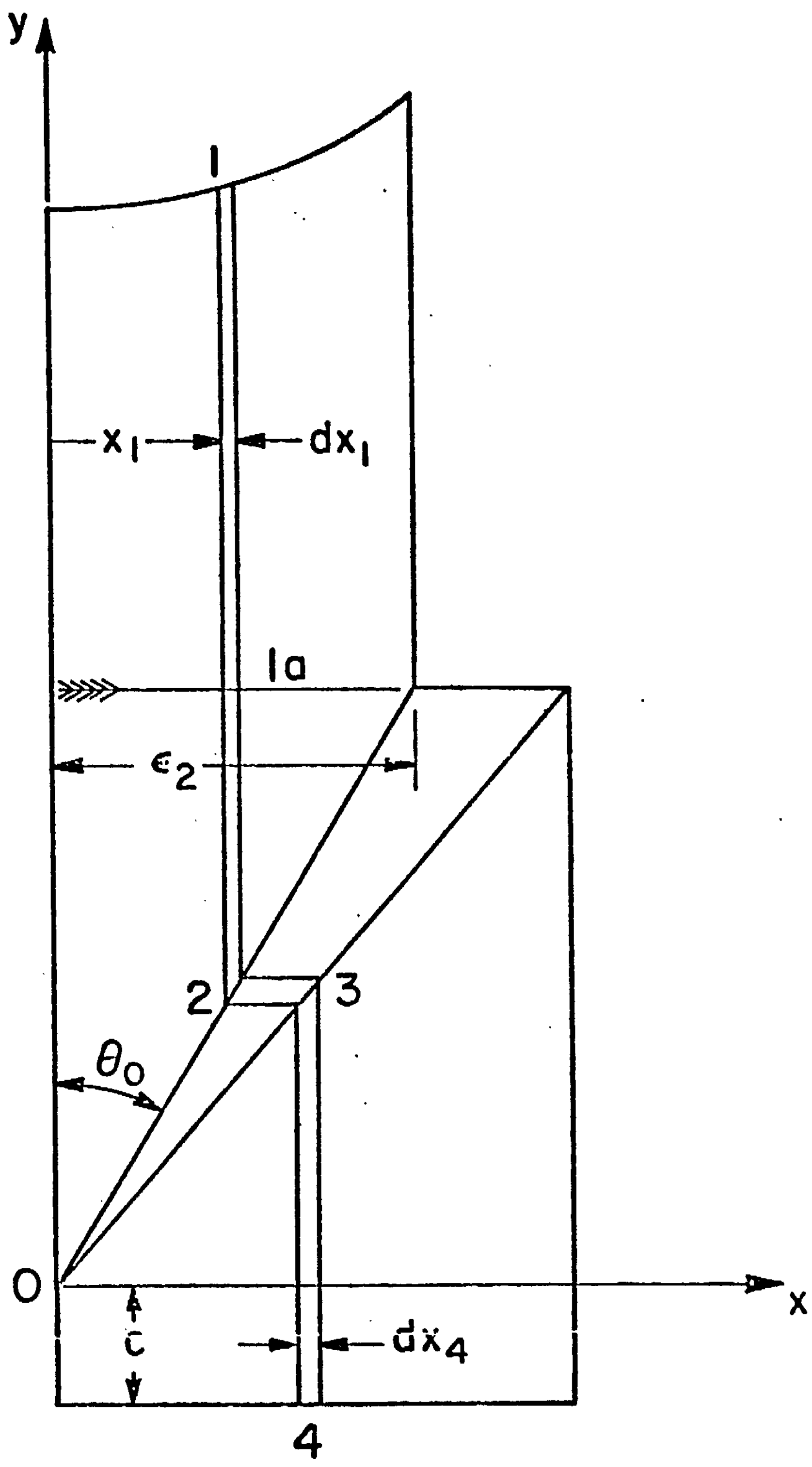

Figure 4-6

The location of point 2 can similarly be found from

$$y_2 = x_2 \cot \theta_o \tag{4-22}$$

and the resistance component from 1a to 2 is given by

$$dR_{1a-2} = \frac{(\varepsilon_2 - x_2) \cot \theta_o}{k_m \, dx_1} \tag{4-23}$$

where the fact that $dx_2 = dx_1$ has been used.

On examining the interval ftom point 2 to point 3, the thickness of this section can be written as

$$dy_2 = \cot \theta_o \cdot dx_2 \tag{4-24}$$

and the length is determined from

$$x_3 - x_2 = \frac{\varepsilon_1 \, x_2}{r_o \sin \theta_o} \tag{4-25}$$

so that the resistance for this section can be written as

$$dR_{2-3} = \frac{\varepsilon_1 \, x_1}{r_o \cos \theta_o \, k_m \, dx_1} \tag{4-26}$$

again noting that $x_1 = x_2$, $dx_1 = dx_2$.

For the final section, the vertical position of point 3 is given by

$$y_3 = \left[\frac{r_o \cos \theta_o}{w}\right] x_3 \tag{4-27}$$

so that

$$dy_3 = \left[\frac{r_o \cos \theta_o}{w}\right] dx_3 \tag{4-28}$$

By noting here that $dy_2 = \cot \theta_o \, dx_2$ and that $dy_3 = dy_2$, dx_3 is related to dx_1 by

$$dx_3 = \left[\frac{w}{r_o \sin \theta_o}\right] dx_1 \tag{4-29}$$

since $dx_2 = dx_1$. Since the length of this segment is given by

$$y_3 - y_4 = x_2 \cot \theta_o + c \tag{4-30}$$

the component resistance is obtained as

$$dR_{3-4} = \frac{r_o \sin\theta_o [x_2 \cot\theta_o + c]}{k_m\, w\, dx_1} \qquad (4\text{-}31)$$

Finally, then, since the four components described above form a series thermal circuit through the typical cell, the total strip resistance is obtained as the sum of the four resistances

$$dR_I = dR_{1-1a} + dR_{1a-2} + dR_{2-3} + dR_{3-4} \qquad (4\text{-}32)$$

Using equations (4-21), (4-23), (4-26), and (4-31) in (1-32), the strip resistance can be written, after algebraic rearrangement, as

$$dR_I = \frac{A_1 + B_1 x_1 + C_1\sqrt{\beta^2 - x_1^2}}{k_m\, dx_1} \qquad (4\text{-}33)$$

where

$$A_1 \equiv \frac{\kappa - \varepsilon_2 \cot\theta_o}{k_f/k_m} + \varepsilon_2 \cot\theta_o + \frac{r_o c \sin\theta_o}{w}$$

$$B_1 \equiv \frac{r_o \cos\theta_o}{w} + \frac{\varepsilon_1}{r_o \cos\theta_o} - \frac{\cot\theta_o}{k_f/k_m} \qquad (4\text{-}34)$$

and $C_1 \equiv -k_m/k_f$

Noting that each strip, by virtue of the assumed adiabat locations, forms a thermal link acting in parallel with all other such strips, the total conductance can be found for sub-region I by integration of the inverse of equation (4-33) over the range $0 \leq x_1 \leq \varepsilon_2$. Thus the total conductance for sub-region I becomes

$$K_I = \int_o^{\varepsilon_2} \frac{k_m dx_1}{A_1 + B_1 x_1\; C_1\sqrt{\beta^2 - x_1^2}} \qquad (4\text{-}35)$$

with A_1, B_1, and C_1 as defined in equations (4-34).

4.3.2 Sub-Region II

The geometry pertinent to the examination of sub-region II is illustrated in figure 4-7 and as can be seen from this figure, its treatment will be similar to that for sub-region I. Indeed, the major distinction between the two regions is that the special consideration given to point 1a of figure 4-6 need not be considered in the treatment of sub-region II.

Without going through the details, since they are very similar to those for sub-region I, the resistance for the strip of width dx_1 in the fluid region is presented here without the accompanying derivation. This resistance is given by

$$dR_{II} = \frac{A_2 + B_2\, x_1 + C_2\sqrt{\beta^2 - x_1^2}}{k_m dx_1} \tag{4-36}$$

where

$$A_2 \equiv \frac{\kappa k_m}{k_f} + \frac{r_o c \sin\theta_o}{w}$$

$$B_2 \equiv \frac{r_o \cos\theta_o}{w} + \frac{\varepsilon_1}{r_o \cos\theta_o} - \frac{\cot\theta_o}{k_f/k_m} \tag{4-37}$$

$$C_2 = -\,k_m/k_f$$

For this region, since again each strip forms a thermal link in parallel with all other such strips, the total conductance is obtained by integration of the reciprocal of equation (4-36) over the interval $\varepsilon_2 \le x_1 < w-\varepsilon_1$. This yields the result that

$$K_{II} = \int_{\varepsilon_2}^{w-\varepsilon_1} \frac{k_m\, dx_1}{[A_2 + B_2\, x_1 + C_2\sqrt{\beta^2 - x_1^2}]} \tag{4-38}$$

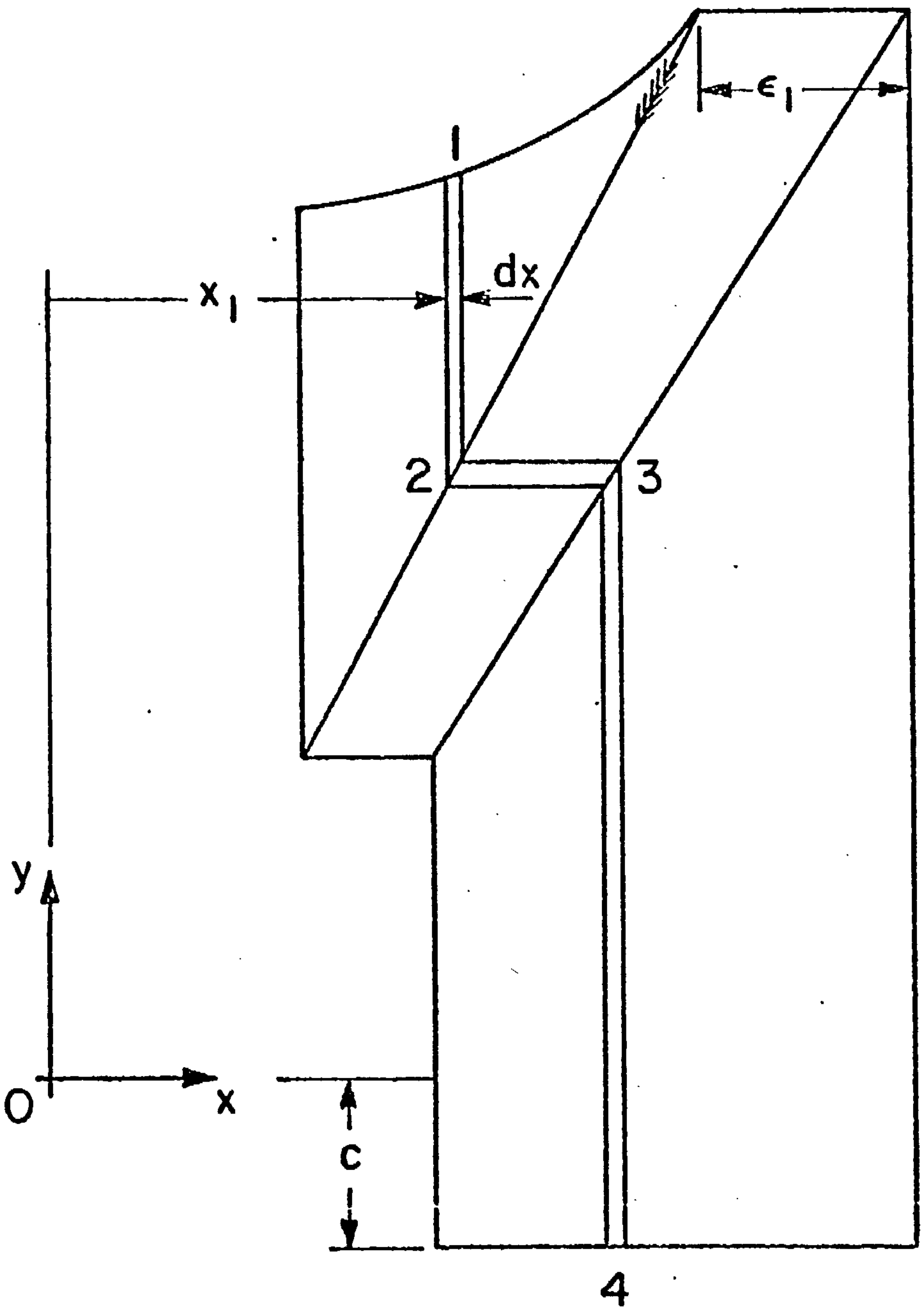

Figure 4-7

with A_2, B_2, and C_2 defined by equations (4-37).

4.3.3 Overall Heat Transfer

The two sub-region conductances given by equations (4-35) and (4-38) themselves act thermally in parallel with each other and as a result their conductances are additive to form the overall conductance.

Thus

$$K = \int_{o}^{\varepsilon_2} \frac{k_m dx_1}{[A_1 + B_1 x_1 + C_1\sqrt{\beta^2 - x_1^2}]} + \int_{\varepsilon_2}^{w-\varepsilon_1} \frac{k_m dx_1}{[A_2 + B_2\, x_1 + C_2\sqrt{\beta^2 - x_1^2}]} \quad \text{(4-3}$$

To determine h_{eq}, the equivalent heat transfer coefficient, the conductance of the wall material lying between the groove root and the exterior wall surface must be discounted, and this is best done using resistances. Defining the resistance as the reciprocal of the conductance, as is usual, by

$$R = 1/K \quad \text{(4-40)}$$

then the resistance associated with the equivalent heat transfer coefficient is given by

$$R_{eq} = 1/K - (c + \varepsilon_2 \cot \theta_o)/k_m w \quad \text{(4-41)}$$

which leads to the equivalent heat transfer coefficient lower limit

$$h_{eq} = \frac{w}{K} + \frac{(c + \varepsilon_2 \cot \theta_o)}{k_m}^{-1} \quad \text{(4-42)}$$

Defining the Nusselt number as before, then,

$$Nu_f = \frac{h_{eq}}{Nk_f} \quad \text{(4-43)}$$

the lower limit for the groove Nusselt number can be determined from

$$Nu_f \frac{k_f}{k_m} = \left[\frac{k_m}{2K} + \frac{\varepsilon_2 \cot \theta_o + c}{2w} \right]^{-1} \quad \text{(4-44)}$$

The expression, equation (4-44), for the groove Nusselt number lower limit was programmed for evaluation on a digital computer. The integrals entailed in equation (4-39) and required for evaluation of (4-44) were numerically integrated using a modified Simpson's rule algorithm. The program listing appears in Appendix B of this report with only the results presented here. The results are presented in Tabular form in Table 4-2.

4.4 Results and Conclusions

As previously mentioned, the results for the heat transfer upper limit are presented in Table 4-1 and those for the lower limit in Table 4-2. To minimize the uncertainty of the actual conductance, the average value of the upper and lower values can be used. This limits the possible inaccuracy of using this value to one half of the difference between the upper and lower values determined earlier. This has been used with some success by Yovanovich, Schneider and Strong [37] in their evaluation of apparent composite conductivities for square fibers in a matrix. Since there is no motivation for using an estimation procedure other than the arithmetic averaging described above, this procedure will be used here.

The arithmetic average value of the product $Nu_f \cdot k_f/k_m$ was computed and the range of uncertainty about this mean value established for land area ratios (symmetric grooves) of 0.01, 0.10 and 0.25, half-groove angles of 20, 30, and 40 degrees, conductivity ratios, k_f/k_m, of 0.1, 0.01156, and 0.001, and values of the normalized apparent contact angle, $\alpha/(\pi/2 - \theta_o)$, of 0.05, 0.25, 0.50, and 1.00. These results are presented in Table 4-3.

It is observed that in general the range of uncertainty about the mean value is lowest for a conductivity ratio of 0.1, with this uncertainty increasing as the land area ratio increases and as the conductivity ratio decreases. While the uncertainty indicated represents the maximum possible

Table 4-2

Groove Nusselt Number Lower Limit

$Nu_f \cdot k_f/k_m$

d	k_f/k_m	$\varepsilon_1 = \varepsilon_2$	x_α 0.05	0.25	0.50	1.00
1.0	0.1	0.01	0.9498	0.7674	0.6382	0.4967
		0.25	0.6027	0.4749	0.3956	0.3150
		0.49	~0	~0	~0	~0
	0.01156	0.01	0.2858	0.1875	0.1409	1.1007
		0.25	0.1404	0.0951	0.0751	0.0578
		0.49	~0	~0	~0	~0
	0.001	0.01	0.0596	0.0290	0.0200	0.0134
		0.25	0.0244	0.0131	0.0098	0.0073
		0.49	~0	~0	~0	~0
1.5	0.1	0.01	0.5780	0.4787	0.4096	0.3330
		0.25	0.3480	0.2905	0.2537	0.2142
		0.49	~0	~0	~0	~0
	0.01156	0.01	0.1664	0.1136	0.0891	0.0676
		0.25	0.0778	0.0567	0.0474	0.0390
		0.49	~0	~0	~0	~0
	0.001	0.01	0.0331	0.0171	0.0124	0.0090
		0.25	0.0129	0.0077	0.0061	0.0049
		0.49	~0	~0	~0	~0
2.0	0.1	0.01	0.402	0.3402	0.298	0.250
		0.25	0.2384	0.2059	0.1850	0.1619
		0.49	~0	~0	~0	~0
	0.01156	0.01	0.114	0.079	0.064	0.051
		0.25	0.0517	0.0396	0.0343	0.0294
		0.49	~0	~0	~0	~0
	0.001	0.01	0.0213	0.0117	0.0089	0.0067
		0.25	0.0083	0.0053	0.0044	0.0037
		0.49	~0	~0	~0	~0

error that may be incurred, since the limit studies provide the upper and lower bound for the heat transfer, there is no means available to decrease these bounds except to solve the thermal problem described in chapter 3. This is the subject of chapter 5.

With the uncertainty ranging from ±23 percent to ±98 percent, the band within which the actual solution lies is not sufficiently narrow to allow use of these results as estimations for the actual heat transfer characteristics. This is particularly true in consideration that the groove mean temperature drop depends inversely upon the equivalent heat transfer coefficient and hence inversely upon the groove Nusselt number. When numbers having an error band approaching ±100 percent are inverted, the resulting band, in this case on the thermal resistance, is extremely large indeed. With the mean groove temperature drop directly dependent upon the groove resistance to heat transfer, it is concluded that the limit study will be of little utility for prediction purposes. Its purpose will then be to serve as a check on the validity of the numerical results presented in the next chapter.

Table 4-3

Average Groove Nusselt Number

$\overline{Nu}_f \cdot k_f/k_m$

d	k_f/k_m	$\varepsilon_1 = \varepsilon_2$	x_α	$\overline{Nu}_f \cdot k_f/k_m$	Uncertainty ± %
1.0	0.1	0.01	0.05	1.5068	37.0
			0.25	1.1467	33.1
			0.50	1.0774	40.8
			1.00	0.6482	23.4
		0.25	0.05	1.3703	56.0
			0.25	1.0167	53.3
			0.50	0.8126	51.3
			1.00	0.6753	53.4
		0.49	0.05	0.9315	100
			0.25	0.6384	100
			0.50	0.5034	100
			1.00	0.5494	100
		0.01156	0.05	1.0018	71.5
			0.25	0.6512	71.2
			0.50	0.4582	69.2
			1.00	0.3033	66.8
1.0	0.01156	0.25	0.05	0.9252	84.8
			0.25	0.5977	84.1
			0.50	0.4667	83.9
			1.00	0.4911	88.2
		0.49	0.05	0.704	100
			0.25	0.4186	100
			0.50	0.3251	100
			1.00	0.5044	100
	0.001	0.01	0.05	0.8085	92.6
			0.25	0.4672	93.8
			0.50	0.3204	93.8
			1.00	0.2243	94.0
		0.25	0.05	0.7628	96.8
			0.25	0.4265	97.0
			0.50	0.3283	97.0
			1.00	0.4585	98.4
		0.49	0.05	0.6034	100
			0.25	0.3069	100
			0.50	0.2335	100
			1.00	0.4982	100

1.5	0.1	0.01	0.05	019232	37.4
			0.25	0.7209	33.6
			0.50	0.5754	28.8
			1.00	0.433	23.1
		0.25	0.05	0.8183	57.5
			0.25	0.644	54.9
			0.50	0.533	52.4
			1.00	0.4523	52.6
		0.49	0.05	0.5595	100
			0.25	0.4281	100
			0.50	0.3562	100
			1.00	0.3664	100
	0.01156	0.01	0.05	0.6196	73.1
			0.25	0.4158	72.7
			0.50	0.2967	70.0
			1.00	0.2024	66.6
		0.25	0.05	0.5796	86.6
			0.25	0.404	86.0
			0.50	0.3237	85.3
			1.00	0.3277	88.1
1.5	0.01156	0.49	0.05	.4576	100
			0.25	.3105	100
			0.50	.2520	100
			1.00	.3366	100
	0.001	0.01	0.05	0.5112	93.5
			0.25	0.3082	94.5
			0.50	0.2122	94.2
			1.00	0.1496	94.0
		0.25	0.05	0.4970	97.4
			0.25	0.3052	97.5
			0.50	0.2396	97.5
			1.00	0.1496	94.0
		0.49	0.05	0.4115	100
			0.25	0.2437	100
			0.50	0.1927	100
			1.00	0.3326	100
2.0	0.1	0.01	0.05	0.6389	37.1
			0.25	0.5122	33.6
			0.50	0.4186	28.8
			1.00	0.3249	23.0

2.0	0.1	0.25	0.05	0.5604	57.5
			0.25	0.4612	55.4
			0.50	0.3932	53.0
			1.00	0.3399	52.4
		0.49	0.05	0.3838	100
			0.25	0.3152	100
			0.50	0.2729	100
			1.00	0.2749	100
	0.01156	0.01	0.05	0.4294	74.1
			0.25	0.2982	73.5
			0.50	0.2167	70.5
			1.00	0.1520	66.4
		0.25	0.05	0.4064	87.3
			0.25	0.3014	86.9
			0.50	0.2480	86.2
			1.00	0.2459	88.0
		0.49	0.05	0.3258	100
			0.25	0.2423	100
			0.50	0.2041	100
			1.00	0.2525	100
2.0	.001	0.01	0.05	0.3598	94.1
			0.25	0.2267	94.8
			0.50	0.1577	94.4
			1.00	0.1122	94.0
		0.25	0.05	0.3568	97.7
			0.25	0.2371	97.7
			0.50	0.1905	97.7
			1.00	0.2295	98.3
		0.49	0.05	0.3009	100
			0.25	0.1992	100
			0.50	0.1630	100
			1.00	0.2497	100

Chapter 5

Finite Element Analysis

5.1 Introduction

The reasons for selecting the finite element method for use in this analysis were briefly discussed in chapter three of this report. The prime motivation for preference of the finite element method over other numerical solution techniques is its flexibility in analysing solution domains of irregular geometry. Recalling the problem geometry of figure 3-3, the solution method used for this problem will certainly require this flexibility.

It is the purpose of this chapter to present briefly the underlying principles governing the application of finite element techniques to heat conduction analysis and to discuss its application to the trapezoidal groove heat transfer problem. Some of the difficulties encountered in applying the method to this particular problem are indicated and the procedure by which these difficulties were surmounted is presented. In concluding the chapter an analysis is presented for estimating the accuracy of the obtained results. This is done using the results of a case study used to examine the convergence characteristics for this problem. It is felt that the combination of parameters used in this study presents a severe test on the method and that the accuracy for all other cases considered will be at least as good as the estimates obtained from this case study.

5.2 The Finite Element Method

The finite element method is a relatively recent numerical solution technique to be employed in the anlysis of heat conduction problems. First introduced to the solution of field problems in 1965 [39,40], the finite element method has since been the subject of several investigations [41-44]. While these investigations were concerned with alternate derivations of the governing functional equation and with the treatment of the transient terms appearing in the governing differential equation, application of the method was restricted to the cartesian coordinate system. In a more recent investigation by Schneider [45], extension of the method was made to include its application to any orthogonal curvilinear coordinate system. This development will be adopted here with the details of the analysis presented in Appendix C. The derivation of the variational statement for application of the finite element method to heat conduction analysis follows directly.

5.2.1 Preliminary Remarks

The development of the governing variational statement will be performed for a general orthogonal curvilinear coordinate system and the results reduced to those corresponding to the cartesian system to be used in this analysis. The general orthogonal coordinate system is illustrated in figure 5-1 with u_1, u_2, and u_3 used to denote the three principal curvilinear coordinate directions. In general, the coordinates of an orthogonal curvilinear coordinate system can be related to the cartesian coordinates, x, y, and

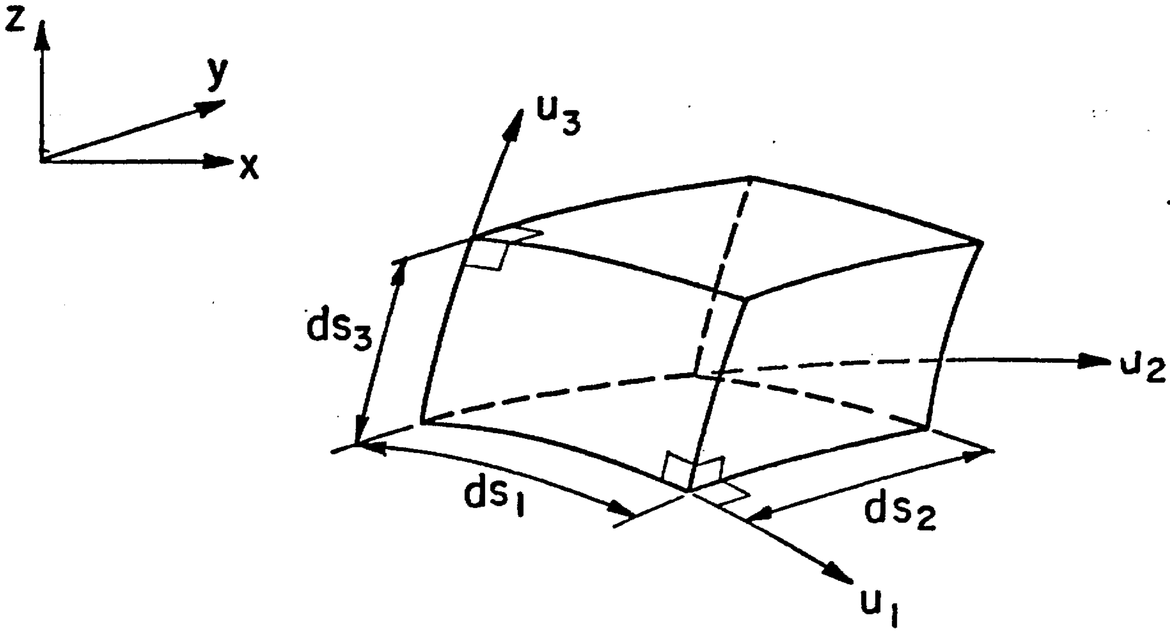

Figure 5-1

z by relations of the form

$$x = x\ (u_1,\ u_2,\ u_3)$$
$$y = y\ (u_1,\ u_2,\ u_3) \qquad (5\text{-}1)$$
$$z = z\ (u_1,\ u_2,\ u_3)$$

Using these relations, the magnitude of an arbitrary differential vector in space, $d\vec{s}$, can be determined from

$$(ds)^2 = g_1(du_1)^2 + g_2(du_2)^2 + g_3(du_3)^2 \qquad (5\text{-}2)$$

where the metric or Lamé coefficients of transformation are defined by [30]

$$g_i = \left(\frac{\partial x}{\partial u_i}\right)^2 + \left(\frac{\partial y}{\partial u_i}\right)^2 + \left(\frac{\partial z}{\partial u_i}\right)^2\ ,\ i = 1,2,3 \qquad (5\text{-}3)$$

Clearly for a differential length, say in the u_i-direction, the relationship of equation (5-2) becomes simply

$$ds_i = \sqrt{g_i}\ \ du_i \qquad (5\text{-}4)$$

Similarly the area and volume elements can be written as

$$dA_i = \sqrt{g_j g_k}\ \ du_j\ du_k,\quad i = 1,2,3 \quad i \neq j \neq k \qquad (5\text{-}5)$$

and $$dV = \sqrt{g}\ \ du_1 du_2 du_3 \qquad (5\text{-}6)$$

where the convention has been used that the direction of the area element be taken normal to the surface in an outward sense and the definition has been made that

$$\sqrt{g} = \sqrt{g_1 g_2 g_3} \qquad (5\text{-}7)$$

By applying the first law of thermodynamics to the differential control volume of figure 5-1 and by using the above relationships for length, area, and volume, the governing differential equation for heat conduction can be written as [30]

$$\frac{\partial}{\partial u_1}\left[\frac{k_1\sqrt{g}}{g_1}\frac{\partial T}{\partial u_1}\right] + \frac{\partial}{\partial u_2}\left[\frac{k_2\sqrt{g}}{g_2}\frac{\partial T}{\partial u_2}\right] + \frac{\partial}{\partial u_3}\left[\frac{k_3\sqrt{g}}{g_3}\frac{\partial T}{\partial u_3}\right]$$

$$+ P\sqrt{g} = \sqrt{g}\,\rho c_p \frac{\partial T}{\partial t} \qquad (5\text{-}8)$$

where Fourier's Law of heat conduction has been used to describe the local transfer of heat within the continuum.

Boundary conditions to be applied to the solution of equation (5-8) can be written in general (except for non-linearized radiative conditions) as

$$T = T_A(u_1,u_2,u_3,t) \qquad (5\text{-}9a)$$

over a portion S_1 of the boundary sufaces and

$$k_n \frac{\partial T}{\partial n} + hT + C = 0 \qquad (5\text{-}9b)$$

over the remaining surface S_2. In equation (5-9b), n is the outward normal to the boundary surface over S_2.

The initial condition, in the case of transient solutions, is represented by

$$T(u_1,u_2,u_3,o) = T_o(u_1,u_2,u_3) \qquad (5\text{-}9c)$$

5.2.2 Variational Statement

If the concept of a variational principle is to be applied to the solution of heat conduction problems, then the governing differential equation (5-8) must correspond to the Euler equation for the corresponding variational problem [46]. Considering a particular instant of time in this development, time derivatives will be treated as prescribed functions of the spatial coordinates, u_1, u_2, and u_3. This approach leads to a quasi-variational statement but rigor is restored with respect to the variational calculus when a steady-state solution is sought and time derivatives are set to zero.

Proceeding with the approach taken here and invoking the requirement that the equation (5-8) be the Euler equation corresponding the same, as yet unknown, variational statement, we set

$$\int_{u_1}\int_{u_2}\int_{u_3} \{\frac{\partial}{\partial u_1}[\frac{k_1\sqrt{g}}{g_1}\frac{\partial T}{\partial u_1}] + \frac{\partial}{\partial u_2}[\frac{k_2\sqrt{g}}{g_2}\frac{\partial T}{\partial u_2}] + \frac{\partial}{\partial u_3}[\frac{k_3\sqrt{g}}{g_3}\frac{\partial T}{\partial u_3}]$$

$$+ P\sqrt{g} - \sqrt{g}\,\rho C_p \frac{\partial T}{\partial t}\}\ \delta T\ du_1 du_2 du_3 = 0 \qquad (5\text{-}10)$$

where the first variation of temperature, δT, has been introduced.

Denoting by I_1 the first integral of equation (5-10) and integrating by parts gives

$$I_1 = \int_{u_2}\int_{u_3} [\frac{k_1\sqrt{g}}{g_1}\frac{\partial T}{\partial u_1}\delta T]\Big|_{u_1=u_1(u_2,u_3)} du_2 du_3$$

$$- \int_{u_1}\int_{u_2}\int_{u_3} [\frac{k_1\sqrt{g}}{g_1}\frac{\partial T}{\partial u_1}]\ \frac{\partial}{\partial u_1}(\delta T) du_1 du_2 du_3 \qquad (5\text{-}11)$$

where $u_1(u_2, u_3)$ represents the locus of values that the u_1 coordinate takes on, as a function of the remaining two coordinates, as the boundary surface of the solution domain is traversed. Employing the commutability property of the differential and variational opertors, equation (5-11) can be wriiten as

$$I_1 = \int_{S_2} [\frac{k_1}{\sqrt{g_1}} \frac{\partial T}{\partial u_1} \quad \delta T] \Big|_{\text{boundary}} \ell_1 ds$$

$$- \frac{1}{2} \delta \int_{u_1}\int_{u_2}\int_{u_3} f_1 (\frac{\partial T}{\partial u_1})^2 \, du_1 du_2 du_3 \qquad (5\text{-}12)$$

where the definition has been made that

$$f_i = \frac{k_i \sqrt{g}}{g_i} \quad , \quad i = 1,2,3, \qquad (5\text{-}13)$$

Further, it has been recognized in writing equation (5-12) that

$$\sqrt{g_2 g_3} \, du_2 du_3 = \ell_1 ds \qquad (5\text{-}14)$$

with ℓ_1 the direction cosine of the bounding surface with respect to the coordinate direction u_1 and also that the variation of temperature over S_1 is by definition zero so that there is no contribution to the first integral of equation (5-11) resulting from integration over the portion S_1 of the boundary. Integrals similar to equation (5-12) arise from consideration of the conduction terms for the other two coordinate directions. Additional details of the derivation are presented in Appendix C.

Determination of the variational form for the remaining two integrals of equation (5-10) follows by a direct application of the calculus of variations. Collecting the components and assembling to provide the quasi-variational equivalent to equation (5-8) yields

$$\{\iiint_{u_1 u_2 u_3} \{\frac{f_1}{2}\left(\frac{\partial T}{\partial u_1}\right)^2 + \frac{f_2}{2}\left(\frac{\partial T}{\partial u_2}\right)^2 + \frac{f_3}{2}\left(\frac{\partial T}{\partial u_3}\right)^2$$

$$-P\sqrt{g}T + \sqrt{g}\rho C_p T\}\ du_1 du_2 du_3\}$$

$$- \iint_{s_2} \{hT + C\}\delta T\ dS_2 = 0 \qquad (5\text{-}15)$$

where the identity has been used that

$$\left[\frac{k_1}{\sqrt{g_1}} \frac{\partial T}{\partial u_1} \ell_1 + \frac{k_2}{\sqrt{g_2}} \frac{\partial T}{\partial u_2} \ell_2 + \frac{k_3}{\sqrt{g_3}} \frac{\partial T}{\partial u_3} \ell_3\right] dS_2 = k_n \frac{\partial T}{\partial n} dS_2 \qquad (5\text{-}16)$$

together with the boundary condition statement, equation (5-9b). A final application of the variational calculus to the surface integral of equation (5-15) leads to the result

$$\delta\left[\iiint_{u_1 u_2 u_3} \{\frac{f_1}{2}\left(\frac{\partial T}{\partial u_1}\right)^2 + \frac{f_2}{2}\left(\frac{\partial T}{\partial u_2}\right)^2 + \frac{f_3}{2}\left(\frac{\partial T}{\partial u_3}\right)^2\right.$$

$$- P\sqrt{g}T + \sqrt{g}\rho C_p \left(\frac{\partial T}{\partial t}\right)T\}\ du_1 du_2 du_3$$

$$\left. + \iint_{S_2} \{\frac{hT^2}{2} + CT\}\ dS_2\right] = 0 \qquad (5\text{-}17)$$

Equation (5-17) is the quasi-variational statement referred to earlier and its satisfaction, within the limits of the treatment of time dependent terms adopted here, is equivalent to satisfying the differential equation (5-8) from which it has been derived.

5.2.3 Spatial Discretization

To enable application of the finite element method to the variational statement of equation (5-17) it will be useful to define the following vectors and matrices. The first, a vector very similar to the gradient field vector of a cartesian frame [33], will be defined by

$$\{G\}^T = \{\frac{\partial T}{\partial u_1}, \frac{\partial T}{\partial u_2}, \frac{\partial T}{\partial u_3}\} \tag{5-18}$$

This vector will be referred to as the curvilinear field vector, although, since the curvilinear coordinates do not directly reflect physical distances, the components of (5-18) are not physical gradients unless accompanied by their corresponding metric coefficients. The second, a matrix analogous to the property matrix of cartesian system, is defined by

$$[R] = \begin{bmatrix} f_1(u_1,u_2,u_3) & o & o \\ o & f_2(u_1,u_2,u_3) & o \\ o & o & f_3(u_1,u_2,u_3) \end{bmatrix} \tag{5-19}$$

This matrix shall be referred to as the effective curvilinear property matrix. The remaining vectors, at this point continuous functions of the spatial curvilinear coordinates, are defined by

$$\begin{aligned} \{T\} &= \{T(u_1,u_2,u_3)\} \\ \{P\} &= \{P(u_1,u_2,u_3)\} \\ \{C\} &= \{C(u_1,u_2,u_3)\} \\ \{\dot{T}\} &= \{\frac{\partial T}{\partial t}\} \end{aligned} \tag{5-20}$$

Using the above defined vectors and matrices, the variational statement (5-17) can be written as

$$\delta\left[\int_{u_1}\int_{u_2}\int_{u_3}\left[\frac{1}{2}\{G\}^T[R]\{G\} - \sqrt{g}\{T\}^T\{P\} + \rho C_p\sqrt{g}\{T\}^T\{\dot{T}\}\right]du_1du_2du_3\right.$$

$$\left. + \int_{S_2}\left[\frac{h}{2}\{T\}^T\{T\} + \{T\}^T\{C\}\right]dS_2\right] = 0 \qquad (5\text{-}21)$$

With the variational statement expressed in vector notation, we now consider the fundamental concept of the finite element method, that the solution domain can be spatially subdivided into a collection of finite elements. Over each of these elements, an approximate solution is assumed which contains a specified number of arbitrary parameters representative of the nodal degrees of freedom. It is the object of the finite element method to determine the values for these nodal degrees of freedom by the approximate satisfaction of the variational statement (5-21).

Approximating the unknown temperature distribution by the approximation

$$\{T\} = [N_1, N_2 \cdots\ ]\begin{Bmatrix} T_1 \\ T_2 \\ \vdots \end{Bmatrix} = \{N_i\}^T\{T_i\} \qquad (5\text{-}22)$$

the curvilinear field vector can immediately be written as:

$$\{G\} = \begin{bmatrix} \partial N_1/\partial u_1 & \partial N_2/\partial u_1 & \cdots \\ \partial N_1/\partial u_2 & \partial N_2/\partial u_2 & \cdots \\ \partial N_1/\partial u_3 & \partial N_2/\partial u_3 & \cdots \end{bmatrix}\begin{Bmatrix} T_1 \\ T_2 \\ \vdots \end{Bmatrix} = [B]\{T_i\} \qquad (5\text{-}23)$$

In the above the N_i's are the shape function [ ] for the element and their form and number will depend on the type of element under consideration. Having made the approximation of equation (5-22), the approximate functional corresponding to equation (5-21) becomes a function of only the unknown nodal temperatures, T_i, $i = 1,2,3,$. Finding the stationary value of this functional by taking its first ariation with respect to T then becomes equivalent to simply differentiating the approximate functional with respect to each nodal temperature in turn, and setting the result equal to zero.

Performing the indicated differentiation, and recalling that the instantaneous thermal behavior is considered in this treatment, leads to the matrix-differential equations.

$$[k]\{T_i\} + \{P\}\{\dot{T}_i\} = \{f\} \qquad (5\text{-}24)$$

where

$$[k] = \sum_{e=1}^{n}\Big[\iiint_{V_e} [B]^T[R]\,[B]du_1du_2du_3$$

$$+ \iint_{S_{2_e}} h\,\{N_i\}\,\{N_i\}^T dS_2\Big] \qquad (5\text{-}25a)$$

$$[P] = \sum_{e=1}^{n}\iiint_{V_e} \rho C_p\,\sqrt{g}\;\{N_i\}\,\{N_i\}^T\,du_1du_2du_3 \qquad (5\text{-}25b)$$

and

$$\{f\} = \sum_{e=1}^{n}\Big[\iiint_{V_e} \sqrt{g}\,\{N_i\}\,\{P\}\,du_1du_2du_3 + \iint_{S_{2_e}} \{N_i\}\,\{C\}\,dS_2\Big] \qquad (5\text{-}25c)$$

In the above, integration of the functional over the solution domain volume has been replaced with a summation of volume integrations, each integration being local to the element characterized by the index of summation, e. Treatment of the transient terms is presented in Appendix C but for the present purpose of examining the steady state thermal behavior the time derivatives can be set to zero

$$\{\dot{T}_i\} = 0 \qquad (5\text{-}26)$$

resulting in the matrix equations

$$[k]\,\{T_i\} = \{f\} \qquad (5\text{-}27)$$

where since we are not considering the case of internal heat generation, the heat generation submatrix appearing in {f} can also be set to zero.

$$\{P\} = 0 \qquad (5\text{-}28)$$

Solving the matrix equationsoof equation (5-27) will then provide the approximate solution for the temperature field by means of determining the temperature at the field node points, T_I, $i = 1,2,3,$

5.3 Application to Trapezoidal Groove Heat Transfer

We now consider the application of the finite element method as described above to the problem of direct interest in this work, that of determining the heat transfer characteristics for trapezoidal shaped grooves. The problem geometry is repeated in figure 5-2 from figure 3-3 for ease of reference by the reader.

Examination of the figure suggests tht due to the complex geometric description of the solution domain and component boundaries, the coordinate system most suitable for use in effecting the solution is the cartesian coordinate system. The transformation equations in reference to the material presented in section 5.2.1 are given simply by

$$x = x;\ y = y;\ z = z \qquad (5\text{-}29)$$

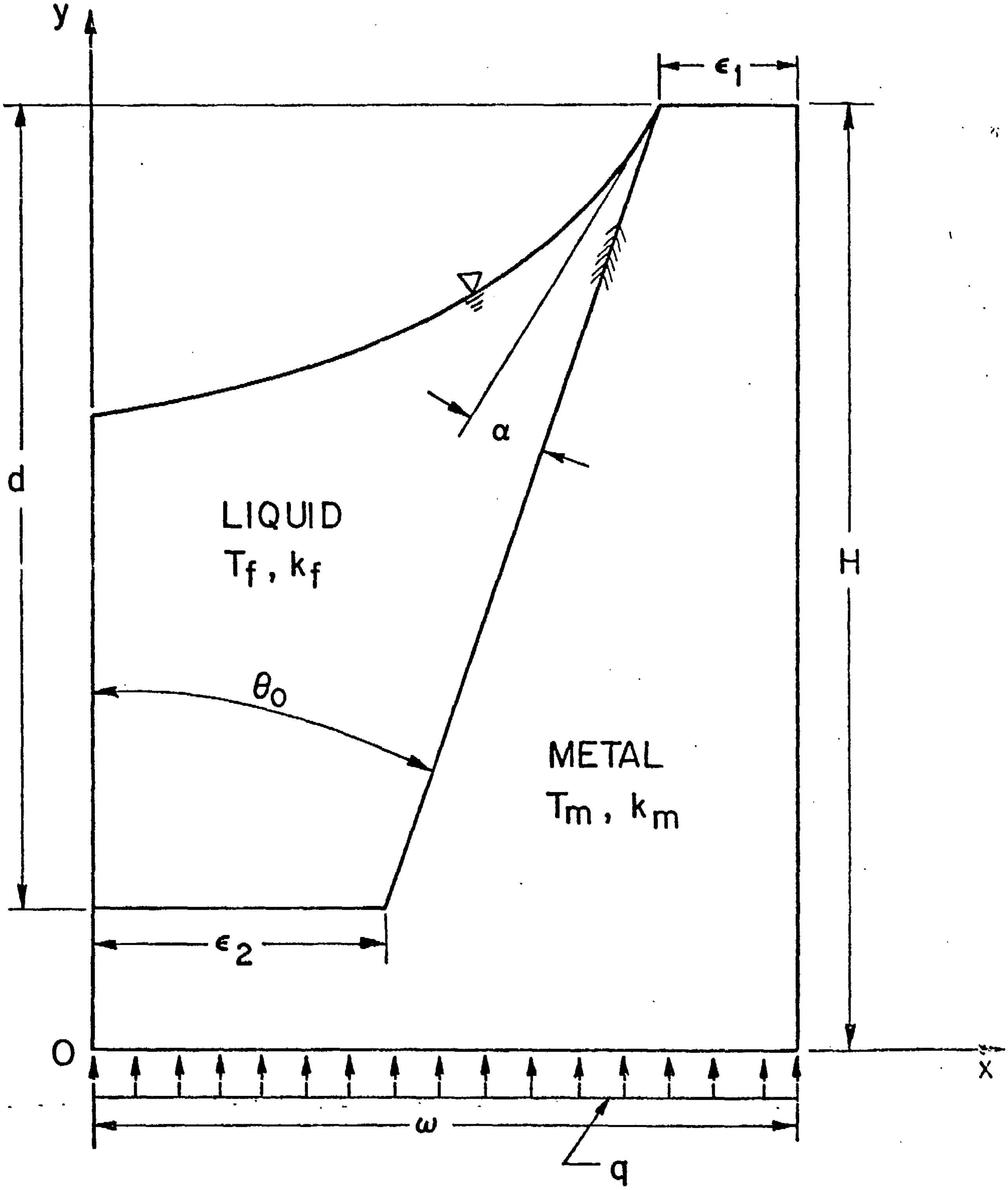

y
ϵ_1
d
H
α
LIQUID
T_f , k_f
θ_0
METAL
T_m , k_m
ϵ_2
O
x
ω
q

Figure 5-2

with the metric coefficients each being identially unity, $g_1 = g_2 = g_3 = g = 1$. For this case, and considering isotropic materials, the effective curvilinear property matrix becomes the diagonal matrix

$$[R] = \begin{bmatrix} k & o & o \\ o & k & o \\ o & o & k \end{bmatrix} \qquad (5\text{-}30)$$

where the conductivity to be used in equation (5-30) will be the liquid or solid conductivity respectively depending upon whether the element under consideration is in the liquid or solid region of the solution domain. For accuracy of representation of the thermal behavior for this problem, since the volume integrations of equation (5-25) usually require a numerical integration procedure, it is important that the solid/liquid interface form a bounding surface for adjacent interface elements rather than to allow a step change in the thermal properties to occur within a single element. The above modification of the effective curvilinear property matrix in the general formulation is all that is required to adapt it for use with the cartesian coordinate system. Further simplifications can be made, however.

Considering the boundary condition specification as indicated in general by equation (5-9b)

$$k_n \frac{\partial T}{\partial n} + hT + C = 0 \qquad (5\text{-}9b)$$

the non-homogeneous term, hT, can be interpreted as part of the specification for boundary conditions of the Cauchy type. Not having Cauchy, or in this application convective, boundary conditions present on any exterior surface of the solution domain, the surface integral of equation (5-25a) will be identically zero.

The constant term of the boundary condition specification is representative of a Neumann type boundary condition. Having a prescribed flux of q, the constant C will be determined by

$$C = q \tag{5-31}$$

This specification is applicable over the surface defined by y = 0 in figure 5-2. In the special case of an adiabatic surface, as for example over the surfaces defined by x = 0, x = w for $0 \leq y \leq H$, and for y = H for $w \leq \varepsilon_1 \leq x \leq w$, the constant C will be zero and its contribution to the surface integral of equation (5-25C) will be zero. These boundaries therefore require no special treatment whatsoever in their implementation and are called natural boundary conditions. As was seen earlier the Dirichlet boundary over the liquid free surface is also a natural boundary condition to the Finite Element Method as developed here.

A program has been developed which, using a compatible data input subroutine, will assemble and solve the matrix equations (5-27) to yield as a solution the temperatures at the discrete nodal points. Using this computed temperature field, the various derived quantities of interest in this investigation can be computed. The most important derived quantity of interest here is the equivalent heat transfer coefficient to be associated with the heat transfer from the groove root to the vapor core.

The 'finite element' selected for use in the analysis of the trapezoidal groove heat transfer is the general quadrilateral, linear, isoparametric element. The details of the element shape functions and stiffness matrix will not be discussed here but can be found in finite element texts [33,34] with the details presented very explicitly in the paper by Shah and Kobayashi [47]. This particular element has a general quadrilateral shape and maintains the flexibility of degeneration to a triangle by the assignment of two of the four nodes to the same physical location in space. A summary of the derivations pertinent to this element are, however, presented in Appendix F of this report.

Due to the large degree of detail which would be required to explain fully the internal operation of the solution program, the details of its operation will also not be discussed in this report. Further, these details are of no consequence with respect to the thermal problem under consideration; it must simply be ascertained that the appropriate sub-functions of the program components are being performed correctly. Let it suffice for purposes of this investigation to demonstrate the correct operation of the program components by example. In Appendix C of this report where the finite element formulation of the heat conduction equation is developed for any orthogonal curvilinear coordinate system, two examples are considered for verification of the development; a problem in the polar spherical coordinate system and one in the oblate spheroidal coordinate system. The fact that the solution program used for this investigation is the same as that used for the verification examples, with the exception of the input data subroutine, and the fact that these examples indicate excellent agreement of the finite element results with known analytic solutions, provides confidence that the solution program is functioning correctly.

The input data subroutine, being unique to each problem tackled using such a program as that developed for this investigation, is an important consideration in applying the finite element method. Indeed, in this work considerable difficulty was experienced due to a not entirely 'appropriate' input of the nodal locations, element distribution, and element shapes for the initial mesh generation subroutines. These types of difficulty, however, are extremely problem dependent and are often difficult to anticipate and can only be detected during an examination of the convergence characteristics for a particular problem. In this regard, it is the authors' firm opinion that the heat transfer problem tackled in this particular investigation is an extremely difficulty one indeed, by any method of attack. The reasons for arriving at this conclusion are briefly presented below.

In examining the behavior of heat transfer across trapezoidal grooves in the case of moderate temperature heat pipes, the working fluid is typically of low thermal conductivity, eg. water, methanol, ammonia, etc., while the pipe structure is typically metallic and consequently has a significantly higher thermal conductivity, eg., stainless steel, carbon steel, aluminum, copper, etc. The conductivity ratio, k_f/k_m, for these combinations can therefore range from approximately 0.03 for water/stainless steel pipes to approximately 0.0014 for methanol/copper heat pipes. Numerically enforcing inferface compatibility for problems having such a severe conductivity ratio is extremely, difficult except for problems of very simple geometry. The solution to such problems must be able to adequately describe the interfacial heat transfer characteristics at component boundaries within the solution domain.

Further, the above problem is compounded by the geometric characteristics of the trapezoidal groove problem. This arises for two reasons. Firstly the liquid free surface geometry is such that it the meniscus attachment point, the liquid thickness vanishes. This results in an extremely local region over which the bulk of the heat transfer is concentrated. The second, serving to compound the first, is that the metal section extends fully to the vapor core. This affords the heat flow a low resistance path to the meniscus contact region and further concentrates the heat flow in this region. A solution program must then be sufficiently flexible to be able to 'pick up' the large gradients existing near the meniscus contact and blend this region into the remaining portion of the solution domain where the heat flow is less concentrated and gradients are smaller.

5.4 Problems in Effecting the Solution

In effecting the finite element solution to the trapezoidal groove heat transfer problem, several difficulties were encountered which had to be resolved before confidence in the numerical results could be established. These difficulties are related to the spatial discretization of the solution domain and the influence that the method of subdivision has on the finite element solution of the heat transfer problem. With this application of the finite element method by the authors being the first application in which difficulty of application was experienced, the above named cause of the problem was not immediately obvious and a systemmatic check of the entire solution program was necessitated. Since all of the checks employed that are not directly related to the input data subroutine indicated that the program components were functioning correctly, these will not be discussed here. Indeed, many checks performed directly on the input subroutine also indicated that even the input subroutine was operating correctly; that is, the location, numbering and allocation of the nodes and elements was being performed as intended. Thus the problem is not one of incorrect input of information but rather of the influence that the method of subdivision has on effecting a solution using the finite element method. The difficulties encountered in the solution are discussed briefly in the sections that follow but only to the extent to which they are relevant to the problem area to which the difficulties have been attributed.

5.4.1 Mesh Generation Scheme I

The first mesh generation arrangment was constructed with the intent that a larger number of small elements be located near the meniscus contact point. In consideration of the anticipated local concentration of the heat flow in this region, this type of element allocation was deemed necessary in order to obtain reliable results while keeping the program storage requirements within the limits afforded by the available computational facilites. As will be seen, this is indeed a desirable objective of the mesh generator. The problem with this generation scheme, concluded after many tedious verification procedures, is in the method of allocation and in particular in the shape of the elements near the meniscus contact region. A more detailed description of this generator will be given below.

Before discussing the generator, however, we present the test-case used for evaluation of the computational scheme convergence characteristics. It was felt that to examine the convergence characteristics, an extreme computational situation should be used. In this way, when an estimate of the solution accuracy is available, computational results for less severe cases should be at least as accurate as those obtained for the test situation. Feeling,however, that the computations will be relatively insensitive to the groove half-angle, within moderate bounds, a value of twenty degrees was used for the groove half-angle. An exposed land area ratio (symmetric groove configuration) of 25 per cent land area to total apparent area was used since this case will yield a significant degree of heat flow concentration. The extreme case of the conductivity ratio, k_f/k_m, of 0.001 was also used since this also augments the heat flow concentration. Finally, an apparent contact angle of 2.5 degrees was used, also for the reasons given above. It is felt that any problems configuration and property dependent will become apparent for this combination of parameters. The characteristics of the first mesh generator are given below for this parameter combination.

The first mesh generation scheme used a virtual origin established at the intersection of the groove centerline with the extrapolation of the groove sidewall plane. This is illustrated in figure 5-3. Radial lines emanating from this origin were constructed with the region used ranging from the wall exterior surface to the liquid free surface over the angular range of $0 \leq \theta \leq \theta_o$. In order to provide a higher degree of detail near the meniscus contact a finer angular division between the radial lines was used near $\theta = \theta_o$ than near θ-o. The details of the actual subdivision scheme used to provide this gradation will not be presented here since they will not add to the problem understanding. Within the metal region extending over $0 \leq \theta \leq \theta_o$, horizontal lines were used to provide the remaining boundaries for the elements. Within the liquid, the radial distance between the groove root and the liquid free surface was further subdivided non-uniformly to provide the smaller elements required near the meniscus contact point. A non-uniform linear scheme was used within the remainder of the metal region of the solution domain. The resulting mesh is illustrated in figure 5-3 for a crude mesh subdivision.

The results of a preliminary examination of the convergence characteristics for the sharp V case, 0.5 land area ratio and conductivity ratio of 0.01156 are presented in figure 5-4. As can be seen from the figure, convergence 'looks' monotone and asymptotic to a limiting value. Calculation indicates, however, that the limit has not been approached. Unfortunately, the last data point presented represents the limit for available storage core on the IBM 360/75 computing installation at the University of Waterloo. It was in the search for verifying that the limit was near the last computational

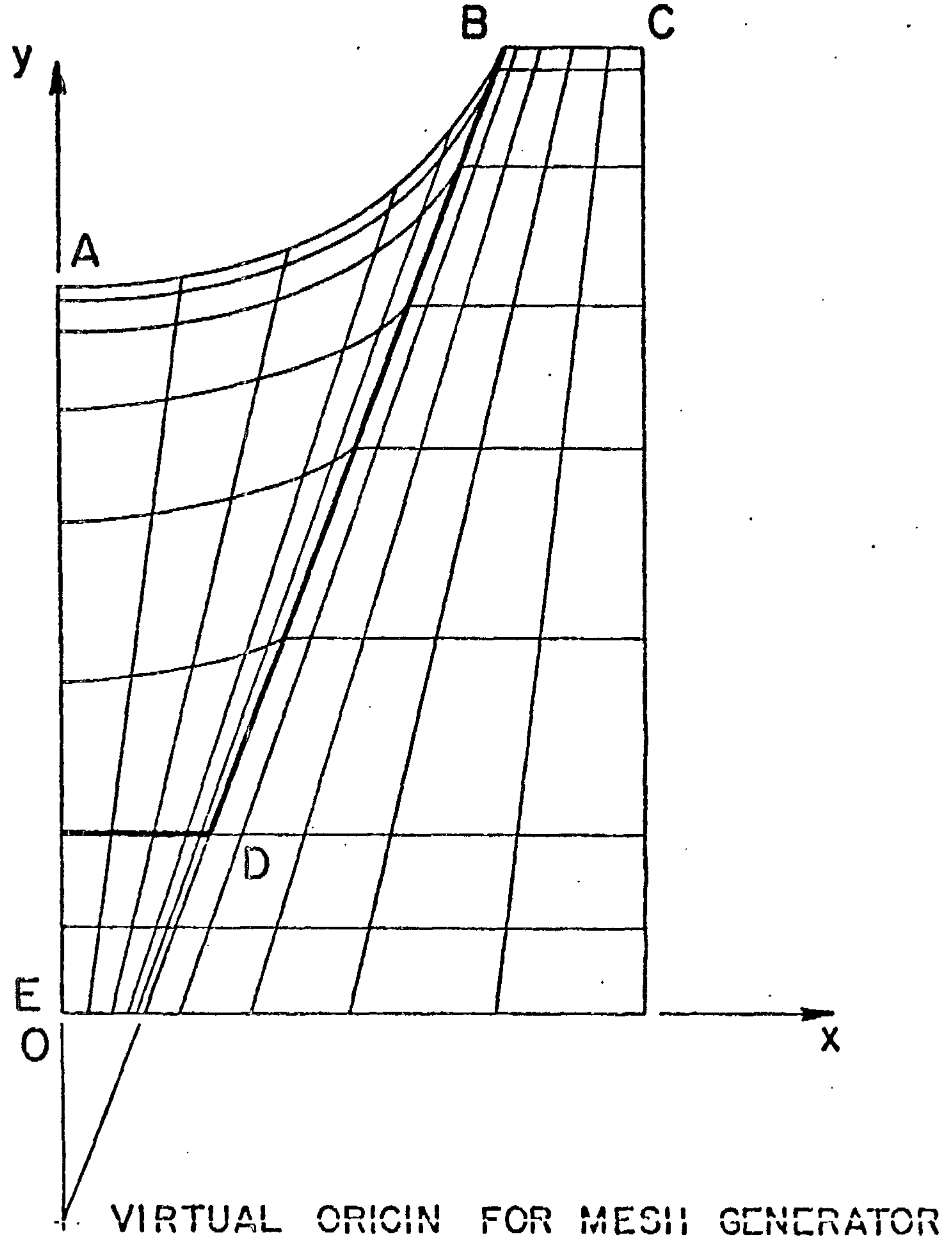

Figure 5-3

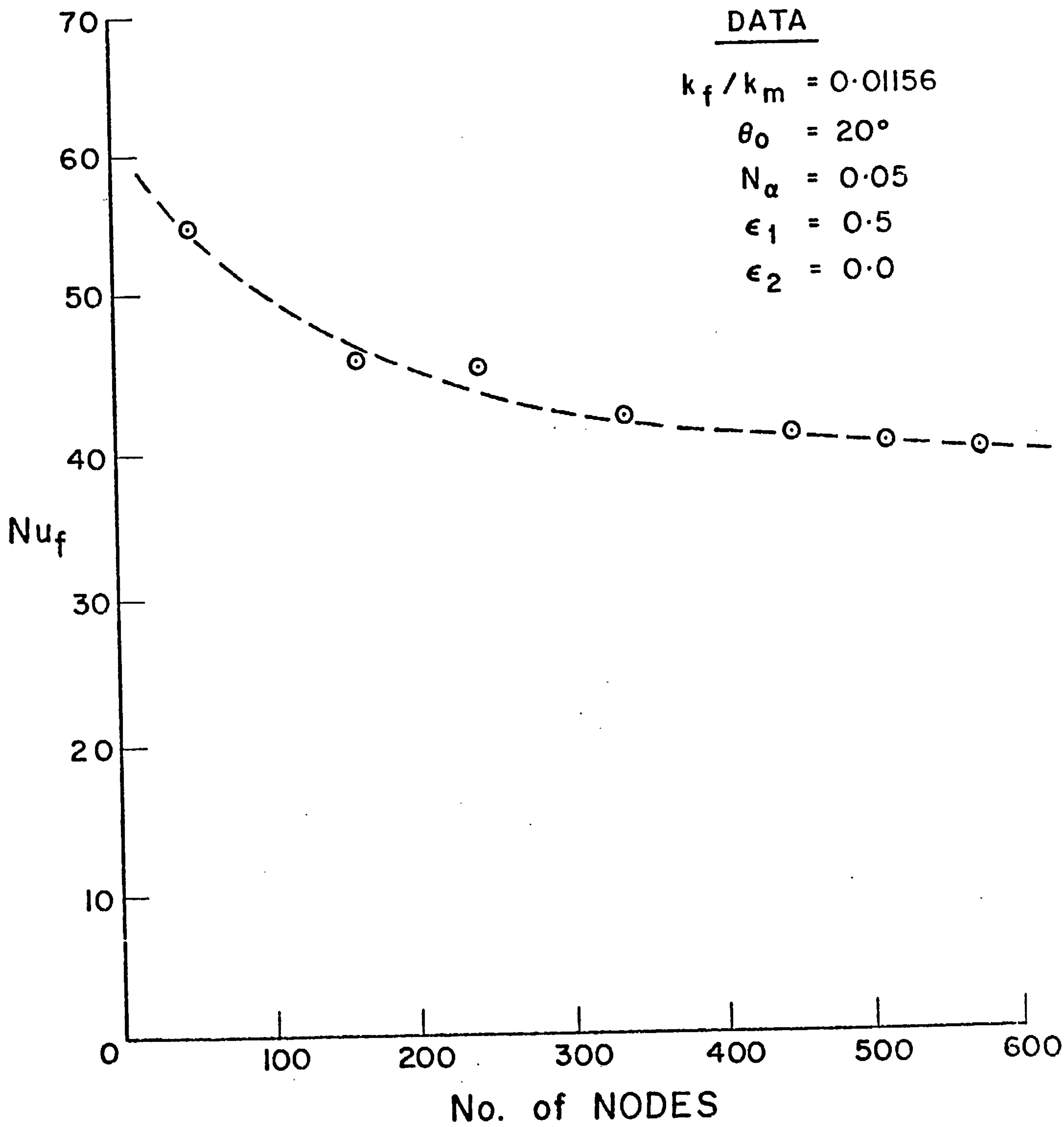
DATA
$k_f/k_m = 0{\cdot}01156$
$\theta_0 = 20°$
$N_\alpha = 0{\cdot}05$
$\epsilon_1 = 0{\cdot}5$
$\epsilon_2 = 0{\cdot}0$
70
60
50
40
Nu_f
30
20
10
0
100
200
300
400
500
600
No. of NODES

Figure 5-4

data point that the problem area associated with this mesh generation scheme was discovered.

To examine the convergence characteristics in greater detail, the IBM 370/158 'virtual machine' was used which allows much larger core usage. On this system, additional points computed for the above case departed from the asymptotic nature exhibited in figure 5-4 and fell increasingly far below the anticipated asymptote.

The results for the more severe test case using the 370/158 system are shown in figure 5-5. The results referred to henceforth will apply to the more severe test case parameter combination described earlier. As can be seen from the figure, an initial approach towards a convergence limit is indicated by the results but as the number of nodes is further increased beyond 1600 the results drop off sharply. It is not so much the range of values taken on by the Nusselt number (note the expanded ordinate scale) but the trend of the results which is most disturbing. If these results were accepted, the question would have to be answered, "Where are these results going?", and this is not determinable from the convergence characteristics of figure 5-5.

It was concluded therefore that the mesh generation scheme described above will be inadequate to describe the thermal behavior of this problem. The reasons for its inadequacy are attributed to two independent characteristics of this mesh generation scheme and are briefly outlined below.

The first potential cause for the apparent erratic behavior displayed by figure 5-5 is the combination of the variable mesh generation

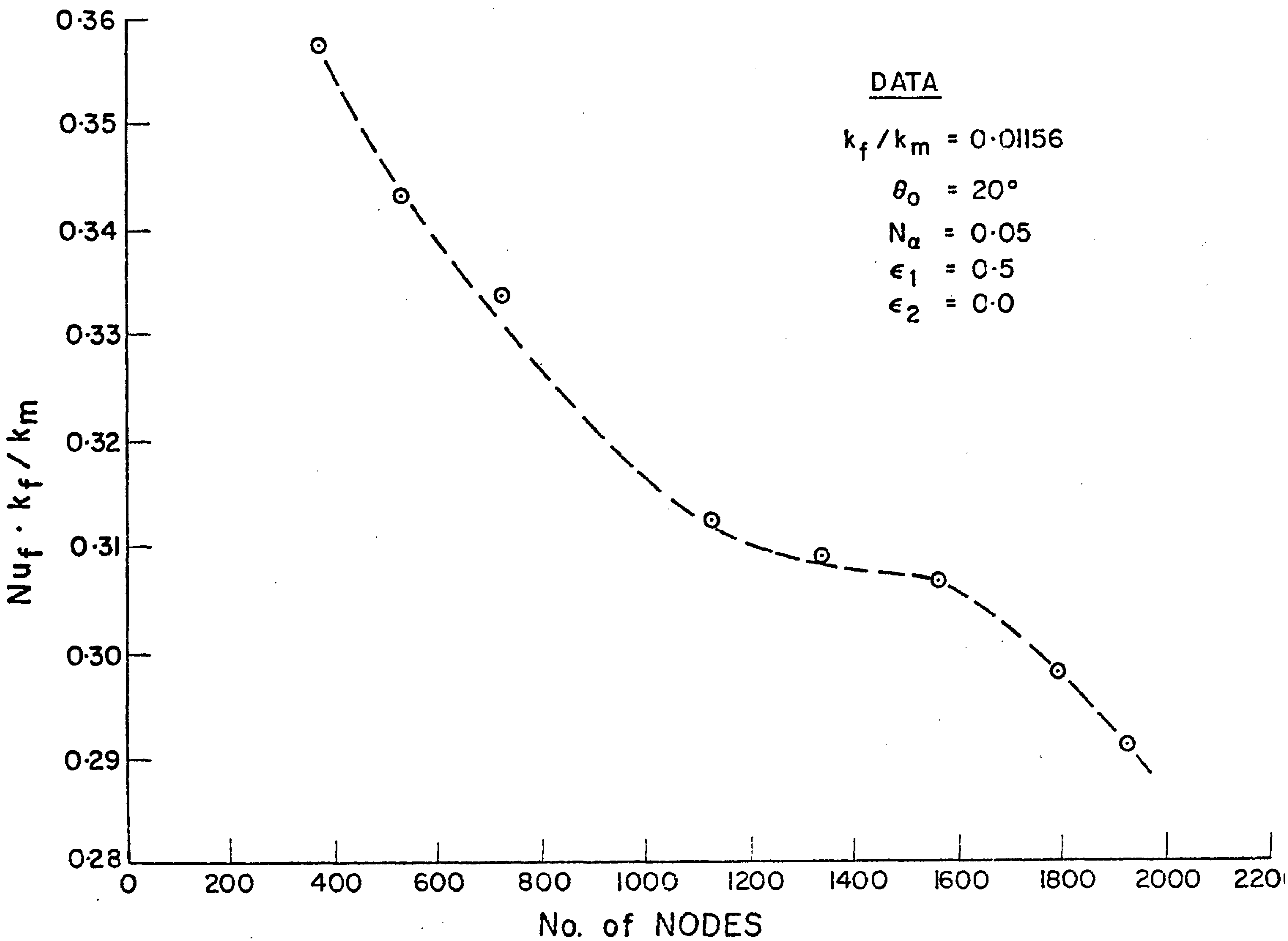
DATA
$k_f / k_m = 0{\cdot}01156$
$\theta_o = 20°$
$N_\alpha = 0{\cdot}05$
$\epsilon_1 = 0{\cdot}5$
$\epsilon_2 = 0{\cdot}0$
$Nu_f \cdot k_f / k_m$
No. of NODES
0·36
0·35
0·34
0·33
0·32
0·31
0·30
0·29
0·28
0
200
400
600
800
1000
1200
1400
1600
1800
2000

Figure 5-5

schemes for the two independent directions used to obtain the total generation pattern. This is best visualized with reference to figure 5-3. In order to obtain greater detail of the solution in the radial direction (from the virtual origin) near the meniscus contact region, the element thickness in that direction is small not only near the meniscus contact, point B, but also at the groove centerline, point A. Conversely, while the variable mesh in traversing the liquid region, from point A to B, provides (finer) subdivision near point B, the element 'lengths' near point A are large by comparison. The net result of the independent gradation for each direction is a series of elements with aspect ratios very much different from unity existing near point A of the figure. Similar effects are obtained near point C, D, and E of figure 5-3. With aspect ratios of 1000:1 and higher in these regions, it is clear that the thermal influence of two nodes on each other in any given 'direction' may be 1000 times more, or less, than that for the other 'direction'. Without expounding on the details of the effects of very large or very small aspect ratios, let it suffice for purposes of this report to say that certain of the inter-nodal influences become dwarfed, or indeed lost, upon assembly into the overall stiffness matrix, particularly when computing using single precision arithmetic.

The second deficiency of the first mesh generation scheme is its introduction of highly skewed elements into the solution domain. Unfortunately, predominance of these highly skewed elements is (almost) exclusively in the region near the meniscus contact with the groove wall and as a result any detrimental behavior resulting from their skewed character will be markedly reflected in the solution. Due to the general nature of the general quadrilateral finite element used in this work, the volume integration of equation (5-25a) is performed numerically in the solution program using Gauss-point integration. The influence of highly skewed elements on the solution accuracy is reflected through a reduced accuracy of the numerical integration for these elements. It is felt that this skewed character for some of the elements is the second cause for the poor convergence characteristics of the first mesh generation scheme.

While the influence of the second item above would be in the form of a misrepresentation of the thermal problem, the influence of the first item, in addition to contribution to the misrepresentation, is to provide very small and very large diagonal elements in the coefficient matrix (5-25a). The effect of the small diagonal elements was observed in the solution through nodal heat flow imbalances as large as 100 percent of the imposed heat flow rate. Clearly, now, this subdivision scheme is unacceptable for use with this problem.

5.4.2 Mesh Generation Scheme II

A second mesh generation scheme, a modification of the first scheme described above, was also found to be unacceptable for this problem but for different reasons than for those of the first scheme. This second scheme sought to alleviate the problems associated with the first generation scheme while maintaining the same basic mechanism for achieving element size variation throughout the solution domain. The corrective measures that were taken proved to be effective but unfortunately due to the built in safeguard in this scheme to keep the aspect ratio near unity for all elements, a very large number of elements are required. Indeed, for this scheme even at 2000 nodes within the solution domain, the computational results were far from being near a converged state. The convergence characteristics for the second mesh generation scheme are presented in figure 5-6. A brief discussion of the second mesh generation scheme is given below but the purpose of this discussion does not warrant a detailed description of its nature.

The prime departure of this scheme from the previous one is that given a prescribed number of nodes, their distribution is rearranged to maintain element aspect ratios near unity. In order to universally achieve this it was also necessary to relax the transition from the coarse regions to the finer regions, and this, of course, necessitates the use of more elements to achieve a prescribed degree of detail near the meniscus contact region. The redistribution of elements mentioned above was effected by imposing a fixed number of elements across the test section thickness, and as the typical cell is traversed from the outer surface to the inner surface, elements are 'passed' from the metal section to the liquid section in accordance with the respective cross-sectional area changes. In this way a greater degree of aspect ratio uniformity, were achieved using this generation scheme, and while the resultant convergence characteristics exhibited monotonic behavior as illustrated in figure 5-6, the additional elements required to obtain the required detail near the meniscus contact region makes this generator impractical for use on this problem. Indeed, as can be seen from figure 5-6, when comparing ordinate scales here with that of figure

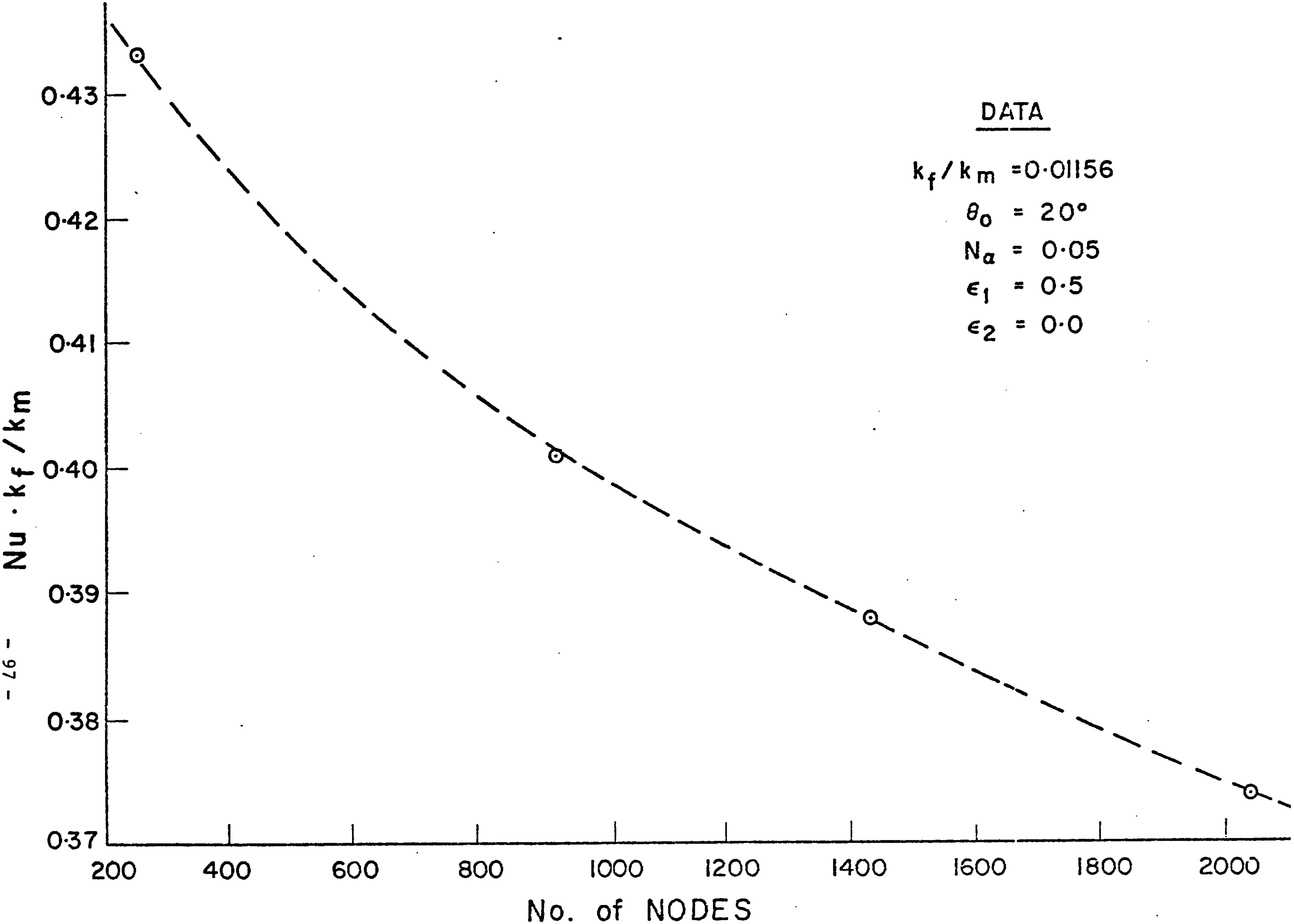

DATA
k_f / k_m = 0·01156
θ_o = 20°
N_α = 0·05
ϵ_1 = 0·5
ϵ_2 = 0·0
$Nu \cdot k_f / k_m$
0·43
0·42
0·41
0·40
0·39
0·38
0·37
200
400
600
800
1000
1200
1400
1600
1800
2000
No. of NODES

Figure 5-6

5-5, the last data point from the second generator has not even reached the starting point of the first generator. In view of this, and the fact that the convergence slope at 2000 nodal degrees of freedom is far from that of a 'near converged' situation, this generator was discarded as being impractical to apply with the available computational facilities. A third generator, which proved to be adequate for the purposes intended, was devised instead and used for the subsequent parametric study. This generation scheme is described in the following section.

5.5 Successful Application of the Method

In this section the third, successful, mesh generation scheme is presented along with the associated convergence characteristics. The third generation scheme was developed entirely as a new and different subdivision scheme and does not incorporate any of the underlying ideas which led to the first two schemes. The object still remains to provide detail near the meniscus contact point, however, but while the former two methods accomplished this, the third enables in addition a more compatible gradation to the coarser elements and is also relatively free from highly skewed elements.

The convergence characteristics for the three conductivity ratios to be considered, k_f/k_m = 0.1, 0.01156, and 0.001, are also presented in this section. Finally, an extrapolation technique is utilized to provide an estimate on the solution accuracy. The expected solution accuracy is found to be sufficient for the purpose intended by this investigation.

5.5.1 Mesh Generation Scheme III

In this third mesh generator the virtual origin concept used in the previous two generators is discarded entirely. Instead, a deliberate attempt has been made to orient the elements in a fashion which more closely resembles the anticipated thermal field set up within the solution domain. In effecting this orientation of elements, it is also strived to keep the elements as close as possible to rectangular in shape and to maintain the aspect ratio within a moderate range. A schematic of the spatial subdivision scheme is presented in figure 5-7 for a crude subdivision. The diagram is only representative of the element allocation, however, and is not to scale.

In this subdivision scheme, a single parameter. NE1 is used as input. The remaining spatial subdivision is determined from the lengths associated with the appropriate section of the typical cell. One exception to this determination is the subdivision parameter, NF, in the fluid region which is taken as one-half the value of NE1 (to the nearest larger integral value). This is felt to be adequate since over the bulk of the liquid region, little heat is flowing while near the meniscus contact point the coalescence of the element boundaries at a single node at the contact point yields element thicknesses which are here sufficiently small to 'pick-up' the larger gradients in this region. The details of the generation procedure will not be presented here since the algebraic 'bookkeeping' becomes rather messy for this scheme, but a few of the salient features are indicated in the following paragraphs.

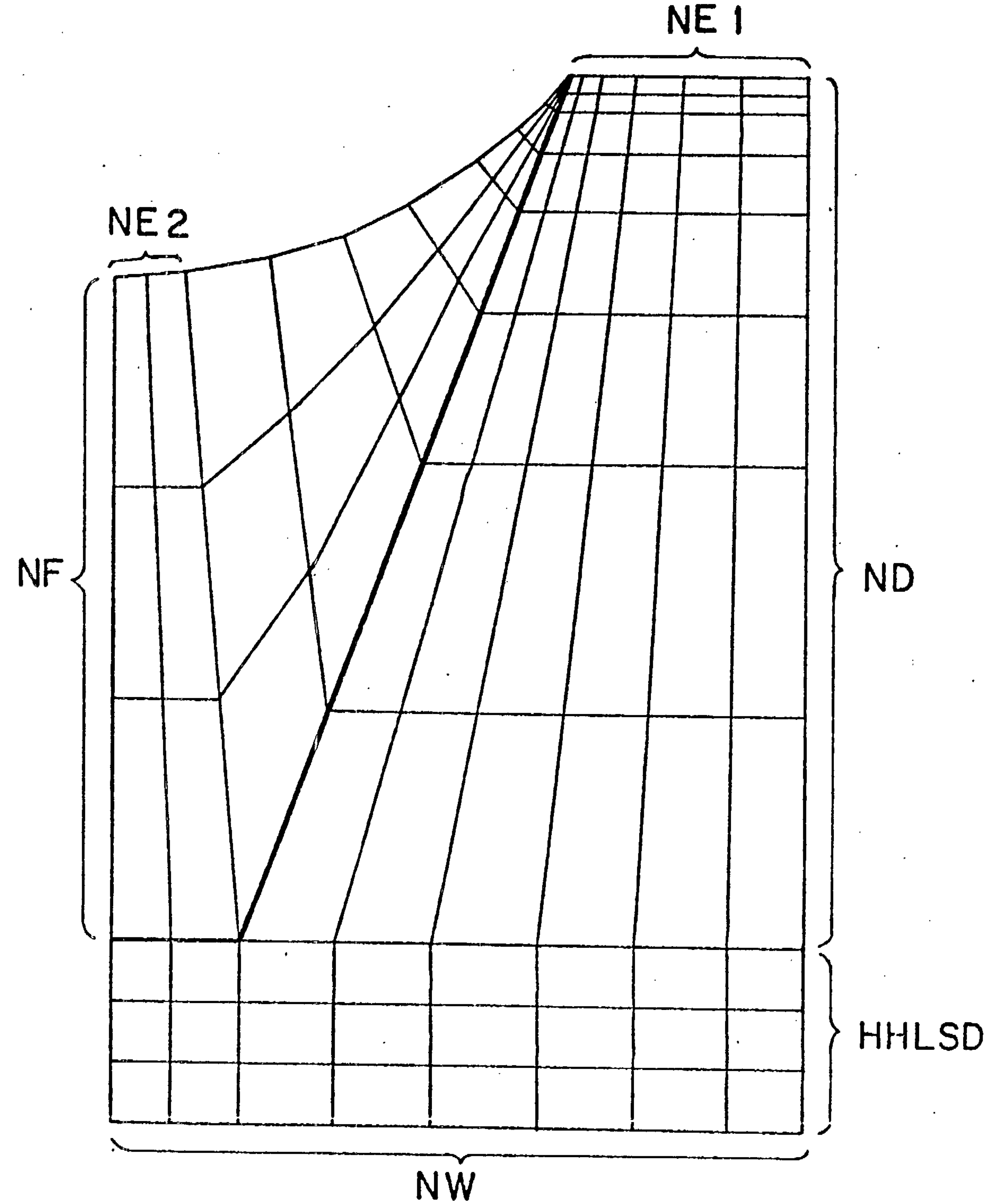

Figure 5-7

Firstly, the inter-element boundaries formed by the lines joining the liquid free surface to the groove wall are constructed by providing a transitional development from the near-to-vertical case near the groove root to the case near the meniscus attachment point where those boundaries form the base of an isosceles triangle hinged at the attachment point. This transition scheme provides element boundaries for this direction which are suggestive of the anticipated heat flow lines over the length of the groove wall. In the other direction these lines are subdivided equally to provide the remaining element boundaries. The scheme also provides elements, although rotated with respect to a cartesian set of axes, which are near rectangular in shape, certainly far more so than the elements resulting from the previous two generators. Further, the use of appropriate dimensions in determining the number of element subdivisions in a particular direction yields elements with an aspect ratio nearer to unity.

The second feature of this subdivision scheme is the use of a transition mesh in the metal 'fin' section of the groove. The mesh in this region has been graded from a uniform one at the groove root plane, where the field is expected to be relatively uniform, to a non-linear one at the metal fin tip providing greater detail near the meniscus attachment point, where the gradients are expected to be large and non-linear. A non-linear spacing has also been employed in the direction along the groove wall as the groove wall is traversed from root to tip. Although in this metal region elements of poor aspect ratio are generated near the upper right side of figure 5-7, these elements are of little consequence with respect to their contribution to the thermal behavior. Their use is thus justified in consideration of the gains available in the more consequential region near the meniscus attachment point.

As will be seen in the next section, this third subdivision scheme provides solutions which display a monotone, asymptotic behavior as the number of nodal points in the discretized description of the thermal problem is increased.

5.5.2 Convergence Characteristics

The third mesh generation scheme was used in the solution program and the convergence characteristics obtained for the three conductivity ratios, $k_f/k_m = 0.1$, 0.01156, and 0.001. The results of the convergence study are presented for these cases in figures 5-8, 5-9, and 5-10 respectively with the remaining solution parameters being those of the test case described earlier. It is clear from examination of these figures that convergence is both monotone and asymptotic for this mesh subdivision scheme. It is also clear from a cross-comparison of the three convergence plots that the conductivity ratio strongly influences the rate of convergence of the results and that the extremely low ratio of 0.001 is indeed a severe test on the solution program. Even for this severe case, however, examination of figure 5-11, where the convergence trends are presented on non-expanded axes, indicates that the computed solution for 1800 nodal points is near its asymptotic value and that the effort and expenditure required to achieve a further improvement on the accuracy will be prohibitively large.

The above discussion has been concerned with the convergence characteristics of the derived quantity, the groove equivalane Nusselt number. Perhaps a more fundamental indicator of convergence, however, is the functional of equation (5-17) whose value is being made stationary by the variational statement. Treating the solution for each degree of subdivision as an approximate solution, the better the approximate solution is, the closer this functional will move towards its extreme value, which is obtainable only in the limit where the exact solution is achieved. The rate of convergence of this functional provides, therefore, an additional check on the solution credibility as well as an estimate of the closeness of the solution to its asymptote. The convergence characteristics for the functional are presented in figure 5-11. As seen from the figure the convergence trends of the functional are very similar to those for the derived equivalent Nusselt number. This realization offers further support, then, that the third mesh generation scheme has been successful in providing a spatial subdivision which, in conjunction with the solution program, will yield reliable solutions. The accuracy of these solutions will be estimated in the following section.

5.5.3 Accuracy of the Results

In this section an estimate will be made for the accuracy of the aforementioned results using a hyperbolic extrapolation technique. The data appearing in the previous graphs is presented in tabular form in Table 5-1 for the test case studied.

Table 5-1

NE1	No. of Nodes	$Nu \cdot k_f/k_m$
3	65	0.501
5	141	0.469
7	276	0.445
10	547	0.425
12	741	0.416
14	1020	0.407
15	1136	0.403
16	1317	0.400
17	1448	0.396
19	1828	0.390

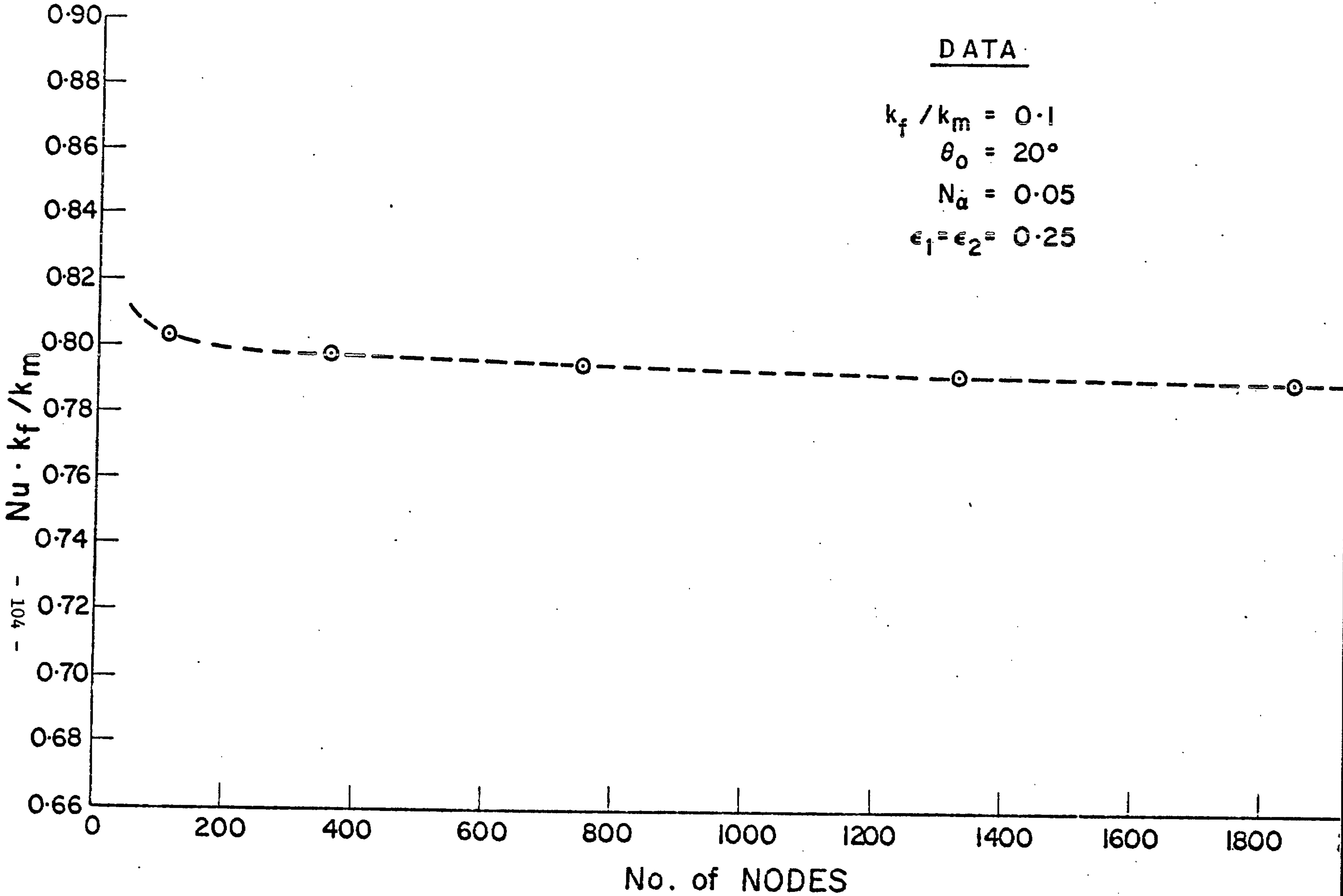
DATA
$k_f / k_m = 0 \cdot 1$
$\theta_0 = 20°$
$N_\alpha = 0 \cdot 05$
$\epsilon_1 = \epsilon_2 = 0 \cdot 25$
$Nu \cdot k_f / k_m$
0·90
0·88
0·86
0·84
0·82
0·80
0·78
0·76
0·74
0·72
0·70
0·68
0·66
0
200
400
600
800
1000
1200
1400
1600
1800
No. of NODES

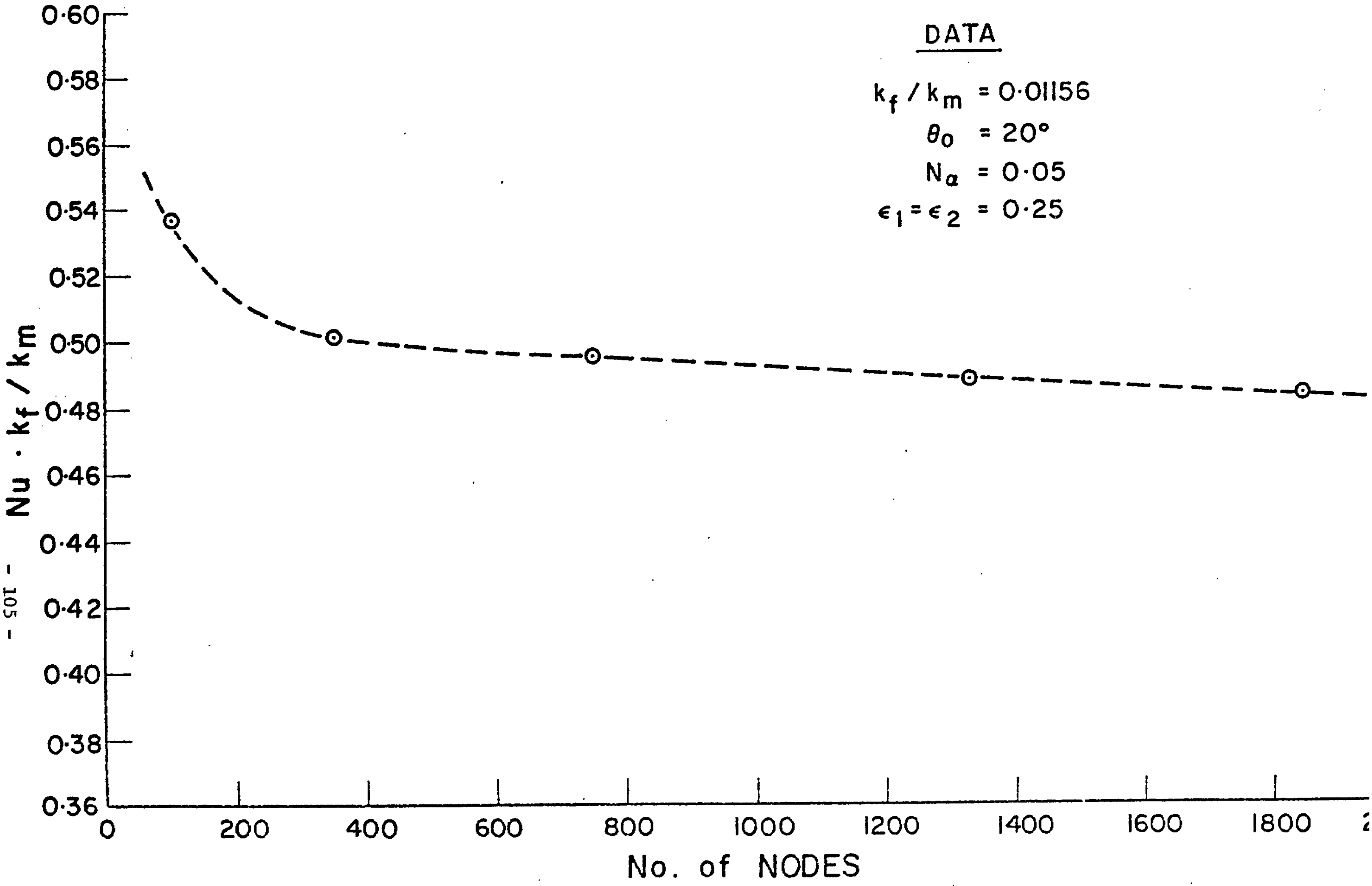
DATA
$k_f / k_m = 0.01156$
$\theta_o = 20°$
$N_\alpha = 0.05$
$\epsilon_1 = \epsilon_2 = 0.25$
0·60
0·58
0·56
0·54
0·52
0·50
0·48
0·46
0·44
0·42
0·40
0·38
0·36
$Nu \cdot k_f / k_m$
0
200
400
600
800
1000
1200
1400
1600
1800
No. of NODES

Figure 5.9

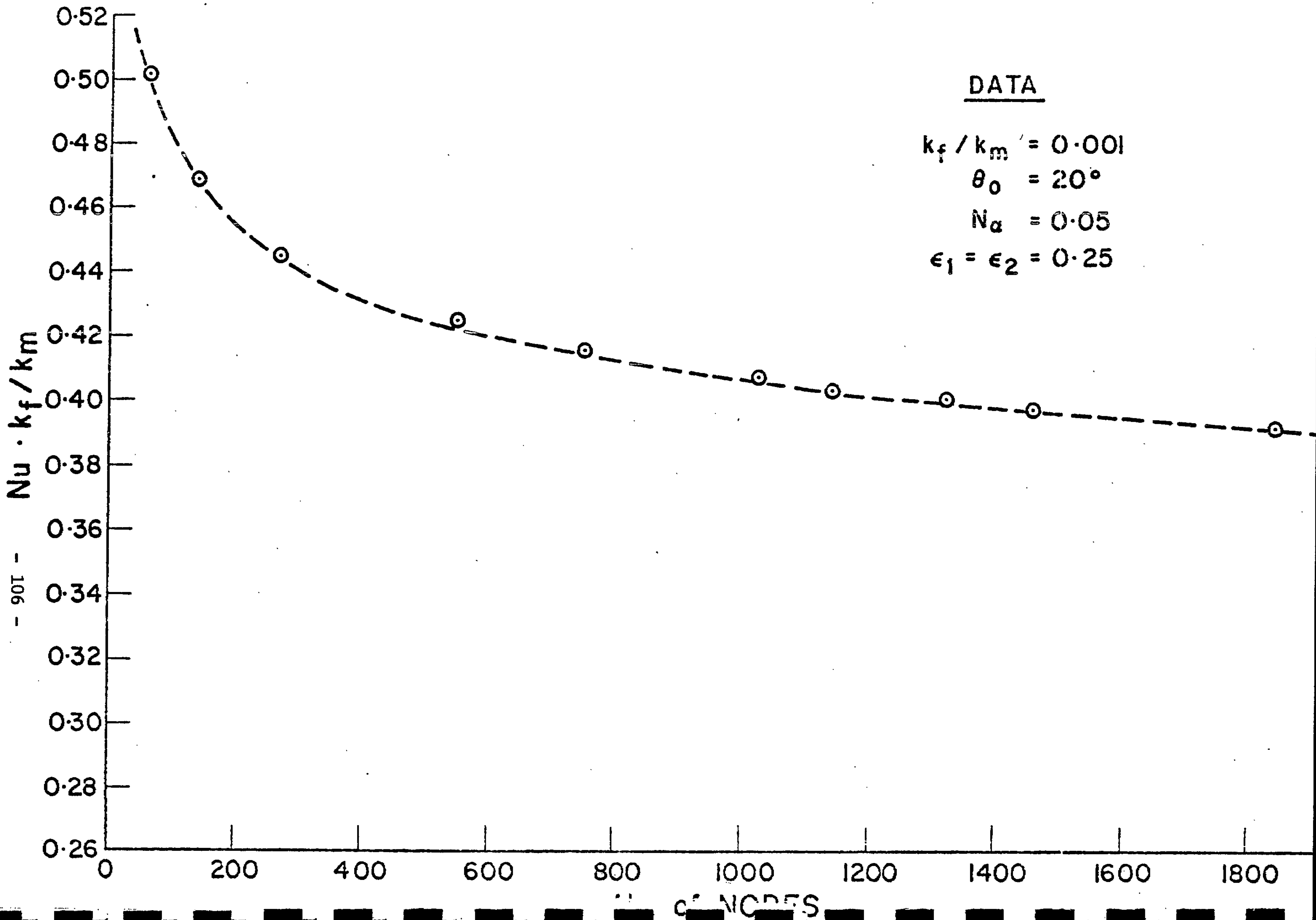
DATA
$k_f / k_m = 0.001$
$\theta_0 = 20°$
$N_\alpha = 0.05$
$\epsilon_1 = \epsilon_2 = 0.25$
$Nu \cdot k_f / k_m$
0·52
0·50
0·48
0·46
0·44
0·42
0·40
0·38
0·36
0·34
0·32
0·30
0·28
0·26
0
200
400
600
800
1000
1200
1400
1600
1800

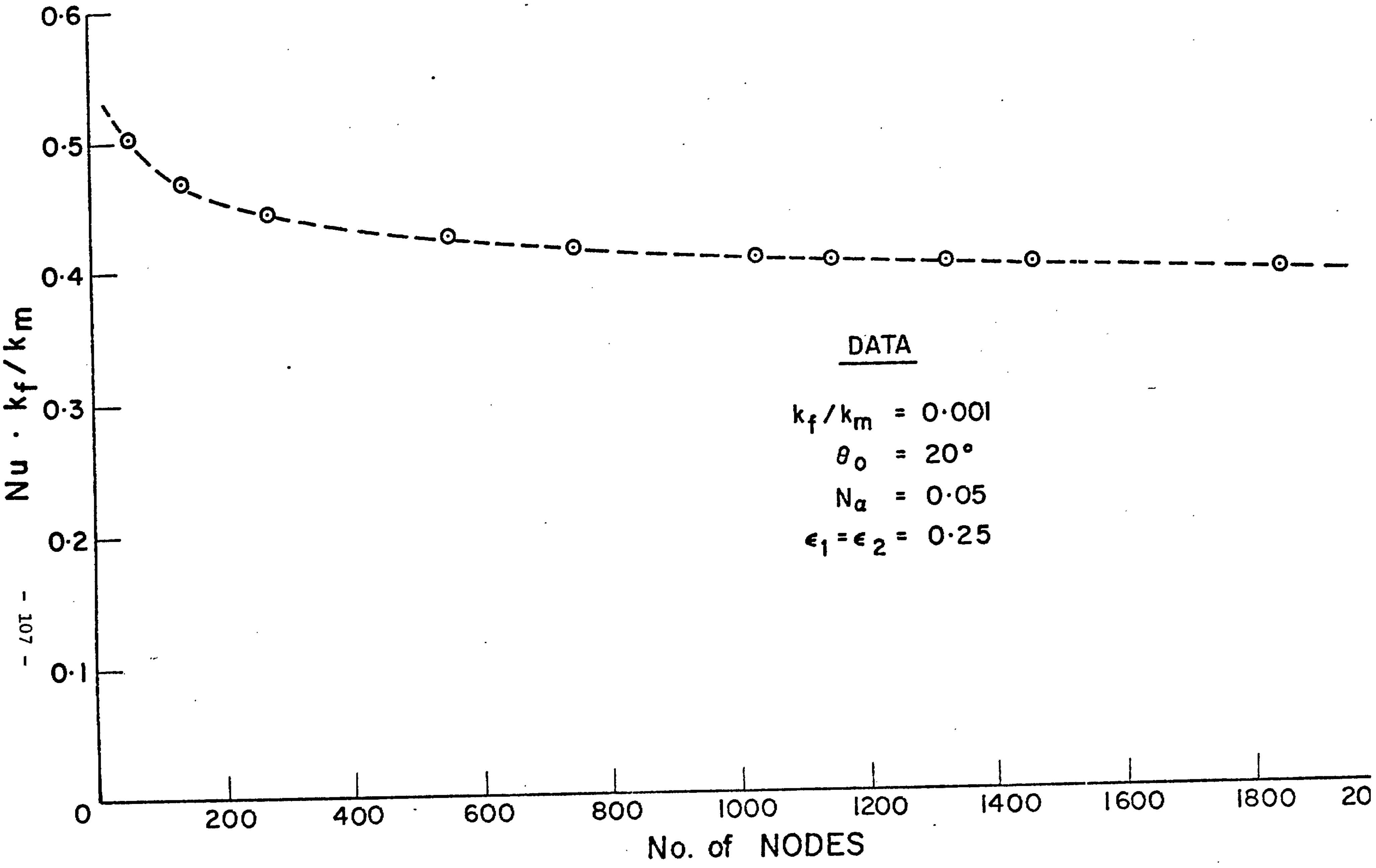
0·6
0·5
0·4
0·3
0·2
0·1
0
Nu · k_f / k_m
200
400
600
800
1000
1200
1400
1600
1800
20
No. of NODES
DATA
k_f / k_m = 0·001
θ_o = 20°
N_a = 0·05
$\epsilon_1 = \epsilon_2$ = 0·25

Figure 5-11

Anticipating that the convergence curve follows a path displaying an inverse dependence on the number of nodal degrees of freedom, and observing this basic trend in the convergence plots, the hyperbolic conic section appears to be a reasonable candidate for description of the convergence behavior. In addition, an asymptotic limit must be provided by the describing curve since we know the numerical solution asymptotically approaches the exact solution as the number of nodal degrees of freedom becomes infinitely large (excepting machine round-off errors). Since the hyperbolic curve description provides the above characteristics, it will be used in an extrapolation for purposes of error estimation. The estimation is performed in the following fashion.

Using the numerical data of Table 5-1, a least squares minimization is performed to fit the data to a general hyperbola of the form

$$Nu_f \cdot k_f / k_m = \frac{C_1}{(N-C_2)} + C_3 \qquad (5\text{-}32)$$

If an acceptable fit is obtained, extrapolation of the analytical expression describing the curve is made for N becoming infinitely large. Clearly from the above expression (5-32) the approximation of the limiting value is given by

$$\lim_{N\to\infty} [Nu_f \cdot k_f / k_m] \approx C_3 \qquad (5\text{-}33)$$

A program was written which, using the data of Table 5-1, performed a least squares curve fit of the data to the model equation (5-32). Excellent agreement was found between the data and the equation with parameters given by

$$Nu_f \cdot k_f/k_m = \frac{25.80}{N+139.5} + 0.3820 \qquad (5\text{-}34)$$

The maximum error incurred over the entire range of data was only 1.4 per cent. Using the approximation for the asymptotic value given by equation (5-33), the estrapolated asymptote is given by

$$[Nu_f \cdot k_f/k_m]_{N\to\infty} \simeq 0.382$$

Comparison of this asymptote with the last computed value yields an expected error in this value of 1.96 per cent. Adding to this value the maximum error incurred by the correlation equation within the range of the data of 1.4 per cent yields a potential error in the last value of 3.36 per cent for this extreme parameter combination.

Based on the good correlation agreement of the model equation with the data, and evaluation of the analytic asymptote of the correlation equation, it is expected that the actual error in the solution will be less than five per cent which provides a safety margin of fifty per cent on the incurred error. Since this test case represents a severe combination of physical and geometric parameters, it is anticipated that the errors incurred for the remaining parameter combinations will be less than five per cent.

5.6 Comparison with a Limiting Analytical Solution

As a further check on the solutions program operation, the solution from the finite element analysis will be computed for the case where an anlytic solution is known. This is a very restrictive case but it serves the purpose well of verifying correct operation of the solution program.

The case study under examination is that for which the conductivity ratio is taken to be unity. In this case the problem is clearly a single component problem and becomes a member of the constriction resistance class of problem. Further, to enable an analytic solution an equivalent full groove condition must be assumed in the groove. The land area ratio (symmetric groove) will be maintained at the former value of 0.25, and the mesh generation routine developed for the multi-component problem will be used, even though it may not be an ideal subdivision scheme for this problem.

The problem geometry and boundary conditions for this verification problem are illustrated in figure 5-12. The adiabatic boundaries remain as they were previously prescribed. The isothermal boundary is now applied at $y = H$ over the range $0 \leq x \leq 1-\varepsilon_1$. Over the lower surface a uniform heat flux is prescribed. It is noted here that the analytical solution to be discussed is applicable to the situation where the lower surface is maintained at a second isothermal temperature but that this very nearly corresponds to a uniform flux condition over this surface for the dimensions considered in this problem. The physical dimensions for the verification example are $H = 1.4737$, $w = 1.0$, and $\varepsilon_1 = \varepsilon_2 = 0.25$, and the conductivity for each region is taken to be unity.

The analytical solution to the above described problem, in determining the total thermal resistance, can be expressed in terms of the Jacobian Elliptic functions and Elliptic integrals of the first kind [48]

$$R_T = \frac{K'(\lambda)}{K(\lambda)} \tag{5-37}$$

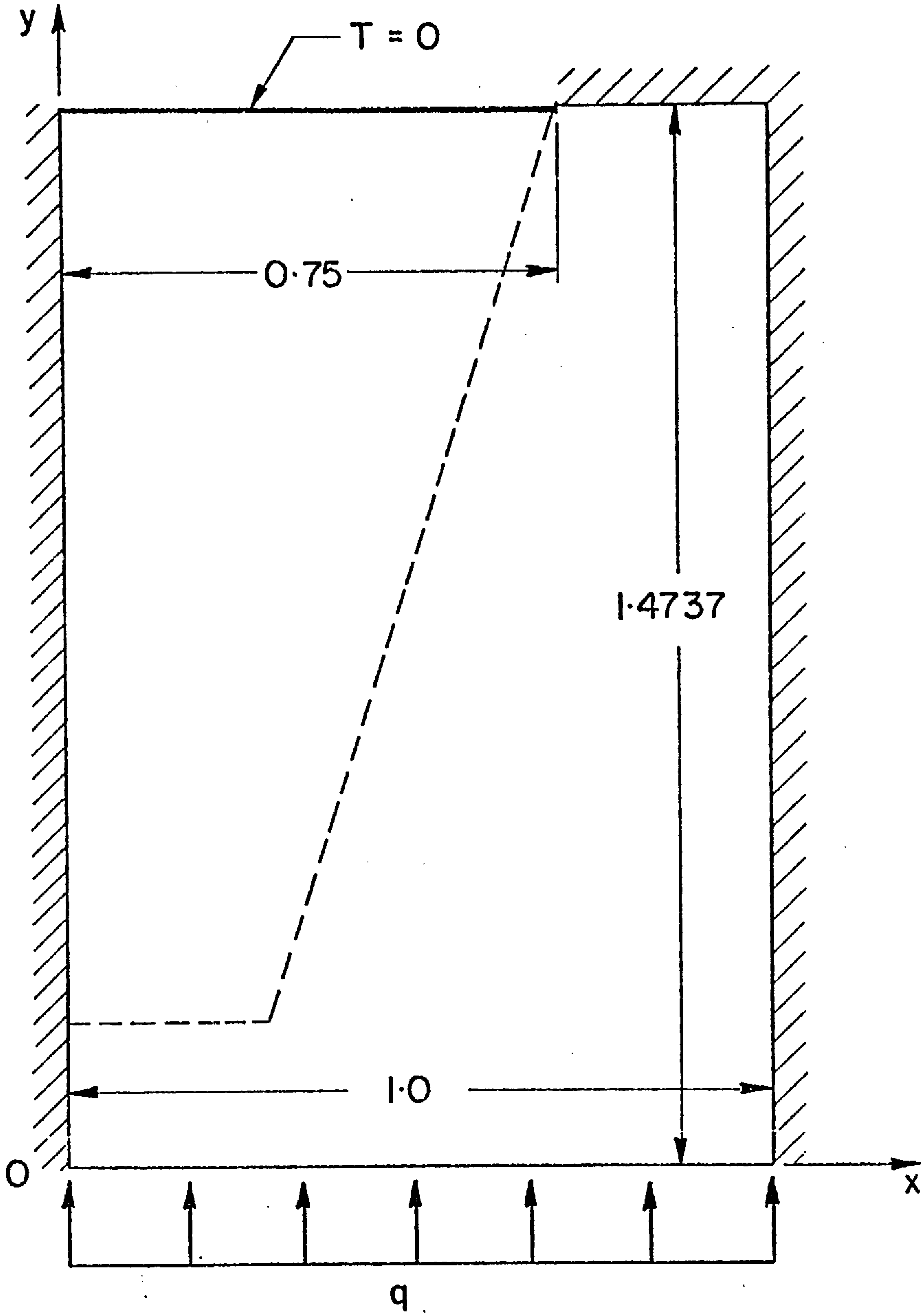

Figure 5-12

where the modulus λ is determined from

$$\lambda = \kappa \text{ sn } \left(\frac{(1-\varepsilon_1)}{w} K(\kappa), \kappa \right) \tag{5-37}$$

where sn denotes the Jacobian Elliptic sine amplitude function, K denotes the complete elliptic integral of the first kind, and κ, a second modulus, is determined from

$$\frac{K'(\kappa)}{K(\kappa)} = \frac{H}{w} \tag{5-38}$$

Here $H/w = 1.4737$ and using equation (5-38) and interpolating from the tables in Abramowitz and Stegun [49] yields a value for the second modulus of

$$\kappa = 0.38027 \tag{5-39}$$

Note the modulus used here is the square root of the Abramowitz and Stegun modulus, m, and is merely a matter of convention. Using this modulus the associated complete elliptic integral of the first kind can be determined to be

$$K(\kappa) = 1.6327 \tag{5-40}$$

The first modulus, λ, is then found using equation (5-37) from

$$\lambda = 0.38027 \text{ sn } (1.2246, .38027 \tag{5-41}$$

This determination, however, is not an easy one. Returning to Abramowitz and Stegun [49] for guidance, the Jacobian sine amplitude function can be related to the Jacobian Theta functions, appropriately defined in the reference, by

$$\text{sn}(u,\kappa) = \theta_s(v,\kappa)/\theta_n(v,\kappa) \tag{5-42}$$

where $$v = \pi u/2K(\kappa) \tag{5-43}$$

Following the evaluation procedure suggested by Abramowitz and Stegun [49], the first modulus can be determined to be

$$\lambda = 0.3530 \tag{5-44}$$

Finally, using this value in the expression for the total resistance, equation (5-36), yields the result

$$R_{T_{exact}} = 1.5246 \tag{5-45}$$

for this geometric configuration.

Determination of the total resistance using the finite element program developed for the trapezoidal groove problem, with the appropriate input data of, in particular, $X_\alpha = 1.0$ and $k_f/k_m = 1.0$, led directly to a value for the total resistance of

$$R_{T_{FEM}} = 1.5268 \tag{5-46}$$

which agrees with the 'exact' analytical value to within 0.15 per cent. The remarkable agreement obtained for this verification example suggests, indeed, that reliable operation and accurate solutions can be obtained using the finite element solution program.

5.7 Conclusions

In the foregoing chapter, the basic ideas underlying the application of the finite element method to heat conduction analysis were introduced. The variational statement governing the finite element analysis of the heat conduction phenomenon was developed in a general fashion, so as to be applicable to any general orthogonal curvilinear coordinate system. The generalized results were seen to easily reduce to those corresponding to the cartesian coordinate frame utilized in the analysis of the trapezoidal groove heat transfer problem. Application of the method was made to the trapezoidal groove problem with its appropriate boundary conditions.

It was found, however, that the application to the trapezoidal groove heat transfer problem is, indeed, not as straight forward as it might at first appear. The problem under examination in this work was found to be very special with respect to both its physical and geometric characteristics. The special character of the problem foiled the attempts made in the development of the first two mesh generation schemes to provide reliable solutions of adequate accuracy.

Finally, after a great deal of effort, a third mesh generation scheme was developed which displays monotone, asymptotic, convergence characteristics. An estimation of the accuracy of the resultant solution indicated that for the severe test case examined, having a conductivity ration of $k_f/k_m = 0.001$, solutions accurate to within approximately five per cent are expected, with the numerical value being larger than the exact value due to the extremizing nature of the variational statement for the problem. Solution accuracy, although this will be presented in a subsequent chapter, is considerably improved as the conductivity ratio is increased towards a value of unity.

Finally, a verification example, for which an analytic solution is available, was computed and compared with the analytical value for the particular problem. The conductivity ratio for this example was, in fact, unity. The excellent agreement displayed by the 0.15 per cent error obtained for this example verifies correct program functioning and also demonstrates that improved accuracy is available for more moderate conductivity ratios.

Chapter 6

Numerical Results

6.1 Introduction

It is the purpose of this chapter to present the numerically predicted values for the equivalent groove Nusselt number which result from applying the finite element analysis developed in the preceding chapter to the problem under consideration in this investigation. Due to the nature of a numerical solution, however, the Nusselt number is available for only a discrete number of combinations of the problem parameters. Parameter combinations were therefore selected in such a fashion as to span a broad range of the variables and yet to be of practical utility. The number of test cases considered within this range is necessarily limited by cost and time considerations for the solution procurement. It is nevertheless felt by the investigators that the combinations presented in this chapter are indeed representative of situations of practical concern and that sufficient cases are presented to allow a meaningful interpolation of the results for situations that are not precisely described by the actual parameter values used in the study.

6.2 Parametric Study

Grooves of symmetric cross-section only are considered here but the program of Appendix D maintains the flexibility of solving the non-symmetric cross-section if it should be required by future investigators. In spite of the restriction to symmetric groove cross-sections, however, there are still four remaining independent solution parameters which must be considered. In view of this four parameter characterization, it is clear that the use of an increasing number of values for each of the independent parameters will soon cause the parametric study to become prohibitively expensive and time consuming.

The four parameters upon which the equivalent groove Nusselt number is dependent are given below.

The first is the apparent contact angle that the liquid free surface makes with the metal groove wall. In this study a normalized value is used for this angle and is given by $x_\alpha = \alpha/(\pi/2 - \theta_o)$ where θ_o is the groove half-angle. Clearly the range of x_α is $0 \leq x_\alpha \leq 1$. Four values of this parameter are considered in the study; x_α = 0.05, 0.25, 0.50, and 1.00. It is anticipated that due to hydrodynamic considerations of replenishment flow of working fluid to the evaporation sites, a value of $x_\alpha = 0.0$ cannot be physically sustained. The smallest value considered for x_α is therefore a value of 0.05. In the other limit, a full groove condition is indicated by a value of $x_\alpha = 1.00$. The intermediate value of 0.5 lies midway in the x_α range. The final value of 0.25 is provided in the region where a marked dependence is expected to occur in order to provide a more complete description of the dependence on this parameter. The expected higher sensitivity in the region of small x_α is supported by the numerical results.

The second parameter considered is the groove land area ratio. Due to the assumed symmetry of the geometry this is equal to the groove root area ratio. The groove land area ratio, ε, is defined as the ratio of the exposed land area of the fin tip to the total area of the typical cell. While the minimum value that this parameter can take on is necessarily zero, the maximum value is limited to 0.5 by the symmetry condition on the cross-section. The three values of ε selected for use in the parametric study are $\varepsilon = 0.01$, 0.25 and 0.49 with the exclusion of exact values of 0.0 and 0.50 due to the mesh generation requirements of the program. A value of $\varepsilon = 0.0$, that is no land area at all, corresponds to a groove profile of sharp 'V' configuration. In the other extreme, a value of $\varepsilon = 0.50$ dictates for a symmetric groove that the projected area is either originating from the groove fin tip or from the groove root. This profile is the rectangular profile common in moderate capacity, longitudinally extruded heat pipes. The intermediate value of $\varepsilon = 0.25$ is considered in order to provide a more complete description of the heat transfer dependence on this parameter.

The third parameter, d, is the groove depth in relation to the groove typical cell width and is an important parameter in considering the viscous losses experienced by the working fluid. While there are no physical limits on the range of values that can be considered (excepting unrealistically small values) it was felt by the investigators that the three cases $d = 1.0$, 1.5, and 2.0 would encompass the range of values typically encountered in heat pipe designs.

The final parameter considered in the heat transfer analysis is the conductivity ratio of the liquid to metal thermal conductivities. The high value considered of 0.1 represents an upper limit on the conductivity ratio while the low value of 0.001 represents an expected lower limit on the conductivity ratio, again considering typical moderate temperature heat pipe applications. The intermediate value was chosen as 0.01156 since it corresponds to a methanol/stainless steel heat pipe materials combination.

The numerical results of the parametric study to determine the equivalent groove Nusselt number are presented in tabular form in Tables 6-1, 6-2, and 6-3 for the conductivity ratios $k_f/k_m = 0.1$, 0.01156, and 0.001 respectively. The product $Nu_f \cdot k_f/k_m$ is treated as the dependent variable since, due to the normalization of the thermal problem with respect to the metal properties, a smaller overall variation results than would result by treating Nu_f as the dependent variable.

The numerical results are also presented graphically in figures 6-1 through 6-9. Here the systematic progression is assumed of fixing the conductivity ratio and land area ratio, and plotting the dependence of $Nu_f \cdot k_f/k_m$ on x_α with the groove depth d appearing as the parameter. In the progression, the land area ratio is monotonically increased through its range for a fixed conductivity ratio and then the conductivity ratio incremented to its next value.

A discussion of the results follows.

Table 6-1

$Nu \cdot k_f/k_m$

For Trapezoidal Grooves

			x_α			
k_f/k_m	d	$\varepsilon_1 = \varepsilon_2$	0.05	0.25	0.50	1.00
0.1	1.0	0.01	1.1336	.9422	.2056	.6628
0.1		0.25	1.0724	.9069	.7921	.6938
0.1		0.49	.8464	.7085	.6264	.5551
0.1	1.5	0.01	.7519	.6381	.5538	.4642
0.1		0.25	.7262	.6348	.5721	.5098
0.1		0.49	.5992	.5287	.4839	.4419
0.1	2.0	0.01	.5559	.4793	.4210	.3578
0.1		0.25	.5487	.4914	.4511	.4104
0.1		0.49	.4694	.4254	.3963	.3685

Table 6-2

$Nu \cdot k_f/k_m$

For Trapezoidal Grooves

k_f/k_m	d	$\varepsilon_1 = \varepsilon_2$	x_α 0.05	0.25	0.50	1.00
.01156	1.0	0.01	.5392	.4481	.4101	.3807
.01156		0.25	.6144	.5401	.5136	.4946
.01156		0.49	.4745	.4270	.4106	.3993
.01156	1.5	0.01	.3792	.3163	.2901	.2697
.01156		0.25	.4501	.3998	.3816	.3625
.01156		0.49	.3809	.3510	.3405	.3332
.01156	2.0	0.01	.2912	.2479	.2295	.2152
.01156		0.25	.3638	.3333	.3220	.3136
.01156		0.49	.3201	.2990	.2916	.2963

Table 6-3

$Nu \cdot k_f/k_m$

For Trapezoidal Grooves

k_f/k_m	d	$\varepsilon_1 = \varepsilon_2$	x_α 0.05	0.25	0.50	1.00
.001	1.0	0.01	.3688	.3483	.3421	.3389
.001		0.25	.4975	.4745	.4697	.4671
.001		0.49	.3953	.3828	.3802	.3788
.001	1.5	0.01	.2610	.2504	.2480	.2464
.001		0.25	.3723	.3618	.3596	.3581
.001		0.49	.3265	.3199	.3127	.2178
.001	2.0	0.01	.2030	.1957	.1942	.1907
.001		0.25	.3105	.3040	.3022	.3017
.001		0.49	.2793	.2752	.2744	.2737

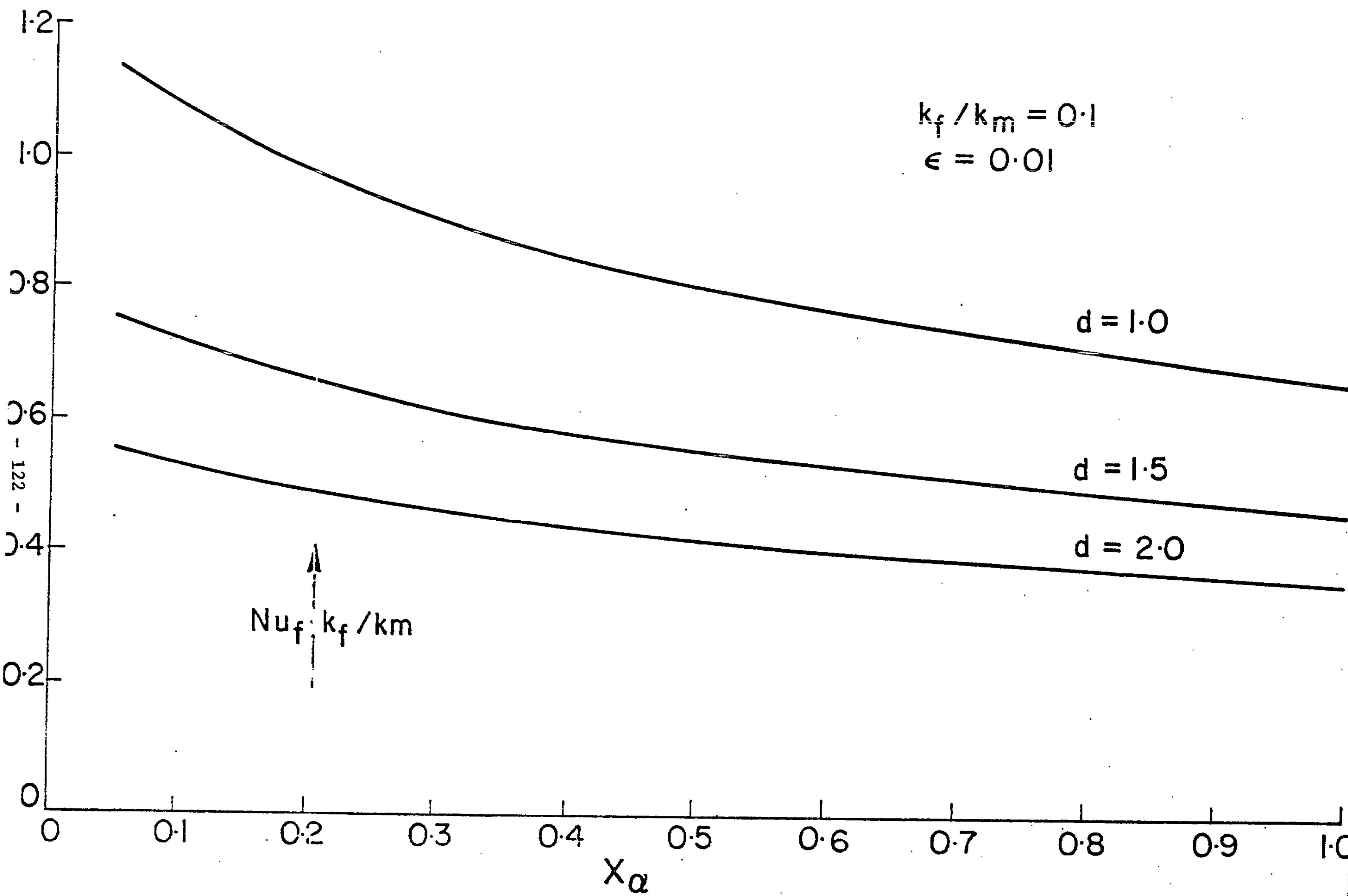
1·2
1·0
0·8
0·6
0·4
0·2
0
$k_f / k_m = 0·1$
$\epsilon = 0·01$
d = 1·0
d = 1·5
d = 2·0
$Nu_f \cdot k_f / km$
0
0·1
0·2
0·3
0·4
0·5
0·6
0·7
0·8
0·9
1·0
X_α

Figure 6-1

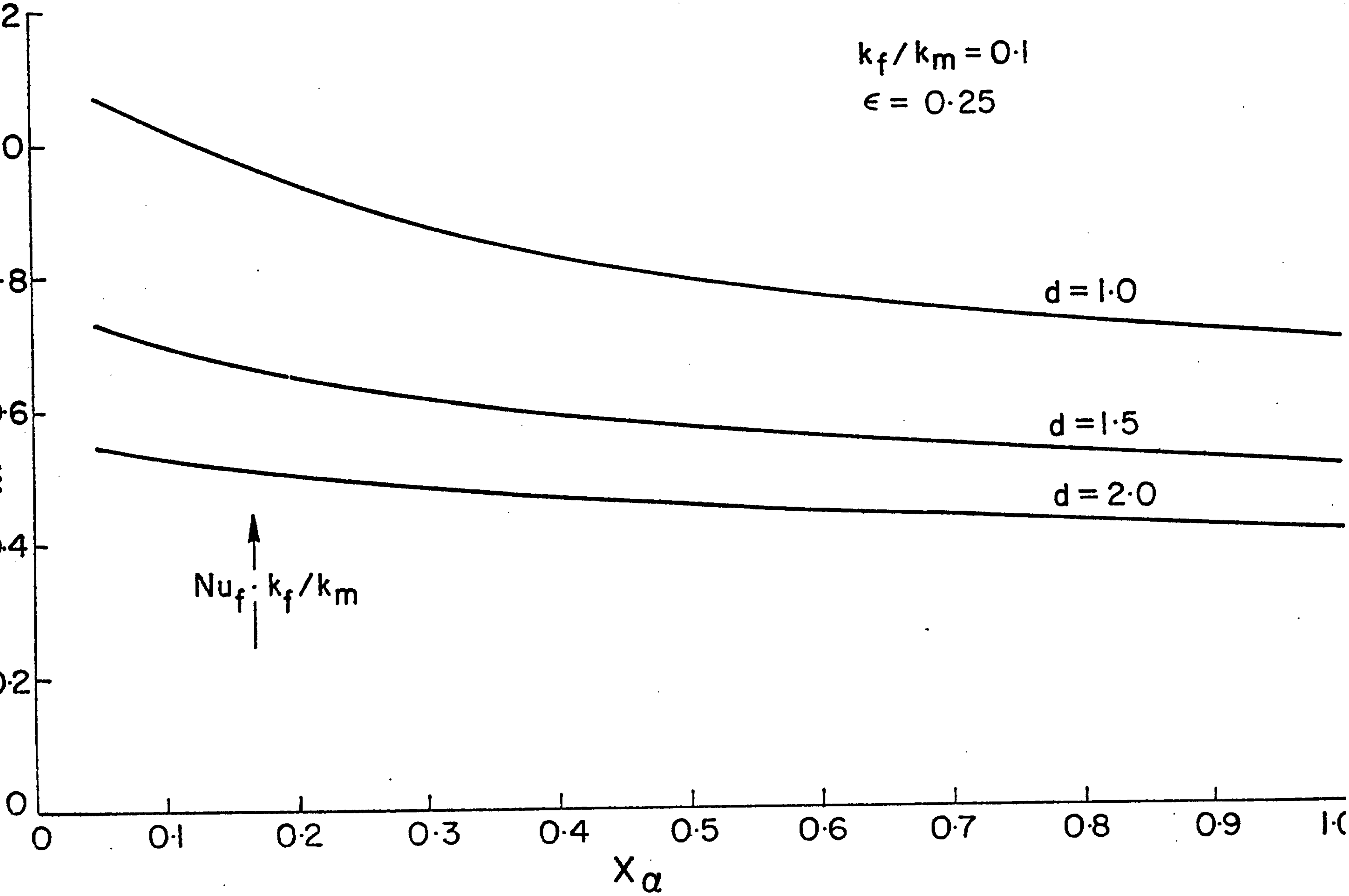

$k_f/k_m = 0{\cdot}1$
$\epsilon = 0{\cdot}25$
$d = 1{\cdot}0$
$d = 1{\cdot}5$
$d = 2{\cdot}0$
$Nu_f \cdot k_f/k_m$
X_a
0
0·1
0·2
0·3
0·4
0·5
0·6
0·7
0·8
0·9
1·0
1·2

Figure 6-2

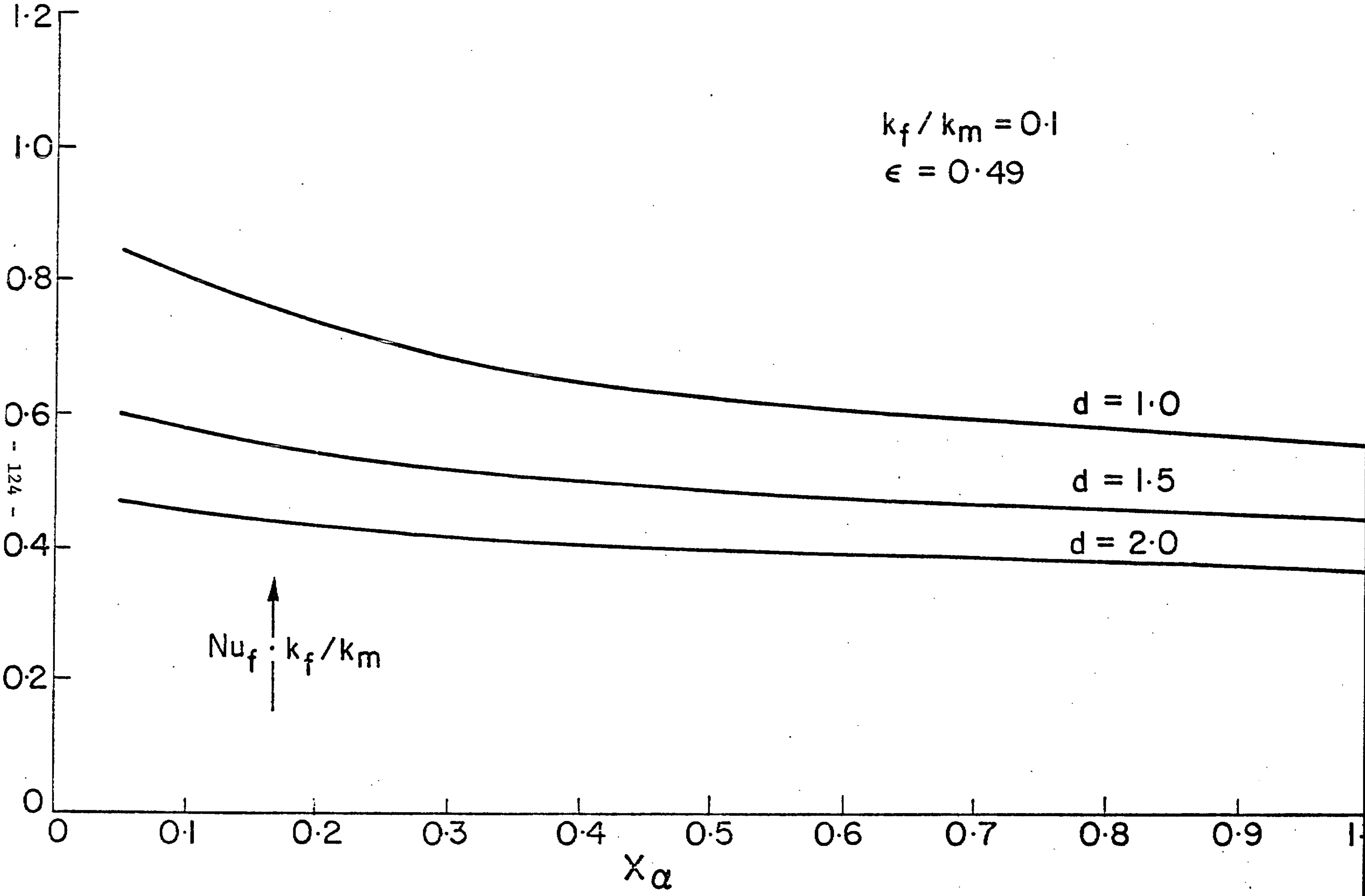

1·2
1·0
0·8
0·6
0·4
0·2
0
0
0·1
0·2
0·3
0·4
0·5
0·6
0·7
0·8
0·9
1
$k_f / k_m = 0·1$
$\epsilon = 0·49$
d = 1·0
d = 1·5
d = 2·0
$Nu_f \cdot k_f / k_m$
X_α

Figure 6-3

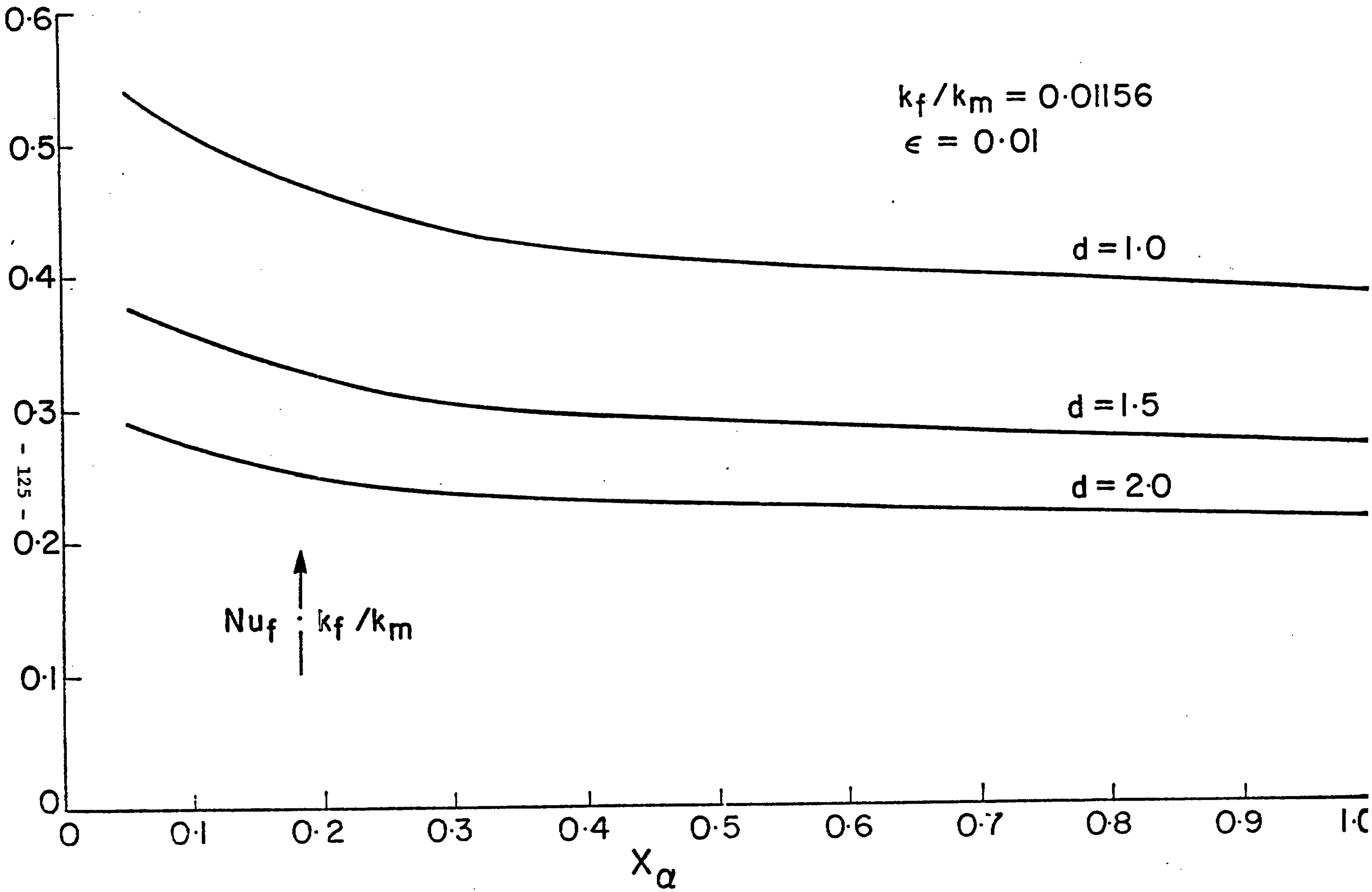

$k_f/k_m = 0{\cdot}01156$
$\epsilon = 0{\cdot}01$
d = 1·0
d = 1·5
d = 2·0
$Nu_f \cdot k_f/k_m$
X_α
0·6
0·5
0·4
0·3
0·2
0·1
0
0
0·1
0·2
0·3
0·4
0·5
0·6
0·7
0·8
0·9
1·0

Figure 6-4

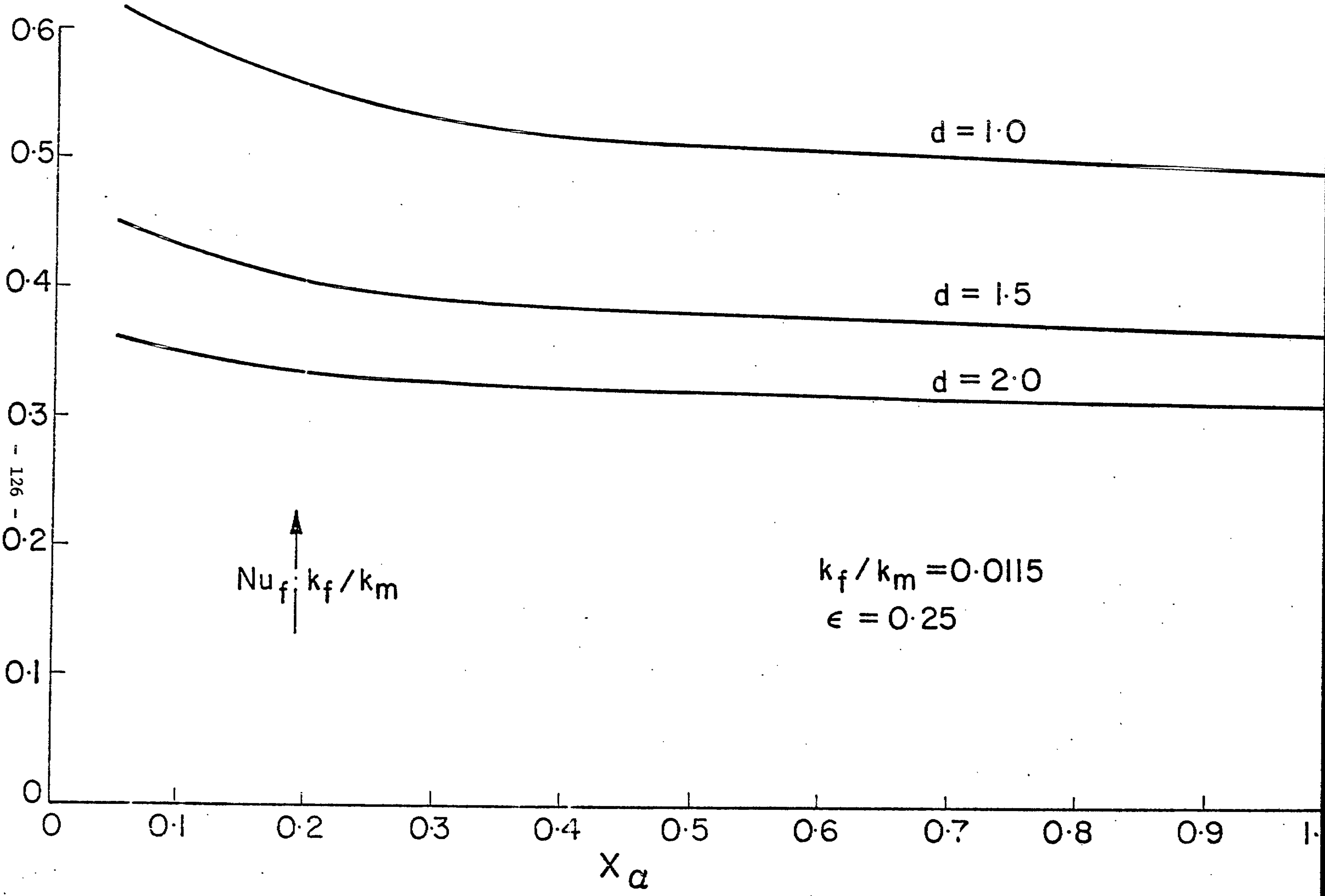
0·6
0·5
0·4
0·3
0·2
0·1
0
d = 1·0
d = 1·5
d = 2·0
$Nu_f\ k_f/k_m$
$k_f/k_m = 0{\cdot}0115$
$\epsilon = 0{\cdot}25$
0
0·1
0·2
0·3
0·4
0·5
0·6
0·7
0·8
0·9
1·
X_a

igu -5

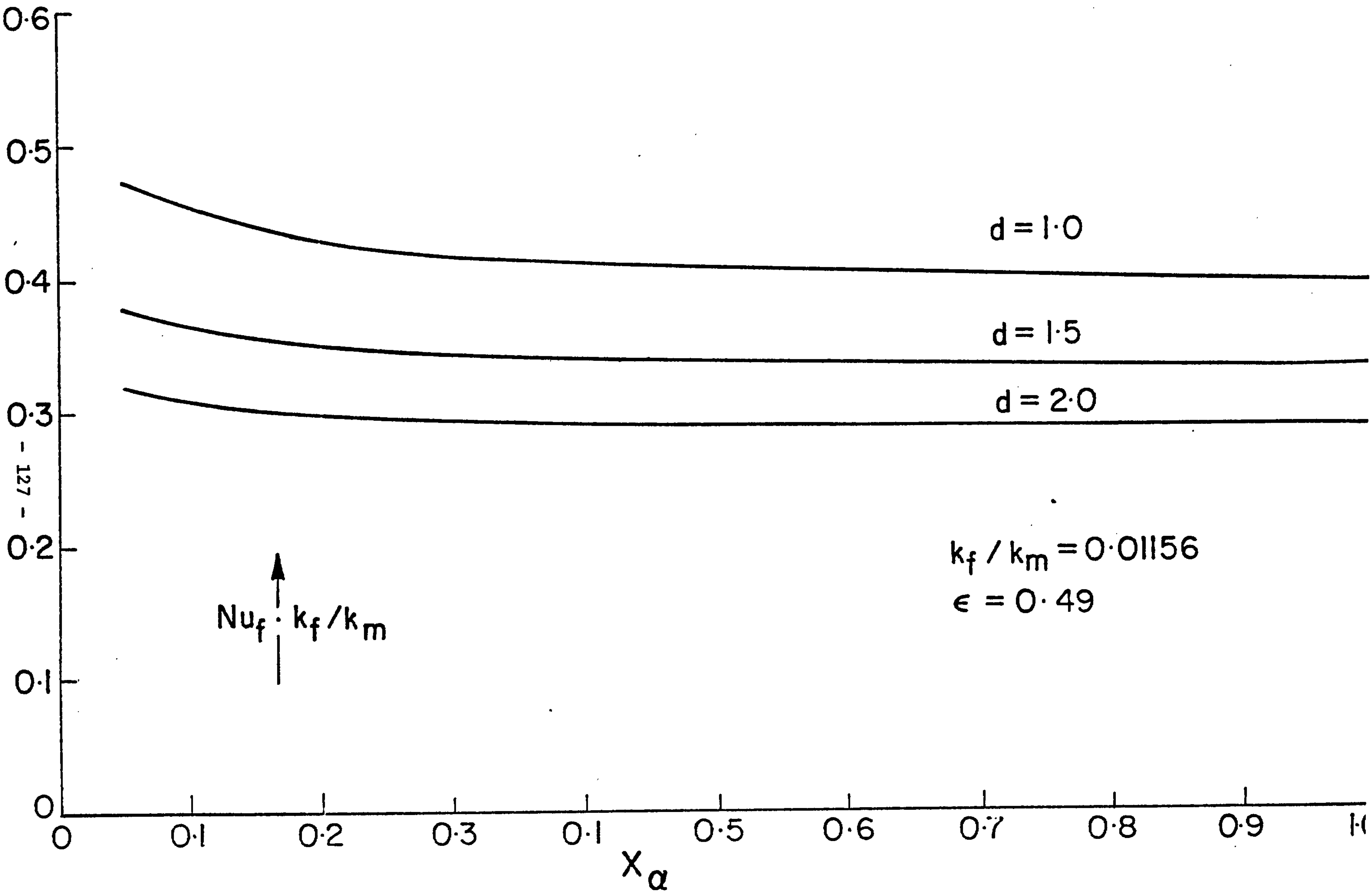
0·6
0·5
0·4
0·3
0·2
0·1
0
d = 1·0
d = 1·5
d = 2·0
kf / km = 0·01156
ε = 0·49
Nuf · kf /km
0
0·1
0·2
0·3
0·1
0·5
0·6
0·7
0·8
0·9
Xα

Figure 6-6

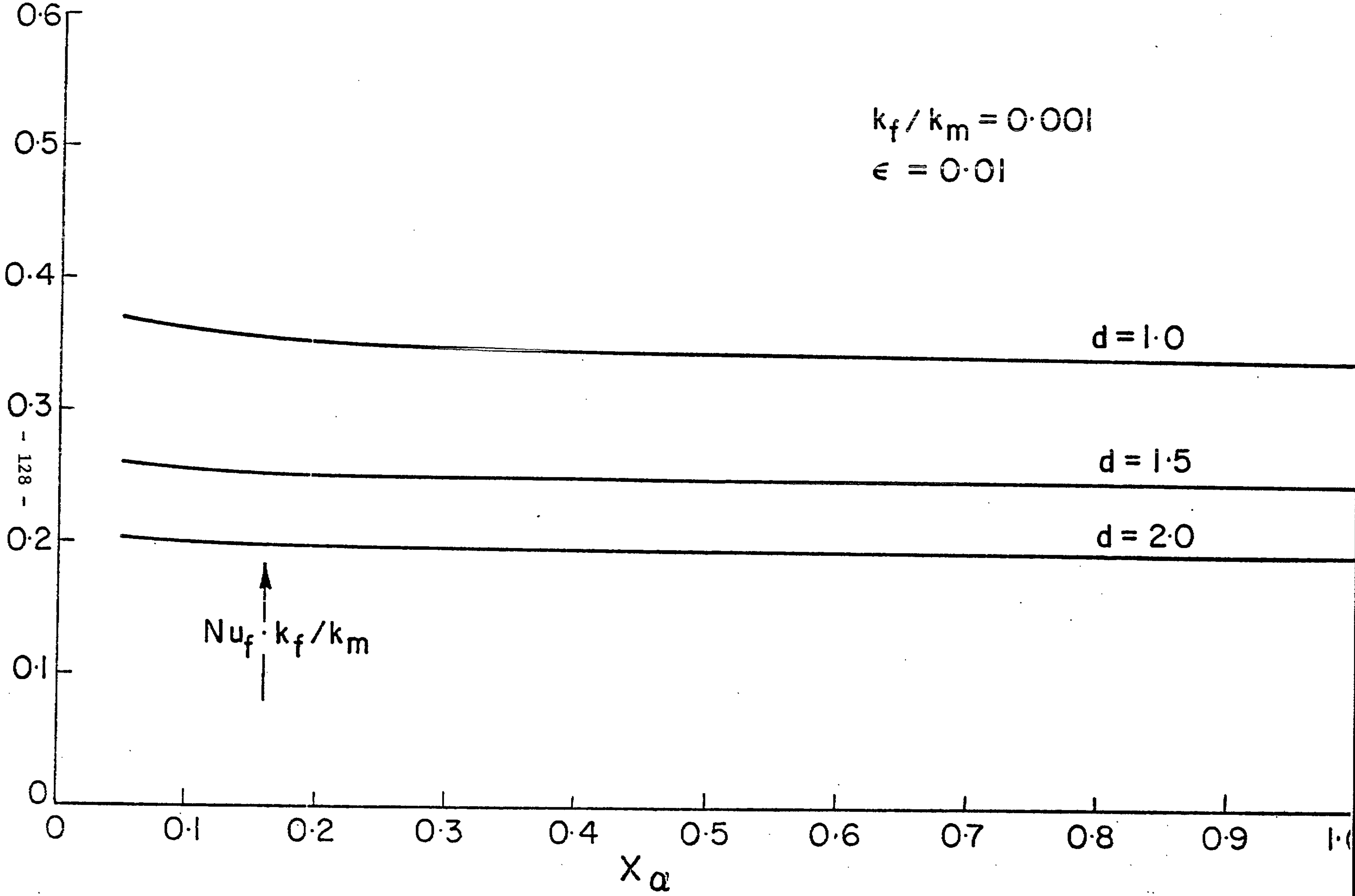
0·6
0·5
0·4
0·3
0·2
0·1
0
$k_f / k_m = 0·001$
$\epsilon = 0·01$
d = 1·0
d = 1·5
d = 2·0
$Nu_f \cdot k_f / k_m$
0
0·1
0·2
0·3
0·4
0·5
0·6
0·7
0·8
0·9
X_α

Figure 6-7

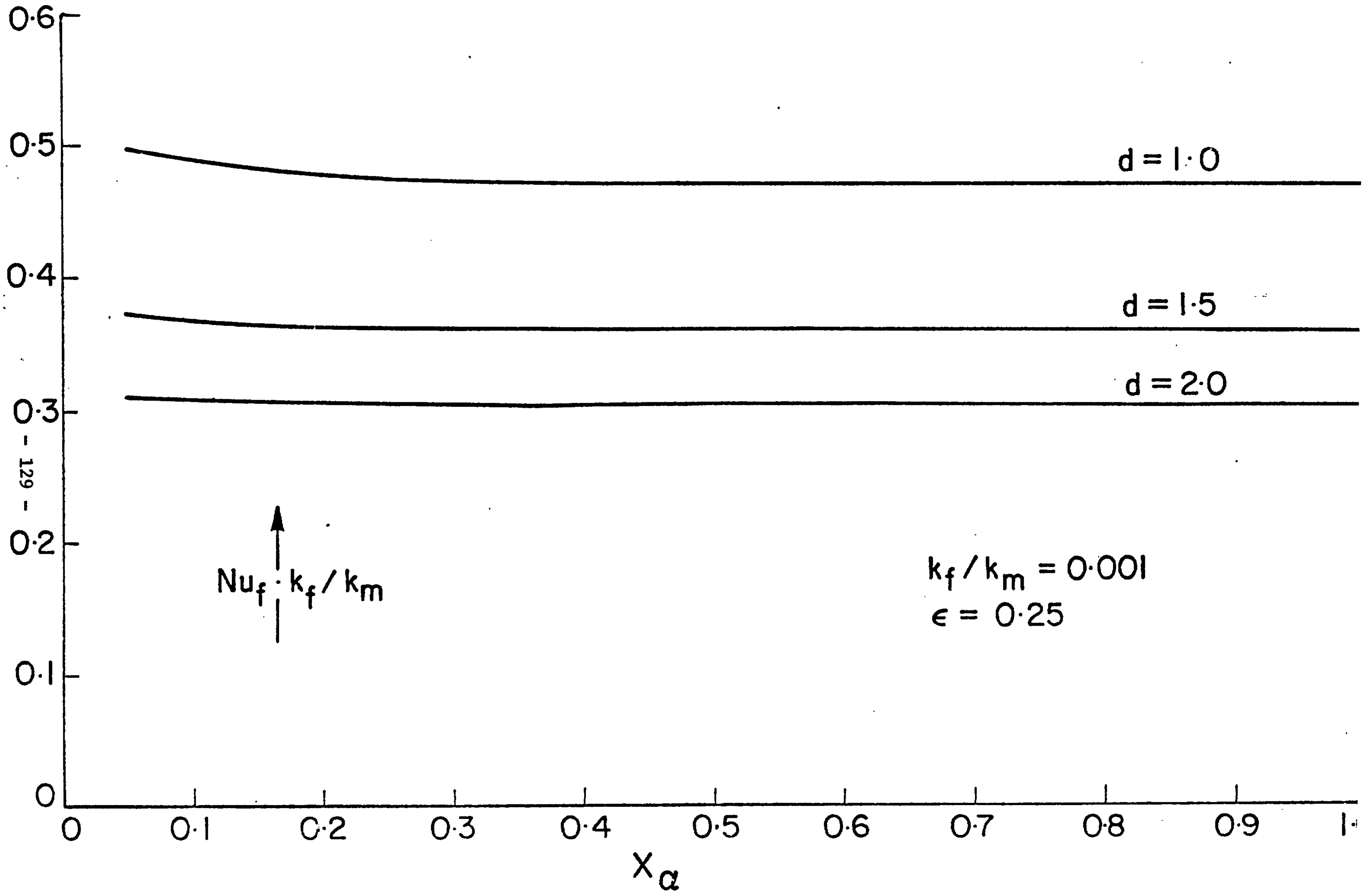
0·6
0·5
0·4
0·3
0·2
0·1
0
d = 1·0
d = 1·5
d = 2·0
$Nu_f \cdot k_f / k_m$
$k_f / k_m = 0{\cdot}001$
$\epsilon = 0{\cdot}25$
0
0·1
0·2
0·3
0·4
0·5
0·6
0·7
0·8
0·9
1·
X_α

Figure 6-8

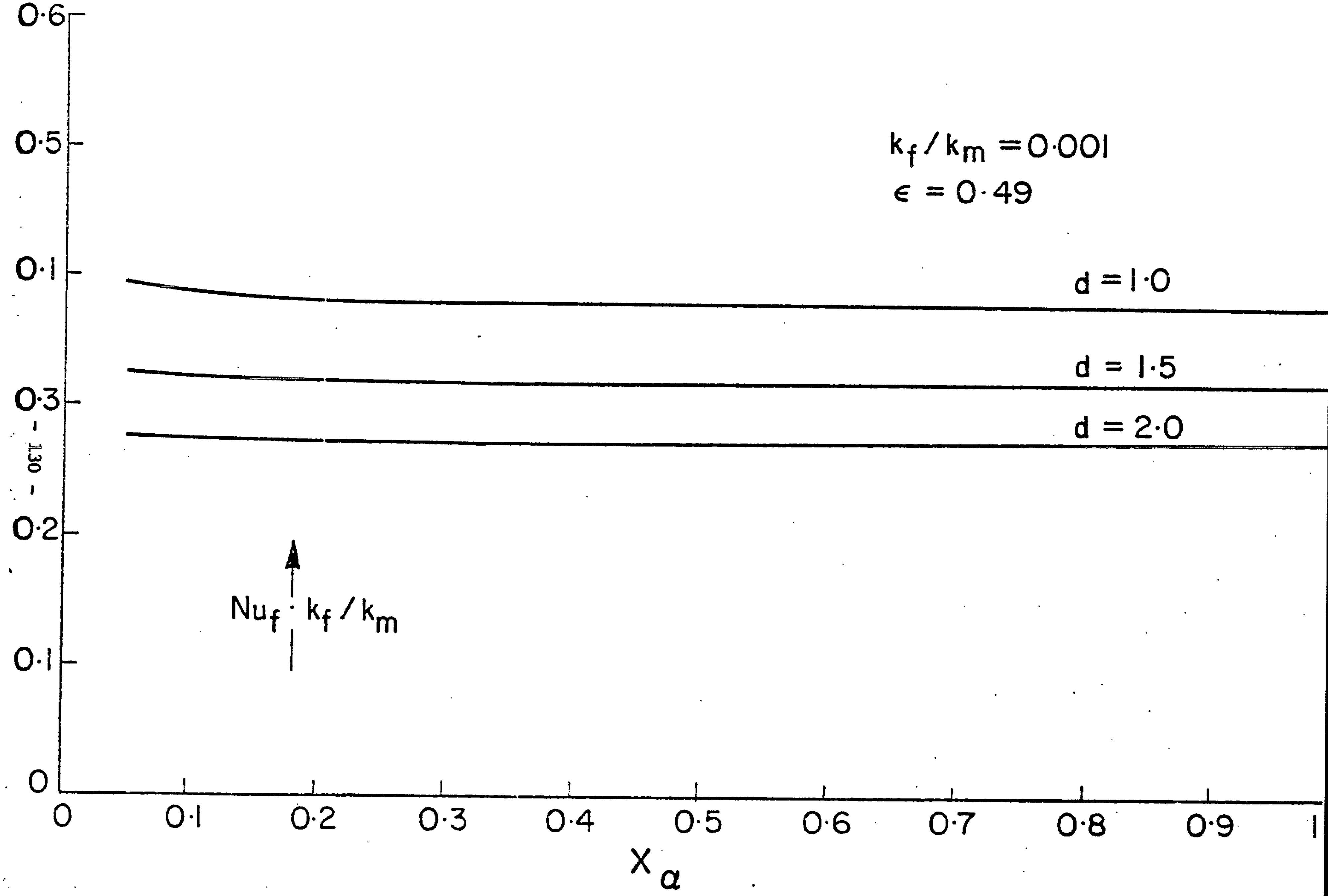
0·6
0·5
0·1
0·3
0·2
0·1
0
$k_f / k_m = 0·001$
$\epsilon = 0·49$
d = 1·0
d = 1·5
d = 2·0
$Nu_f \cdot k_f / k_m$
0
0·1
0·2
0·3
0·4
0·5
0·6
0·7
0·8
0·9
1
X_α

Figure 6-9

6.3 Discussion of the Results

On examining the characteristics of figures 6-1 through 6-9, it becomes clear that in every case the equivalent Nusselt number decreases monotonically with increasing x_α. Indeed, this is to be expected since in all cases it is the low thermal conductivity of the liquid working fluid that causes a preferential migration of the heat flow. This migration is through the metal to the location where the escape route through the liquid, in conjunction with the resistance of the metal heat flow path, offers the least resistance to the heat flow. For the cases considered this will invariably result in a concentration of the heat flow lines near the meniscus contact with the groove wall. Clearly, then, the shorter the liquid path that must be traversed in this region, the lower will be the total resistance and consequently the equivalent Nusselt number will be higher for these shorter liquid path cases. Now, the problem geometry dictates that the liquid heat flow path will be reduced as the apparent contact angle, and hence x_α for all other parameters fixed, is decreased. Thus, it is to be expected that, as x_α is decreased from the full groove condition, $x_\alpha = 1.0$, to a state of near tangency, $x_\alpha = 0.05$, the groove equivalent Nusselt number will increase. This expected behavior is consistent with that displayed by the numerical results. It is noted here, however, that the dependence of the groove Nusselt number on x_α is a relatively mild one. This is in contrast with the extremely sensitive behavior suggested by a previous solution [16] in which the metal groove wall was assumed isothermal from the root to the fin tip. The relaxed dependence on x_α displayed by figures 6-1 through 6-9 illustrates the importance that the active participation of the metal section has on the determination of the overall heat transfer for the composite problem. This influence is particularly important in the region near the meniscus contact since the local concentration of the heat flow there results in a rapidly changing groove wall temperature in this region, which is in contradiction to the formerly assumed isothermal condition.

The second trend which is observed in the numerical results is that as the groove depth increases, the groove Nusselt number decreases. This too is consistent with the problem physics. Following the arguments above, it is anticipated that there will be a large adjustment of the thermal flow field in the region near the meniscus contact, and thus the dominating influence in the determination of the metal/liquid interaction stems from this region. Consequently, in the remainder of the fin the flow field is quasi-uniform in the sense that local gradients are primarily determined by the total heat flow rate, and the local area, with only small contributions due to the bulk fluid adjacent to these regions. As a result, the influence of increasing d will be to add a section of pure conductive, variable area, metal in addition to that for the case of smaller groove depth. A secondary influence of increasing the depth for a fixed land area ratio is that the problem geometry is necessarily altered. Thus, θ_o changes, with the associated influence on $x_\alpha = \alpha/(\pi/2 - \theta_o)$, and even the local behavior at the meniscus contact is slightly altered. Here, then, we see that the variation of one parameter has an influence on the interpretation of the trends displayed by another. Taking into account this influence, calculation indicates that it is primarily the conductive differences in the metal which account for the decreasing Nusselt number dependence with increasing groove depth.

The influence of the conductivity ratio, k_f/k_m, is to decrease the product $Nu_f \cdot k_f/k_m$ as the conductivity ratio is decreased. This also is physically consistent since as the conductivity of the liquid decreases, the heat flow becomes more concentrated within the metal, particularly near the fin tip. This increased heat flow concentration results in a higher resistance within the metal section, and is additive to the higher liquid film resistance due directly to its decreased thermal conductivity. This behavior is consistent with a decreasing $Nu_f \cdot k_f/k_m$ product with decreasing conductivity ratio.

The influence of changing land area ratio, however, is not monotonic as in the case of the previous three parameters, but rather produces, generally, a maximum value of the product $Nu_f \cdot k_f/k_m$ within the three cases studied for a land area ratio of $\varepsilon = 0.25$. Exception to this occurs at small apparent contact angles for a conductivity ratio of $k_f/k_m = 0.1$. Considering the range of this land area ratio, $0 \leq \varepsilon \leq 0.5$, the geometric changes resulting from changes in ε as the full range is traversed, are severe. Indeed, due to the severe geometric changes incurred by the variation of ε, it is difficult to anticipate precisely the influence of this parameter on the overall heat transfer since the resulting geometric changes influence both the liquid and the metal region geometries, and consequently the liquid/metal thermal interaction. It is felt that the maximum value of the $Nu_f \cdot k_f/k_m$ product is the result of a favorable balance between the changing pure conductive resistance and the changing liquid/metal interaction, each of which is changing at a different rate. This observed behavior is consistent for the combinations of parameters considered in this report.

6.4 Correlations of the Equivalent Nusselt Number

As we have noted earlier, the equivalent groove Nusselt number is dependent upon four parameters. As a consequence correlation efforts become extremely complicated when attempting to maintain acceptable accuracy. For example, if the observed trends are second order in each of the parameters, then three correlation parameters are required to account for the dependence on x_α, say, and for each of these parameters, three additional parameters are required to account for the dependence on d, and so on. This yields a total of $3^4 = 81$ correlation parameters and results in a correlation equation of extreme complexity. In contrast, if only a few parameters are employed, the resulting correlation may be of inadequate accuracy to be of significant practical utility. In this work a compromise has been adopted to yield a correlation of manageable complexity while maintaining adequate accuracy for engineering calculations.

On examination of figures 6-1 through 6-9, it was felt that a two parameter correlation of each curve independently of the form

$$Nu_f \cdot k_f / k_m = A \ln (x_\alpha) + B \qquad (6\text{-}1)$$

might provide adequate accuracy for engineering purposes. Indeed application of equation (6-1) to each of the curves independently using a least squares curve-fit subroutine yielded a maximum correlation error at the data points of four per cent. It is anticipated, however, that with the inclusion of the remaining three parameter dependencies, the obtainable accuracy will become somewhat relaxed.

Incorporating next the dependence of $Nu_f \cdot k_f/k_m$ on the land area ratio, ε, a correlation equation of the form

$$Nu_f \cdot k_f/k_m = [A_{11}\varepsilon + A_{12}] \ln(x_\alpha) + [B_{11}\varepsilon^2 + B_{12}\varepsilon + B_{13}] \qquad (6\text{-}2)$$

was found to relax the obtainable accuracy to approximately five per cent.

A further inclusion of the dependence on the groove depth was made by assuming the above correlation constants to be of the form

$$\begin{aligned} A_{11} &= A_{111}\, D + A_{112} \\ A_{12} &= A_{121}\, D + A_{122} \\ B_{11} &= B_{111}\, D + B_{112} \\ B_{12} &= B_{121}\, D + B_{122} \\ B_{13} &= B_{131} \exp(B_{132}\, D) + B_{133} \end{aligned} \qquad (6\text{-}3)$$

Application of the correlation constants (6-3) in equation (6-2) yielded a further relaxation requirement on the accuracy to approximately six per cent.

Inclusion of the final correlation parameter, the conductivity ratio, k_f/k_m, was made by considering the influence to be dependent on $\ln(k_f/k_m)$ and assuming this influence to be quadratic in $\ln(k_f/k_m)$. This yielded a maximum correlation error at the data points of seven per cent, with errors of this order occuring at only a few locations for the case where $k_f/k_m = 0.1$.

The final correlation equation for the equivalent groove Nusselt number is given by

$$Nu_f \cdot k_f/k_m = A \ln(x_\alpha) + B \tag{6-4}$$

where

$$A = A_1 [-.389 d + 1]\varepsilon + A_2 [-.376 d + 1] \tag{6-5}$$

$$\begin{aligned} B = {} & B_1 [-.29 \ d + 1]\varepsilon^2 \\ & + B_2 [-.228 d + 1]\varepsilon \\ & + B_3 [5.368 \exp(-1.295 D) + 1] \end{aligned} \tag{6-6}$$

and finally

$$A_1 = .0056 \ln^2(k_f/k_m) + .1025 \ln(k_f/k_m) + .4511 \tag{6-7}$$

$$A_2 = -.0098 \ln^2(k_f/k_m) - .1413 \ln(k_f/k_m) - .5251 \tag{6-8}$$

$$B_1 = .0336 \ln^2(k_f/k_m) + .4557 \ln(k_f/k_m) - 1.0821 \tag{6-9}$$

$$B_2 = -.0407 \ln^2(k_f/k_m) - .5090 \ln(k_f/k_m) - .2668 \tag{6-10}$$

$$B_3 = .0105 \ln^2(k_f/k_m) + .1254 \ln(k_f/k_m) + 0.4986 \tag{6-11}$$

A comparison of the correlation values for $Nu_f \cdot k_f/k_m$ with the numerical data points is presented in Table 6-4. It is seen from the table that the largest errors, 7.01, 6.28, 5.77, 5.66, and 5.13 per cent, are confined to the case where $k_f/k_m = 0.1$. All other cases yield errors less than five per cent. Indeed, as the entries for $k_f/k_m = 0.0116$ are examined, the correlation agreement is within four per cent. The maximum error of correlation for $k_f/k_m = 0.001$ is further reduced to 3.4 per cent. It is felt that a maximum correlation error of seven per cent is adequate for most heat pipe analysis and design

Table 6-4

COND RATIO	D	E	XALPHA	(KF/KM)* NU(CORR)	(KF/KM)* NU(ACT)	% ERROR
0.1000	1.0000	0.0100	0.0500	1.1267	1.1336	-0.6120
0.1000	1.0000	0.0100	0.2500	0.8766	0.9427	-7.0162
0.1000	1.0000	0.0100	0.5000	0.7688	0.8056	-4.5625
0.1000	1.0000	0.0100	1.0000	0.6611	0.6628	-0.2520
0.1000	1.0000	0.2500	0.0500	1.0611	1.0724	-1.0507
0.1000	1.0000	0.2500	0.2500	0.8688	0.9069	-4.1994
0.1000	1.0000	0.2500	0.5000	0.7860	0.7981	-1.5174
0.1000	1.0000	0.2500	1.0000	0.7032	0.6938	1.3495
0.1000	1.0000	0.4900	0.0500	0.8375	0.8464	-1.0530
0.1000	1.0000	0.4900	0.2500	0.7030	0.7085	-0.7821
0.1000	1.0000	0.4900	0.5000	0.6450	0.6264	2.9726
0.1000	1.0000	0.4900	1.0000	0.5871	0.5551	5.7615
0.1000	1.5000	0.0100	0.0500	0.7995	0.7519	6.3369
0.1000	1.5000	0.0100	0.2500	0.6248	0.6381	-2.0835
0.1000	1.5000	0.0100	0.5000	0.5495	0.5538	-0.7678
0.1000	1.5000	0.0100	1.0000	0.4743	0.4642	2.1738
0.1000	1.5000	0.2500	0.0500	0.7675	0.7262	5.6848
0.1000	1.5000	0.2500	0.2500	0.6322	0.6348	-0.4160
0.1000	1.5000	0.2500	0.5000	0.5739	0.5721	0.3108
0.1000	1.5000	0.2500	1.0000	0.5156	0.5098	1.1372
0.1000	1.5000	0.4900	0.0500	0.6108	0.5992	1.9279
0.1000	1.5000	0.4900	0.2500	0.5148	0.5287	-2.6204
0.1000	1.5000	0.4900	0.5000	0.4735	0.4839	-2.1406
0.1000	1.5000	0.4900	1.0000	0.4322	0.4419	-2.1866
0.1000	2.0000	0.0100	0.0500	0.5611	0.5559	0.9365
0.1000	2.0000	0.0100	0.2500	0.4617	0.4793	-3.6664
0.1000	2.0000	0.0100	0.5000	0.4189	0.4210	-0.4925
0.1000	2.0000	0.0100	1.0000	0.3761	0.3578	5.1219
0.1000	2.0000	0.2500	0.0500	0.5625	0.5487	2.5165
0.1000	2.0000	0.2500	0.2500	0.4842	0.4914	-1.4699
0.1000	2.0000	0.2500	0.5000	0.4504	0.4511	-0.1460
0.1000	2.0000	0.2500	1.0000	0.4167	0.4104	1.5366
0.1000	2.0000	0.4900	0.0500	0.4727	0.4694	0.7009
0.1000	2.0000	0.4900	0.2500	0.4154	0.4254	-2.3490
0.1000	2.0000	0.4900	0.5000	0.3907	0.3963	-1.4038
0.1000	2.0000	0.4900	1.0000	0.3661	0.3685	-0.6604
0.0116	1.0000	0.0100	0.0500	0.5387	0.5392	-0.0909
0.0116	1.0000	0.0100	0.2500	0.4504	0.4481	0.5228
0.0116	1.0000	0.0100	0.5000	0.4124	0.4101	0.5677
0.0116	1.0000	0.0100	1.0000	0.3744	0.3807	-1.6513
0.0116	1.0000	0.2500	0.0500	0.6064	0.6144	-1.2974
0.0116	1.0000	0.2500	0.2500	0.5430	0.5401	0.5305
0.0116	1.0000	0.2500	0.5000	0.5156	0.5136	0.3959
0.0116	1.0000	0.2500	1.0000	0.4883	0.4946	-1.2736
0.0116	1.0000	0.4900	0.0500	0.4761	0.4745	0.3420
0.0116	1.0000	0.4900	0.2500	0.4375	0.4270	2.4504
0.0116	1.0000	0.4900	0.5000	0.4208	0.4106	2.4874
0.0116	1.0000	0.4900	1.0000	0.4042	0.3993	1.2180

0.0116	1.5000	0.0100	0.0500	0.3842	0.3792	1.3277
0.0116	1.5000	0.0100	0.2500	0.3226	0.3163	1.979
0.0116	1.5000	0.0100	0.5000	0.2960	0.2901	2.033
0.0116	1.5000	0.0100	1.0000	0.2694	0.2697	-0.0967
0.0116	1.5000	0.2500	0.0500	0.4567	0.4501	1.4621
0.0116	1.5000	0.2500	0.2500	0.4119	0.3998	3.033
0.0116	1.5000	0.2500	0.5000	0.3927	0.3816	2.8963
0.0116	1.5000	0.2500	1.0000	0.3734	0.3685	1.3237
0.0116	1.5000	0.4900	0.0500	0.3730	0.3809	-2.076
0.0116	1.5000	0.4900	0.2500	0.3452	0.3510	-1.664
0.0116	1.5000	0.4900	0.5000	0.3332	0.3405	-2.153
0.0116	1.5000	0.4900	1.0000	0.3212	0.3332	-3.607
0.0116	2.0000	0.0100	0.0500	0.2792	0.2912	-4.137
0.0116	2.0000	0.0100	0.2500	0.2441	0.2479	-1.543
0.0116	2.0000	0.0100	0.5000	0.2290	0.2295	-0.232
0.0116	2.0000	0.0100	1.0000	0.2139	0.2152	-0.623
0.0116	2.0000	0.2500	0.0500	0.3563	0.3638	-2.054
0.0116	2.0000	0.2500	0.2500	0.3303	0.3333	-0.905
0.0116	2.0000	0.2500	0.5000	0.3191	0.3220	-0.911
0.0116	2.0000	0.2500	1.0000	0.3078	0.3136	-1.834
0.0116	2.0000	0.4900	0.0500	0.3193	0.3201	-0.264
0.0116	2.0000	0.4900	0.2500	0.3022	0.2990	1.084
0.0116	2.0000	0.4900	0.5000	0.2949	0.2916	1.137
0.0116	2.0000	0.4900	1.0000	0.2876	0.2863	0.451
0.0010	1.0000	0.0100	0.0500	0.3645	0.3688	-1.176
0.0010	1.0000	0.0100	0.2500	0.3500	0.3483	0.494
0.0010	1.0000	0.0100	0.5000	0.3438	0.3424	0.410
0.0010	1.0000	0.0100	1.0000	0.3376	0.3389	-0.387
0.0010	1.0000	0.2500	0.0500	0.4874	0.4975	-2.029
0.0010	1.0000	0.2500	0.2500	0.4752	0.4745	0.146
0.0010	1.0000	0.2500	0.5000	0.4699	0.4697	0.050
0.0010	1.0000	0.2500	1.0000	0.4647	0.4671	-0.517
0.0010	1.0000	0.4900	0.0500	0.3977	0.3953	0.606
0.0010	1.0000	0.4900	0.2500	0.3877	0.3828	1.285
0.0010	1.0000	0.4900	0.5000	0.3834	0.3802	0.847
0.0010	1.0000	0.4900	1.0000	0.3791	0.3788	0.085
0.0010	1.5000	0.0100	0.0500	0.2620	0.2610	0.365
0.0010	1.5000	0.0100	0.2500	0.2519	0.2504	0.585
0.0010	1.5000	0.0100	0.5000	0.2475	0.2480	-0.192
0.0010	1.5000	0.0100	1.0000	0.2432	0.2464	-1.307
0.0010	1.5000	0.2500	0.0500	0.3748	0.3723	0.678
0.0010	1.5000	0.2500	0.2500	0.3663	0.3618	1.232
0.0010	1.5000	0.2500	0.5000	0.3626	0.3596	0.826
0.0010	1.5000	0.2500	1.0000	0.3589	0.3581	0.218
0.0010	1.5000	0.4900	0.0500	0.3200	0.3265	-1.981
0.0010	1.5000	0.4900	0.2500	0.3130	0.3199	-2.151
0.0010	1.5000	0.4900	0.5000	0.3100	0.3187	-2.745
0.0010	1.5000	0.4900	1.0000	0.3069	0.3176	-3.424
0.0010	2.0000	0.0100	0.0500	0.2037	0.2030	0.366
0.0010	2.0000	0.0100	0.2500	0.1980	0.1957	1.179
0.0010	2.0000	0.0100	0.5000	0.1955	0.1942	0.689
0.0010	2.0000	0.0100	1.0000	0.1931	0.1927	0.191
0.0010	2.0000	0.2500	0.0500	0.3065	0.3105	-1.274
0.0010	2.0000	0.2500	0.2500	0.3016	0.3040	-0.783
0.0010	2.0000	0.2500	0.5000	0.2995	0.3028	-1.090
0.0010	2.0000	0.2500	1.0000	0.2974	0.3017	-1.432
0.0010	2.0000	0.4900	0.0500	0.2867	0.2743	2.634
0.0010	2.0000	0.4900	0.2500	0.2825	0.2752	2.669
0.0010	2.0000	0.4900	0.5000	0.2808	0.2744	2.323
0.0010	2.0000	0.4900	1.0000	0.2790	0.2737	1.938

calculations of engineering interest, and that the correlation equations (6-4) - (6-11) adequately maintain this agreement while keeping the correlation equation manageable.

6.5 Conclusions

In the present chapter of this report the results of a parametric study to explore the dependence of the equivalent groove Nusselt number on the four parameters, the apparent contact angle, the groove land area ratio, the groove depth, and the liquid/metal thermal conductivity ratio, were presented. These results were found to be self-consistent in their behavioral characteristics and to generally display the dependencies that are anticipated from consideration of the physics of the underlying thermal problem under investigation. The displayed trends however, illustrate a somewhat relaxed dependence on the apparent contact angle than that given by a previous approximate solution [16]. This demonstrates the importance of the contribution to the overall thermal problem that is due to the metal fin region and that the problem analysed is truly a composite thermal problem. Both the liquid region, the metal region, and the thermal interaction between the two regions along their common interface, are important contributions to the total problem solution and must all be considered.

Finally, in closing the chapter, a correlation equation has been determined which interpolates the numerical data with a maximum error of seven per cent. It is felt that this correlation equation will be adequate for most engineering applications of heat pipe analysis and design.

Chapter 7

Application of the Results

7.1 Introduction

In the previous chapter a study was conducted to determine the influence of the apparent contact angle, the groove land area ratio, the groove depth, and the liquid/metal thermal conductivity ratio, on the equivalent groove Nusselt number. These factors are all important considerations in designing a heat pipe to meet prescribed operating conditions. In many cases, however, a compromise must often be found, in particular for the geometric details of the grooves, which strikes a balance between counteracting thermal and hydrodynamic influences of a parameter change. For example, if the pipe conductance must not fall below a prescribed minimum value, then parameter changes on the groove cross-section can be effected to provide the required conductance value. However, the design changes made must not sufficiently alter the hydrodynamics of the pipe such that the available capillary forces cannot provide a sufficient recirculation rate to meet the thermal loading requirements of the particular heat pipe application. This balance, however, is not the subject of this report and will not be dealt with further here.

For a given heat pipe design, of the four variable parameters examined in chapter 6 of this report there are three which are fixed by the design, while the fourth remains free to vary as the operational conditions dictate. This fourth parameter is the apparent contact angle, and, having selected a particular set of design parameters, is the only parameter which will lead to heat pipe exterior surface temperature variations within each of the evaporator, adiabatic, and condenser sections of the heat pipe. Indeed the apparent contact angle variation is itself implicitly dependent upon the operational temperature and pressure, the imposed thermal loading, the groove material and transport fluid properties, the change of working fluid present, and the groove geometry for the particular heat pipe application of interest.

Since an examination of each of the above influences independently would require an investigation of enormous proportions, this chapter is directed at determining the influence that the working contact angle will have on the surface temperature distribution of an operational heat pipe. The results of this analysis can then be used as a basis for evaluating the need for future, more fundamental investigations into the contact angle behavior.

7.2 Case I

7.2.1 Pipe Geometry and Thermal Loading

The computer code developed under the CRC 6656-1 (SCS) program will be used to determine the surface temperature distribution for a heat pipe having the specifications indicated below. The influence of the minimum break-away contact angle on the surface temperature variation will also be examined. The heat pipe specifications follow:

Pipe:

$L_e = 1.67$ ft.

$L_a = 0.646$ ft.

$L_c = 2.33$ ft.

$L = 4.646$ ft.

$r_{out} = .02083$ ft.

$r_{in} = .0188$ ft.

Material = S.S. type 304 ($k_m = 10 \frac{Btu}{hr.ft.^oF}$

V-grooves:	Pitch = 1056 per foot
	Depth = 6.67×10^{-4} ft.
	$\theta_o = 35.38^o$
Arteries:	Number = 3 arteries with 2 sizes 1) .120 in. I.D. (2 layers of screen), (1) 2) .060 in. I.D. (7 layers of screen), (2)
	Material = 150 mesh, .003 in. thick type 316 stainless steel screen
	Configuration = interference fit across a diameter, in-line
Working fluid:	Fluid = methanol, laboratory grade $k_f \doteq 0.1156$ Btu/hr.ft.^{o}F
Thermal loading:	Evaporator Flux = 15,000 Btu/hr.ft.^{2} (uniform over evaporator)
	Ambient Condenser Temperature = 0^oF
	Condenser External Surface Heat Transfer Coefficient = 1000 Btu/hr.ft.^{2}F (uniform over condenser)
	Total Heat Transfer Rate = 3280 Btu/hr = 961 watts

For the heat pipe specifications described above, two relatively extreme values for the minimum break-away contact angle are examined; $\alpha_{ba} = 2^o$ and $\alpha_{ba} = 20^o$. The determination of the local apparent contact angle will be performed using the hydrodynamic flow model of the previous report [16]. The effect of varying the minimum break-away contact angle in the analysis is to limit the highest value that the equivalent heat transfer coefficient can attain in the evaporator region. It is assumed in this examination that, once the angular recession has reached the minimum break-away contact angle, the liquid level recession is sufficiently moderate and the sensitivity to liquid level is sufficiently low that the equivalent heat transfer coefficient will remain constant at its break-away angle value. This assumption requires verification and indeed, investigation, but for the purposes intended here it will suffice.

7.2.2 Numerical Results

The heat pipe analysis program was executed for the two test cases described above with the subroutine for the determination of h_{eq} modified to reflect the results of this work. The groove side heat transfer coefficient, h_{eq}, and the pipe exterior surface temperature distribution resulting from these two test cases are presented in Tables 7-1 through 7-4.

We will examine first the case where the minimum break-away contact angle is assumed to be $\alpha_{ba} = 20^o$. The equivalent heat transfer coefficient for this case, presented in Table 7-1, varies from a low value of 3422 Btu/(hr.ft^2.^{o}F) in the extreme condenser groove region to a high value of 4050 Btu/(hr.ft^2.^{o}F) in the extreme evaporator region. The overall variation for a minimum break-away contact angle of 20^o is 18.4 per cent. Of this variation, there is only a 2.9 per cent variation over the evaporator region while the condenser variation in h_{eq} is 6.1 per cent.

The relatively large region of uniform h_{eq} in the evaporator is the result of an assumed break-away contact angle of 20 deg. This assumption of a large break-away contact angle results in a condition of full angular recession occurring relatively early in the hydrodynamic development of the return liquid flow. The additional assumption taken here, that the equivalent heat transfer coefficient will not change appreciably with moderate liquid level recession, leads to a large region of uniform

h_{eq} on the evaporator, and thus a small variation in the equivalent heat transfer coefficient over this region.

The relative uniformity of h_{eq} over each of the evaporator and condenser sections is reflected in Table 7-2 by a similar uniformity of the surface temperature distribution. Indeed, since the metal conductivity is large relative to the liquid conductivity, $k_m/k_f = 86.5$, heat conduction within the pipe wall tends to reduce the fractional variation of the surface temperature for each section below that exhibited by the equivalent heat transfer coefficient. The evaporator surface temperature variation for this case is only 0.4 per cent while the condenser variation is 1.19 per cent. It is seen that the relative proportion of evaporator to condenser non-uniformity is very close to that for the equivalent heat transfer coefficient but that the magnitudes are greatly reduced. This magnitude reduction is due to the isothermalizing character of the higher conductivity wall material.

Relaxing the value of the minimum break-away contact angle to allow angular recession of the liquid to a contact angle of 2 degrees results in the equivalent heat transfer coefficient distribution presented in Table 7-3. It is seen from Table 7-3 that the initial distribution and development of h_{eq} is identical to the previous case, as it must be. Exception to this occurs, however, in the evaporator section of the pipe since, here, the relaxed limitation on contact angle recession allows additional hydrodynamic development to occur prior to the onset of liquid level recession.

The additional development allowed in the contact angle recession is most visibly displayed in Table 7-3 by a larger equivalent heat transfer coefficient in the extreme evaporator regions. Indeed in this example the equivalent heat transfer coefficient exceeds that for the previous case, in the extreme evaporator region, by 32.6 per cent. This is a substantial increase in h_{eq} and is due to its increased sensitivity at low contact angles.

The maximum variation of the equivalent heat transfer coefficient is 34.6 per cent over the evaporator region and remains at 6.1 per cent for the condenser region. There is clearly a marked dependence of the evaporator equivalent heat transfer coefficient on the minimum break-away contact angle.

Examining the surface temperature variation, for this case presented in Table 7-4, the temperature variation over the external surface is again attenuated by the heat conduction within the higher conductivity heat pipe wall. In the evaporator region, the h_{eq} variation of 32.6 per cent is reflected in the surface temperature by a variation of only 4.8 per cent. The variation over the condenser region is unaffected by the change in the value of α_{ba}. The influence of this change in the minimum break-away contact angle has been to increase the pipe overall conductance by approximately 8 per cent. Thus although a substantial influence of α_{ba} is felt on h_{eq}, the resultant effect on the pipe conductance is considerably less pronounced.

7.3 Case II

In this section a second example problem is considered and the influence of the minimum break-away contact angle on the pipe exterior surface temperature variation and on the pipe overall conductance is investigated.

Table 7-1

HEAT PIPE ANALYSIS
GROOVE SIDE COEFF(BTU/HR-SQ.FT-F)

Z/L	PSI (DEGREES)									
	9.0	27.0	45.0	63.0	81.0	99.0	117.0	135.0	153.0	171.0
0.014	4050.	4050.	4050.	4050.	4050.	4050.	4050.	4050.	4050.	4050.
0.042	4050.	4050.	4050.	4050.	4050.	4050.	4050.	4050.	4050.	4050.
0.069	4050.	4050.	4050.	4050.	4050.	4050.	4050.	4050.	4050.	4050.
0.097	4050.	4050.	4050.	4050.	4050.	4050.	4050.	4050.	4050.	4050.
0.125	4050.	4050.	4050.	4050.	4050.	4050.	4050.	4050.	4050.	4050.
0.153	4050.	4050.	4050.	4050.	4050.	4050.	4050.	4050.	4050.	4050.
0.181	4050.	4050.	4050.	4050.	4050.	4050.	4050.	4050.	4050.	4050.
0.208	4050.	4050.	4050.	4050.	4050.	4050.	4050.	4050.	4050.	4050.
0.236	4050.	4050.	4050.	4050.	4050.	4050.	4050.	4050.	4050.	4050.
0.264	4050.	4050.	4050.	4050.	4050.	4050.	4050.	4050.	4050.	4050.
0.292	4049.	4050.	4050.	4050.	4050.	4050.	4050.	4050.	4050.	4049.
0.319	3989.	4050.	4050.	4050.	4050.	4050.	4050.	4050.	4050.	3989.
0.347	3934.	4050.	4050.	4050.	4050.	4050.	4050.	4050.	4050.	3934.
0.375	3812.	3812.	3812.	3812.	3812.	3812.	3812.	3812.	3812.	3812.
0.403	3774.	3774.	3774.	3774.	3774.	3774.	3774.	3774.	3774.	3774.
0.431	3739.	3739.	3739.	3739.	3739.	3739.	3739.	3739.	3739.	3739.
0.458	3707.	3707.	3707.	3707.	3707.	3707.	3707.	3707.	3707.	3707.
0.486	3678.	3678.	3678.	3678.	3678.	3678.	3678.	3678.	3678.	3678.
0.514	3632.	3602.	3582.	3569.	3563.	3563.	3569.	3582.	3602.	3632.
0.542	3609.	3582.	3563.	3551.	3545.	3545.	3551.	3563.	3582.	3609.
0.569	3588.	3563.	3546.	3535.	3529.	3529.	3535.	3546.	3563.	3588.
0.597	3570.	3546.	3530.	3520.	3514.	3514.	3520.	3530.	3546.	3570.
0.625	3554.	3531.	3516.	3506.	3501.	3501.	3506.	3516.	3531.	3554.
0.653	3539.	3518.	3503.	3494.	3489.	3489.	3494.	3503.	3518.	3539.
0.681	3526.	3506.	3492.	3482.	3478.	3478.	3482.	3492.	3506.	3526.
0.708	3514.	3495.	3481.	3473.	3468.	3468.	3473.	3481.	3495.	3514.
0.736	3504.	3485.	3472.	3464.	3459.	3459.	3464.	3472.	3485.	3504.
0.764	3495.	3477.	3464.	3456.	3452.	3452.	3456.	3464.	3477.	3495.
0.792	3487.	3469.	3457.	3449.	3445.	3445.	3449.	3457.	3469.	3487.
0.819	3480.	3463.	3451.	3443.	3439.	3439.	3443.	3451.	3463.	3480.
0.847	3474.	3457.	3445.	3438.	3434.	3434.	3438.	3445.	3457.	3474.
0.875	3469.	3453.	3441.	3434.	3430.	3430.	3434.	3441.	3453.	3469.
0.903	3466.	3449.	3438.	3430.	3427.	3427.	3430.	3438.	3449.	3466.
0.931	3463.	3447.	3435.	3428.	3424.	3424.	3428.	3435.	3447.	3463.
0.958	3461.	3445.	3433.	3426.	3423.	3423.	3426.	3433.	3445.	3461.
0.986	3460.	3444.	3433.	3425.	3422.	3422.	3425.	3433.	3444.	3460.

Table 7-2

HEAT PIPE ANALYSIS

SURFACE TEMPERATURES (DEG. FAHR.)

Z/L	PSI (DEGREES)									
	9.0	27.0	45.0	63.0	81.0	99.0	117.0	135.0	153.0	171.[illegible]
0.014	23.89	23.89	23.89	23.89	23.89	23.89	23.89	23.89	23.89	23.89
0.042	23.89	23.89	23.89	23.89	23.89	23.89	23.89	23.89	23.89	23.[illegible]
0.069	23.89	23.89	23.89	23.89	23.89	23.89	23.89	23.89	23.89	23.89
0.097	23.89	23.89	23.89	23.89	23.89	23.89	23.89	23.89	23.89	23.89
0.125	23.89	23.89	23.89	23.89	23.89	23.89	23.89	23.89	23.89	23.89
0.153	23.89	23.89	23.89	23.89	23.89	23.89	23.89	23.89	23.89	23.89
0.181	23.89	23.89	23.89	23.89	23.89	23.89	23.89	23.89	23.89	23.89
0.208	23.89	23.89	23.89	23.89	23.89	23.89	23.89	23.89	23.89	23.89
0.236	23.89	23.89	23.89	23.89	23.89	23.89	23.89	23.89	23.89	23.89
0.264	23.89	23.89	23.89	23.89	23.89	23.89	23.89	23.89	23.89	23.89
0.292	23.89	23.89	23.89	23.89	23.89	23.89	23.89	23.89	23.89	23.[illegible]
0.319	23.94	23.89	23.89	23.89	23.89	23.89	23.89	23.89	23.89	23.[illegible]
0.347	23.99	23.90	23.89	23.89	23.89	23.89	23.89	23.89	23.90	23.[illegible]9
0.375	16.66	16.66	16.66	16.66	16.66	16.66	16.66	16.66	16.66	16.[illegible]
0.403	16.66	16.66	16.66	16.66	16.66	16.66	16.66	16.66	16.66	16.[illegible]
0.431	16.66	16.66	16.66	16.66	16.66	16.66	16.66	16.66	16.66	16.66
0.458	16.66	16.66	16.66	16.66	16.66	16.66	16.66	16.66	16.66	16.6[illegible]
0.486	16.66	16.66	16.66	16.66	16.66	16.66	16.66	16.66	16.66	16.65
0.514	11.02	11.01	11.00	10.99	10.98	10.98	10.99	11.00	11.01	11.[illegible]
0.542	11.01	10.99	10.98	10.98	10.97	10.97	10.98	10.98	10.99	11.01
0.569	11.00	10.98	10.97	10.97	10.96	10.96	10.97	10.97	10.98	11.[illegible]
0.597	10.99	10.97	10.96	10.96	10.95	10.95	10.96	10.96	10.97	10.[illegible]
0.625	10.98	10.96	10.95	10.95	10.94	10.94	10.95	10.95	10.96	10.97
0.653	10.97	10.95	10.94	10.94	10.94	10.94	10.94	10.94	10.95	10.[illegible]
0.681	10.96	10.95	10.94	10.93	10.93	10.93	10.93	10.94	10.95	10.[illegible]
0.708	10.95	10.94	10.93	10.93	10.92	10.92	10.93	10.93	10.94	10.95
0.736	10.94	10.93	10.92	10.92	10.92	10.92	10.92	10.92	10.93	10.94
0.764	10.94	10.93	10.92	10.91	10.91	10.91	10.91	10.92	10.93	10.9[illegible]
0.792	10.93	10.92	10.91	10.91	10.91	10.91	10.91	10.91	10.92	10.9[illegible]
0.819	10.93	10.92	10.91	10.91	10.90	10.90	10.91	10.91	10.92	10.93
0.847	10.92	10.92	10.91	10.90	10.90	10.90	10.90	10.91	10.92	10.9[illegible]
0.875	10.92	10.91	10.90	10.90	10.90	10.90	10.90	10.90	10.91	10.9[illegible]
0.903	10.92	10.91	10.90	10.90	10.89	10.89	10.90	10.90	10.91	10.92
0.931	10.92	10.91	10.90	10.90	10.89	10.89	10.90	10.90	10.91	10.[illegible]
0.958	10.92	10.91	10.90	10.89	10.89	10.89	10.89	10.90	10.91	10.9[illegible]
0.986	10.92	10.91	10.90	10.89	10.89	10.89	10.89	10.90	10.91	10.9[illegible]

Table 7-3

HEAT PIPE ANALYSIS
GROOVE SIDE COEFF(BTU/HR-SQ.FT-F)

Z/L	PSI (DEGREES) 9.0	27.0	45.0	63.0	81.0	99.0	117.0	135.0	153.0	171.0
0.014	4701.	5371.	5371.	5371.	5371.	5371.	5371.	5371.	5371.	4701.
0.042	4673.	5371.	5371.	5371.	5371.	5371.	5371.	5371.	5371.	4673.
0.069	4622.	5371.	5371.	5371.	5371.	5371.	5371.	5371.	5371.	[illegible]
0.097	4555.	5371.	5371.	5371.	5371.	5371.	5371.	5371.	5371.	[illegible]
0.125	4480.	5371.	5371.	5371.	5371.	5371.	5371.	5371.	5371.	[illegible]
0.153	4402.	5371.	5371.	5371.	5371.	5371.	5371.	5371.	5371.	[illegible]
0.181	4325.	5371.	5371.	5371.	5371.	5371.	5371.	5371.	5371.	[illegible]
0.208	4250.	5371.	5371.	5371.	5371.	5371.	5371.	5371.	5371.	[illegible]
0.236	4179.	4860.	5371.	5371.	5371.	5371.	5371.	5371.	4860.	[illegible]
0.264	4112.	4566.	5371.	5371.	5371.	5371.	5371.	5371.	4566.	[illegible]
0.292	4049.	4381.	5371.	5371.	5371.	5371.	5371.	5371.	4381.	[illegible]
0.319	3989.	4245.	4765.	5371.	5371.	5371.	5371.	4765.	4245.	[illegible]
0.347	3934.	4136.	4446.	5103.	5371.	5371.	5103.	4446.	4136.	[illegible]
0.375	3812.	3812.	3812.	3812.	3812.	3812.	3812.	3812.	3812.	[illegible]
0.403	3774.	3774.	3774.	3774.	3774.	3774.	3774.	3774.	3774.	3774.
0.431	3739.	3739.	3739.	3739.	3739.	3739.	3739.	3739.	3739.	[illegible]
0.458	3707.	3707.	3707.	3707.	3707.	3707.	3707.	3707.	3707.	[illegible]
0.486	3678.	3678.	3678.	3678.	3678.	3678.	3678.	3678.	3678.	[illegible]
0.514	3632.	3602.	3582.	3569.	3563.	3563.	3569.	3582.	3602.	[illegible]
0.542	3609.	3582.	3563.	3551.	3545.	3545.	3551.	3563.	3582.	[illegible]
0.569	3588.	3563.	3546.	3535.	3529.	3529.	3535.	3546.	3563.	[illegible]
0.597	3570.	3546.	3530.	3520.	3514.	3514.	3520.	3530.	3546.	[illegible]
0.625	3554.	3531.	3516.	3506.	3501.	3501.	3506.	3516.	3531.	3554.
0.653	3539.	3518.	3503.	3494.	3489.	3489.	3494.	3503.	3518.	[illegible]
0.681	3526.	3506.	3492.	3482.	3478.	3478.	3482.	3492.	3506.	[illegible]
0.708	3514.	3495.	3481.	3473.	3468.	3468.	3473.	3481.	3495.	3514.
0.736	3504.	3485.	3472.	3464.	3459.	3459.	3464.	3472.	3485.	[illegible]
0.764	3495.	3477.	3464.	3456.	3452.	3452.	3456.	3464.	3477.	[illegible]
0.792	3487.	3469.	3457.	3449.	3445.	3445.	3449.	3457.	3469.	3487.
0.819	3480.	3463.	3451.	3443.	3439.	3439.	3443.	3451.	3463.	[illegible]
0.847	3474.	3457.	3445.	3438.	3434.	3434.	3438.	3445.	3457.	[illegible]
0.875	3469.	3453.	3441.	3434.	3430.	3430.	3434.	3441.	3453.	[illegible]
0.903	3466.	3449.	3438.	3430.	3427.	3427.	3430.	3438.	3449.	[illegible]
0.931	3463.	3447.	3435.	3428.	3424.	3424.	3428.	3435.	3447.	[illegible]
0.958	3461.	3445.	3433.	3426.	3423.	3423.	3426.	3433.	3445.	3461.
0.986	3460.	3444.	3433.	3425.	3422.	3422.	3425.	3433.	3444.	[illegible]

Table 7-4

HEAT PIPE ANALYSIS

SURFACE TEMPERATURES (DEG. FAHR.)

Z/L	PSI (DEGREES)									
	9.0	27.0	45.0	63.0	81.0	99.0	117.0	135.0	153.0	171.
0.014	23.27	22.93	22.89	22.88	22.88	22.86	22.88	22.89	22.93	23.2
0.042	23.29	22.93	22.89	22.88	22.88	22.88	22.88	22.89	22.93	23.2
0.069	23.32	22.93	22.89	22.88	22.88	22.88	22.88	22.89	22.93	23.32
0.097	23.37	22.94	22.89	22.88	22.88	22.86	22.88	22.89	22.94	23.3
0.125	23.42	22.94	22.89	22.88	22.88	22.86	22.88	22.89	22.94	23.4
0.153	23.47	22.95	22.89	22.88	22.88	22.88	22.88	22.89	22.95	23.47
0.181	23.53	22.96	22.89	22.88	22.88	22.86	22.88	22.89	22.96	23.5
0.208	23.59	22.96	22.89	22.88	22.88	22.86	22.88	22.89	22.96	23.5
0.236	23.68	23.23	22.92	22.89	22.88	22.88	22.89	22.92	23.23	23.6
0.264	23.76	23.41	22.94	22.89	22.88	22.88	22.89	22.94	23.41	23.76
0.292	23.84	23.53	22.96	22.89	22.88	22.88	22.89	22.96	23.53	23.8
0.319	23.91	23.67	23.28	22.93	22.89	22.89	22.93	23.28	23.67	23.
0.347	23.97	23.78	23.50	23.08	22.91	22.91	23.08	23.50	23.78	23.97
0.375	16.66	16.66	16.66	16.66	16.66	16.66	16.66	16.66	16.66	16.
0.403	16.66	16.66	16.66	16.66	16.66	16.66	16.66	16.66	16.66	16.
0.431	16.66	16.66	16.66	16.66	16.66	16.66	16.66	16.66	16.66	16.6
0.458	16.66	16.66	16.66	16.66	16.66	16.66	16.66	16.66	16.66	16.6
0.486	16.65	16.65	16.65	16.65	16.65	16.65	16.65	16.65	16.65	16.6
0.514	11.02	11.01	10.99	10.99	10.98	10.98	10.99	10.99	11.01	11.
0.542	11.01	10.99	10.98	10.97	10.97	10.97	10.97	10.98	10.99	11.01
0.569	11.00	10.98	10.97	10.96	10.96	10.96	10.96	10.97	10.98	10.
0.597	10.98	10.97	10.96	10.95	10.95	10.95	10.95	10.96	10.97	10.
0.625	10.97	10.96	10.95	10.95	10.94	10.94	10.95	10.95	10.96	10.97
0.653	10.96	10.95	10.94	10.94	10.93	10.93	10.94	10.94	10.95	10.
0.681	10.96	10.95	10.94	10.93	10.93	10.93	10.93	10.94	10.95	10.9
0.708	10.95	10.94	10.93	10.92	10.92	10.92	10.92	10.93	10.94	10.9
0.736	10.94	10.93	10.92	10.92	10.92	10.92	10.92	10.92	10.93	10.9
0.764	10.94	10.93	10.92	10.91	10.91	10.91	10.91	10.92	10.93	10.9
0.792	10.93	10.92	10.91	10.91	10.91	10.91	10.91	10.91	10.92	10.9
0.819	10.93	10.92	10.91	10.90	10.90	10.90	10.90	10.91	10.92	10.9
0.847	10.92	10.91	10.91	10.90	10.90	10.90	10.90	10.91	10.91	10.9
0.875	10.92	10.91	10.90	10.90	10.90	10.90	10.90	10.90	10.91	10.9
0.903	10.92	10.91	10.90	10.90	10.89	10.89	10.90	10.90	10.91	10.92
0.931	10.92	10.91	10.90	10.89	10.89	10.89	10.89	10.90	10.91	10.9
0.958	10.91	10.91	10.90	10.89	10.89	10.89	10.89	10.90	10.91	10.9
0.986	10.91	10.90	10.90	10.89	10.89	10.89	10.89	10.90	10.90	10.

7.3.1 Pipe Geometry and Thermal Loading

The second example considered in this section is examined for identical pipe, working fluid, and thermal loading characteristics as the previous example, with one exception. The thermal conductivity of the working fluid is taken to be 1.0 Btu/(hr-ft-^{o}F), and, while this is a somewhat ficticious consideration, it is designed to illustrate the dependence of the heat pipe behavior on the fluid/metal thermal conductivity ratio. Further, the case of k_f/k_m = 0.1 will serve as an extreme case since it was found in chapter 6 of this report that the sensitivity of h_{eq} on α_{ba} was highest where the conductivity ratio, k_f/k_m, was also the highest, within the range of parameters examined. That is, the more closely the liquid thermal conductivity approaches that of the solid, the more highly dependent the heat transfer becomes on the liquid cross-sectional configuration.

7.3.2 Numerical Results

The results of executing the heat pipe prediction program for the case of k_f/k_m = 0.1 are presented in Tables 7-5 to 7-6 for an assumed minimum break-away angle of 20 degrees. From Table 7-5, the overall variation of h_{eq} has increased to 25.5 per cent ranging from a low value of 5472 to a maximum value of 7491. This is to be compared with the variation for k_f/k_m = 0.01156 of 18.4 per cent. In this case the evaporator variation has increased to 3.9 per cent and the condenser variation to 8.5 per cent. Again a relatively large uniform region over the evaporator surface is present due to the large minimum break-away angle of 20 degrees.

The surface temperature variation, again de-sensitized by the high wall thermal conductivity, is only 0.4 per cent over the evaporator and 1.0 per cent over the condenser surface. The relatively low surface temperature variations exhibited here may also be in part attributed to the large equivalent heat transfer coefficients in this case which more closely link the wall temperatures to the uniform vapor temperature. For example in the extreme evaporator regions, the value of h_{eq} is 1.85 times its former value while in the extreme condenser region it is 1.75 times its former value. Thus we see that, while the variation of h_{eq} has increased, the surface temperature variation for this case has decreased. Considering now the case where α_{ba} = 2 degrees, the additional hydrodynamic development of the liquid return flow has substantially increased the extreme evaporator equivalent heat transfer coefficient to 10,684, an increase of 42.6 per cent. The evaporator equivalent heat transfer coefficient variation has correspondingly increased to 48.2 per cent with the condenser region again remaining as it was for the 20 degree break-away angle case.

Once again, the isothermalizing of the pipe wall, and the close thermal link with the vapor core temperature has limited the surface temperature variation, Table 7-8, over the evaporator region to 3.67 per cent. The condenser surface temperature variation again remains unchanged from the 20 degree break-away angle case. The overall pipe thermal conductance has increased by the change of α_{ba} by approximately 7 per cent from the 20 degree case. These moderate increases of the overall pipe conductance with relatively severe changes in the equivalent heat transfer coefficient provide an indication that heat pipes of high performance design may often be limited in their performance characteristics by the thermal behavior of the heat pipe

Table 7-5

HEAT PIPE ANALYSIS
GROOVE SIDE COEFF (BTU/HR-SQ.FT-F)

Z/L	PSI (DEGREES)									
	9.0	27.0	45.0	63.0	81.0	99.0	117.0	135.0	153.0	171.0
0.014	7491.	7491.	7491.	7491.	7491.	7491.	7491.	7491.	7491.	7491.
0.042	7491.	7491.	7491.	7491.	7491.	7491.	7491.	7491.	7491.	7491.
0.069	7491.	7491.	7491.	7491.	7491.	7491.	7491.	7491.	7491.	7491.
0.097	7491.	7491.	7491.	7491.	7491.	7491.	7491.	7491.	7491.	7491.
0.125	7491.	7491.	7491.	7491.	7491.	7491.	7491.	7491.	7491.	7491.
0.153	7491.	7491.	7491.	7491.	7491.	7491.	7491.	7491.	7491.	7491.
0.181	7491.	7491.	7491.	7491.	7491.	7491.	7491.	7491.	7491.	7491.
0.208	7491.	7491.	7491.	7491.	7491.	7491.	7491.	7491.	7491.	7491.
0.236	7491.	7491.	7491.	7491.	7491.	7491.	7491.	7491.	7491.	7491.
0.264	7491.	7491.	7491.	7491.	7491.	7491.	7491.	7491.	7491.	7491.
0.292	7469.	7491.	7491.	7491.	7491.	7491.	7491.	7491.	7491.	[illegible]
0.319	7345.	7491.	7491.	7491.	7491.	7491.	7491.	7491.	7491.	[illegible]
0.347	7210.	7491.	7491.	7491.	7491.	7491.	7491.	7491.	7491.	[illegible]
0.375	6916.	6916.	6916.	6916.	6916.	6916.	6916.	6916.	6916.	6916.
0.403	6824.	6824.	6824.	6824.	6824.	6824.	6824.	6824.	6824.	[illegible]
0.431	6740.	6740.	6740.	6740.	6740.	6740.	6740.	6740.	6740.	6740.
0.458	6663.	6663.	6663.	6663.	6663.	6663.	6663.	6663.	6663.	[illegible]
0.486	6592.	6592.	6592.	6592.	6592.	6592.	6592.	6592.	6592.	6592.
0.514	6480.	6408.	6359.	6329.	6314.	6314.	6329.	6359.	6408.	[illegible]
0.542	6425.	6359.	6314.	6285.	6271.	6271.	6285.	6314.	6359.	[illegible]
0.569	6376.	6314.	6272.	6245.	6232.	6232.	6245.	6272.	6314.	6376.
0.597	6331.	6274.	6234.	6209.	6197.	6197.	6209.	6234.	6274.	6331.
0.625	6292.	6238.	6200.	6176.	6164.	6164.	6176.	6200.	6238.	6292.
0.653	6256.	6205.	6169.	6146.	6135.	6135.	6146.	6169.	6205.	6256.
0.681	6225.	6176.	6141.	6119.	6109.	6109.	6119.	6141.	6176.	[illegible]
0.708	6196.	6150.	6116.	6095.	6085.	6085.	6095.	6116.	6150.	6196.
0.736	6171.	6126.	6094.	6074.	6064.	6064.	6074.	6094.	6126.	6171.
0.764	6149.	6105.	6075.	6055.	6045.	6045.	6055.	6075.	6105.	6149.
0.792	6130.	6087.	6057.	6038.	6029.	6029.	6038.	6057.	6087.	6130.
0.819	6113.	6072.	6042.	6024.	6014.	6014.	6024.	6042.	6072.	6113.
0.847	6099.	6059.	6030.	6011.	6002.	6002.	6011.	6030.	6059.	[illegible]
0.875	6088.	6048.	6019.	6001.	5992.	5992.	6001.	6019.	6048.	[illegible]
0.903	6078.	6039.	6011.	5993.	5984.	5984.	5993.	6011.	6039.	[illegible]
0.931	6072.	6033.	6005.	5987.	5978.	5978.	5987.	6005.	6033.	[illegible]
0.958	6067.	6028.	6001.	5983.	5974.	5974.	5983.	6001.	6028.	[illegible]
0.986	6065.	6026.	5999.	5981.	5972.	5972.	5981.	5999.	6026.	[illegible]

Table 7-6

HEAT PIPE ANALYSIS

SURFACE TEMPERATURES (DEG. FAHR.)

Z/L	PSI (DEGREES)									
	9.0	27.0	45.0	63.0	81.0	99.0	117.0	135.0	153.0	171.
0.014	20.59	20.59	20.59	20.59	20.59	20.59	20.59	20.59	20.59	[illegible]
0.042	20.59	20.59	20.59	20.59	20.59	20.59	20.59	20.59	20.59	[illegible]
0.069	20.59	20.59	20.59	20.59	20.59	20.59	20.59	20.59	20.59	[illegible]
0.097	20.59	20.59	20.59	20.59	20.59	20.59	20.59	20.59	20.59	[illegible]
0.125	20.59	20.59	20.59	20.59	20.59	20.59	20.59	20.59	20.59	[illegible]
0.153	20.59	20.59	20.59	20.59	20.59	20.59	20.59	20.59	20.59	[illegible]
0.181	20.59	20.59	20.59	20.59	20.59	20.59	20.59	20.59	20.59	[illegible]
0.208	20.59	20.59	20.59	20.59	20.59	20.59	20.59	20.59	20.59	[illegible]
0.236	20.59	20.59	20.59	20.59	20.59	20.59	20.59	20.59	20.59	[illegible]
0.264	20.59	20.59	20.59	20.59	20.59	20.59	20.59	20.59	20.59	[illegible]
0.292	20.59	20.59	20.59	20.59	20.59	20.59	20.59	20.59	20.59	[illegible]
0.319	20.63	20.60	20.59	20.59	20.59	20.59	20.59	20.59	20.60	[illegible]
0.347	20.67	20.63	20.59	20.59	20.59	20.59	20.59	20.59	20.6[illegible]	[illegible]
0.375	15.24	15.24	15.24	15.24	15.24	15.24	15.24	15.24	15.24	[illegible]
0.403	15.24	15.24	15.24	15.24	15.24	15.24	15.24	15.24	15.24	[illegible]
0.431	15.24	15.24	15.24	15.24	15.24	15.24	15.24	15.24	15.24	[illegible]
0.458	15.24	15.24	15.24	15.24	15.24	15.24	15.24	15.24	15.24	[illegible]
0.486	15.24	15.24	15.24	15.24	15.24	15.24	15.24	15.24	15.24	[illegible]
0.514	11.05	11.04	11.03	11.02	11.02	11.02	11.02	11.03	11.04	[illegible]
0.542	11.04	11.03	11.02	11.01	11.01	11.01	11.01	11.02	11.03	[illegible]
0.569	11.03	11.02	11.01	11.00	11.00	11.00	11.00	11.01	11.02	[illegible]
0.597	11.02	11.01	11.00	11.00	10.99	10.99	11.00	11.00	11.01	[illegible]
0.625	11.01	11.00	10.99	10.99	10.99	10.99	10.99	10.99	11.00	[illegible]
0.653	11.01	10.99	10.99	10.98	10.98	10.98	10.98	10.99	10.99	[illegible]
0.681	11.00	10.99	10.98	10.98	10.97	10.97	10.98	10.98	10.99	[illegible]
0.708	10.99	10.98	10.97	10.97	10.97	10.97	10.97	10.97	10.98	[illegible]
0.736	10.99	10.98	10.97	10.96	10.96	10.96	10.96	10.97	10.98	[illegible]
0.764	10.98	10.97	10.96	10.96	10.96	10.96	10.96	10.96	10.97	[illegible]
0.792	10.98	10.97	10.96	10.96	10.95	10.95	10.96	10.96	10.97	[illegible]
0.819	10.97	10.96	10.96	10.95	10.95	10.95	10.95	10.96	10.96	[illegible]
0.847	10.97	10.96	10.95	10.95	10.95	10.95	10.95	10.95	10.96	[illegible]
0.875	10.97	10.96	10.95	10.95	10.95	10.95	10.95	10.95	10.96	[illegible]
0.903	10.96	10.96	10.95	10.95	10.94	10.94	10.95	10.95	10.96	[illegible]
0.931	10.96	10.95	10.95	10.94	10.94	10.94	10.94	10.95	10.95	[illegible]
0.958	10.96	10.95	10.95	10.94	10.94	10.94	10.94	10.95	10.95	[illegible]
0.9[illegible]6	10.96	10.95	10.95	10.94	10.94	10.94	10.94	10.95	10.95	[illegible]

Table 7-7

HEAT PIPE ANALYSIS
GROOVE SIDE COEFF (BTU/HR-SQ.FT-F)

Z/L	PSI (DEGREES) 9.0	27.0	45.0	63.0	81.0	99.0	117.0	135.0	153.0	171.
0.014	9066.	10684.	10684.	10684.	10684.	10684.	10684.	10684.	10684.	[illegible]
0.042	8998.	10684.	10684.	10684.	10684.	10684.	10684.	10684.	10684.	[illegible]
0.069	8875.	10684.	10684.	10684.	10684.	10684.	10684.	10684.	10684.	[illegible]
0.097	8714.	10684.	10684.	10684.	10684.	10684.	10684.	10684.	10684.	8714.
0.125	8532.	10684.	10684.	10684.	10684.	10684.	10684.	10684.	10684.	[illegible]
0.153	8344.	10684.	10684.	10684.	10684.	10684.	10684.	10684.	10684.	[illegible]
0.181	8157.	10684.	10684.	10684.	10684.	10684.	10684.	10684.	10684.	[illegible]
0.208	7976.	10684.	10684.	10684.	10684.	10684.	10684.	10684.	10684.	[illegible]
0.236	7804.	9450.	10684.	10684.	10684.	10684.	10684.	10684.	9450.	[illegible]
0.264	7642.	8738.	10684.	10684.	10684.	10684.	10684.	10684.	8738.	[illegible]
0.292	7489.	8291.	10684.	10684.	10684.	10684.	10684.	10684.	8291.	[illegible]
0.319	7345.	7962.	9220.	10684.	10684.	10684.	10684.	9220.	7962.	[illegible]
0.347	7210.	7700.	8448.	10038.	10684.	10684.	10038.	8448.	7700.	[illegible]
0.375	6916.	6916.	6916.	6916.	6916.	6916.	6916.	6916.	6916.	[illegible]
0.403	6824.	6824.	6824.	6824.	6824.	6824.	6824.	6824.	6824.	[illegible]
0.431	6740.	6740.	6740.	6740.	6740.	6740.	6740.	6740.	6740.	[illegible]
0.458	6663.	6663.	6663.	6663.	6663.	6663.	6663.	6663.	6663.	[illegible]
0.486	6592.	6592.	6592.	6592.	6592.	6592.	6592.	6592.	6592.	[illegible]
0.514	6480.	6408.	6359.	6329.	6314.	6314.	6329.	6359.	6408.	[illegible]
0.542	6425.	6359.	6314.	6285.	6271.	6271.	6285.	6314.	6359.	[illegible]
0.569	6376.	6314.	6272.	6245.	6232.	6232.	6245.	6272.	6314.	[illegible]
0.597	6331.	6274.	6234.	6209.	6197.	6197.	6209.	6234.	6274.	6331.
0.625	6292.	6238.	6200.	6176.	6164.	6164.	6176.	6200.	6238.	[illegible]
0.653	6256.	6205.	6169.	6146.	6135.	6135.	6146.	6169.	6205.	[illegible]
0.681	6225.	6176.	6141.	6119.	6109.	6109.	6119.	6141.	6176.	[illegible]
0.708	6196.	6150.	6116.	6095.	6085.	6085.	6095.	6116.	6150.	[illegible]
0.736	6171.	6126.	6094.	6074.	6064.	6064.	6074.	6094.	6126.	6171.
0.764	6149.	6105.	6075.	6055.	6045.	6045.	6055.	6075.	6105.	[illegible]
0.792	6130.	6087.	6057.	6038.	6029.	6029.	6038.	6057.	6087.	[illegible]
0.819	6113.	6072.	6042.	6024.	6014.	6014.	6024.	6042.	6072.	6113.
0.847	6099.	6059.	6030.	6011.	6002.	6002.	6011.	6030.	6059.	[illegible]
0.875	6088.	6048.	6019.	6001.	5992.	5992.	6001.	6019.	6048.	[illegible]
0.903	6078.	6039.	6011.	5993.	5984.	5984.	5993.	6011.	6039.	[illegible]
0.931	6072.	6033.	6005.	5987.	5978.	5978.	5987.	6005.	6033.	[illegible]
0.958	6067.	6028.	6001.	5983.	5974.	5974.	5983.	6001.	6028.	[illegible]
0.986	6065.	6026.	5999.	5981.	5972.	5972.	5981.	5999.	6026.	[illegible]

Table 7-8

HEAT PIPE ANALYSIS

SURFACE TEMPERATURES (DEG. FAHR.)

Z/L	PSI (DEGREES) 9.0	27.0	45.0	63.0	81.0	99.0	117.0	135.0	153.0	171.
0.014	20.18	19.95	19.93	19.93	19.93	19.93	19.93	19.93	19.95	[illegible]
0.042	20.20	19.95	19.93	19.93	19.93	19.93	19.93	19.93	19.95	20.[illegible]
0.069	20.22	19.95	19.93	19.93	19.93	19.93	19.93	19.93	19.95	20.[illegible]
0.097	20.25	19.96	19.93	19.93	19.93	19.93	19.93	19.93	19.96	20.[illegible]
0.125	20.29	19.96	19.93	19.93	19.93	19.93	19.93	19.93	19.96	20.[illegible]
0.153	20.33	19.96	19.93	19.93	19.93	19.93	19.93	19.93	19.96	20.[illegible]
0.181	20.37	19.97	19.93	19.93	19.93	19.93	19.93	19.93	19.97	20.[illegible]
0.208	20.41	19.97	19.93	19.93	19.93	19.93	19.93	19.93	19.97	20.4[illegible]
0.236	20.47	20.15	19.95	19.93	19.93	19.93	19.93	19.95	20.15	20.4[illegible]
0.264	20.52	20.27	19.96	19.93	19.93	19.93	19.93	19.96	20.27	20.[illegible]
0.292	20.57	20.36	19.97	19.93	19.93	19.93	19.93	19.97	20.36	20.[illegible]
0.319	20.61	20.45	20.18	19.95	19.93	19.93	19.95	20.18	20.45	20.[illegible]1
0.347	20.66	20.52	20.33	20.05	19.94	19.94	20.05	20.33	20.52	20.[illegible]
0.375	15.23	15.23	15.23	15.23	15.23	15.23	15.23	15.23	15.23	15.[illegible]
0.403	15.23	15.23	15.23	15.23	15.23	15.23	15.23	15.23	15.23	15.[illegible]
0.431	15.23	15.23	15.23	15.23	15.23	15.23	15.23	15.23	15.23	15.[illegible]
0.458	15.23	15.23	15.23	15.23	15.23	15.23	15.23	15.23	15.23	15.[illegible]
0.486	15.23	15.23	15.23	15.23	15.23	15.23	15.23	15.23	15.23	15.[illegible]
0.514	11.05	11.04	11.03	11.02	11.02	11.02	11.02	11.03	11.04	11.[illegible]
0.542	11.04	11.03	11.02	11.01	11.01	11.01	11.01	11.02	11.03	11.[illegible]
0.569	11.03	11.02	11.01	11.00	11.00	11.00	11.00	11.01	11.02	11.[illegible]
0.597	11.02	11.01	11.00	10.99	10.99	10.99	10.99	11.00	11.01	11.[illegible]
0.625	11.01	11.00	10.99	10.99	10.98	10.98	10.99	10.99	11.00	11.[illegible]
0.653	11.00	10.99	10.98	10.98	10.98	10.98	10.98	10.98	10.99	11.[illegible]
0.681	11.00	10.99	10.98	10.97	10.97	10.97	10.97	10.98	10.99	[illegible]
0.708	10.99	10.98	10.97	10.97	10.96	10.96	10.97	10.97	10.98	[illegible]
0.736	10.98	10.97	10.97	10.96	10.96	10.96	10.96	10.97	10.97	[illegible]
0.764	10.98	10.97	10.96	10.96	10.96	10.96	10.96	10.96	10.97	[illegible]
0.792	10.97	10.97	10.96	10.95	10.95	10.95	10.95	10.96	10.96	[illegible].97
0.819	10.97	10.96	10.95	10.95	10.95	10.95	10.95	10.95	10.96	[illegible]
0.847	10.97	10.96	10.95	10.95	10.94	10.94	10.95	10.95	10.96	[illegible]
0.875	10.96	10.96	10.95	10.94	10.94	10.94	10.94	10.95	10.96	[illegible]
0.903	10.96	10.95	10.95	10.94	10.94	10.94	10.94	10.95	10.95	[illegible]
0.931	10.96	10.95	10.95	10.94	10.94	10.94	10.94	10.95	10.95	[illegible]
0.958	10.96	10.95	10.94	10.94	10.94	10.94	10.94	10.94	10.95	[illegible]
0.986	10.96	10.95	10.94	10.94	10.94	10.94	10.94	10.94	10.95	[illegible]

wall. Substantially more severe changes might be expected if an aluminum or copper pipe wall material were used in place of the stainless steel one considered here. The results are, nevertheless, consistent with the anticipated behavioral characteristics, with the relatively weak dependence of the pipe overall conductance attributable to a pipe wall limited operational mode.

7.4 Closure

An examination has been conducted in this chapter to study the effect of the assumed minimum break-away contact angle on heat pipe performance for the two test cases cited in the text. It was found that while the equivalent heat transfer coefficient exhibited substantial variation with the minimum break-away contact angle, the resultant effect on the pipe exterior surface temperature variation is considerably de-sensitized. This de-sensitization is attributable in part to the isothermalizing nature of the high conductivity pipe wall material and also in part to the high magnitude of the equivalent heat transfer coefficient which causes the pipe wall temperature distribution to lie close to the uniform vapor temperature. In interpretting these results, however, and in drawing conclusions regarding the heat pipe thermal behavior, it must be remembered that the observed influences are application and heat pipe design dependent.

Chapter 8

Discussion and Conclusions

8.1 Summary

It has been the object of the investigation presented in this report to determine the heat transfer characteristics of grooved heat pipe walls. In particular this study is directed at determination of the 'equivalent heat transfer coefficient' which provides the thermal link between a hypothetical surface, the groove root surface, and the isothermal vapor core. Since the majority of the temperature drop encountered in high capacity, moderate temperature heat pipes will occur in the groove region, accurate prediction of the groove thermal behavior is fundamental to the accurate prediction of the overall performance of heat pipes of this design.

The analyses presented within this report consider the general case of grooves having arbitrary, trapezoidal cross-section with the single exception that symmetric groove configurations are exclusively treated, i.e. the exposed fin tip area is equal to the groove root area. While this restriction must be placed on the interpretation of the results, the problem description and, indeed, the solution program, both maintain the flexibility of applicability to the non-symmetric situation. Two limiting cases of the general trapezoidal groove shape are commonly used in heat pipe applications. These are the case of zero land area, the triangular V-groove, and the case of fifty per cent land area, the rectangular groove.

A mathematical description of the groove heat transfer problem was presented in Chapter three of this report. It was concluded in that chapter that the heat transfer problem is primarily one of conductive heat transport through the metal/liquid composite from the groove root surface to the vapor core. It is assumed, however, that the hydrodynamic analysis has been performed elsewhere and that the liquid cross-section at any location within the pipe is fully determined. It became clear through the analytical solution development of Chapter three that a complete analytical solution to the equivalent heat transfer coefficient problem is unattainable using current mathematical methods. This realization led to two alternatives for determination of the groove heat transfer characteristics; determination of upper and lower bounds which when averaged yield a band of solution uncertainty which is acceptable for engineering purposes, or a complete numerical solution to the composite heat transfer problem.

Chapter four of this report is devoted to a study which establishes upper and lower limits by which the actual heat transfer is bounded. The theorems of Elrod [35] were used in this analysis but unfortunately the resultant range of uncertainty is unacceptably large to allow direct application of the results. The calculated limits still serve as a check, however, on the now required numerical solution since the numerical results must be between the two bounds previously calculated. The numerical results which were computed for the groove heat transfer problem satisfy this requirement.

Convinced that a complete numerical solution is required to provide an acceptable solution, the finite element method was selected as being the most appropriate numerical method for use in this problem. The prime motivation for selection of the finite element method over other available computational methods is its capability of providing the geometric flexibility demanded by the problem configuration. Nevertheless, application of the method was not direct.

The thermal problem under consideration here displays a remarkable combination of influences. While there is a very high degree of detail required to adequately describe the thermal field near the meniscus contact point, the remaining bulk of the cross-sectional geometry is sufficiently significant in its thermal behavior that it cannot be discounted. This leads to a situation where a relatively large region must be discretized in order to 'pick up' its thermal characteristics, and within this region there exists a sub-region requiring extreme geometric subdivision to adequately describe its thermal behavior. Such a combination foiled the first two attempts at a viable mesh subdivision scheme. Finally, after a critical examination of the first two mesh generators, a third scheme was devised which met the problem requirements. The problems encountered in devising an acceptable solution procedure is in support of the conclusions of Chapter three, that the problem is indeed complex.

The finite element method was described in Chapter five and a derivation presented for application of the method in any general orthogonal curvilinear coordinate system. The very close similarity of the resultant functional to the commonly used cartesian form allows extension of the method to be made to these coordinate systems with a minimum of effort. Application of these generalized results was made to the cartesian coordinate system which is used to describe the trapezoidal groove problem.

Several problems were encountered in the application of the finite element method to the trapezoidal groove problem, with these problems being related exclusively to the spatial subdivision scheme. Briefly, these problem areas resulted from the use of elements having aspect ratios much different from unity and from the use of skewed diamond-shaped elements. A great deal of effort was expended in overcoming these difficulties with the third, final mesh generation scheme providing acceptable results.

The third mesh generation scheme was applied to the extreme parameter combination case of $k_f/k_m = 0.001$, $\varepsilon_1 = \varepsilon_2 = 0.25$, $x_\alpha = 0.05$, and $\theta_o = 20$ deg. The numerical results exhibited a monotone and asymptotic behavior as the number of degrees of freedom of the solution was increased. Extrapolation of the numerical data suggested that the solution error at the last data point would be less than five per cent. In further support of the numerical results, a second case for which an exact analytic solution is available was computed. In this example, a conductivity ratio of unity and a full groove condition were examined, clearly not as severe a test as the previous case. Nevertheless, the excellent agreement displayed by the 0.15 per cent error for this case fully supports correct functioning of the solution program.

A parametric study was conducted in Chapter six to determine the influence of the problem parameters on the equivalent heat transfer coefficient. Four parameters are considered here; the conductivity ratio, k_f/k_m, the groove depth, d, the groove land area ratio, ε, and the apparent normalized contact angle, x_α. Parameter variations were considered that encompass the range of most practical interest. A correlation equation, provided for convenience in application, interpolates the numerical data with a maximum error of correlation of seven per cent. Since the heat transfer is dependent on four independent parameters, improvement in the correlation agreement can only be obtained at the expense of additional complexity. As was found in applying the results in a typical heat pipe application, as demonstrated by the results of Chapter eight, the surface temperature distribution is relatively insensitive to the variation of the equivalent heat transfer coefficient. This behavior is typical of many heat pipe applications.

8.2 Conclusions

It is concluded, based on the arguments presented in Chapter three, that conduction is the prime mode of heat transfer within the metal/liquid composite region of grooved heat pipe walls. Although other modes are definitely present, they are of secondary importance relative to the conductive contribution to the heat transfer. These secondary influences are further de-emphasized by the apparent insensitivity of the pipe external surface temperature variation on variations in the internal equivalent heat transfer coefficients for typical applications.

With a limit study failing to sufficiently narrow the band of uncertainty in its resultant values, the heat conduction equation and boundary conditions were formulated for solution by the finite element method. Indeed, the current finite element formulation of the heat conduction equation was expanded in this report to include its application to any general orthogonal curvilinear coordinate system. With this in hand, reduction to the cartesian coordinate frame is direct.

The finite element method was successfully used to solve the groove heat transfer problem. In effecting the solution, however, several problems were experienced and were exclusively related to the mesh generation scheme used to subdivide the continuum. These problems reflect directly the complex nature of the problem under consideration in this report. Equally important, however, is the warning that these problem areas offer to the finite element user. Although the method offers geometric flexibility, care must be exercised when large departures from square, orthogonal elements are required if the linear isoparametric quadrilateral element is used.

Having finally devised a reliable mesh generation scheme, the equivalent heat transfer coefficient was computed for the combinations of parameters deemed to be of practical import. It was found that the dependence of the heat transfer on the apparent contact angle is relatively weak when compared to the severe dependence displayed by the approximate model presented in a previous report [16]. The trends, however, are consistent with that previous model.

It was found by application of these results that even for variations in the equivalent heat transfer coefficient approaching fifty per cent, the influence on the surface temperature variation was less than ten per cent. This conclusion is extremely application dependent, but for heat pipes operating in the moderate temperature range, it is most probably a typical result. This result is an attractive one in the design of heat pipes. The precise details of the groove flow need not be exactly known a priori in order to obtain an approximate solution since the sensitivity of the pipe surface temperatures on local liquid cross-section is not extremely severe.

References

1. Katzoff, S., "Heat Pipes and Vapor Chambers for Thermal Control of Spacecraft", AIAA Progress in Astronautics and Aeronautics: Thermophysics of Spacecraft and Planetary Bodies, edited by G. B. Heller, Vol. 20, Academic Press, New York, 1967.

2. Basiulis, A., Eallondardo, C. M., and Kendall, B. M., "Heat Pipe System for Space Shuttle TWTA", AIAA 8th Thermophysics Conference, July 16-18, 1973, AIAA paper 73-755.

3. Roukis, J., Rogovin, J. and Swerdling, B., "Heat Pipe Applications to Space Vehicles", AIAA 6th Thermophysics Conference, April 26-28, 1971, AIAA paper 71-410.

4. Tawil, M., Alario, J., Prager, R., and Bullock, R., "Heat Pipe Applications for the Space Shuttle", AIAA 7th Thermophysics Conference, April 10-12, 1972, AIAA paper 72-272.

5. Scallon Jr., T. R., and Robinson, G. A., "Heat Pipe Thermal Control System Concept for the Space Station", AIAA 7th Thermophysics Conference, April 10-12, 1972, AIAA paper 72-261.

6. Edestein, F., Swerdling, B., and Kosson, B., "Development of a Self-Priming High-Capacity Heat Pipe for Flight on OAO-C", AIAA 7th Thermophysics Conference, April 10-12, 1972, AIAA paper 72-258.

7. Bienert, W., and Kroliczek, E., "Experimental High Performance Heat Pipes for the OAO-C Spacecraft", SAE/ASME/AIAA Life Support and Environmental Control Conference", July 12-14, 1971, ASME paper 71-Av-26.

8. Mock, P. R., Marcus, B. D., and Edelman, E. A., "Communications Technology Satellite: AIAA/ASME 1974 Thermophysics and Heat Transfer Conference, July 15-17, 1974, AIAA paper 74-749.

9. Winter, E. R. F., and Barsch, W. O., "The Heat Pipe", Advances in Heat Transfer, Vol. 7, edited by T. F. Irvine and J. P. Hartnett, Academic Press, New York, 1971.

10. Bressler, R. G., and Wyatt, P. W., "Surface Wetting Through Capillary Grooves", Trans. ASME, Journal of Heat Transfer, February, 1970.

11. Kosson, R., Hembach, R., Edelstein, F., and Tawil, M., "A Tunnel Wick 100,000 Watt-inch Heat Pipe", AIAA 7th Thermophysics Conference, April 10, 1972, AIAA paper 72-273.

12. Edwards, D. K., Gier, K. D., Ayyaswamy, P. S., and Catton, I., "Evaporation and Condensation in Circumferential Grooves on Horizontal Tubes", ASME/AICHE Heat Transfer Conference, August 5-8, 1973, ASME paper 73-HT-25.

13. Berger, M. E., and Feldman Jr., K. T., "Analysis of Circumferentially Grooved Heat Pipe Evaporators", ASME Winter Annual Meeting, November 11-15, 1973, ASME paper 73-WA/HT-13.

14. Gier, K. D., and Edwards, D. K., "Flooding and Dry-up Limits of Circumferential V-Grooves", AIAA/ASME 1974 Thermophysics and Heat Transfer Conference, July 15-17, 1974, AIAA paper 74-722.

15. Grover, G. M., Cotter, T. P., and Erickson, G. F., "Structures of Very High Thermal Conductance", appearing in "Heat Pipes", AIAA Selected Reprint Series, Volume 16, Chang-Lin Tien editor, reprinted from Journal of Applied Physics, American Institute of Physics, New York, N.Y., Volume 35, No. 6, 1964.

16. Schneider, G. E., and Yovanovich, M. M., "Three-Dimensional Thermal Analysis of a High Capacity Heat Pipe with Circumferential V-Grooves", final report of a study conducted for the Communications Research Centre, CRC 6656-1 (SCS) program.

17. Sun, K. H., and Tien, C. L., "Simple Conduction Model for Steady State Heat Pipe Performance", AIAA Journal, American Institute of Aeronautics and Astronautics, New York, N.Y., Vol. 10, No. 8, August, 1972.

18. Ayyaswamy, P. S., Catton, I., and Edwards, D. K., "Capillary Flow in Triangular Grooves", ASME Winter Annual Meeting, November 11-15, 1973, ASME paper 73-WA/HT-21.

19. Knacke, O., and Stranski, I. N., "The Mechanism of Evaporation", Progress in Metal Physics, Vol. 6, 1956, pp. 181-235.

20. Wyllie, G., "Evaporation and Surface Structure of Liquids", Proceedings of the Royal Society of London, Series A, Vol. 197, No. 1050, June 1949, pp. 383-395.

21. Schrage, R. W., A Theoretical Study of Interphase Mass Transfer, Columbia University Press, New York, N.Y., 1953.

22. Bornhorst, W. J., "Irreversible Thermodynamics of a Phase Change", Ph.D. Dissertation, Massachusetts Institute of Technology, Cambridge, Mass., June 1966.

23. Bornhorst, W. J., and Hatsopoulos, G. N., "Analysis of a Liquid Vapor Phase Change by the Methods of Irreversible Thermodynamics", Transactions of the ASME, Journal of Applied Mechanics, Vol. 34, No. 4, Dec. 1967, pp. 840-846.

24. Kucherov, R. Ya., and Rikenglaz, L. E., "On Hydrodynamic Boundary Conditions for Evaporation and Condensation", Soviet Physics JETP, Vol. 37 (10), No. 1, Jan. 1960, pp. 88-89.

25. Labunstov, D. A., "An Analysis of Evaporation and Condensation Processes", Teplofizika Vysokikh Temperatur, Vol. 5, No. 4, July-August 1967, pp. 647-654.

26. Feldman, K. T. Jr., and Berger, M. E., "Analysis of a High-Heat-Flux Water Heat Pipe Evaporator", Technical Report ME 62 (73) ONR-012-2, September 1973, pp. 91-94.

27. Ferrell, J. K., and Alleavitch, J., "Vaporization Heat Transfer in Capillary Wick Structures", AIChE Preprint 6, presented at the Eleventh National Heat Transfer Conference AIChE-ASME, Minneapolis, Minn., Aug. 3-6, 1969.

28. Ferrell, J. K. and Johnson, H. R., "The Mechanism of Heat Transfer in the Evaporator Zone of a Heat Pipe", ASME Paper No. 70-HT/SpT-12, presented at the ASME Space Technology and Heat Transfer Conference, Los Angeles, California, June 1970.

29. Kreith, F., Principles of Heat Transfer, 2nd ed., International Textbook Company, Scranton, Penn., 1966.

30. Yovanovich, M. M., Advanced Heat Conduction, Hemisphere Publishing Corporation, Washington, D.C., (1976).

31. Schneider, G. E., Strong, A. B., and Yovanovich, M. M., "A Physical Approach to the Finite Difference Solution of the Conduction Equation in Orthogonal Curvilinear Coordinates", presented at the ASME Winter Annual Meeting, Houston, Texas, Nov. 30 - Dec. 4, 1975, ASME Paper No. 75-WA/HT-94.

32. Schneider, G. E., Strong, A. B., and Yovanovich, M. M., "Finite Difference Modelling of the Heat Conduction Equation in General Orthogonal Curvilinear Coordinates Using Taylor Series Expansion", proceedings of the AICA Conference on Advances in Computer Methods for Partial Differential Equations, R. Vichnevetsky (ed.), June 27-29, 1975.

33. Desai, C. S., and Abel, J. F., Introduction to the Finite Element Method, Van Nostrand Reinhold Company, 1972.

34. Huebner, K. H., The Finite Element Method for Engineers, John Wiley and Sons, Inc., New York, N.Y., 1975.

35. Elrod, H. G., "Two Simple Theorems for Establishing Bounds on the Total Heat Flow in Steady-State Heat-Conduction Problems with Convective Boundary Conditions", Journal of Heat Transfer, Vol. 96, Series C, No. 1, 1974, pp. 65-70.

36. Smythe, W. R., Static and Dynamic Electricity, 3rd ed., McGraw-Hill Book Company, New York, N.Y., 1968.

37. Yovanovich, M. M., Schneider, G. E., and Strong, A. B., "Transverse Apparent Thermal Conductivity of Long Rectangular Fibers in a Matrix", presented at AIChE-ASME Heat Transfer Conference, San Francisco, Calif., Aug. 11-13, 1975, ASME Paper No. 75-HT-26.

38. Standard Mathematical Tables, Nineteenth Edition, S. M. Selby ed., The Chemical Rubber Company, Cleveland, Ohio, 1971.

39. Zienkiewicz, O. C., and Cheung, Y. K., "Finite Elements in the Solution of Field Problems", The Engineer, Vol. 220, 1965, pp. 507-510.

40. Visser, W., "A Finite Element Method for Determination of Non-Stationary Temperature Distribution and Thermal Deformations", Proceedings of the Conference on Matrix Methods in Structural Mechanics, held at the Air Force Institute of Technology, Wright-Patterson Air Force Base, Ohio, 1965, pp. 925-944.

41. Emery, A. F., "The Use of Singularity Programming in Finite Difference and Finite Element Computations of Temperature", Transactions of the ASME, Journal of Heat Transfer, Vol. 95, Series C, No. 3, August, 1973, pp. 344-351.

42. Wilson, E. L., and Nickell, R. E., "Application of the Finite Element Method to Heat Conduction Analysis", Nuclear Engineering and Design, Vol. 4, 1966, pp. 276-286.

43. Warzee, G., "Finite Element Analysis of Transient Heat Conduction - Application of the Weighted Residual Process", Computer Methods in Applied Mechanics and Engineering, Vol. 3, 1974, pp. 255-268.

44. Zienkiewicz, O. C., and Parekh, C. J., "Transient Field Problems: Two-Dimensional and Three-Dimensional Analysis by Isoparametric Finite Elements", International Journal for Numerical Methods in Engineering, Vol. 2, 1970, pp. 61-71.

45. Schneider, G. E., "Finite Element Formulation of the Heat Conduction Equation in General Orthogonal Curvilinear Coordinates", presented at the ASME Winter Annual Meeting, Houston, Texas, Nov. 30 - Dec. 4, 1975, ASME Paper No.

46. Hildebrande, F.B., Methods of Applied Mathematics, 2nd edition, Prentice-Hall Inc., Englewood Cliffs, New Jersey, 1965.

47. Shah, S.N., and Kobayashi, S., "The Matrix Method for the Analysis of Metal Forming Processes," unpublished manuscript.

48. Costello, F. A., "Heat Flux Through a Strip-Heated Flat Plate", Transactions of the ASME, Journal of Heat Transfer, February, 1971, pp. 124-125.

49. Abramowitz, M., and Stegun, I. A., "Handbook of Mathematical Functions", Dover Publications, New York, pp. 589-592.

50. Carslaw, H. S., and Jaeger, J. C., "Conduction of Heat in Solids", Oxford University Press, London, 1959.

51. Zienkiewicz, O. C., Finite Elements in Engineering Science, McGraw-Hill Book Company, London, 1971.

52. Gurtin, M. E., "Variational Principles for Linear Initial-Value Problems", Quarterly Journal of Applied Mathematics, Vol. 22, 1964, p. 252.

53. Finlayson, B. A., and Scriven, L. E., "On the Search for Variational Principles", International Journal of Heat and Mass Transfer, Vol. 10, 1967, pp. 799-821.

Appendix A

Geometric Description of Trapezoidal Groove Section

We are in this section concerned with the geometric description of the heat transfer analysis cross-section for heat transfer from trapezoidal grooves. The groove region is filled with a liquid, the heat pipe working fluid, while the remainder of the section is composed of the heat pipe containment wall material. The analysis geometry is illustrated in figure A-1.

Locating the origin of a cartesian coordinate system as shown in the figure, the heat flow symmetry boundaries are defined by the surfaces $x = 0$ and $x = \omega$. The pipe external surface is defined by the surface $y = 0$. In general the cross-section will not consist of a sharp 'V' configuration so that a land area and groove root area are defined having thicknesses ε_1 and ε_2 respectively. For symmetric grooves $\varepsilon_1 = \varepsilon_2$. The groove section is further typified by a groove half-angle of θ_o while the second angle characterizing the heat transfer is the apparent contact angle α. The remaining parameters to be used in the geometric analysis are indicated in the figure.

The groove root surface is defined by $y = HLSD$ over the domain $0 \leq x \leq \varepsilon_2$, and the groove land area is defined by $y = H$ over the domain $(\omega - \varepsilon_1) \leq x \leq \omega$. The liquid/metal groove interface is given, then, by the relation

$$(y - HLSD) = (x - \varepsilon_2) \cot\theta_o \qquad \text{(A-1)}$$

over the domain $\varepsilon_2 \leq x \leq (\omega - \varepsilon_1)$.

The liquid free surface, circular in cross-section in the absence of gravitational forces, can be characterized by a free surface radius of curvature, β, where β can be determined from [16]

$$\beta = \frac{r_o \sin\theta_o}{\cos(\alpha + \theta_o)} \tag{A-2}$$

where

$$r_o = (\omega - \varepsilon_1)/\sin\theta_o \tag{A-3}$$

and, locating a virtual origin at the intersection of the plane x = 0 with the groove liquid/surface interface, the separation of the free surface radius of curvature center and then this virtual origin, κ_1, is given by [16]

$$\kappa_1 = \frac{r_o \cos\alpha}{\cos(\alpha + \theta_o)} \tag{A-4}$$

Further the separation of the virtual origin and the origin of figure A-1 is given by

$$0(\text{figure A-1}) - 0(\text{virtual}) = \varepsilon_2 \cot\theta_o - \text{HLSD} \tag{A-5}$$

Defining a parameter, K, by

$$K \equiv \kappa - (\varepsilon_2 \cot\theta_o - \text{HLSD}) \tag{A-6}$$

the equation describing the free surface is

$$(y - K)^2 + x^2 = \beta^2 \tag{A-7}$$

Expanding and rearranging equation (A-7) leads to

$$y^2 - 2K\ y + (K^2 - \beta^2 + x^2) = 0 \tag{A-8}$$

from which, solving for the roots of (A-8), the free surface description becomes

$$y = K - \sqrt{\beta^2 - x^2} \tag{A-9}$$

where only the smallest of the roots is an admissible one. The domain of applicability of equation (A-9) is the domain $0 \leqslant x \leqslant (\omega - \varepsilon_1)$. For the special case of a full groove condition, the limiting value of equation (A-9) for $\beta \to \infty$ is not immediately clear. For this case, however, the free surface description is given simply by

$$y = H \tag{A-10}$$

as is apparent from the figure.

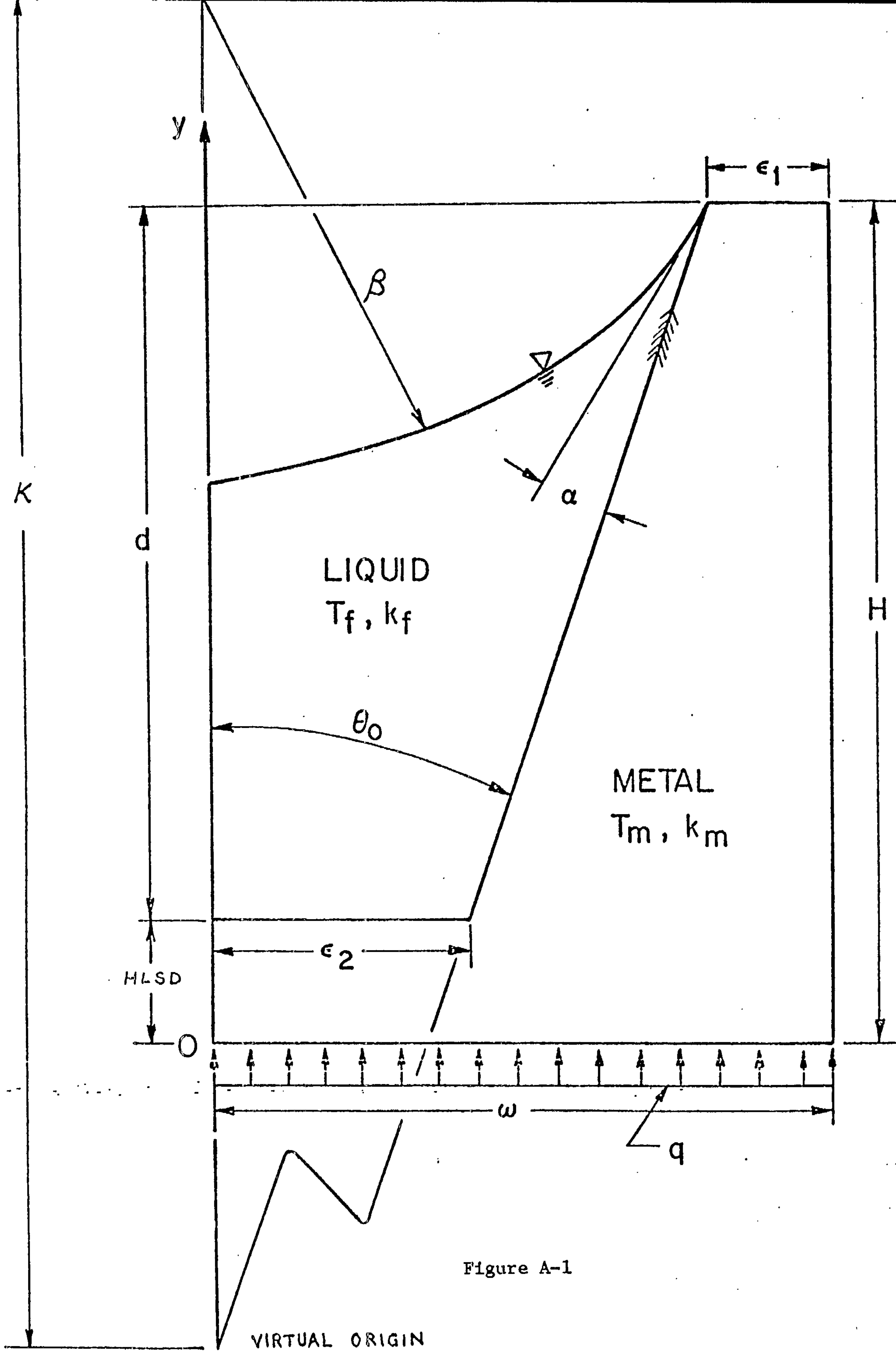
y
ε1
β
K
d
H
α
LIQUID
Tf , kf
θ0
METAL
Tm , km
ε2
HLSD
O
ω
q
VIRTUAL ORIGIN

Figure A-1

Appendix B

Programs for Heat Transfer Limit Evaluation

B.1 Introduction

In this appendix the program listings for the evaluation of the upper and lower groove heat transfer limits are presented. The programs serve only as mechanism for evaluation of the integrals presented in Chapter 4 of this report and as a result there will be no discussion here of the underlying theory. Both programs use a modified Simpson's Rule algorithm, the subroutine of which is included in the listings. To aid the interested reader, a brief nomenclature is included for the listings.

B.2 Groove Heat Transfer Lower Limit Program Nomenclature

The pertinent symbolic Fortran names used in the program for evaluation of the lower limit are presented here with frequent use made of the variables introduced in Chapter 4 of this report. Since duplication of certain mainline variables occurs in subroutine DINTGL, only mainline variables will be included in the nomenclature.

A1 = A_1

A2 = A_2

B1 = B_1

B2 = B_2

BETA = β

C = $H - d$

C1 = C_1

C2 = C_2

COND1 = k_m

COND2 = k_f

D = d

DINTGL = subroutine for integral evaluation

DKAPPA = K

DLIM1 = integration limit

DLIM2 = integration limit

DLIM3 = integration limit

DNUM = $Nu_f \equiv heq/(N \cdot k_f)$

DNUM = $Nu_m = heq/(N \cdot k_m)$

E1 = ε_1

E2 = ε_2

Fx1 = integrand for integral I

Fx2 = integrand for integral II

H = H

HEQ = heq

I,J,K,L = array subscripts to allow parameter variation

PI = π

Ro = r_o

RTOT = R_T

REQ = 1/(heq w)

THETA = θ_o(in degrees)

THRAD = θ_o(in radians)

U1 = $1/R_I$

$$U2 = 1/R_{II}$$

$$UTOT = 1/R_T$$

$$W = w$$

$$XALPHA = \alpha/(\pi/2 - \theta_o)$$

B.3 Groove Heat Transfer Lower Limit Program Listing

The program listing for evaluation of the lower groove heat transfer limit is presented on the following three pages.

```
C-----------------------------------------------------------------------
C
C              GROOVE HEAT TRANSFER LOWER LIMIT
C
C-----------------------------------------------------------------------
C
      IMPLICIT REAL*8(A-H,O-Z)
      DIMENSION E1(3),E2(3),D(3),COND2(3),XALPHA(4)
      EXTERNAL FX1,FX2
      COMMON/ONE/A1,B1,C1,BETA,A2,B2,C2
C
C---------INPUT DATA
C
      PI = 3.14159265388793
      C = 0.1
      COND1 = 1.0
      W = 1.0
      READ(5,1)  (E1(L),L=1,3)
    1 FORMAT(3F10.5)
      READ(5,2)  (E2(L),L=1,3)
    2 FORMAT(3F10.5)
      READ(5,3)  (D(K),K=1,3)
    3 FORMAT(3F10.5)
      READ(5,4)  (COND2(J),J=1,3)
    4 FORMAT(3F10.5)
      READ(5,5)  (XALPHA(I),I=1,4)
    5 FORMAT(4F10.5)
      WRITE(6,1)  (E1(L),L=1,3)
      WRITE(6,2)  (E2(L),L=1,3)
      WRITE(6,3)  (D(K),K=1,3)
      WRITE(6,4)  (COND2(J),J=1,3)
      WRITE(6,5)  (XALPHA(I),I=1,4)
      DO 25  L=1,3
      DO 26  K=1,3
      DO 27  J=1,3
      DO 28  I=1,4
C
C---------PRELIMINARY CALCULATIONS
C
      THRAD = DATAN((W-E1(L)-E2(L))/D(K))
      IF(XALPHA(I).GE.1.0)  XALPHA(I) = 0.999
      ALPHA = XALPHA(I)*(PI/2.-THRAD)
      H = (W-E1(L))/DTAN(THRAD)
      RC = (W-E1(L))/DSIN(THRAD)
      BETA = RC*DSIN(THRAD)/DCOS(ALPHA+THRAD)
      DKAPPA = RC*DCOS(ALPHA)/DCOS(ALPHA+THRAD)
      A1 = (DKAPPA-E2(L)/DTAN(THRAD))/(COND2(J)/COND1)
     *     + E2(L)/DTAN(THRAD) + RC*C*DSIN(THRAD)/W
      B1 = RC*DCOS(THRAD)/W + E1(L)/(RC*DCOS(THRAD))
     *     - 1./(DTAN(THRAD)*COND2(J)/COND1)
      C1 = -COND1/COND2(J)
      A2 = DKAPPA/(COND2(J)/COND1) + RC*C*DSIN(THRAD)/W
      B2 = RC*DCOS(THRAD)/W + E1(L)/(RC*DCOS(THRAD))
     *     - 1./(DTAN(THRAD)*COND2(J)/COND1)
      C2 = -COND1/COND2(J)
```

```
C
C---------LIMITS OF INTEGRATION
C
      DLIM1 = 0.0
      DLIM2 = F2(L)
      DLIM3 = RO*DSIN(THRAD)
C
C---------INTEGRAL EVALUATION
C
      CALL DINTGL(DLIM1,DLIM2,FX1,DINT1)
      CALL DINTGL(DLIM2,DLIM3,FX2,DINT2)
C
C---------COMPUTATION OF REQUIRED RESULTS
C
      U1 = DINT1
      U2 = DINT2
      UTOT = U1+U2
      RTOT = 1./UTOT
      REQ = RTOT - (C+F2(L)/DTAN(THRAD))/(COND1*W)
      HEQ = 1./(REQ*W)
      DNUF = HEQ*2.*W/COND2(J)
      DNUM = DNUF*COND2(J)/COND1
C
C---------OUTPUT
C
      WRITE(6,10)
   10 FORMAT('1',////,20X,'ESTABLISHING GROOVE HEAT TRANSFER',
     *                    ' LOWER LIMIT',//)
      THETA = THRAD*180./PI
      WRITE(6,11)  THETA
   11 FORMAT(' ',20X,'HALF GROOVE ANGLE = ',F7.3,' DEGREES',/)
      ALPDEG = ALPHA*180./PI
      WRITE(6,12)  ALPDEG
   12 FORMAT(' ',20X,'APPARENT CONTACT ANGLE = ',F7.3,' DEGREES',/)
      WRITE(6,13)  W
   13 FORMAT(' ',20X,'GROOVE CELL HALF-WIDTH = ',F7.3,/)
      WRITE(6,14)  F1(L)
   14 FORMAT(' ',20X,'LAND AREA RATIO = ',F7.3,/)
      WRITE(6,15)  F2(L)
   15 FORMAT(' ',20X,'GROOVE ROOT WIDTH RATIO = ',F7.3,/)
      DLGTH = R+C
      WRITE(6,16)  DLGTH
   16 FORMAT(' ',20X,'TEST SECTION LENGTH = ',F7.3,/)
      WRITE(6,17)  D(K)
   17 FORMAT(' ',20X,'ACTUAL GROOVE DEPTH = ',F7.3,/)
      WRITE(6,18)  COND1
   18 FORMAT(' ',20X,'CONDUCTIVITY ONE = ',F8.4,/)
      WRITE(6,19)  COND2(J)
   19 FORMAT(' ',20X,'CONDUCTIVITY TWO = ',F9.5,/)
      WRITE(6,20)  DNUF
   20 FORMAT(' ',20X,'NU(BASED ON KF) = ',F10.5,/)
      WRITE(6,21)  DNUM
   21 FORMAT(' ',20X,'NU * KF/KM = ',F9.5,/)
   28 CONTINUE
   27 CONTINUE
```

```
   26  CONTINUE
   25  CONTINUE
       WRITE(6,22)
   22  FORMAT('1')
       STOP
       END
C
C
C
       SUBROUTINE DINTGL(A,B,F,YNT)
       IMPLICIT REAL*8(A-H,O-Z)
       NN = 10
  101  CONTINUE
       H = (B-A)/NN
       SUM = (F(A)+F(B))/4. + (F(A+H/2.)+F(B-H/2.))/3.
     *               + 11.*(F(A+H)+F(B-H))/12.
       NNN = NN-2
       DO 102  N=2,NNN
       SUM = SUM+F(A+N*H)
  102  CONTINUE
       YNT = SUM*H
       IF(NN.EQ.10)  GO TO 103
       ERR = DABS((YNT-YNTO)/YNT)
       IF(ERR.LT.1.D-04)  GO TO 105
  103  CONTINUE
       NN = NN*2
       YNTO = YNT
       IF(NN.LE.40000)  GO TO 101
       WRITE(6,104)
  104  FORMAT(' ',/,10X,'INTEGRAL NOT CONVERGENT AT 40000',
     *                                ' SUBDIVISIONS',/)
  105  CONTINUE
       RETURN
       END
C
C
C
       FUNCTION FX1(X)
       IMPLICIT REAL*8(A-H,O-Z)
       COMMON/CNF/A1,B1,C1,BETA,A2,B2,C2
       FX1 = 1./(A1+B1*X+C1*DSQRT(BETA**2-X**2))
       RETURN
       END
C
C
C
       FUNCTION FX2(X)
       IMPLICIT REAL*8(A-H,O-Z)
       COMMON/CNF/A1,B1,C1,BETA,A2,B2,C2
       FX2 = 1./(A2+B2*X+C2*DSQRT(BETA**2-X**2))
       RETURN
       END
```

B.4 Groove Heat Transfer Upper Limit Program Nomenclature

The program nomenclature used for evaluation of the upper limit for the trapezoidal groove heat transfer follows closely that of the lower limit determination program. Where exceptions occur they are either self-explanatory or of no consequence, as for example in the case of localized working variables. As a result of the nomenclature similarities of the two limit prediction programs, a second nomenclature will not be presented here.

B.5 Groove Heat Transfer Upper Limit Program Listing

The program listing for evaluation of the upper groove heat transfer limit is presented on the final three pages of this appendix.

```
C--------------------------------------------------------------------
C
C             GROOVE HEAT TRANSFER UPPER LIMIT
C
C--------------------------------------------------------------------
C
      IMPLICIT REAL*8(A-H,O-Z)
      DIMENSION E1(3),E2(3),D(3),XALPHA(4)
      EXTERNAL FX1,FX2
      COMMON/ONE/DKAPPA,THRAD,COND1,COND2(3),RC,W,DPAR1,DPAR2,J
C
C---------INPUT DATA
C
      PI = 3.141592653589793
      C = 0.1
      COND1 = 1.0
      W = 1.0
      READ(5,1)  (E1(L),L=1,3)
    1 FORMAT(3F10.5)
      READ(5,2)  (E2(L),L=1,3)
    2 FORMAT(3F10.5)
      READ(5,3)  (D(K),K=1,3)
    3 FORMAT(3F10.5)
      READ(5,4)  (COND2(J),J=1,3)
    4 FORMAT(3F10.5)
      READ(5,5)  (XALPHA(I),I=1,4)
    5 FORMAT(4F10.5)
      WRITE(6,1)  (E1(L),L=1,3)
      WRITE(6,2)   (E2(L),L=1,3)
      WRITE(6,3)  (D(K),K=1,3)
      WRITE(6,4)  (COND2(J),J=1,3)
      WRITE(6,5)  (XALPHA(I),I=1,4)
      DO 25  L=1,3
      DO 26  K=1,3
      DO 27  J=1,3
      DO 28  I=1,4
C
C---------PRELIMINARY CALCULATIONS
C
      THRAD = DATAN((W-E1(L)-E2(L))/D(K))
      IF(XALPHA(I).GE.1.0)  XALPHA(I) = 0.999
      ALPHA = XALPHA(I)*(PI/2.-THRAD)
      H = D(K) +C
      RC = (W-E1(L))/DSIN(THRAD)
      BETA = RC*DSIN(THRAD)/DCOS(ALPHA+THRAD)
      DKAPPA = RC*DCOS(ALPHA)/DCOS(ALPHA+THRAD)
      DPAR1 = DKAPPA*DSIN(THRAD)
      DPAR2 = DKAPPA-RC*DCOS(THRAD)
C
C---------LIMITS OF INTEGRATION
C
      DLIM11 = BETA
      DLIM2 = DSQRT(W**2+(DKAPPA-RC*DCOS(THRAD))**2)
      DLIM12 = DLIM11+0.005*(DLIM2-DLIM11)
      DLIM3 = DKAPPA-E2(L)/DTAN(THRAD)
```

```
C
C---------INTEGRAL EVALUATION
C
      CALL DINTGL(DLIM11,DLIM12,FX1,DINT11)
      CALL DINTGL(DLIM12,DLIM2,FX1,DINT12)
      CALL DINTGL(DLIM2,DLIM3,FX2,DINT2)
C
C---------COMPUTATION OF REQUIRED RESULTS
C
      R11 = DINT11
      R12 = DINT12
      R1 = R11+R12
      R2 = DINT2
      R3 = (H-D(K))/(COND1*W)
      RTOT = R1+R2+R3
      DNUF = 2./((RTOT-R3)*COND2(J))
      DNUM = DNUF*COND2(J)/COND1
C
C---------OUTPUT
C
      WRITE(6,10)
   10 FORMAT('1',////,20X,'ESTABLISHING GROOVE HEAT TRANSFER',
     *                    ' UPPER LIMIT',//)
      THETA = THRAD*180./PI
      WRITE(6,11) THETA
   11 FORMAT(' ',20X,'HALF GROOVE ANGLE = ',F7.3,' DEGREES',/)
      ALFDEG = ALPHA*180./PI
      WRITE(6,12) ALFDEG
   12 FORMAT(' ',20X,'APPARENT CONTACT ANGLE = ',F7.3,' DEGREES',/)
      WRITE(6,13) W
   13 FORMAT(' ',20X,'GROOVE CELL HALF-WIDTH = ',F7.3,/)
      WRITE(6,14) E1(L)
   14 FORMAT(' ',20X,'LAND AREA RATIO = ',F7.3,/)
      WRITE(6,15) E2(L)
   15 FORMAT(' ',20X,'GROOVE ROOT WIDTH RATIO = ',F7.3,/)
      WRITE(6,16) H
   16 FORMAT(' ',20X,'TEST SECTION LENGTH = ',F7.3,/)
      WRITE(6,17) D(K)
   17 FORMAT(' ',20X,'ACTUAL GROOVE DEPTH = ',F7.3,/)
      WRITE(6,18) COND1
   18 FORMAT(' ',20X,'CONDUCTIVITY ONE = ',F8.4,/)
      WRITE(6,19) COND2(J)
   19 FORMAT(' ',20X,'CONDUCTIVITY TWO = ',F9.5,/)
      WRITE(6,20) DNUF
   20 FORMAT(' ',20X,'NU(BASED ON KF) = ',F10.5,/)
      WRITE(6,21) DNUM
   21 FORMAT(' ',20X,'NU * KF/KM = ',F9.5,/)
   28 CONTINUE
   27 CONTINUE
   26 CONTINUE
   25 CONTINUE
      WRITE(6,22)
   22 FORMAT('1')
      STOP
      END
```

```
C
C
C
      SUBROUTINE DINTGL(A,B,F,YNT)
      IMPLICIT REAL*8(A-H,O-Z)
      NN = 10
  101 CONTINUE
      H = (B-A)/NN
      SUM = (F(A)+F(B))/4. + (F(A+H/2.)+F(B-H/2.))/3.
     *               + 11.*(F(A+H)+F(B-H))/12.
      NNN = NN-2
      DO 102  N=2,NNN
      SUM = SUM+F(A+N*H)
  102 CONTINUE
      YNT = SUM*H
      IF(NN.EQ.10)  GO TO 103
      ERR = DABS((YNT-YNTO)/YNT)
      IF(ERR.LT.1.D-04)  GO TO 105
  103 CONTINUE
      NN = NN*2
      YNTO = YNT
      IF(NN.LE.40000)  GO TO 101
      WRITE(6,104)
  104 FORMAT(' ',/,10X,'INTEGRAL NOT CONVERGENT AT 40000',
     *                            ' SUBDIVISIONS',/)
  105 CONTINUE
      RETURN
      END
C
C
C
      FUNCTION FX1(X)
      IMPLICIT REAL*8(A-H,O-Z)
      COMMON/ONE/DKAPPA,THRAD,COND1,COND2(3),RO,W,DPAR1,DPAR2,J
      GF = DARSIN(DPAR1/X) - THRAD
      GM = DARCOS(DPAR2/X) - GF
      FX1 = 1./((COND2(J)*GF + COND1*GM)*X)
      RETURN
      END
C
C
C
      FUNCTION FX2(X)
      IMPLICIT REAL*8(A-H,O-Z)
      COMMON/ONE/DKAPPA,THRAD,COND1,COND2(3),RO,W,DPAR1,DPAR2,J
      GF = DARSIN(DPAR1/X) - THRAD
      GM = DARSIN(W/X) - GF
      FX2 = 1./((COND2(J)*GF + COND1*GM)*X)
      RETURN
      END
```

Appendix C

Finite Element Formulation of the Heat Conduction Equation in General Orthogonal Curvilinear Coordinates

C.1 Introduction

In the analytic solution of heat conduction and other potential field problems, the governing differential equation is conventionally formulated in one of the three coordinate systems; cartesian, circular cylinder, or spherical. Since the governing differential equation results from the application of the first law of thermodynamics, in the case of heat conduction, to a control volume of differential dimensions, this is always possible. Where the bounding surfaces of the solution domain lend themselves to one of these coordinate system, many solutions are available [50]. Considerable difficulty is experienced, however, when such geometric compatibility is not present.

It is sometimes possible in these cases to set up a system of coordinates which are 'more natural' to the field of interest, in this work that of heat conduction [30], such that the coordinate surfaces conform to the lines of flow and potential surfaces, and moreover that they offer geometric conformity with the bounding surfaces. The nature of such a coordinate system is determined by the geometry of the bounding surfaces, by the field behavior at the boundaries, by specifying the nature and position of field singularities, or by a combination of the above influences. In many instances these more natural coordinates allow a simple and tractable solution where use of the conventional three systems leaves the solution unmanageable.

For the above reasons, it is important that the heat conduction analyst be proficient in the use of orthogonal curvilinear coordinate systems. Unfortunately, however, while multi-directional problems can be reduced through their use to problems dependent upon a single curvilinear coordinate, there remains a large number of problems for which this is not the case, but for which the heat flow is predominantly unidirectional in nature. For these problems, where a numerical solution may be required, the advantages gained analytically through the use of curvilinear coordinates may be available through their use in the numerical solution of the problem.

In this work the numerical solution procedure of interest is the finite element method. First introduced to the solution of field problems in 1965 [39,40], the finite element method as applied to field problems has since been the subject of several investigations [41-44]. In many of these investigations the work has been directed at alternate derivations of the governing functional equation and at examining the treatment of transient terms appearing in the differential equation. In all cases, however, where application of the method is made, the cartesian coordinate system has been used.

It is the intent of this paper, therefore, to introduce to the finite element method as applied to conduction heat transfer the use of general orthogonal curvilinear coordinate systems. This will be accomplished by developing the governing functional equation with appropriate boundary conditions in a general orthogonal curvilinear frame. The resultant functional equation is well suited for solutions using the finite element method. Due to the nature of orthogonal curvilinear coordinate systems when appropriately chosen, their use in the finite element method serves to automatically provide a variable mesh subdivision in accordance with the problem requirements. This is a result of the transformation behavior near field singularities or geometric boundaries. This behavior leads to a finer or coarser curvilinear coordinate spacing, in terms of physical distances, as is appropriate to the local features it must describe. As a consequence, a simple uniform subdivision scheme in the curvilinear frame, very simple to implement in an automatic mesh generation routine, may result in a highly complex or distorted physical subdivision which may be more appropriate for the problem analysis. Appropriate choice of coordinate system is, of course, prerequisite to obtaining this advantage. For the class of problems in which the bounding surfaces form part of an orthogonal curvilinear net, this advantage can provide substantial savings both in computational time for solution and in programming effort. Two examples are presented to demonstrate the application of these results. The coordinate systems considered are the spherical and the oblate spheroidal coordinate systems.

C.2 Preliminary Remarks

Before proceeding with the development of the governing functional equation, it will be instrumental to consider a general orthogonal curvilinear coordinate system as illustrated in Figure C-1. Here u_1, u_2, and u_3 are used to denote the three principal directions in the curvilinear frame with x, y, and z denoting those of the corresponding cartesian system. In general, the cartesian coordinates can be related to the curvilinear ones through relations of the general form [30]

$$x = x(u_1, u_2, u_3)$$
$$y = y(u_1, u_2, u_3) \qquad \text{(C-1)}$$
$$z = z(u_1, u_2, u_3)$$

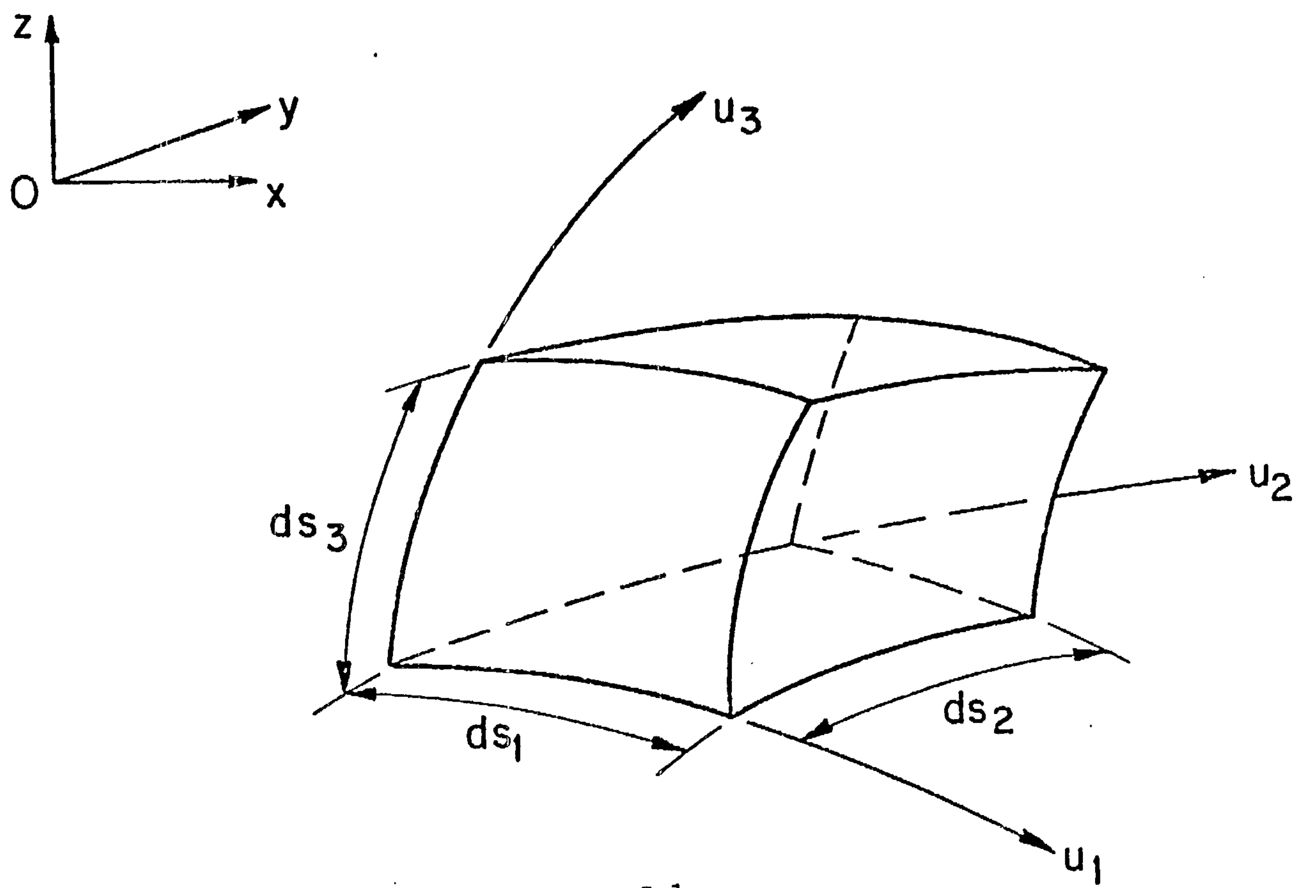

Figure C-1

In curvilinear space, a differential line element, $d\vec{s}$, can in turn be related back to the cartesian coordinates and is given by

$$d\vec{s} = \hat{i}\ dx + \hat{j}\ dy + \hat{k}\ dz \qquad \text{(C-2)}$$

By using the transformation relations (1), and the orthogonality properties of the coordinate directions, the magnitude of the vector $d\vec{s}$ can be given simply by

$$(ds)^2 = g_1(du_1)^2 + g_2(du_2)^2 + g_3(du_3)^2 \qquad \text{(C-3)}$$

where the metric or Lame coefficients of transformation are defined by [30]

$$g_i = \left(\frac{\partial x}{\partial u_i}\right)^2 + \left(\frac{\partial y}{\partial u_i}\right)^2 + \left(\frac{\partial z}{\partial u_i}\right)^2 , \quad i = 1, 2, 3 \tag{C-4}$$

These metric coefficients relate the curvilinear frame to the cartesian one from which it was derived.

Clearly for a length in the u_i direction where $du_j = du_k = 0$ the relationship is simply

$$ds_i = \sqrt{g_i}\, du_i \tag{C-5}$$

In a similar fashion the area element can be formed by

$$dA_i = \sqrt{g_j g_k}\, du_j\, du_k, \quad \begin{matrix} i = 1, 2, 3 \\ i \neq j \neq k \end{matrix} \tag{C-6}$$

where the convention has been used that the direction of the area element be taken normal to the surface in an outward sense. Finally, the volume element in curvilinear space is given by

$$dV = \sqrt{g}\, du_1\, du_2\, du_3 \tag{C-7}$$

where by definition

$$\sqrt{g} \equiv \sqrt{g_1 g_2 g_3} \tag{C-8}$$

By using the above relationships for length, area, and volume in an orthogonal curvilinear coordinate system, and by applying the first law of thermodynamics to the differential volume element of Fig. C-1, the governing differential equation can be written as [30]

$$\frac{\partial}{\partial u_1}\left[\frac{k_1\sqrt{g}}{g_1}\frac{\partial T}{\partial u_1}\right] + \frac{\partial}{\partial u_2}\left[\frac{k_2\sqrt{g}}{g_2}\frac{\partial T}{\partial u_2}\right] + \frac{\partial}{\partial u_3}\left[\frac{k_3\sqrt{g}}{g_3}\frac{\partial T}{\partial u_3}\right] + P\sqrt{g}$$

$$= \sqrt{g}\, \rho Cp \frac{\partial T}{\partial t} \tag{C-9}$$

where Fourier's law of heat conduction has been used to describe the local transfer of heat within the continuum.

The boundary conditions to be applied at the bounding surfaces of the solution domain (excepting non-linearized radiative conditions) will in general be given by

$$T = T_A(u_1, u_2, u_3, t) \tag{C-10a}$$

over S_1, and

$$\frac{k_1}{\sqrt{g_1}}\frac{\partial T}{\partial u_1}\,\ell_1 + \frac{k_2}{\sqrt{g_2}}\frac{\partial T}{\partial u_2}\,\ell_2 + \frac{k_3}{\sqrt{g_3}}\frac{\partial T}{\partial u_3}\,\ell_3 + hT + C = 0 \tag{C-10b}$$

over S_2 where ℓ_1, ℓ_2, and ℓ_3 are the direction cosines of the bounding surfaces with respect to the curvilinear coordinates u_1, u_2, and u_3 respectively. Alternatively, condition (C-10b) can be stated as

$$k_n \frac{\partial T}{\partial n} + hT + C = 0 \text{ over } S_2 \tag{C-10c}$$

where n is taken as the outward normal to the bounding surface over S_2.

The initial condition is represented simply by

$$T(u_1, u_2, u_3, o) = T_o(u_1, u_2, u_3) \tag{C-10d}$$

C.3 Variational Statement

If the concept of a variational principle is to be applied to the solution of heat conduction problems, then the governing differential equation (C-9) must correspond to the Euler equation for the corresponding variational problem. In this treatment we shall for simplicity of presentation and application follow the approach taken by Visser [40], Zienkiewicz and Parekh [44], and Zienkiewicz [51] where a particular instant of time is considered. In this way, time derivatives of temperature and of physical parameters can be treated as prescribed functions of the spatial coordinates u_1, u_2, and u_3. This is in contrast to the use of convolution integrals in time put forward by Gurtin [52] in establishing a true variational principle. The instantaneous considerations adopted here lead to a quasi-variational statement and can readily be converted to a restricted variational statement as indicated by Finlayson and Scriven [53]. The true variational approach, however, has been applied by Wilson and Nickell [42] in a cartesian coordinate frame and could also be extended to a general orthogonal curvilinear system by following arguments similar to those presented in this work.

Proceeding with the approach adopted here, and invoking the above requirement, we set

$$\int_{u_1}\int_{u_2}\int_{u_3} \{\frac{\partial}{\partial u_1}[\frac{k_1\sqrt{g}}{g_1}\frac{\partial T}{\partial u_1}] + \frac{\partial}{\partial u_2}[\frac{k_2\sqrt{g}}{g_2}\frac{\partial T}{\partial u_2}] + \frac{\partial}{\partial u_3}[\frac{k_3\sqrt{g}}{g_3}\frac{\partial T}{\partial u_3}]$$

$$+ P\sqrt{g} - \sqrt{g}\,\rho C_p \frac{\partial T}{\partial t}\} \delta T du_1 du_2 du_3 = 0 \qquad \text{(C-11)}$$

where we have introduced the first variation of temperature, δT. Considering now the first integral of equation (C-11) and denoting it by I_1, we have

$$I_1 = \int_{u_2}\int_{u_3}\left[\int_{u_1} \frac{\partial}{\partial u_1}[\frac{k_1\sqrt{g}}{g_1}\frac{\partial T}{\partial u_1}\right]\delta T\, du_1]du_2 du_3 \qquad \text{(C-12)}$$

Integrating (C-12) by parts and using the commutative property of the differential and variational operators yields

$$I_1 = \int_{u_2}\int_{u_3} \left[\frac{k_1\sqrt{g}}{g_1} \frac{\partial T}{\partial u_1} \delta T\right]\Bigg|_{u_1 = u_1(u_2,u_3)} du_2 du_3$$

$$- \int_{u_1}\int_{u_2}\int_{u_3} \left[\frac{k_1\sqrt{g}}{g_1} \frac{\partial T}{\partial u_1}\right] \frac{\partial}{\partial u_1} (\delta T) du_1 du_2 du_3 \qquad \text{(C-13)}$$

where $u_1(u_2,u_3)$ represents the locus of values that the u_1 coordinate takes on, as a function of the remaining two coordinates, as the bounding surface of the solution domain is traversed. Again using the commutability of the differential and variational operators, namely here that

$$\frac{\partial T}{\partial u_1} \frac{\partial}{\partial u_1} (\delta T) = \frac{\partial T}{\partial u_1} \delta\left(\frac{\partial T}{\partial u_1}\right) = \frac{1}{2} \delta\left[\left(\frac{\partial T}{\partial u_1}\right)^2\right] \qquad \text{(C-14)}$$

and simultaneously rearranging the integrand of the first integral of (C-13) we can write

$$I_1 = \int_{u_2}\int_{u_3} \left[\left[\frac{k_1}{\sqrt{g_1}} \frac{\partial T}{\partial u_1} \delta T\right] \sqrt{g_2 g_3}\right]\Bigg|_{u_1 = u_1(u_2,u_3)} du_2 du_3$$

$$- \frac{1}{2} \int_{u_1}\int_{u_2}\int_{u_3} \left[\frac{k_1\sqrt{g}}{g_1}\right] \left(\frac{\partial T}{\partial u_1}\right)^2 du_1 du_2 du_3 \qquad \text{(C-15)}$$

Finally, we recognize that $\sqrt{g_2 g_3}\, du_2 du_3$ when evaluated over $u_1 = u_1(u_2,u_3)$ on the boundary is simply the projection of the surface element dS on the u_2-u_3 plane and can be represented by

$$\sqrt{g_2 g_3}\,\Big|_{u_1 = u_1(u_2,u_3)} du_2\, du_3 = \ell_1\, dS \qquad \text{(C-16)}$$

This leads to the result that

$$I_1 = \iint_{S_1 + S_2} \left[\frac{k_1}{\sqrt{g_1}} \frac{\partial T}{\partial u_1} \delta T\right] \Bigg|_{\text{boundary}} \ell_1 \, dS$$

$$- \frac{1}{2} \int_{u_1} \int_{u_2} \int_{u_3} f_1 \left(\frac{\partial T}{\partial u_1}\right)^2 du_1 du_2 du_3 \tag{C-17}$$

where the definition has been made that

$$f_i = \frac{k_i \sqrt{g}}{g_i} \; ; \quad i = 1, 2, 3 \tag{C-18}$$

Further, by virtue of the specified temperature condition over the surface S_1 (by definition, the surface variation in temperature over S_1 will be zero), equation (C-17) reduces to the final result for this term

$$I_1 = \iint_{S_2} \left[\frac{k_1}{\sqrt{g_1}} \frac{\partial T}{\partial u_1} \delta T\right] \Bigg|_{\text{boundary}} \ell_1 \, d\, S_2$$

$$- \frac{1}{2} \delta \int_{u_1} \int_{u_2} \int_{u_3} f_1 \left(\frac{\partial T}{\partial u_1}\right)^2 du_1 du_2 du_3 \tag{C-19}$$

Expressions similar to equation (C-19) can readily be derived for the other two coordinate directions by following the procedure illustrated above. Only a systematic rotation of the subscripts in equation (C-19) is required for its adaptation to the other coordinate directions.

For the heat generation term of equation (C-11), considering only a spatial dependence of the generation rate, a direct application of the calculus of variations allows the heat generation term to be written as

$$\int_{u_1}\int_{u_2}\int_{u_3} P\sqrt{g}\ \delta T\ du_1 du_2 du_3 = \delta\int_{u_1}\int_{u_2}\int_{u_3} [P\sqrt{g}\ T]\ du_1 du_2 du_3 \qquad \text{(C-20)}$$

and similarly for the transient term, recalling that time derivatives are treated as being spatially prescribed, we have

$$\int_{u_1}\int_{u_2}\int_{u_3} \sqrt{g}\ \rho\ C_p \frac{\partial T}{\partial t}\ \delta T\ du_1\ du_2\ du_3 = \delta\int_{u_1}\int_{u_2}\int_{u_2} [\sqrt{g}\ \rho\ C_p(\frac{\partial T}{\partial t})T]du_1 du_2 du_3 \qquad \text{(C-21)}$$

Collecting the component equations (C-19), (C-20) and (C-21) to reform equation (C-11) we have

$$\delta\ \{\int_{u_1}\int_{u_2}\int_{u_3} \{\frac{f_1}{2}\ \frac{\partial T}{\partial u_1})^2 + \frac{f_2}{2}(\frac{\partial T}{\partial u_2})^2 + \frac{f_3}{2}\ (\frac{\partial T}{\partial u_3})^2 - P\sqrt{g}\ T$$

$$+ \sqrt{g}\ \rho C_p (\frac{\partial T}{\partial t})\ T\ \}du_1 du_2 du_3\ \}$$

$$-\iint_{S_2}\{\frac{k_1}{\sqrt{g_1}}\ \frac{\partial T}{\partial u_1}\ell_1 + \frac{k_2}{\sqrt{g_2}}\ \frac{\partial T}{\partial u_2}\ell_2 + \frac{k_3}{\sqrt{g_3}}\ \frac{\partial T}{\partial u_3}\ell_3\}\delta T dS_2 = 0 \qquad \text{(C-22)}$$

which can more conveniently be written, using boundary condition statements (C-10b) and (C-10c), as

$$\delta\{\int_{u_1}\int_{u_2}\int_{u_3} \{\frac{f_1}{2}\ (\frac{\partial T}{\partial u_1})^2 + \frac{f_2}{2}\ (\frac{\partial T}{\partial u_2})^2 + \frac{f_3}{2}\ (\frac{\partial T}{\partial u_3})^2 - P\sqrt{g}\ T$$

$$+ \sqrt{g}\ \rho C_p (\frac{\partial T}{\partial t})T\}du_1 du_2 du_3\}$$

$$+\iint_{S_2} [hT + C]\delta T\ dS_2 = 0 \qquad \text{(C-23)}$$

Finally, a further application of the variational calculus to the surface integral yields the variational statement

$$\delta\left\{\int_{u_1}\int_{u_2}\int_{u_3}\{\frac{f_1}{2}(\frac{\partial T}{\partial u_1})^2 + \frac{f_2}{2}(\frac{\partial T}{\partial u_2})^2 + \frac{f_3}{2}(\frac{\partial T}{\partial u_3})^2 - P\sqrt{g}T\right.$$

$$+ \sqrt{g}\,\rho C_p(\frac{\partial T}{\partial t})\,T\}du_1du_2du_3$$

$$\left.+\iint_{S_2}[\frac{hT^2}{2} + CT]dS_2\right\} = 0 \qquad \text{(C-24)}$$

Equation (C-24) above is the quasi-variational principle referred to earlier in this section, and its satisfaction, within the limits of the treatment of time dependent terms adopted here, is equivalent to satisfying the differential equation (C-9) from which it was derived.

C.4 Spatial Discretization

Before proceeding directly to the spatial discretization of the solution domain for application of the finite element method, it will be useful to define the following vectors and matrices. The first is a vector very similar to the gradient field vector [33] of a cartesian frame and will be defined by

$$\{G\}^T = \{\frac{\partial T}{\partial u_1}, \frac{\partial T}{\partial u_2}, \frac{\partial T}{\partial u_3}\} \qquad \text{(C-25)}$$

This vector will be henceforth referred to as the curvilinear field vector, although, since the curvilinear coordinates do not directly reflect physical distances, the components of (C-25) are not physical gradients unless accompanied by their corresponding metric coefficients. The second, a matrix analogous to the property matrix of a cartesian system, is defined by

$$[R] = \begin{bmatrix} f_1(u_1,u_2,u_3) & o & o \\ o & f_2(u_1,u_2,u_3) & o \\ o & o & f_3(u_1,u_2,u_3) \end{bmatrix} \qquad \text{(C-26)}$$

This matrix shall be referred to as the effective curvilinear property matrix. For completeness, the remaining vectors requiring definition are

$$\begin{aligned} \{T\} &= \{T(u_1,u_2,u_3)\} \\ \{P\} &= \{P(u_1,u_2,u_3)\} \\ \{C\} &= \{C(u_1,u_2,u_3)\} \end{aligned} \qquad \text{(C-27)}$$

and $\qquad \{\dot{T}\} = \{\frac{\partial T}{\partial t}\}$

It must be remembered that the vectors defined above at this stage remain continuous functions of the spatial coordinates in the curvilinear frame. Using their definitions, equations (C-25), (C-26) and (C-27), the variational statement (C-24) can be written in vector notation as

$$\delta \left\{ \int_{u_1}\int_{u_2}\int_{u_3} \{\frac{1}{2}\,\{G\}^T[R]\{G\} - \sqrt{g}\,\{T\}^T\{P\} + \sqrt{g}\,\rho C_p\,\{T\}^T\{\dot{T}\}\}du_1du_2du_3 + \iint_{S_2}\{\frac{h}{2}\,\{T\}^T\{T\} + \{T\}^T\,\{C\}\,\}dS_2 \right\} = 0 \qquad \text{(C-28)}$$

Having expressed the variational statement in vector notation, we now consider the fundamental concept of the finite element method, that the solution domain can be spatially sub-divided into a collection of finite elements, for each of which an approximate solution is assumed. This approximate solution will contain a specified number of arbitrary parameters, representative of the nodal degrees of freedom, whose determination is the object of the method. The determination of these nodal values for the independent variable is performed by the approximate satisfaction of the variational statement (C-28).

Approximating the unknown temperature distribution within a single element by the approximation

$$\{T\} \approx [N_1, N_2, \ldots] \begin{Bmatrix} T_1 \\ T_2 \\ \cdot \\ \cdot \\ \cdot \end{Bmatrix} = \{N_i\}^T \{T_i\} \tag{C-29}$$

the curvilinear field vector can immediately be written as

$$\{G\} = \begin{bmatrix} \partial N_1/\partial u_1 & \partial N_2/\partial u_1 & \cdots \\ \partial N_1/\partial u_2 & \partial N_2/\partial u_2 & \cdots \\ \partial N_1/\partial u_3 & \partial N_2/\partial u_2 & \cdots \end{bmatrix} \begin{Bmatrix} T_1 \\ T_2 \\ \cdot \\ \cdot \\ \cdot \end{Bmatrix} \equiv [B]\ \{T_i\} \tag{C-30}$$

In the above, the N_i's are the shape functions [33] for the element under consideration and their form and number will depend on the type of element selected for the problem at hand.

By using the equations (C-29) and (C-30) in (C-28), the variational statement for the approximate solution becomes

$$\delta \left[\sum_{e=1}^{n} \iiint_{V_e} \left[\frac{1}{2} \{T_i\}^T [B]^T [R] [B] \{T_i\} - \sqrt{g}\ \{T_i\}^T \{N_i\}\{P\} \right. \right.$$
$$\left. + \rho c_p \sqrt{g}\ \{T_i\}^T \{N_i\}\{N_i\}^T \{\dot{T}_i\} \right] du_1\, du_2\, du_3$$
$$\left. + \iint_{S_{2_e}} \left[\frac{h}{2} \{T_i\}^T \{N_i\}\{N_i\}^T \{T_i\} + \{T_i\}^T \{N_i\}\{C\} \right] dS_{2_e} \right.$$
$$= 0 \tag{C-31}$$

where the global integration over the entire field has been replaced by a summation of integrals, each integral being local to the element characterized by the summation index, e.

The approximate variational statement (C-31) can be written more compactly by

$$\delta F = 0 \tag{C-32}$$

where F, the approximate functional, denotes the expression within the outermost parentheses of (C-31). The approximate functional F, however, is a function only of the unknown nodal temperatures, T_i, $i = 1, 2, 3, \ldots$. Finding the stationary value of this functional by taking its first variation with respect to T then becomes equivalent to simply differentiating F with respect to each nodal temperature in turn, and setting the result equal to zero.

Performing the indicated differentiation, and recalling that the instantaneous thermal behavior is considered in this treatment, leads to the matrix-differential equations

$$[K]\ T_i + [P]\ \dot{T}_i = f \tag{C-33}$$

where

$$[K] = \sum_{e=1}^{n} \int_{V_e} [B]^T\ [R]\ [B]\ du_1\ du_2\ du_3 + \int_{S_{2_e}} h\ \{N_i\}^T\ \{N_i\}\ dS_2 \tag{C-34a}$$

$$[P] = \sum_{e=1}^{n} \int_{V_e} \rho c_p\ \sqrt{g}\ \{N_i\}^T\ \{N_i\}\ du_1\ du_2\ du_3 \tag{C-34b}$$

and

$$\{f\} = \sum_{e=1}^{n} \int_{V_e} \sqrt{g}\{N_i\}^T\ \{P\}\ du_1\ du_2\ du_3 + \iint_{S_{2_e}} \{N_i\}^T\ \{c\}\ dS_2 \tag{C-34c}$$

Solving the matrix-differential equations, (C-33), will provide the approximate solution for the temperature field. This is the ultimate objective of the analysis in applying the method. To effect the solution to (C-33), however, additional information is required to accommodate the time dependence of the equations. Following Zienkiewicz and Parekh [[illegible]], this time dependence is approximated here by finite differences over the time interval from t to t + Δt.

Evaluating (C-33) at time t + Δt/2 and using the first central difference quotient to approximate the first time derivative, we have

$$[K]\,\{T_i\}_{t+\frac{\Delta t}{2}} + [P]\left[\{T_i\}_{t+\Delta t} - \{T_i\}_t\right]/\Delta t = \{f\} \qquad \text{(C-35)}$$

where [K], [P], and {f}, if time dependent are assigned their mid-interval values. Noting that for this approximation scheme

$$\{T_i\}_{t+\frac{\Delta t}{2}} = \left[\{T_i\}_{t+\Delta t} + \{T_i\}_t\right]/2 \qquad \text{(C-36)}$$

we have

$$([K] + 2[P]/\Delta t)\,\{T_i\}_{t+\frac{\Delta t}{2}} = \frac{2[P]}{\Delta t}\{T_i\}_t + \{f\} \qquad \text{(C-37)}$$

with $$\{T_i\}_{t+\Delta t} = 2\,\{T_i\}_{t+\frac{\Delta t}{2}} - \{T_i\}_t \qquad \text{(C-38)}$$

These last two equations, (C-37) and (C-38), provide a convenient scheme to complete the integration. Other alternatives, however, are also available for the treatment of the time dependence [51]. The algebraic equations (C-37) with (C-38) and the coefficient matrix definitions (C-34) define the approximate solution using the finite element method in general orthogonal curvilinear coordinates. It can easily be demonstrated that these equations reduce to those for the cartesian case. In fact for a cartesian coordinate system where $g_1 = g_2 = g_3 = g = 1$ the analogy between the gradient field vector and the curvilinear field vector, and between the property matrix and the effective curvilinear property matrix, is complete, and becomes an equivalence. Thus the limiting behavior of these expressions is in accordance with our experience.

C.5 Application of the Results

The utility of the expressions derived in this work will be demonstrated here by means of two examples. However, since the treatment of heat generation and time dependent terms appearing in the governing differential equation is straightforward and follows accepted procedures, the examples presented will be restricted to the case of steady-state heat conduction. In both cases, linear isoparametric quadrilateral elements are used with the shape functions applied in the curvilinear coordinate frame.

The first example considers heat conduction through a spherical shell of inner radius r_i and outer radius r_o. The curvilinear (spherical) plane defined by $\theta = \alpha$ has a flux distribution prescribed while that defined by $\theta = \pi/2$ is maintained at a uniform temperature, $T = 0$. The remaining two boundaries have a zero normal gradient prescribed. The problem geometry is that illustrated in Fig. C-2 and axisymmetric heat transfer is considered. The case of $\alpha = 5.0$ degrees is examined.

Denoting the curvilinear (spherical) coordinates by

$$u_1 = r, \; u_2 = \theta, \; u_3 = \psi \qquad \text{(C-39)}$$

The metric coefficients are derived from equation (C-4):

$$
\begin{aligned}
g_1 &= 1 \\
g_2 &= r^2 \\
g_3 &= r^2 \sin^2\theta
\end{aligned}
\qquad \text{(C-40)}
$$

and

$$\sqrt{g} = r^2 \sin\theta$$

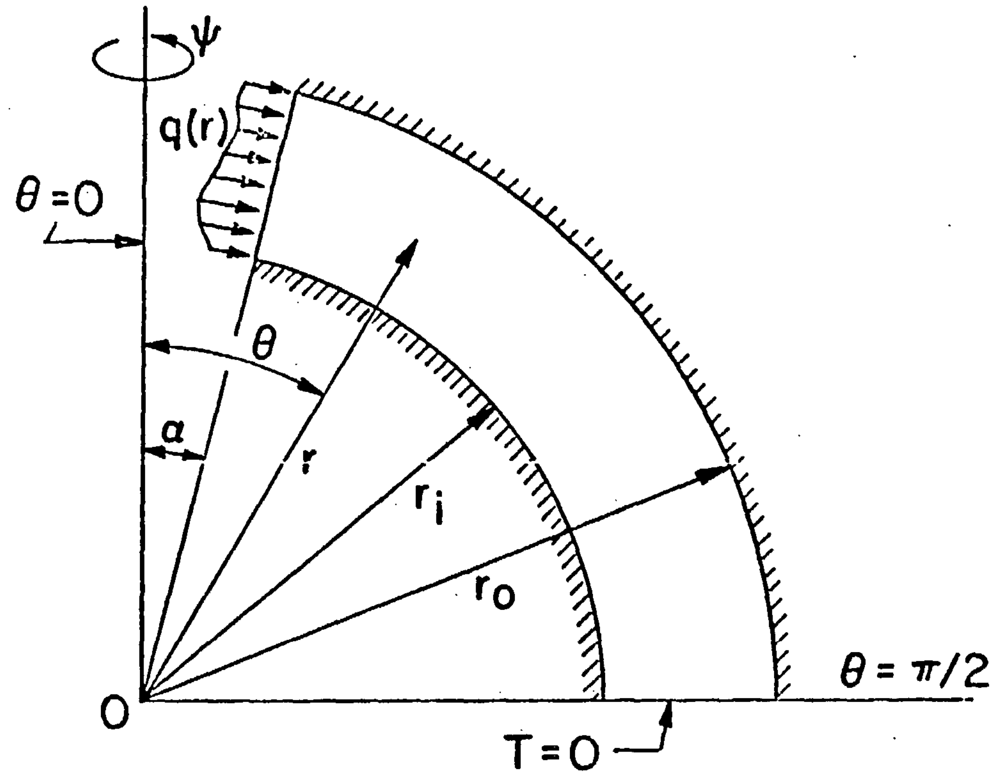

Figure C-2

From the above, the elements of the effective curvilinear property matrix can be found. Considering the axi-symmetric nature of the problem, the effective curvilinear property matrix becomes simply

$$[R] = \begin{bmatrix} k\, r^2 \sin\theta & 0 \\ 0 & k \sin\theta \end{bmatrix} \qquad \text{(C-41)}$$

Excepting boundary condition specification, then, this is the only modification required to allow a standard finite element program to treat this problem. Boundary condition specification for the flux prescribed cases to be considered are treated in the usual fashion by applying equivalent nodal heat flow rates at the appropriate nodes.

When the flux distribution applied over the conical section, $\theta = \alpha$, is equivalent to prescribing an isothermal boundary there, an exact solution is available [30]. For this case the flux distribution varies inversely with the radial coordinate

$$q = \frac{c}{r} \qquad \text{(C-42)}$$

and a non-dimensional thermal resistance can be determined to be

$$Rk\, r_o = \frac{1}{2\pi(1 < \varepsilon)} \ln \left[\frac{1}{\tan(\alpha/2)}\right] \qquad \text{(C-43)}$$

where $\varepsilon \equiv r_i/r_o$. Application of the flux distribution (C-42) to the problem at hand yields results which compare favorably with the exact solution. The comparison is presented in Table C-1 for three values of the parameter ε.

Since the method of subdivision used for the case of an isothermal cone is adequate to describe the thermal behavior of this problem, a further extension was made to consideration of a uniform flux boundary condition for $\theta = \alpha$. The convergence characteristics for this problem are shown in Fig. C-3 where the non-dimensional thermal resistance obtained from the finite element solution is presented as a function of the number of nodal points, NNP, used in the spatial discretization.

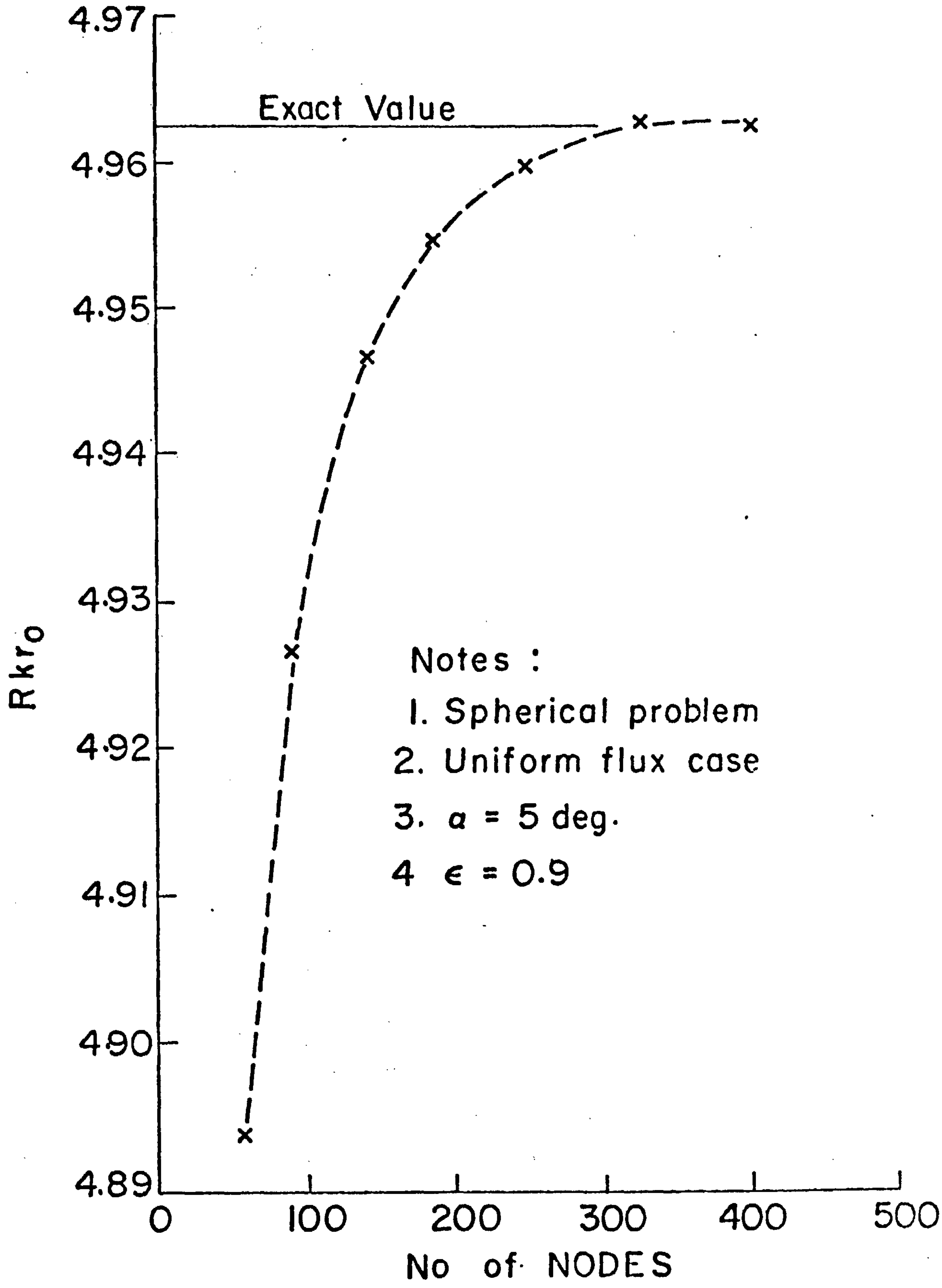
4.97
4.96
4.95
4.94
4.93
4.92
4.91
4.90
4.89
Rkro
Exact Value
Notes :
1. Spherical problem
2. Uniform flux case
3. α = 5 deg.
4 ε = 0.9
0
100
200
300
400
500
No of NODES

Figure C-3

The figure indicates a rapid and stable convergence to the limiting value.

Table 1

Comparison of FEM and Exact Solutions for Spherical Problem

α	ε	No. of Nodes	Rkr_o (ref. 14)	Rkr_o (present)	% Difference
5 degrees	.1	800	0.5537	0.5511	-0.47
5 degrees	.5	400	0.9967	0.9942	-0.25
5 degrees	.9	200	4.9836	4.9717	-0.24

To indicate the effect of the two different boundary conditions on the thermal resistance, Fig. C-4 was constructed. Here the ratio of resistances, that due to a uniform flux and that due to an isothermal boundary at $\theta = \alpha$, is plotted versus the radii ratio, ε. It can be seen from the figure that for ε approaching unity, the difference between the results for the two boundary conditions vanishes, as it should. However, for small ε the resistance resulting from a uniform flux over $\theta = \alpha$ exceeds that due to an isothermal specification by as much as 15 per cent. Higher deviations are expected for $\varepsilon < 0.1$. This example provides another illustration of the importance that boundary condition specification plays in determining the thermal resistance of any system. As was intended, however, this example also serves to illustrate the ease of application of the results presented in this paper.

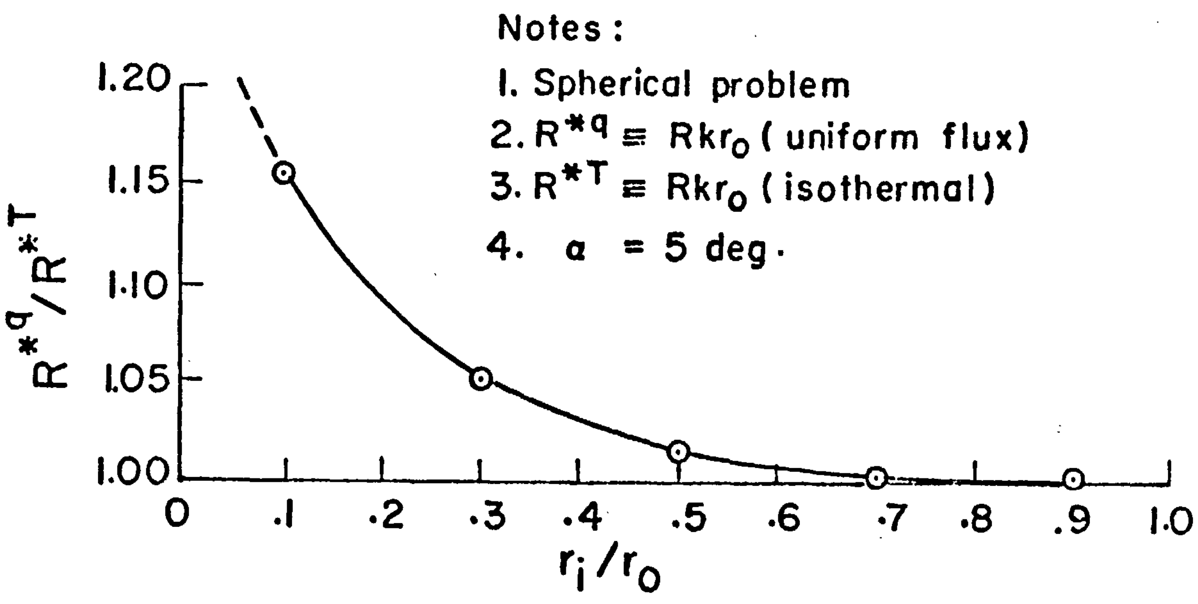

Figure C-4

The second example presented here considers the flow of heat from a thin circular disk located on a semi-infinite solid. Over the disk surface a prescribed flux distribution will be assumed while over the remaining free surface of the half-space the boundary is taken to be impervious to heat transfer. Again axi-symmetric heat transfer will be considered. The cross-section of the problem geometry is illustrated in Fig. C-5. The boundary at infinity has a prescribed temperature ($T = 0$) boundary specification.

In the case of an isothermal condition over the disk, the resultant temperature field becomes one dimensional in the oblate spheroidal coordinate, η, and a solution is readily obtained [30]. For other boundary conditions, however, this is not the case but departures from this one-

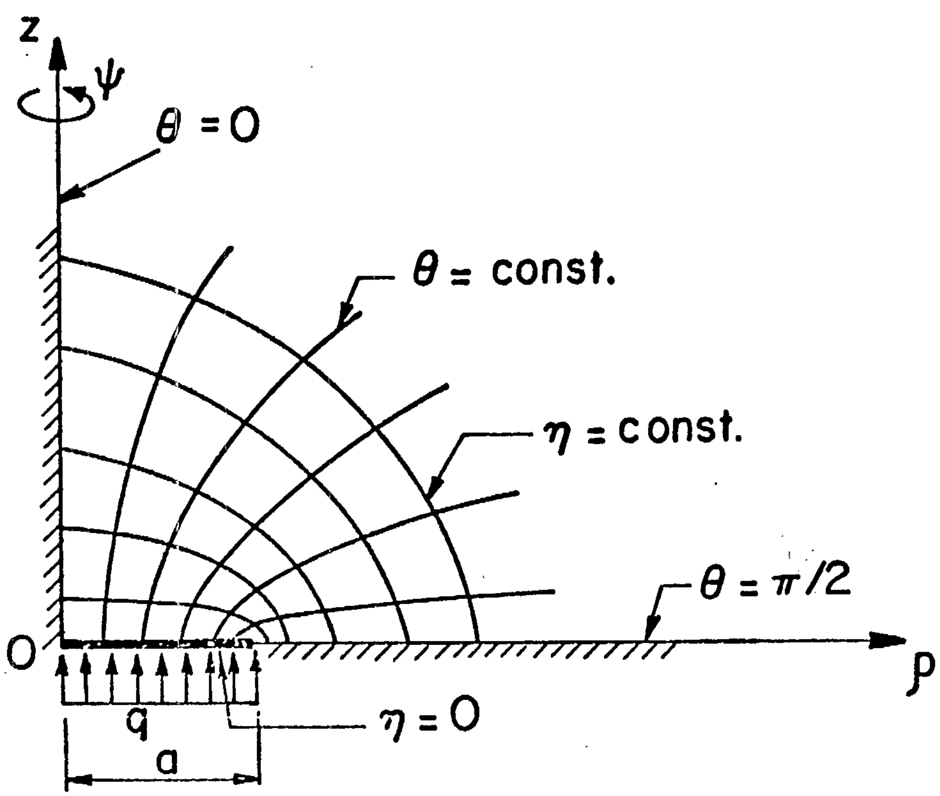

Figure C-5

dimensionality are expected to be small when compared with those experienced when using a cartesian, circular cylinder, or spherical coordinate system. This then suggests that the oblate spheroidal coordinate system is a 'natural' one to use for analysis purposes when considering the geometry of Fig. C-5.

The oblate spheroidal coordinate system is defined by the transformation equations

$$\begin{aligned} x &= a \cosh\eta \sin\theta \cos\psi \\ y &= a \cosh\eta \sin\theta \sin\psi \\ z &= a \sinh\eta \cos\theta \end{aligned} \qquad \text{(C-44)}$$

where a is the generating disk radius. Using the transformation equations (C-44) the metric coefficients can easily be determined to be

$$g_\eta = g_\theta = a^2 \ (\cosh^2\eta - \sin^2\theta)$$

$$g_\psi = a^2 \cosh^2\eta \sin^2\theta \qquad \text{(C-45)}$$

and $$\sqrt{g} = a^3 \ (\cosh^2\eta - \sin^2\theta) \cosh\eta \sin\theta$$

where the coordinates η, θ, and ψ are those indicated in figure C-5. Surfaces corresponding to lines of constant η and lines of constant θ describe ellipsoids and hyperboloids of revolution respectively when represented on a cartesian set of axes. The coordinate ψ represents the angular measure about the oz axis. It was found numerically and can be demonstrated analytically that $\eta_\infty \approx 10$ will suffice for the location of the boundary at infinity for heat transfer purposes.

Having found the metric coefficient of transformation, the effective curvilinear property matrix for this problem is given by

$$[R] = \begin{bmatrix} ak \cosh\eta \sin\theta & 0 \\ 0 & ak \cosh\eta \sin\theta \end{bmatrix} \qquad \text{(C-46)}$$

With the effective curvilinear property matrix defined and the flux prescribed boundary then treated in the usual fashion, the problem solution is now possible. In this example, a uniform flux distribution over the disk surface will be considered.

The dimensionless constriction resistance defined by $R^* \equiv Rka$, where R is the total thermal resistance based upon the mean disk surface temperature, is shown in Fig. C-6 plotted versus the number of nodal points used to effect the solution. Again the convergence characteristics indicate a rapid and stable approach toward its limiting value. The value of 0.269 obtained using 800 nodes compares favorably with the exact solution for this problem of 0.27019 [50].

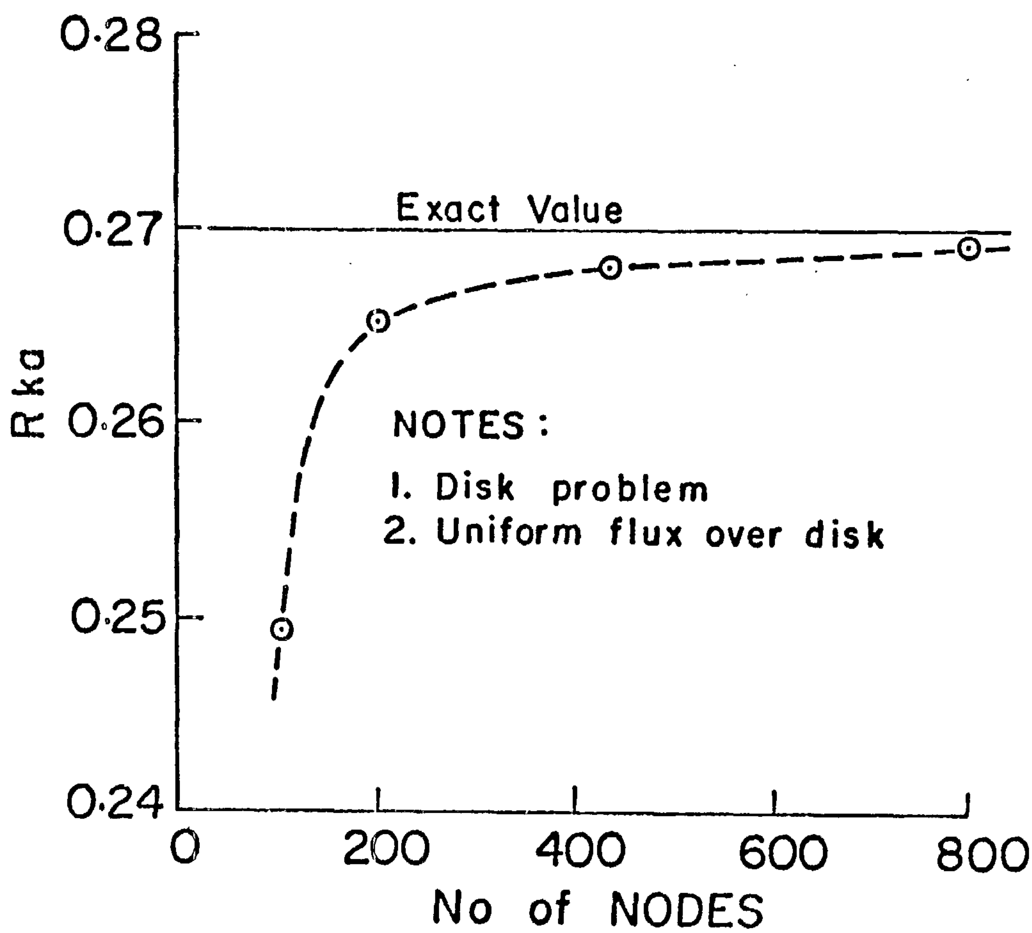

Figure C-6

Examining the solution behavior still further, a plot of the solution error in per cent is presented in Fig. C-7 as a function of the number of nodal points used in the mesh subdivisions. Indeed, from the figure it is seen that an error of less than 2 per cent is incurred when only 200 nodes are used to represent the continuum. Both the ease of application and the accuracy of the results indicate the utility of this work in analysing problems having a convenient 'natural' coordinate system.

C.6 Discussion and Conclusions

A quasi-variational 'principle' has been derived in this paper which describes the conduction of heat within a continuum. The derivation presented herein extends those currently available by its explicit consideration of general orthogonal curvilinear coordinate systems in the formulation of the governing variational statement for the heat conduction problem. This is of considerable utility since many problems have associated with them a natural or quasi-natural coordinate system.

Using this variational statement, a function equation, application of the finite element method is made by subdividing the solution domain into a collection of finite curvilinear elements, as is fundamental to the method. Over each of these elements an approximate solution is assumed, following the usual procedures, and a system of simultaneous equations results. After application of boundary conditions, solution of this system of equations leads to the required approximate solution for the temperature field by means of determining the temperature at each of the nodes used in the discretized curvilinear solution domain.

It was found convenient when using matrix notation to represent the governing functional equations, to define a 'curvilinear field vector' and an 'effective curvilinear property matrix' as these arise naturally

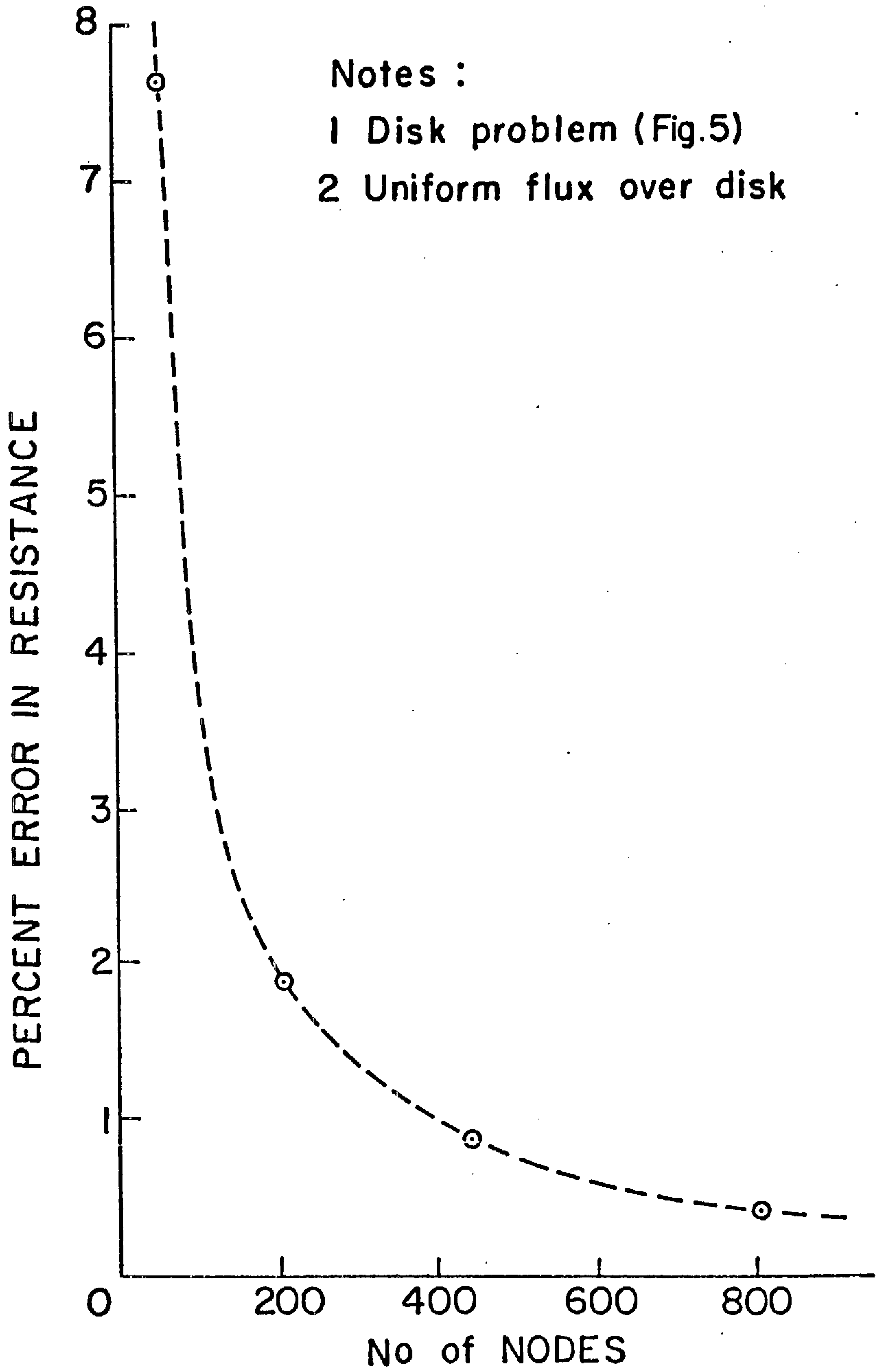
Notes :
1 Disk problem (Fig.5)
2 Uniform flux over disk
PERCENT ERROR IN RESISTANCE
8
7
6
5
4
3
2
1
0
200
400
600
800
No of NODES

Figure C-7

in the derivation. With these definitions, the matrix form of the variational statement bears a strong resemblance to the cartesian form in popular usage. This fact makes application of the results extremely easy and straightforward requiring minimal modification to existing finite element programs. Indeed, the results of this work reduce identically to those for the cartesian case when the appropriate metric coefficients defining the cartesian coordinate system are used.

Two examples have been presented which illustrate the ease of application of the results to other than the cartesian coordinate system. The spherical coordinate system and the oblate spheroidal coordinate system are the two systems used in the examples. In both cases the solution converged rapidly and monotonically to its limiting value. In particular by the second example, where only 800 nodes were used to represent a semi-infinite body and approximately 0.5 per cent accuracy was obtained, the utility of formulating the variational problem in the appropriate coordinate frame becomes clear.

These results will find application to contact problems, problems involving semi-infinite or infinite domains, and generally to problems where a coordinate system, more natural than the cartesian one, exists to describe the problem geometry and field behavior. The nature of these coordinate systems is to provide an automatic mesh generation, for uniform subdivision in the curvilinear coordinates, which locates smaller and larger elements (in terms of real physical size) throughout the domain as appropriate to the problem. These systems can also be used locally within larger systems and matched along common boundaries or joined using a relatively crude transition mesh. The net result in problems where there exists a more appropriate coordinate system will be a savings in both storage requirements and computational time to achieve a prescribed accuracy of solution.

Appendix D

Finite Element Groove Heat Transfer Prediction Program

D.1 Introduction

In this section the prediction program used for determination of the heat transfer characteristics of heat pipe walls having trapezoidal shaped grooves is presented. The program utilizes the finite element method for providing an approximate, numerical solution of Laplace's equation within the two component groove section discussed in Chapter 3 of this report. Due to its bookkeeping and manipulation complexity, however, the details of implementation of the method will not be presented here since the necessary discussion would be unduly lengthy and is not warranted in consideration of the objectives of this research. Sufficient proof has been presented earlier, in Chapter 5 of this report, that the program components are functioning correctly.

It was also brought forward in the discussions of Chapter 5 that large amounts of computer core were required to effect an accurate solution. As a result, the current program cannot be effectively run on the IBM 360/75 computing installation, which, until recently was the single installation available at the University of Waterloo. Instead, the program presented in this appendix is designed for use with the IBM 370/158 'virtual machine' installation now available at this University. As a result, a great deal of caution must be exercized if utilization of this program is attempted with other computational facilities, and even then the accuracy of the resulting output, unless sufficient core is available, may be questionable. The large core required by the solution program to provide a solution of acceptable accuracy is a reflection of the complex nature of the problem being investigated in this research.

D.2 Input Information

The program as presented in the final pages of this chapter utilizes an automatic mesh generation routine developed specifically for the trapezoidal groove problem. As a result only the parametric information necessary to characterize the groove geometry, materials combination, and the mesh refinement are required in the form of input data.

The solution program is directed at the solution of the normalized equations and boundary conditions (3-17) - (3-27). As a result the typical cell width, w, is assigned a value of unity automatically within the program. Further, the boundary condition at the liquid/vapor interface is a Dirichlet condition with a normalized magnitude here of zero. Since the problem is linear in temperature throughout the entire solution field, the further internal assignment has been made that the metal conductivity be unity. This results in a normalization of the temperature field with respect to the metal conductivity. Finally, the thickness of the pipe wall between the groove lower surface and the pipe exterior surface has been given a value of 0.1. The one-dimensional resistance of this thickness is later discounted in order to establish the 'equivalent' groove resistance and hence determine the groove equivalent heat transfer coefficient.

The remaining information required as input data to completely characterize the problem consists of, NE1, the number of lateral subdivisions within the metal fin section, IPRINT, a printing code parameter, THETA, the groove half-angle, XALPHA, the normalized apparent contact angle, COND(2), the fluid conductivity or in the normalized case the conductivity ratio kf/km, E1, the fin tip land area ratio, and E2, the groove root land area ratio. This information is fed into the program via two data cards.

The first data card consists of the parameters NE1 and IPRINT punched according to a 2I5 format. A value for NE1 of 19 was found acceptable in the convergence studies of Chapter 5 for the third mesh generation routine. A non-zero value for the IPRINT code parameter will cause the mesh generation details to be printed. This includes the x and y coordinates for each nodal point as well as a listing by element number of the element associated nodes and the material type for the element. Material type one indicates a metal element while material type two indicates an element within the liquid region of the solution domain. If the value of IPRINT is not supplied on this first data card, a value of zero will be assigned by most computing installations.

The second data card contains the remaining parameters specifications in the following order; THETA, XALPHA, COND(2), E1, E2. This information is supplied according to a 5F10.5 format.

THETA is the groove half-angle and is supplied in units of degrees. The second parameter, XALPHA $\equiv \alpha/(\pi/2 - \theta_o)$, is the normalized apparent and takes on values ranging from 0.0 to 1.0. The third parameter, COND(2), due to the internal specification that COND(1) = 1.0, is the fluid/metal thermal conductivity ratio, k_f/k_m. The final two parameters, E1 and E2 are the fin tip and groove root land area ratios respectively and can take on values in the range $0 \leq \{^{E1}_{E2}\} \leq 1.0$.

D.3 Program Listing

With the above input information the problem specification is complete. The prediction program listing is presented in the remaining pages of this chapter.

FILE: GROOVE FORTRAN A UNIVERSITY OF WATERLOO CONVERSATIONAL MONITOR SYSTEM

```
C-----------------------------------------------------------------------
C
C                 GROOVE HEAT TRANSFER - FINITE ELEMENTS
C
C-----------------------------------------------------------------------
C
      COMMON/ONE/NODES,X(2000),Y(2000),IE(2000,5),NFI(75),NFJ(75),
     *SUFFIX(75,2),ISEN1,R(2000),Z(2000),A(2000,50),NSFLXC,
     *ISPEC(76),NPN(76),NEL,NTSPEC
      COMMON/TWO/COND(2),W,C,TAVG,RES,DNU,HLSD,FLOW,F
      COMMON/THREE/AC(4,4)
C
C                        MAIN CONTROL PROGRAM
C
      REWIND 1
      CALL INPUT
      CALL SOLVER
      CALL OUTPUT
      STOP
      END
C
C
C                      INFORMATION INPUT
C
      SUBROUTINE INPUT
C
C---------INPUT OF GEOMETRIC AND NODAL DATA, MATERIAL PROPERTIES
C          AND BOUNDARY CONDITIONS
C
      COMMON/ONE/NODES,X(2000),Y(2000),IE(2000,5),NFI(75),NFJ(75),
     *SUFFIX(75,2),ISEN1,R(2000),Z(2000),A(2000,50),NSFLXC,
     *ISPEC(76),NPN(76),NEL,NTSPEC
      COMMON/TWO/COND(2),W,C,TAVG,RES,DNU,HLSD,FLOW,F
      COMMON/PRINT/IPRINT
      PI = 3.141592654
C---------
      READ(5,1001)  NE1,IPRINT
 1001 FORMAT(2I5)
      WRITE(6,1002)  NE1
 1002 FORMAT('NE1 = ',I5)
      READ(5,1003)  D,XALPHA,COND(2),E1,E2
 1003 FORMAT(5E10.5)
      WRITE(6,1003)  D,XALPHA,COND(2),E1,E2
      W = 1.0
      COND(1) = 1.0
      HLSD = 0.1
      THETA = ATAN((W-E1-E2)/D)
      ALPHA = XALPHA*(PI/2.-THETA)
      H = HLSD+D
C---------SUBDIVISION ALLOCATION
      NNE1 = NE1 + 1
      WORK = 2.*D/(E1+W-E2)
      ND = IFIX(WORK*FLOAT(NE1))
      NND = ND + 1
      WORK = E2/(W-E2)
```

```
      NE2 = IFIX(WORK*FLOAT(NE1))
      IF(NE2.EQ.0) NE2=1
      IF(E2.EQ.0.0) NE2 = 0
      NNE2 = NE2 + 1
      NHLSL = NL2 + 1
      NNHLSL = NHLSL + 1
      NW = NE1 + NE2
      NNW = NW + 1
      NF = NE1/2 + 1
      NNF = NF + 1
      NEL = NW + NE2*(NF+NW) + ND*(NF+NE1)
      NNP = NNW + NE2*(NNF+NNW) + NND*(NNF+NE1) - NF
      NEQNS = NNP
      VERTEX = HLSL - E2/TAN(THETA)
      R0 = (W-E1)/SIN(THETA)
      R1 = (W-E1-E2)/SIN(THETA)
      IF((ALPHA+THETA).GT.(0.999*PI/2.)) GO TO 10
      DLVL = VERTEX + (R0/COS(ALPHA+THETA))*(COS(ALPHA)-SIN(THETA))
      IF(DLVL.LE.HLSL) GO TO 15
      GO TO 20
   10 CONTINUE
      DLVL = VERTEX + R0*COS(THETA)
      GO TO 20
   15 WRITE(6,1004)
 1004 FORMAT('0',10X,'GROOVE DEPTH IS TOO SMALL TO ALLOW',
     *                    ' A CONTINUOUS MENISCUS')
      STOP
   20 CONTINUE
C
C                              NODAL POINT COORDINATES
C
C                                 1. FIRST ROW
C
      K = 0
      IF(NE2.EQ.0) GO TO 31
      WORK = E2/FLOAT(NE2)
      DO 30  J=1,NNE2
      K = K+1
      X(K) = (J-1)*WORK
      Y(K) = 0.0
   30 CONTINUE
   31 CONTINUE
      WORK = (W-E2)/FLOAT(NE1)
      DO 32  J=1,NE1
      K = K+1
      X(K) = X(K-1) + WORK
      Y(K) = 0.0
   32 CONTINUE
C
C                                 2. ROWS 2 TO NNE2
C
      THMAX = THETA*E2/(E2+R1)
      IF(NE2.EQ.0) GO TO 51
      DTH = THMAX/NE2
      DO 50  I=1,NNE2
```

```
      TH = (I-1)*DTH
      IF((ALPHA+THETA).GT.(0.999*PI/2.))  GO TO 35
      RS = RO * (COS(ALPHA)*COS(TH) -
     *          SQRT(SIN(THETA)**2-(COS(ALPHA)*SIN(TH))**2))
     *          /COS(ALPHA+THETA)
      GO TO 37
   35 CONTINUE
      RS = RO * COS(THETA)/COS(TH)
   37 CONTINUE
      XMAX = RS*SIN(TH)
      YMAX = VERTEX + RS*COS(TH)
      XMIN = (I-1)*B2/FLOAT(NE2)
      YMIN = ELSD
      DX = (XMAX-XMIN)/FLOAT(NF)
      DY = (YMAX-YMIN)/FLOAT(NF)
      DO 40  J=1,NN1
      K = K+1
      X(K) = XMAX-(J-1)*DX
      Y(K) = YMAX-(J-1)*DY
   40 CONTINUE
      LIM = NNE2-I
      IF(LIM.EQ.0)  GO TO 47
      DY = YMIN/FLOAT(NELSD)
      DO 42  J=1,LIM
      K = K+1
      X(K) = XMIN
      Y(K) = YMIN - J*DY
   42 CONTINUE
      DX = B2/FLOAT(NE2)
      DO 45  J=1,LIM
      K = K+1
      X(K) =  X(K-1) + DX
      Y(K) = Y(K-1)
   45 CONTINUE
   47 CONTINUE
      DX = (W-B2)/FLOAT(NE1)
      DO 49  J=1,NE1
      K = K+1
      X(K) = X(K-1) + DX
      Y(K) = Y(K-1)
   49 CONTINUE
   50 CONTINUE
   51 CONTINUE

                         3. ROWS NNE2 TO NELES1

      DELTH = THETA-THMAX
      XTIP = RO*SIN(THETA)
      YTIP = VERTEX + RO*COS(THETA)
      NELS1 = NL - 1
      DO 60  I=1,NELS1
      ANGLE1 = (FLOAT(I)/FLOAT(ND))*PI/2.
      TH = THMAX + DELTH*(SIN(ANGLE1))**1.00
      IF((ALPHA+THETA).GT.(0.999*PI/2.))  GO TO 52
      RS = RO * (COS(ALPHA)*COS(TH) -
```

```
     +           SQRT(SIN(THETA)**2-(COS(ALPHA)*SIN(TH))**2))
     *           /COS(ALPHA+THETA)
      GO TO 53
   52 CONTINUE
      RS = RC*COS(THETA)/COS(TH)
   53 CONTINUE
      XMAX = RS*SIN(TH)
      YMAX = VERTEX + RS*COS(TH)
      WORK = SQRT((XTIP-XMAX)**2 + (YTIP-YMAX)**2)
      RHC = (R1-WORK)*(1./3. + 4.*ANGLE1/(3.*PI)) + (R0-R1)
      XMIN = RHC*SIN(THETA)
      YMIN = VERTEX + RHC*COS(THETA)
      DX = (XMAX-XMIN)/FLOAT(NF)
      DY = (YMAX-YMIN)/FLOAT(NF)
      DO 55  J=1,NNF
      K = K+1
      X(K) = XMAX-(J-1)*DX
      Y(K) = YMAX-(J-1)*DY
   55 CONTINUE
      DELX = W-XMIN
      DO 57  J=1,NE1
      ANGLE2 = (FLOAT(J)/FLOAT(NE1))*PI/2.
      K = K+1
      X(K) = XMIN + DELX*(1.-COS(ANGLE2))*(FLOAT(I)/FLOAT(NE)) +
     +          (1.-FLOAT(I)/FLOAT(NE))*DELX*FLOAT(J)/FLOAT(NE1)
      Y(K) = YMIN
   57 CONTINUE
   60 CONTINUE
C
C                         4. LAST ROW
C
      K = K+1
      X(K) = XTIP
      Y(K) = YTIP
      DELX = R1
      DO 65  J=1,NE1
      ANGLE2 = (FLOAT(J)/FLOAT(NE1))*PI/2.
      K = K+1
      X(K) = XTIP + DELX*(1.-COS(ANGLE2))
      Y(K) = YTIP
   65 CONTINUE
C
C                   ELEMENT ASSOCIATED INDICES-CLOCKWISE
C                    ROTATIONAL NUMBERING
C
      M = 0
      DO 70  J=1,NW
      M = M+1
      IE(M,1) = J
      IE(M,2) = NNW + NE + NE2 + J
      IE(M,3) = NNW + NE + NE2 + J + 1
      IE(M,4) = J + 1
      IE(M,5) = 1
   70 CONTINUE
      L = 0
```

```
      IF(NE2.EQ.0)  GO TO 86
      DO 85  I=1,NE2
      L = L+1
      M = M+1
      IE(M,1) = IE(M-1,4) + 2
      IE(M,2) = IE(M-1,4) + 1
      IE(M,3) = IE(M,2) + NF + 2*(NE2-I+1) + NE1 + 1
      IE(M,4) = IE(M,3) + 1
      IE(M,5) = 2
      NFN(L) = IE(M,2)
      DO 73  J=2,NF
      M = M+1
      IE(M,1) = IE(M-1,1) + 1
      IE(M,2) = IE(M-1,1)
      IE(M,3) = IE(M-1,4)
      IE(M,4) = IE(M-1,4) + 1
      IE(M,5) = 2
   73 CONTINUE
      LIM = NE2-I
      IF(LIM.EQ.0)  GO TO 76
      DO 75  J=1,LIM
      M = M+1
      IE(M,1) = IE(M-1,1) + 1
      IE(M,2) = IE(M-1,1)
      IE(M,3) = IE(M-1,4)
      IE(M,4) = IE(M,3) + 1
      IE(M,5) = 1
   75 CONTINUE
   76 CONTINUE
      M = M+1
      IE(M,1) = IE(M-1,1) + 1
      IE(M,2) = IE(M-1,1)
      IE(M,3) = IE(M-1,4)
      IE(M,4) = IE(M,1) + 1
      IE(M,5) = 1
      LIM = NE2-I
      IF(LIM.EQ.0)  GO TO 80
      DO 77  J=1,LIM
      M = M+1
      IE(M,1) = IE(M-1,4)
      IE(M,2) = IE(M-1,3)
      IE(M,3) = IE(M,2) + 1
      IE(M,4) = IE(M,1) + 1
      IE(M,5) = 1
   77 CONTINUE
   80 CONTINUE
      DO 82  J=1,NE1
      M = M+1
      IE(M,1) = IE(M-1,4)
      IE(M,2) = IE(M-1,3)
      IE(M,3) = IE(M-1,3) + 1
      IE(M,4) = IE(M-1,4) + 1
      IE(M,5) = 1
   82 CONTINUE
   85 CONTINUE
```

```
 86   CONTINUE
      DO 92  I=1,NELS1
      L = L+1
      N = N+1
      IE(N,1) = IE(N-1,4) + 1
      IE(N,2) = IE(N-1,4) + NNF + NNE1
      IE(N,3) = IE(N,2) + 1
      IE(N,4) = IE(N,1) + 1
      IE(N,5) = 2
      NFR(L) = IE(N,1)
      DO 87  J=2,NE
      N = N+1
      IE(N,1) = IE(N-1,4)
      IE(N,2) = IE(N-1,3)
      IE(N,3) = IE(N,2) + 1
      IE(N,4) = IE(N,1) + 1
      IE(N,5) = 2
 87   CONTINUE
      DO 90  J=1,NE1
      N = N+1
      IE(N,1) = IE(N-1,4)
      IE(N,2) = IE(N-1,3)
      IE(N,3) = IE(N,2) + 1
      IE(N,4) = IE(N,1) + 1
      IE(N,5) = 1
 90   CONTINUE
 92   CONTINUE
      L = L+1
      N = N+1
      IE(N,1) = IE(N-1,4) + 1
      IE(N,2) = IE(N-1,4) + NNF + NNE1
      IE(N,3) = IE(N,2)
      IE(N,4) = IE(N,1) + 1
      IE(N,5) = 2
      NFR(L) = IE(N,1)
      NFR(L+1) = IE(N,2)
      DO 95  J=2,NE
      N = N+1
      IE(N,1) = IE(N-1,4)
      IE(N,2) = IE(N-1,2)
      IE(N,3) = IE(N-1,3)
      IE(N,4) = IE(N,1) + 1
      IE(N,5) = 2
 95   CONTINUE
      DO 97  J=1,NE1
      N = N+1
      IE(N,1) = IE(N-1,4)
      IE(N,2) = IE(N-1,3)
      IE(N,3) = IE(N,2) + 1
      IE(N,4) = IE(N,1) + 1
      IE(N,5) = 1
 97   CONTINUE
C
C
C                       BOUNDARY CONDITIONS
```

```
                         1. SPECIFIED FLUX

      NSFLXC = NW
      DO 100  I=1,NSFLXC
      NFI(I) = I
      NFJ(I) = I+1
      SURFLX(I,1) = 100.
      SURFLX(I,2) = 100.
  100 CONTINUE

                    2. SPECIFIED TEMPERATURE NODES

      NTSPEC = NND + NF2
      DO 102  I=1,NTSPEC
      TSPEC(I) = 0.
  102 CONTINUE

                    EVALUATE SEMI-BANDWIDTH

      MAXDIF = 0
      DO 105  M=1,NEL
      DO 105  J=1,4
      DO 105  I=1,4
      II = IABS(IE(M,I)-IE(M,J))
      IF(II.GT.MAXDIF)  MAXDIF = II
  105 CONTINUE
      ISEMI = MAXDIF + 1

                    DISPLAY PARTS OF INPUT

      WRITE(6,1010)
 1010 FORMAT('1')
      WRITE(6,1011)
 1011 FORMAT(' ',//,32X,'FINITE ELEMENTS')
      WRITE(6,1012)
 1012 FORMAT(' ',31X,'----------------',///)
      WRITE(6,1013)
 1013 FORMAT('0',30X,'BASIC PARAMETERS',//)
      WRITE(6,1014)  NNP
 1014 FORMAT(' ',25X,'NUMBER OF NODAL POINTS.........',I5)
      WRITE(6,1015)  NEL
 1015 FORMAT(' ',25X,'NUMBER OF ELEMENTS.............',I5)
      WRITE(6,1016)  COND(1)
 1016 FORMAT(' ',25X,'CONDUCTIVITY ONE...............',F8.4,
     *                ' BTU/(HR-FT-F)')
      WRITE(6,1017)  COND(2)
 1017 FORMAT(' ',25X,'CONDUCTIVITY TWO...............',F8.4,
     *                ' BTU/(HR-FT-F)')
      WRITE(6,1018)  W
 1018 FORMAT(' ',25X,'TEST SECTION WIDTH.............',F8.4,' FT')
      WRITE(6,1019)  B
 1019 FORMAT(' ',25X,'TEST SECTION LENGTH............',F8.4,' FT')
      WRITE(6,1020)  D
 1020 FORMAT(' ',25X,'ACTUAL GROOVE DEPTH............',F8.4,' FT')
```

```
      WRITE(6,1021)  W1                                                 GRC0386
 1021 FORMAT(' ',25X,'GROOVE LAND WIDTH...............',F8.4,' IN')     GRC0387
      WRITE(6,1022)  W2                                                 GRC0388
 1022 FORMAT(' ',25X,'GROOVE ROOT WIDTH...............',F8.4,' IN')     GRC0389
      THETAW    THETA*180./PI                                           GRC0390
      WRITE(6,1023)  THETAW                                             GRC0391
 1023 FORMAT(' ',25X,'GROOVE HALF ANGLE...............',F8.4,' DEGREES') GRC0392
       ALPHAW = ALPHA*180./PI                                           GRC0393
      WRITE(6,1024)  ALPHAW                                             GRC0394
 1024 FORMAT(' ',25X,'APPARENT CONTACT ANGLE.........',F8.4,' DEGREES') GRC0395
      WRITE(6,2001)  NE1                                                GRC0396
 2001 FORMAT(' ',25X,'NE1..............................',I5)           GRC0397
      WRITE(6,2002)  NE2                                                GRC0398
 2002 FORMAT(' ',25X,'NE2..............................',I5)           GRC0399
      WRITE(6,2003)  NE                                                 GRC0400
 2003 FORMAT(' ',25X,'NE...............................',I5)           GRC0401
      WRITE(6,2004)  NW                                                 GRC0402
 2004 FORMAT(' ',25X,'NW...............................',I5)           GRC0403
      WRITE(6,2005)  NF                                                 GRC0404
 2005 FORMAT(' ',25X,'NF...............................',I5)           GRC0405
      WRITE(6,1025)                                                     GRC0406
 1025 FORMAT(' ',//,30X,'BOUNDARY CONDITIONS',//)                       GRC0407
      WRITE(6,1026)                                                     GRC0408
 1026 FORMAT(' ',30X,'1. SPECIFIED FLUX',/)                             GRC0409
      WRITE(6,1027)                                                     GRC0410
 1027 FORMAT(' ',18X,'NODES',35X,'FLUX',/)                              GRC0411
      DO 110  L=1,NSFLXC                                                GRC0412
      WRITE(6,1028)  NPI(L),NPJ(L),SURFLX(L,1),SURFLX(L,2)              GRC0413
 1028 FORMAT(' ',11X,I5,'  TO  ',I5,22X,F7.3,'   TO   ',F7.3)           GRC0414
  110 CONTINUE                                                          GRC0415
      WRITE(6,1029)                                                     GRC0416
 1029 FORMAT(' ',///,29X,'2. SPECIFIED TEMPERATURE',/)                  GRC0417
      WRITE(6,1030)                                                     GRC0418
 1030 FORMAT(' ',18X,'NODE',32X,'TEMPERATURE',/)                        GRC0419
      DO 115  K=1,NTSPEC                                                GRC0420
      WRITE(6,1031)  NPK(K),TSPEC(K)                                    GRC0421
 1031 FORMAT(' ',16X,I5,35X,F7.3)                                       GRC0422
  115 CONTINUE                                                          GRC0423
      WRITE(6,1032)                                                     GRC0424
 1032 FORMAT('1')                                                       GRC0425
CHECK                                                                   GRC0426
      IF(IPRINT.EQ.0)  GO TO 126                                        GRC0427
      DO 120  I=1,NNP                                                   GRC0428
      WRITE(6,1033)  I,X(I),Y(I)                                        GRC0429
 1033 FORMAT(' ',10X,I5,10X,F8.4,10X,F8.4)                              GRC0430
  120 CONTINUE                                                          GRC0431
      WRITE(6,1032)                                                     GRC0432
      DO 125  M=1,NEL                                                   GRC0433
      WRITE(6,1034)  M,IE(M,1),IE(M,2),IE(M,3),IE(M,4),IE(M,5)          GRC0434
 1034 FORMAT(' ',3X,I5,3X,I5,3X,I5,3X,I5,3X,I5,3X,I5)                   GRC0435
  125 CONTINUE                                                          GRC0436
  126 CONTINUE                                                          GRC0437
CHECK                                                                   GRC0438
      RETURN                                                            GRC0439
      END                                                               GRC0440
```

```
C
C                           MATRIX ASSEMBLY AND SOLUTION
C
      SUBROUTINE SOLVER
C
C------- EVALUATES ELEMENT MATRICES AND ASSEMBLES TO FORM GLOBAL SYSTEM
C------- IMPLEMENTATION OF BOUNDARY CONDITIONS
C------- TRIANGULARIZATION AND SOLUTION
C
      COMMON/ONE/NEQNS,X(2000),Y(2000),IE(2000,5),NPI(75),NPJ(75),
     *SURFLX(75,2),ISEMI,R(2000),Z(2000),A(2000,50),NSFLXC,
     *ISPEC(76),NPN(76),NEL,NISPEC
      CALL MATRIX
      CALL SOLVE(1)
      CALL SOLVE(2)
      RETURN
      END
      SUBROUTINE MATRIX
C
C------- STIFFNESS MATRIX FORMED AND MODIFIED TO INCORPORATE B.C.
C------- LOAD VECTOR FORMED AND MODIFIED TO INCORPORATE B.C.
C
      COMMON/ONE/NEQNS,X(2000),Y(2000),IE(2000,5),NPI(75),NPJ(75),
     *SURFLX(75,2),ISEMI,R(2000),Z(2000),A(2000,50),NSFLXC,
     *ISPEC(76),NPN(76),NEL,NISPEC
      COMMON/TWO/COND(2),W,C,TAVG,RES,DNU,HLSD,FLOW,F
      COMMON/THREE/AC(4,4)
C
C                           INITIALIZE GLOBAL STIFFNESS AND LOAD VECTOR
C
      DO 1  I=1,NEQNS
      R(I) = 0.
      DO 1  J=1,ISEMI
      A(I,J) = 0.
    1 CONTINUE
C
C                           COMPUTE ELEMENT STIFFNESSES AND LOADS
C
      DO 3  N=1,NEL
C
C                           PROPERTY MATRIX
C
      C11 = COND(IE(N,5))
      C12 = 0.
      C21 = 0.
      C22 = COND(IE(N,5))
C
      CALL QUAD(N,C11,C12,C21,C22)
C
C                           ASSEMBLE STIFFNESS MATRIX
C
      DO 2  IN=1,4
      I=IE(N,IN)
      DO 2  JN=1,4
      J = IE(N,JN)-I+1
```

```
      IF(J.LE.0) GO TO 2
      A(I,J) = A(I,J)+AC(IW,JW)
    2 CONTINUE
    3 CONTINUE
      WRITE(1) ((A(I,J),J=1,ISEMI),I=1,NEQNS)
C
C                      CONVERT LINEARLY VARYING SURFACE FLUXES
C                      TO EQUIVALENT NODAL FLOW RATES AND ADD
C                      TO GLOBAL LOAD VECTOR
C
      IF(NSFLXC.EQ.0) GO TO 5
      DO 4 L=1,NSFLXC
      I = NFI(L)
      J = NFJ(L)
      DX = X(J)-X(I)
      DY = Y(J)-Y(I)
      R(I) = R(I)+DX*(SURFLX(L,1)/3.+SURFLX(L,2)/6.)
      R(J) = R(J)+DX*(SURFLX(L,1)/6.+SURFLX(L,2)/3.)
    4 CONTINUE
    5 CONTINUE
C
C                      INTRODUCE KINEMATIC CONSTRAINTS
C                      (GEOMETRIC BOUNDARY CONDITIONS)
C
      IF(NTSPEC.EQ.0) GO TO 7
      DO 6 K=1,NTSPEC
      CALL GEOBDC(TSPEC(K),NPB(K))
    6 CONTINUE
    7 CONTINUE
      RETURN
      END
      SUBROUTINE GEOBDC(T,N)
C
C---------- MODIFIES ASSEMBLAGE STIFFNESS FOR T PRESCRIBED AT NODE N
C
      COMMON/ONE/NEQNS,X(2000),Y(2000),IE(2000,5),NFI(75),NFJ(75),
     *SURFLX(75,2),ISEMI,R(2000),Z(2000),A(2000,50),NSFLXC,
     *TSPEC(76),NPB(76),NEL,NTSPEC
      DO 2 M=2,ISEMI
      K = N-M+1
      IF(K.LE.0) GO TO 1
      R(K) = R(K)-A(K,M)*T
      A(K,M) = 0.
    1 CONTINUE
      K = N+M-1
      IF(K.GT.NEQNS) GO TO 2
      R(K) = R(K)-A(N,M)*T
      A(N,M) = 0.
    2 CONTINUE
      A(N,1) = 1.
      R(N) = T
      RETURN
      END
      SUBROUTINE SOLVE(ICNTRL)
C
```

```
C--------- SOLVES A SET OF LINEAR,SYMMETRIC,'BANDED',SIMULTANEOUS        GRC05510
C          EQUATIONS OF THE FORM A*X=B USING GAUSS-DOOLITTLE DECOMP.      GRC05520
C--------- ONLY DIAGONAL AND RIGHT-OF-DIAGONAL ELEMENTS ARE INPUT IN A    GRC05530
C--------- TRANSFORMATION; J(BANDED) = J-I+1 AND I = I                    GRC05540
C--------- ICNTRL = CONTROL VARIABLE                                      GRC05550
C                       ICNTRL = 1; TRIANGULARIZATION ONLY                GRC05560
C                       ICNTRL = 2; SOLVES FOR R.H.S.                     GRC05570
C--------- SOLUTION RETURNS IN 'B' CONSTANT VECTOR                        GRC05580
                                                                          GRC05590
      COMMON/ONE/NEQNS,X(2000),Y(2000),IE(2000,5),NPI(75),NPJ(75),        GRC05600
     *SURFIX(75,2),ISEMI,B(2000),Z(2000),A(2000,50),NSFLXC,               GRC05610
     *TSPEC(76),NPR(76),NEL,NTSPEC                                        GRC05620
      DO 100  I=1,NEQNS                                                   GRC05630
      Z(I) = B(I)                                                         GRC05640
  100 CONTINUE                                                            GRC05650
      NLESS1 = NEQNS-1                                                    GRC05660
      IF(ICNTRL.EQ.2)  GO TO 3                                            GRC05670
                                                                          GRC05680
                          TRIANGULARIZATION                               GRC05690
                                                                          GRC05700
      DO 2  N=1,NLESS1                                                    GRC05710
      M = N-1                                                             GRC05720
      LIM = MINO(ISEMI,NEQNS-M)                                           GRC05730
      PIVOT = A(N,1)                                                      GRC05740
      DO 2  L=2,LIM                                                       GRC05750
      CP = A(N,L)/PIVOT                                                   GRC05760
      I = M+L                                                             GRC05770
      J = 0                                                               GRC05780
      DO 1  K=L,LIM                                                       GRC05790
      J = J+1                                                             GRC05800
      A(I,J) = A(I,J)-CP*A(N,K)                                           GRC05810
    1 CONTINUE                                                            GRC05820
      A(N,L) = CP                                                         GRC05830
    2 CONTINUE                                                            GRC05840
      GO TO 6                                                             GRC05850
    3 CONTINUE                                                            GRC05860
                                                                          GRC05870
                          SOLVING FOR R.H.S.                              GRC05880
                                                                          GRC05890
      DO 4  N=1,NLESS1                                                    GRC05900
      M = N-1                                                             GRC05910
      LIM = MINO(ISEMI,NEQNS-M)                                           GRC05920
      CP = B(N)                                                           GRC05930
      B(N) = CP/A(N,1)                                                    GRC05940
      DO 4  L=2,LIM                                                       GRC05950
      I = M+L                                                             GRC05960
      B(I) = B(I)-A(N,L)*CP                                               GRC05970
    4 CONTINUE                                                            GRC05980
      B(NEQNS) = B(NEQNS)/A(NEQNS,1)                                      GRC05990
      DO 5  I=1,NLESS1                                                    GRC06000
      N = NEQNS-I                                                         GRC06010
      M = N-1                                                             GRC06020
      LIM = MINO(ISEMI,NEQNS-M)                                           GRC06030
      DO 5  K=2,LIM                                                       GRC06040
      L = M+K                                                             GRC06050
```

```
      R(N) = R(N)-A(N,K)*R(L)
    5 CONTINUE
    6 CONTINUE
      RETURN
      END
C
C                              PRESENTATION OF RESULTS
C
      SUBROUTINE OUTPUT
C
C--------- CALCULATES DERIVED QUANTITIES AND PRINTS RESULTS
C
      COMMON/ONE/NECNS,X(2000),Y(2000),IE(2000,5),NPI(75),NPJ(75),
     *SURFLX(75,2),ISEMI,R(2000),Z(2000),A(2000,50),NSFLXC,
     *TSPEC(76),NPR(76),NEL,NTSPEC
      COMMON/TWO/COND(2),W,C,TAVG,RES,DNU,HLSD,FLOW,F
      CALL CALCNS
      CALL FCLERM(FLOW)
      CALL FNCTNL(F)
      CALL PRINT
      RETURN
      END
      SUBROUTINE CALCNS
C
C--------- PERFORMS MISCELLANEOUS CALCULATIONS
C
      COMMON/ONE/NECNS,X(2000),Y(2000),IE(2000,5),NPI(75),NPJ(75),
     *SURFLX(75,2),ISEMI,R(2000),Z(2000),A(2000,50),NSFLXC,
     *TSPEC(76),NPR(76),NEL,NTSPEC
      COMMON/TWO/COND(2),W,C,TAVG,RES,DNU,HLSD,FLOW,F
C
C                              SURFACE HEAT FLOWS
C
      Q = 0.
      IF(NSFLXC.EQ.0) GO TO 2
      DO 1 L=1,NSFLXC
      I = NPI(L)
      J = NPJ(L)
      DX = X(J)-X(I)
      DY = Y(J)-Y(I)
      Q = Q+DX*(SURFLX(L,1)/3.+SURFLX(L,2)/6.)
      Q = Q+DX*(SURFLX(L,1)/6.+SURFLX(L,2)/3.)
    1 CONTINUE
    2 CONTINUE
C
C                              AVERAGE SURFACE TEMPERATURE
C
      TAVG = 0.
      DO 3 J=1,NSFLXC
      DX = X(J+1)-X(J)
      TAVG = TAVG+DX*(R(J)+R(J+1))
    3 CONTINUE
      TAVG = TAVG/(2.*W)
C
C                              OVERALL THERMAL RESISTANCE
```

```
      RES = (TAVG-TSPEC(1))/C
      RES2 = RES-HLSD/(COND(1)*W)
      DNU = 2./(RES2*COND(2))
      RETURN
      END
      SUBROUTINE PRINT
      COMMON/ONE/NNODS,X(2000),Y(2000),IE(2000,5),NPI(75),NPJ(75),
     *SURFLX(75,2),ISEMI,R(2000),Z(2000),A(2000,50),NSFLXC,
     *TSPEC(76),NPR(76),NEL,NTSPEC
      COMMON/TWO/COND(2),W,C,TAVG,RES,DNU,HLSD,FLOW,F
      COMMON/FIELD/IFPRNT
      WRITE(6,201)
  201 FORMAT(' ',//,27X,'NODAL DATA, TEMPERATURES AND HEAT FLOW',//)
      WRITE(6,202)
  202 FORMAT(' ',3X,'NODE',14X,'X',16X,'Y',18X,'TEMP.',8X,'FLOW',/)
      DO 204  N=1,NNODS
      WRITE(6,203) N,X(N),Y(N),R(N),Z(N)
  203 FORMAT(' ',I6,10X,E12.5,5X,E12.5,10X,F8.3,5X,F8.4)
  204 CONTINUE
      WRITE(6,205)
  205 FORMAT('1')
      WRITE(6,206)
  206 FORMAT(' ',////,40X,'SUMMARY',//)
      WRITE(6,207)  FLOW
  207 FORMAT(' ',/,25X,'SUM OF NODAL FLOWS = ',F8.5,' BTU/HR')
      WRITE(6,208)  F
  208 FORMAT(' ',/,25X,'VALUE OF FUNCTIONAL = ',E13.5)
      WRITE(6,214)  TAVG
  214 FORMAT(' ',//,25X,'AVG. SURFACE TEMP. = ',F7.2,' DEG FAHR')
      WRITE(6,215)  C
  215 FORMAT(' ',/,25X,'TOTAL HEAT FLOW = ',F7.2,' BTU/HR')
      WRITE(6,216)  RES
  216 FORMAT(' ',/,25X,'TOTAL RESISTANCE = ',F8.4,' DEG F/BTU/HR')
      DNU2 = DNU*COND(2)/COND(1)
      WRITE(6,217)  DNU,DNU2
  217 FORMAT(' ',/,25X,'EQUIV. NUSSELT.NO. = ',F8.4,' BTU/(HR-SQ.FT-F)',
     1       //,25X,'(EQ. NU.) * (KF/KM) = ',F8.4,' BTU/(HR-SQ.FT-F)')
      WRITE(6,218)
  218 FORMAT('1')
      RETURN
      END
      SUBROUTINE BOIERN(FLOW)
      COMMON/ONE/NNODS,X(2000),Y(2000),IE(2000,5),NPI(75),NPJ(75),
     *SURFLX(75,2),ISEMI,R(2000),Z(2000),A(2000,50),NSFLXC,
     *TSPEC(76),NPR(76),NEL,NTSPEC
      FLOW = 0.0
      REWIND1
      READ(1) ((A(I,J),J=1,ISEMI),I=1,NNODS)
      DO 100 I1=1,NNODS
      FLUX = 0.0
      I3 = 0
      LIM = ISEMI + I1 - 1
      IF(LIM.GT.NNODS) LIM=NNODS
      DO 200 I2=I1,LIM
```

```
      L3 = L3+1
  200 FLUX = FLUX + A(L1,L3)*R(L2)
      IF(L1.EQ.1) GO TO 100
      LIM = L1
      IF(L1.GT.ISEMI) LIM=ISEMI
      DO 300 L2=2,LIM
      L3 = L1 - L2 + 1
  300 FLUX = FLUX + A(L3,L2)*R(L3)
      Z(L1) = FLUX
  100 FLOW = FLOW + FLUX
      RETURN
      END
      SUBROUTINE FNCTNL(F)
      COMMON/ONE/NEQNS,X(2000),Y(2000),IE(2000,5),NPI(75),NPJ(75),
     *SURFLX(75,2),ISEMI,R(2000),Z(2000),A(2000,50),NSFLXC,
     *ISPEC(76),NPK(76),NEL,NISPEC
      F = 0.0
      DO 100 I=1,NEQNS
      F = F + R(I)*Z(I)
  100 CONTINUE
      F = -0.5*F
      RETURN
      END
      SUBROUTINE QUAD(N,C11,C12,C21,C22)
C
C--------- COMPUTES ELEMENT STIFFNESS FOR N'TH ELEMENT
C--------- LINEAR,QUADRILATERAL,ISOPARAMETRIC,ELEMENT-2 PT. GAUSS QUADR.
C
      REAL*8 B(2,4),C(2,2),BTCB(4,4),CB(2,4),WAQ(4,4)
      REAL*8 DABS,DETJ,GAUSS,PI,RAD,S,T,DBLE
      REAL*8 X12,X13,X14,X23,X24,X34,Y12,Y13,Y14,Y23,Y24,Y34
      COMMON/ONE/NEQNS,X(2000),Y(2000),IE(2000,5),NPI(75),NPJ(75),
     *SURFLX(75,2),ISEMI,R(2000),Z(2000),A(2000,50),NSFLXC,
     *ISPEC(76),NPK(76),NEL,NISPEC
      COMMON/THREE/AQ(4,4)
      C(1,1) = DBLE(C11)
      C(1,2) = DBLE(C12)
      C(2,1) = DBLE(C21)
      C(2,2) = DBLE(C22)
      I = IE(N,1)
      J = IE(N,2)
      K = IE(N,3)
      L = IE(N,4)
      X12 = DBLE(X(I))-DBLE(X(J))
      X13 = DBLE(X(I))-DBLE(X(K))
      X14 = DBLE(X(I))-DBLE(X(L))
      X23 = DBLE(X(J))-DBLE(X(K))
      X24 = DBLE(X(J))-DBLE(X(L))
      X34 = DBLE(X(K))-DBLE(X(L))
      Y12 = DBLE(Y(I))-DBLE(Y(J))
      Y13 = DBLE(Y(I))-DBLE(Y(K))
      Y14 = DBLE(Y(I))-DBLE(Y(L))
      Y23 = DBLE(Y(J))-DBLE(Y(K))
      Y24 = DBLE(Y(J))-DBLE(Y(L))
      Y34 = DBLE(Y(K))-DBLE(Y(L))
```

```
C
C                          INITIALIZE AC MATRIX
C
      DO 1  IW=1,4
      DO 1  JW=1,4
      WAC(IW,JW) = 0.D0
    1 CONTINUE
C
C                          TERMS OF INTGRL (B**T)*C*B OVER VOLUME
C
      NN = 2
      GAUSS = .577350269189626
      DO 10  IGAUSS=1,4
      GO TO (2,3,4,5),IGAUSS
    2 S = GAUSS
      T = GAUSS
      GO TO 6
    3 S = -GAUSS
      T = GAUSS
      GO TO 6
    4 S = GAUSS
      T = -GAUSS
      GO TO 6
    5 S = -GAUSS
      T = -GAUSS
    6 CONTINUE
C
C                          FORM ELEMENTS OF B MATRIX
C
      DETJ = (X13*Y24-Y13*X24)+(X34*Y12-Y34*X12)*S+(X23*Y14-Y23*X14)*T
      DETJ = DETJ/8.
      B(1,1) = (Y24-Y34*S-Y23*T)/(8.*DETJ)
      B(1,2) = (-Y13+Y34*S+Y14*T)/(8.*DETJ)
      B(1,3) = (-Y24+Y12*S-Y14*T)/(8.*DETJ)
      B(1,4) = (Y13-Y12*S+Y23*T)/(8.*DETJ)
      B(2,1) = (-X24+X34*S+X23*T)/(8.*DETJ)
      B(2,2) = (X13-X34*S-X14*T)/(8.*DETJ)
      B(2,3) = (X24-X12*S+X14*T)/(8.*DETJ)
      B(2,4) = (-X13+X12*S-X23*T)/(8.*DETJ)
C
C                          COMPUTE MATRIX PRODUCT C*B
C
      DO 7  IW=1,2
      DO 7  JW=1,4
      CB(IW,JW) = 0.
      DO 7  KW=1,2
      CB(IW,JW) = CB(IW,JW)+C(IW,KW)*B(KW,JW)
    7 CONTINUE
C
C                          COMPUTE (B**T)*C*B PRODUCT
C
      DO 8  IW=1,4
      DO 8  JW=1,4
      BTCB(IW,JW) = 0.
      DO 8  KW=1,2
```

```
      BTCE(IW,JW) = BTCE(IW,JW)+B(KW,IW)*CE(KW,JW)                      GRC08260
    8 CCNTINUE                                                          GRC08270
C                                                                       GRC0828
C                                 FOR PLANAR PRCBLEMS                   GRC0829
C                                                                       GRC08300
      PI = 3.141592653589793                                            GRC0831
      RAD = 1./(2.*PI)                                                  GRC0832
      DC 9  IW=1,4                                                      GRC0833
      DC 9  JW=1,4                                                      GRC0834
      WAC(IW,JW) =WAC(IW,JW)+2.*PI*RAD*DABS(DETJ)*BTCE(IW,JW)*4./(NN**2)GRC0835
    9 CCNTINUE                                                          GRC0836
   10 CCNTINUE                                                          GRC0837
      DC 11 IW=1,4                                                      GRC0838
      DC 11 JW=1,4                                                      GRC0839
      AC(IW,JW) = SNGL(WAC(IW,JW))                                      GRC0840
   11 CCNTINUE                                                          GRC0841
      RETURN                                                            GRC0842
      END                                                               GRC0843
```

Appendix E

Typical Output from Finite Element Groove Heat Transfer Prediction Program

E.1 Introduction

In this appendix a typical output from the finite element prediction program is presented. A value of zero was used for the code parameter IPRINT since the use of a non-zero value is useful primarily during the debugging stage of the mesh generator development. This having been completed and verification made that the mesh generator is functioning correctly, it is unnecessary to display this information with every output.

E.2 Sample Output Description

On the final pages of this appendix a typical output from the groove heat transfer prediction program is presented with a brief description of the output given below. Due to the brevity of the following discussion frequent reference by the reader to the sample output will be helpful.

On the first page of output the 'Basic Parameters' describing the particular case under examination are displayed. This display includes material properties, problem characterization parameters, and various other pertinent geometric parameters. In addition to the above, information relevant to the spatial discretization of the problem solution domain are also presented. For an explanation of these parameters the reader is referred to figure 5-7 of Chapter 5 of this report.

Immediately following the display of the basic parameters, the boundary condition information is displayed. The specified flux boundary conditions over the pipe exterior surface are presented firstly. This information is presented in the form of an assumed linearly varying distribution between two successive nodes ranging from the first flux value reported at the first node number reported to the second value reported at the second node number reported. This is performed for each element having a surface on the pipe external surface. A uniform distribution of magnitude 100 (British units) is assumed internally within the program. Following directly the Neuman boundary condition presentation is the Dirichlet boundary condition specification over the liquid/vapor interface. The interpretation of the output for this condition is direct with an assumed relative value of zero for these nodes.

Where a non-zero value for the code parameter IPRINT is used, two tables, additional to those in the sample output, will be present. The first of these contains a listing of the node number, its global x-coordinate, and its global y-coordinate, in the order mentioned. This will be repeated for each node in the finite element model.

Again for the case of a non-zero value for IPRINT, a six column table will be presented following the table described in the previous paragraph. The horizontal entires of this table are respectively the element number, its associated nodal indices in the order of node one to node four, and the material type for the element. A material type of 1 indicates an element located in the solid region of the solution domain while a material type of 2 indicates an element in the liquid region of the cross-section.

The next portion of the output serves to report the node number, its x and y coordinate value in the global system, the nodal temperature as determined by the solution program and the net nodal heat flow rate imbalance. The net nodal heat flow imbalances reported here can serve as a useful check on the solver accuracy for the system of equations. For all internal nodes these nodal heat flow rate imbalances should all be zero (within the solver accuracy). Experience with the finite element method indicates that relatively large internal net heat flow imbalances result near highly skewed or poor aspect ratio elements. Thus this column also serves as an indicator for the acceptability of the mesh generation scheme. For external nodes, the net nodal heat flow rate imbalances over a given surface must sum to the total heat flow occurring across that particular surface. This also provides a check on the solution since the total heat entering the solution domain must, in the steady state, exit from the solution domain. Thus, for steady-state problems, <u>all</u> of the net nodal heat flow rates should algebraically sum to zero.

The final page of output presents a summary of the pertinent heat transfer data including both the computed and derived quantities of interest. The 'SUM OF NODAL FLOWS' is the quantity mentioned in the preceding paragraph which should sum to zero. This is, of course, relative to the total heat flow rate through the system. The number appearing on the sample output indicates approximately a 0.85 per cent cumulative round-off error when the 1828 nodes as used in this example are employed in discretizing the solution domain. The second entry of the summary is the computed value for the functional being extremized and is of importance when performing convergence studies. The 'AVG. SURFACE TEMP.' is the average computed external pipe surface temperature. The 'EQUIV. NUSSELT NO.' is the computed groove equivalent Nusselt number based upon the liquid thermal conductivity. The remaining entries of the summary are self-evident and relate to the derived quantities of Chapter 3.

E.3 Sample Output

The sample output described in the above section is included in the final pages of this appendix.

FINITE ELEMENTS

BASIC PARAMETERS

NUMBER OF NODAL POINTS.........	1826	
NUMBER OF ELEMENTS.............	1743	
CONDUCTIVITY ONE...............	1.[illegible]	BTU/(HR-FT-F)
CONDUCTIVITY TWO...............	[illegible]. 116	BTU/(HR-FT-F)
TEST SECTION WIDTH.............	1.[illegible]	FT
TEST SECTION LENGTH............	1.4737	FT
ACTUAL GROOVE DEPTH............	1.3737	FT
GROOVE LAND WIDTH..............	[illegible].25[illegible]	FT
GROOVE ROOT WIDTH..............	[illegible].25[illegible]	FT
GROOVE HALF ANGLE..............	2[illegible]	DEGREES
APPARENT CONTACT ANGLE.........	3.[illegible]	DEGREES
NE1............................	1[illegible]	
NE2............................	[illegible]	
NL.............................	52	
NW.............................	2[illegible]	
NF.............................	1[illegible]	

BOUNDARY CONDITIONS

1. SPECIFIED FLUX

NODES			FLUX		
1	TO	2	100.000	TO	100.000
2	TO	3	100.000	TO	100.000
3	TO	4	100.000	TO	100.000
4	TO	5	100.000	TO	100.000
5	TO	6	100.000	TO	100.000
6	TO	7	100.000	TO	100.000
7	TO	8	100.000	TO	100.000
8	TO	9	100.000	TO	100.000
9	TO	10	100.000	TO	100.000
10	TO	11	100.000	TO	100.000
11	TO	12	100.000	TO	100.000
12	TO	13	100.000	TO	100.000
13	TO	14	100.000	TO	100.000
14	TO	15	100.000	TO	100.000
15	TO	16	100.000	TO	100.000
16	TO	17	100.000	TO	100.000
17	TO	18	100.000	TO	100.000
18	TO	19	100.000	TO	100.000
19	TO	20	100.000	TO	100.000
20	TO	21	100.000	TO	100.000
21	TO	22	100.000	TO	100.000
22	TO	23	100.000	TO	100.000
23	TO	24	100.000	TO	100.000
24	TO	25	100.000	TO	100.000
25	TO	26	100.000	TO	100.000

NODE	TEMPERATURE
27	[illegible]
69	[illegible]
109	[illegible]
147	[illegible]
183	[illegible]
217	[illegible]
249	[illegible]
279	[illegible]
309	[illegible]
339	[illegible]
369	[illegible]
399	[illegible]
429	[illegible]
459	[illegible]
489	[illegible]
519	[illegible]
549	[illegible]
579	[illegible]
609	[illegible]
639	[illegible]
669	[illegible]
699	[illegible]
729	[illegible]
759	[illegible]
789	[illegible]
819	[illegible]
849	[illegible]
879	[illegible]
909	[illegible]
939	[illegible]
969	[illegible]
999	[illegible]
1029	[illegible]
1059	[illegible]
1089	[illegible]
1119	[illegible]
1149	[illegible]
1179	[illegible]
1209	[illegible]
1239	[illegible]
1269	[illegible]
1299	[illegible]
1329	[illegible]
1359	[illegible]
1389	[illegible]
1419	[illegible]
1449	[illegible]
1479	[illegible]
1509	[illegible]
1539	[illegible]
1569	[illegible]
1599	[illegible]
1629	[illegible]
1659	[illegible]
1689	[illegible]
1719	[illegible]
1749	[illegible]
1779	[illegible]
1809	[illegible]

NODAL DATA, TEMPERATURES AND HEAT FLOW

NODE	X	Y	TEMP.	FLOW
1	0.	0.0	474.166	2.[illegible]833
2	0.41667E-01	0.0	473.249	4.1659
3	0.83333E-01	0.0	47[illegible].797	4.1651
4	0.12500E+00	0.0	466.729	4.1661
5	0.16667E+00	0.0	461.123	4.166
6	0.20833E+00	0.0	45[illegible].2[illegible]	[illegible].16[illegible]
7	0.25[illegible]E+00	0.0	446.935	4.[illegible]356
8	0.28947E+00	0.0	44[illegible].278	3.9463
9	0.32895E+00	0.0	434.365	3.9459
10	0.36842E+00	0.0	429.236	3.9461
11	0.[illegible].789E+00	0.0	424.771	3.[illegible]64
12	0.44737E+00	0.0	42[illegible].848	3.946[illegible]
13	0.48684E+00	0.0	417.38[illegible]	3.9462
14	0.52632E+00	0.0	414.3[illegible]2	3.946[illegible]
15	0.56579E+[illegible]	0.0	411.566	3.9465
16	0.6[illegible]526E+[illegible]	0.[illegible]	4[illegible]9.137	3.[illegible]465
17	0.64474E+00	0.0	4[illegible]6.969	3.9457
18	0.68421E+00	0.0	4[illegible]5.1[illegible]2	3.9461
19	.72368E+00	0.0	4[illegible]3.46[illegible]	3.946[illegible]
20	.76316E+[illegible]	[illegible].0	4[illegible]2.[illegible]59	3.946[illegible]
21	0.8[illegible]263E+00	0.0	4[illegible].863	3.94[illegible]
22	0.84210E+00	0.0	399.928	3.946[illegible]
23	.88158E+[illegible]	[illegible].[illegible]	399.19[illegible]	3.9462
24	0.921[illegible]5E+[illegible]	.[illegible]	398.667	3.9462
25	0.96[illegible]53E+00	0.0	398.35[illegible]	3.946[illegible]
26	0.1[illegible]E+01	0.0	396.251	1.9735
27	.	[illegible].982[illegible]2E+[illegible]	[illegible].[illegible]	- .[illegible]
28	.	0.99382E+[illegible]	73.92	.
29	.	0.86561E+0[illegible]	135.969	-[illegible].[illegible]
30	.	0.71741E+[illegible]	195.675	- .[illegible]
31	.	0.62921E+[illegible]	2[illegible]4.92	.
32	.	[illegible].541[illegible]1E+[illegible]	287.921	- .[illegible]
33	.	0.45281E+00	32[illegible].[illegible]	- .[illegible]
34	.	0.36461E+0[illegible]	36[illegible].966	-.[illegible]
35	.	0.2764[illegible]E+[illegible]	394.016	-.[illegible]
36	.	[illegible].1682[illegible]E+0[illegible]	429.551	-.[illegible]
37	.	0.10000E+00	466.751	-[illegible].[illegible]11
38	.	0.85714E-01	468.958	-[illegible].[illegible]1
39	.	0.71429E-01	469.328	[illegible].[illegible]2
40	.	0.57143E-01	469.69[illegible]	-.[illegible]1[illegible]
41	0.	0.42857E-01	470.645	-[illegible].[illegible]15
42	0.	0.28571E-01	471.593	-[illegible].[illegible]5
43	0.	0.14286E-01	472.734	[illegible].0015
44	.41667E-01	0.14286E-01	471.916	[illegible].[illegible]5
45	0.83333E-01	0.14286E-01	469.465	.[illegible]7
46	0.12500E+00	0.14286E-01	465.393	.[illegible]
47	0.16667E+00	0.14286E-01	459.772	-[illegible].[illegible]
48	0.20833E+00	0.14286E-01	452.695	[illegible].[illegible]2
49	0.25000E+00	0.14286E-01	445.46[illegible]	[illegible].[illegible]1[illegible]

50	0.28947E+00	0.14286E-01	438.796	0.0017
51	0.32895E+00	0.14286E-01	432.684	0.0013
52	0.36842E+00	0.14286E-01	427.765	0.0015
53	0.40789E+00	0.14286E-01	423.307	0.0007
54	0.44737E+00	0.14286E-01	419.391	0.0003
55	0.48684E+00	0.14286E-01	415.927	0.0012
56	0.52632E+00	0.14286E-01	412.852	0.0006
57	0.56579E+00	0.14286E-01	410.118	0.0004
58	0.60526E+00	0.14286E-01	407.691	0.0003
59	0.64474E+00	0.14286E-01	405.543	0.0002
60	0.68421E+00	0.14286E-01	403.658	0.0009
61	0.72368E+00	0.14286E-01	402.019	-0.0001
62	0.76316E+00	0.14286E-01	400.615	0.0006
63	0.80263E+00	0.14286E-01	399.440	[illegible]
64	0.84210E+00	0.14286E-01	398.486	0.0003
65	0.88158E+00	0.14286E-01	397.748	0.0006
66	0.92105E+00	0.14286E-01	397.225	0.0012
67	0.96053E+00	0.14286E-01	396.912	[illegible]
68	0.10000E+01	0.14286E-01	396.810	0.0014
69	0.13331E-01	0.96213E+00	0.0	-0.1373
70	0.16164E-01	0.39391E+00	73.995	[illegible]
71	0.18998E-01	0.80571E+00	139.126	[illegible]
72	0.21831E-01	0.71749E+00	195.861	[illegible]
73	0.24665E-01	0.62928E+00	245.138	[illegible]
74	0.27499E-01	0.54106E+00	288.133	[illegible]
75	0.30332E-01	0.45285E+00	326.249	[illegible]
76	0.33166E-01	0.36464E+00	361.606	[illegible]
77	0.35999E-01	0.27643E+00	394.520	[illegible]
78	0.38333E-01	0.18821E+00	429.146	[illegible]
79	0.41667E-01	0.1[illegible]E+00	467.962	-0.0031
80	0.41667E-01	0.85714E-01	466.136	-0.0037
81	0.41667E-01	0.71429E-01	468.500	-0.0056
82	0.41667E-01	0.57143E-01	469.670	-0.0017
83	0.41667E-01	0.42857E-01	469.625	-0.0007
84	0.41667E-01	0.28571E-01	470.775	0.0021
85	0.83333E-01	0.28571E-01	468.323	0.0015
86	0.12500E+00	0.28571E-01	464.246	-0.0011
87	0.16667E+00	0.28571E-01	458.58	-0.0017
88	0.20833E+00	0.28571E-01	451.570	[illegible]
89	0.25000E+00	0.28571E-01	443.966	-0.0007
90	0.28947E+00	0.28571E-01	437.199	[illegible]
91	0.32895E+00	0.28571E-01	431.297	[illegible]
92	0.36842E+00	0.28571E-01	426.207	[illegible]
93	0.40789E+00	0.28571E-01	421.775	[illegible]
94	0.44737E+00	0.28571E-01	417.874	[illegible]
95	0.48684E+00	0.28571E-01	414.422	[illegible]
96	0.52632E+00	0.28571E-01	411.356	[illegible]
97	0.56579E+00	0.28571E-01	408.629	[illegible]
98	0.60526E+00	0.28571E-01	406.207	[illegible]
99	0.64474E+00	0.28571E-01	404.064	0.001[illegible]
100	0.68421E+00	0.28571E-01	402.181	0.000[illegible]
101	0.72368E+00	0.28571E-01	400.548	0.0007
102	0.76316E+00	0.28571E-01	399.163	0.00[illegible]
103	0.80263E+00	0.28571E-01	397.968	0.0011
104	0.84210E+00	0.28571E-01	397.014	[illegible]
105	0.88158E+00	0.28571E-01	396.277	-0.0007
106	0.92105E+00	0.28571E-01	395.754	0.000[illegible]
107	0.96053E+00	0.28571E-01	395.442	-0.0011
108	0.10000E+01	0.28571E-01	395.34	0.00[illegible]
109	0.26665E-01	0.98245E+00	0.0	-0.1377

110	.32335E- 1	0.89421E+00	71.218	[illegible]
111	0.38[illegible]2E- 1	0.84596E+00	139.536	[illegible]
112	0.43668E-01	0.71772E+00	196.415	[illegible]
113	0.49334E-01	0.62947E+00	245.777	[illegible]
114	.55[illegible]1E-01	0.54123E+00	288.789	[illegible]
115	.6[illegible]67E-01	0.45298E+00	326.6[illegible]1	[illegible]
116	0.66334E-01	0.36474E+00	361.342	[illegible]
117	0.72[illegible]E-01	0.27649E+00	394.243	[illegible]
118	0.77667E-01	0.18825E+00	427.931	0.00[illegible]
119	.83333E-01	0.1[illegible]E+00	465.497	[illegible]
120	0.83333E-01	0.85714E-01	465.677	[illegible]56
121	.83333E-01	0.71429E-01	466.[illegible]47	[illegible]31
122	0.83333E-01	0.57143E-01	466.612	[illegible]2[illegible]
123	0.83333E- 1	0.42857E-01	467.372	[illegible]
124	0.125[illegible]E+00	0.42857E-01	463.262	[illegible]
125	0.16667E+00	0.42857E-01	457.56[illegible]	[illegible]
126	.2[illegible]833E+00	0.42857E-01	45[illegible].327	.[illegible]007
127	0.25[illegible]E+00	0.42857E-01	442.379	[illegible]
128	0.28947E+00	0.42857E-01	435.475	[illegible]
129	0.32895E+00	0.42857E-01	429.[illegible]3	[illegible]1
130	.36842E+00	0.42857E-01	424.565	[illegible]7
131	0.4[illegible]789E+00	0.42857E-01	42[illegible].169	[illegible]2
132	0.44737E+00	0.42857E-01	416.298	[illegible]
133	0.48684E+00	0.42857E-01	412.867	[illegible]5
134	.52632E+00	.42857E-01	4[illegible]9.616	[illegible]5
135	0.56579E+00	0.42857E-01	4[illegible]7.1[illegible]	[illegible]
136	0.60526E+00	0.42857E-01	4[illegible].636	[illegible]
137	.64474E+00	0.42857E-01	4[illegible]2.55[illegible]	[illegible]4
138	.68421E+00	0.42857E-01	4[illegible].671	[illegible]11
139	0.72368E+00	0.42857E-01	399.[illegible]38	[illegible]
140	0.76316E+00	0.42857E-01	397.639	[illegible]
141	0.8[illegible]263E+00	0.42857E-01	396.406	[illegible]2
142	0.84210E+00	0.42857E-01	395.514	[illegible]2
143	.88158E+00	0.42857E-01	394.776	[illegible]
144	0.92105E+00	0.42857E-01	394.256	[illegible]
145	0.96053E+00	0.42857E-01	393.944	[illegible]1
146	0.10[illegible]E+01	0.42857E-01	393.642	[illegible]7
147	0.4[illegible]22E-01	0.98300E+00	[illegible]	-0.1383
148	0.48519E-01	0.89470E+00	74.591	[illegible]
149	0.57017E-01	0.80640E+00	1[illegible].226	[illegible]
150	0.65515E-01	0.71810E+00	197.349	[illegible]
151	0.74[illegible]13E-01	0.62980E+00	246.853	[illegible]
152	0.82511E-01	0.54150E+00	289.679	[illegible]
153	0.91[illegible]9E-01	0.45320E+00	327.727	[illegible]
154	0.995[illegible]E-01	0.36490E+00	361.832	[illegible]
155	0.1[illegible]E+00	0.2766[illegible]E+00	393.624	[illegible]
156	0.11650E+00	0.18830E+00	425.9[illegible]1	[illegible]
157	0.125[illegible]E+00	0.10000E+00	461.391	[illegible]65
158	.125[illegible]E+00	0.85714E-01	461.545	[illegible]56
159	.125[illegible]E+00	0.71429E-01	461.93[illegible]	[illegible]
160	0.125[illegible]E+00	0.57143E-01	462.512	[illegible]59
161	0.16667E+00	0.57143E-01	456.731	[illegible]25
162	.20833E+00	0.57143E-01	449.196	[illegible]18
163	0.25[illegible]E+00	0.57143E-01	44[illegible].673	[illegible]14
164	0.28947E+00	0.57143E-01	433.[illegible]2	[illegible]7
165	0.32895E+00	0.57143E-01	427.[illegible]2	[illegible]14
166	0.36842E+00	0.57143E-01	422.639	[illegible]14
167	0.40789E+00	0.57143E-01	418.497	[illegible]19
168	0.44737E+00	0.57143E-01	414.665	[illegible]16
169	0.48684E+00	0.57143E-01	411.262	[illegible]11

170	.52632E+[illegible]	[illegible].57143E-01	4[illegible]8.232	[illegible].00[illegible]8
171	.56579E+[illegible]	[illegible].57143E-01	405.531	[illegible].0[illegible]9
172	.60526E+00	0.57143E-01	403.129	[illegible].[illegible]14
173	.64474E+00	0.57143E-01	401.[illegible]1	0.[illegible]
174	.68421E+[illegible]	[illegible].57143E-01	399.129	[illegible].[illegible]9
175	.72368E+[illegible]	[illegible].57143E-01	397.5[illegible]	[illegible].[illegible]12
176	.76316E+[illegible]	0.57143E-01	396.1[illegible]5	[illegible].[illegible]15
177	.80263E+00	0.57143E-01	394.935	0.0011
178	.84210E+00	[illegible].57143E-01	393.985	[illegible].0011
179	[illegible].88158E+00	[illegible].57143E-01	393.251	[illegible].[illegible]
180	[illegible].92105E+00	0.57143E-01	392.73[illegible]	-[illegible].[illegible]2
181	.96053E+00	[illegible].57143E-01	392.419	[illegible].00[illegible]5
182	[illegible].1[illegible]E+01	[illegible].57143E-01	392.317	[illegible].00[illegible]
183	[illegible].53397E-01	.98376E+0[illegible]	.	-[illegible].1391
184	[illegible].64724E-01	[illegible].89539E+0[illegible]	75.119	[illegible].[illegible]
185	[illegible].76[illegible]51E-01	0.80701E+0[illegible]	141.194	[illegible]
186	[illegible].87378E-01	.71863E+[illegible]	198.[illegible]9	[illegible]
187	[illegible].987[illegible]5E-01	[illegible].63[illegible]26E+[illegible]	248.[illegible]	-[illegible]
188	[illegible].11[illegible]3E+00	[illegible].54188E+00	2[illegible]1.414	-[illegible]
189	.12136E+[illegible]	[illegible].4535[illegible]E+0[illegible]	329.[illegible]1	-[illegible]
190	[illegible].13269E+[illegible]	[illegible].36513E+[illegible]	362.[illegible]	[illegible]
191	[illegible].144[illegible]1E+[illegible]	[illegible].27675E+[illegible]	393.32[illegible]	-[illegible]
192	[illegible].15534E+00	[illegible].18838E+[illegible]	423.[illegible]	[illegible]
193	.16667E+[illegible]	[illegible].10[illegible]E+0[illegible]	455.437	-[illegible].[illegible]57
194	.16667E+[illegible]	[illegible].85714E-[illegible]1	455.728	-[illegible].[illegible]51
195	.16667E+[illegible]	[illegible].71429E-01	456.12[illegible]	[illegible]
196	.20[illegible]3E+[illegible]	0.71429E-01	448.240	[illegible].[illegible]43
197	.25[illegible]E+00	[illegible].71429E-01	438.756	[illegible].[illegible]3[illegible]
198	[illegible].28947E+0[illegible]	[illegible].71429E-01	431.[illegible]4	[illegible]
199	[illegible].32895E+[illegible]	[illegible].71429E-01	425.[illegible]2	[illegible]
200	.36842E+00	0.71429E-01	421.[illegible]32	[illegible]13
201	[illegible].[illegible]78[illegible]E+0[illegible]	0.71429E-01	416.758	[illegible]14
202	.44737E+[illegible]	[illegible].71429E-01	412.975	[illegible].0[illegible]14
203	.48684E+[illegible]	[illegible].71429E-01	4[illegible]9.6[illegible]	[illegible]2[illegible]
204	.52632E+[illegible]	0.71429E-01	4[illegible]6.6[illegible]4	[illegible]23
205	.56579E+[illegible]	0.71429E-01	4[illegible]3.923	[illegible]
206	.60526E+[illegible]	[illegible].71429E-01	4[illegible]1.535	[illegible]
207	[illegible].64474E+	[illegible].71429E-01	399.418	[illegible]
208	.68421E+0[illegible]	[illegible].71429E-01	397.554	[illegible]
209	.72368E+[illegible]	0.71429E-01	395.932	[illegible]
210	.76316E+[illegible]	[illegible].71429E-01	394.5[illegible]1	[illegible]11
211	.8[illegible]263E+[illegible]	[illegible].71429E-01	393.375	[illegible]
212	.84210E+0[illegible]	0.71429E-01	392.428	[illegible]
213	[illegible].88158E+00	0.71429E-01	391.696	[illegible]11
214	.921[illegible]5E+[illegible]	[illegible].71429E-01	391.178	[illegible]
215	.9[illegible]53E+[illegible]	[illegible].71429E-01	39[illegible].[illegible]	[illegible]
216	.1[illegible]E+01	0.71429E-01	39[illegible].7[illegible]	[illegible]
217	.[illegible]3E-01	0.98475E+[illegible]	[illegible]	-[illegible].1[illegible]
218	.[illegible]8E-01	0.89628E+0[illegible]	75.[illegible]	[illegible]
219	[illegible].[illegible]9E-01	[illegible].3[illegible]78[illegible]E+[illegible]	142.44[illegible]	[illegible]
220	[illegible].1[illegible]92E+00	[illegible].71933E+0[illegible]	2[illegible].353	-[illegible]
221	[illegible].12342E+00	0.63[illegible]85E+[illegible]	25[illegible].322	-[illegible]
222	[illegible].13757E+[illegible]	[illegible].54238E+0[illegible]	2[illegible]3.[illegible]2	-[illegible]
223	[illegible].15172E+0[illegible]	[illegible].4539[illegible]E+[illegible]	33[illegible].763	-[illegible]
224	[illegible].16587E+00	[illegible].36543E+[illegible]	363.557	-[illegible]
225	[illegible].18[illegible]3E+00	0.27695E+0[illegible]	392.932	-[illegible]
226	[illegible].19[illegible]18E+0[illegible]	[illegible].18348E+0[illegible]	419.375	[illegible]
227	[illegible].2[illegible]833E+0[illegible]	[illegible].1[illegible]E+0[illegible]	447.924	-[illegible]62
228	[illegible].20833E+00	0.85714E-01	447.658	[illegible]57
229	[illegible].25[illegible]E+00	[illegible].85714E-01	436.413	[illegible]54

230	.28947E+00	0.85714E-01	429.334	0.0032
231	0.32895E+00	0.85714E-01	423.913	0.0020
232	0.36842E+00	0.85714E-01	419.140	0.0025
233	0.40789E+00	0.85714E-01	414.955	0.0024
234	.44737E+00	0.85714E-01	411.230	0.0023
235	.48684E+00	0.85714E-01	407.906	0.0025
236	.52632E+00	0.85714E-01	404.933	0.0023
237	0.56579E+00	0.85714E-01	402.275	0.0031
238	.60526E+00	0.85714E-01	399.905	0.0029
239	.64474E+00	0.85714E-01	397.800	0.0031
240	.68421E+00	0.85714E-01	395.947	0.0020
241	0.72368E+00	0.85714E-01	394.332	0.0026
242	.76316E+00	0.85714E-01	392.947	0.0011
243	.80263E+00	0.85714E-01	391.785	0.0007
244	0.84210E+00	0.85714E-01	390.842	0.0027
245	0.88158E+00	0.85714E-01	390.111	0.0003
246	0.92105E+00	0.85714E-01	389.594	0.0008
247	0.96053E+00	0.85714E-01	389.285	0.0015
248	0.10000E+01	0.85714E-01	389.185	0.0019
249	0.83247E-01	0.98596E+00	0.0	-0.1514
250	.97222E-01	0.89737E+00	76.058	0.0
251	.11420E+00	0.80877E+00	143.983	-0.0000
252	.13117E+00	0.72017E+00	202.442	-0.0000
253	0.14815E+00	0.63158E+00	252.737	-0.0000
254	.16512E+00	0.54298E+00	295.855	-0.0000
255	0.18210E+00	0.45439E+00	332.975	-0.0000
256	0.19907E+00	0.36579E+00	364.895	-0.0000
257	0.21605E+00	0.27719E+00	392.563	-0.0000
258	0.23302E+00	0.18860E+00	416.143	-0.0000
259	.25000E+00	0.10000E+00	433.081	-0.0097
260	0.28947E+00	0.10000E+00	427.096	-0.0061
261	0.32895E+00	0.10000E+00	421.812	-0.0031
262	0.36842E+00	0.10000E+00	417.168	-0.0041
263	.40789E+00	0.10000E+00	413.089	-0.0040
264	0.44737E+00	0.10000E+00	409.432	-0.0041
265	.48684E+00	0.10000E+00	406.156	-0.0061
266	0.52632E+00	0.10000E+00	403.219	-0.0054
267	.56579E+00	0.10000E+00	400.589	-0.0037
268	0.60526E+00	0.10000E+00	398.238	-0.0054
269	0.64474E+00	0.10000E+00	396.149	-0.0066
270	.68421E+00	0.10000E+00	394.307	-0.0043
271	.72368E+00	0.10000E+00	392.701	-0.0043
272	0.76316E+00	0.10000E+00	391.323	-0.0064
273	0.80263E+00	0.10000E+00	390.166	-0.0051
274	0.84210E+00	0.10000E+00	389.226	-0.0056
275	0.88158E+00	0.10000E+00	388.499	-0.0061
276	.92105E+00	0.10000E+00	387.983	-0.0048
277	.96053E+00	0.10000E+00	387.676	-0.0017
278	0.10000E+01	0.10000E+00	387.576	0.0074
279	0.94503E-01	0.98750E+00	0.0	-0.1467
280	0.11678E+00	0.91714E+00	62.885	0.0000
281	0.13902E+00	0.84678E+00	120.509	0.0000
282	0.16126E+00	0.77642E+00	172.343	0.0000
283	0.18350E+00	0.70606E+00	218.473	0.0001
284	0.20574E+00	0.63570E+00	259.095	0.0001
285	.22798E+00	0.56534E+00	294.539	0.0002
286	.25022E+00	0.49498E+00	325.148	0.0002
287	.27245E+00	0.42462E+00	351.194	0.0002
288	0.29469E+00	0.35426E+00	372.763	0.0003
289	0.31693E+00	0.28390E+00	389.484	0.0016

290	[illegible].35224E+ [illegible]	[illegible].2839[illegible]E+0[illegible]	387.992	-[illegible].0024
291	.35763E+0[illegible]	[illegible].2839[illegible]E+0[illegible]	386.1[illegible]3	-[illegible].[illegible]27
292	0.42311E+0[illegible]	0.28390E+0[illegible]	384.[illegible]55	-[illegible].[illegible]2
293	[illegible].45863E+0[illegible]	0.28390E+00	381.960	-[illegible].[illegible]017
294	[illegible].49434E+0[illegible]	[illegible].2839[illegible]E+0[illegible]	379.890	-[illegible].[illegible]7
295	[illegible].53[illegible]7E+0[illegible]	0.2839[illegible]E+0[illegible]	377.9[illegible]3	-[illegible].[illegible]22
296	[illegible].56589E+0[illegible]	0.28390E+0[illegible]	376.[illegible]1[illegible]	-[illegible].[illegible]24
297	[illegible].60176E+00	0.28390E+0[illegible]	374.236	-[illegible].0029
298	[illegible].63774E+0[illegible]	[illegible].28390E+0[illegible]	372.594	-[illegible].0027
299	[illegible].67377E+0[illegible]	[illegible].28390E+0[illegible]	371.[illegible]91	-[illegible].[illegible]39
300	[illegible].7[illegible]980E+00	0.28390E+00	369.736	-[illegible].[illegible]17
301	[illegible].746[illegible]E+0[illegible]	0.28390E+0[illegible]	368.532	-[illegible].[illegible]39
302	[illegible].78219E+0[illegible]	[illegible].28390E+0[illegible]	367.484	-[illegible].[illegible]12
303	[illegible].01843E+ [illegible]	.2839[illegible]E+0[illegible]	366.594	-[illegible].[illegible]39
304	[illegible].85[illegible]7[illegible]E+0[illegible]	0.28390E+0[illegible]	365.864	-[illegible].[illegible]37
305	[illegible].891[illegible]E+00	0.28390E+0[illegible]	365.295	-[illegible].[illegible]56
306	[illegible].92732E+00	[illegible].2839[illegible]E+0[illegible]	364.589	-[illegible].0044
307	[illegible].96366E+0[illegible]	[illegible].2839[illegible]E+0[illegible]	364.640	-[illegible].[illegible]051
308	[illegible].1[illegible]E+01	0.2839[illegible]E+0[illegible]	364.565	[illegible].[illegible]27
309	[illegible].10869E+0[illegible]	0.96934E+00	[illegible]	-[illegible].1521
310	[illegible].13[illegible]29E+0[illegible]	[illegible].92[illegible]39E+00	62.2[illegible]	[illegible]
311	[illegible].15168E+0[illegible]	[illegible].85148E+0[illegible]	119.166	[illegible]
312	[illegible].173[illegible]8E+0[illegible]	0.78257E+0[illegible]	17[illegible].51	[illegible]
313	.19448E+0[illegible]	0.71366E+0[illegible]	216.212	[illegible]
314	[illegible].21588E+0[illegible]	[illegible].64475E+0[illegible]	256.494	[illegible]
315	[illegible].23728E+0[illegible]	[illegible].57584E+0[illegible]	291.674	-[illegible]
316	.25867E+00	[illegible].50693E+0[illegible]	322.[illegible]97	[illegible].[illegible]1
317	[illegible].28[illegible]7E+0[illegible]	0.43803E+0[illegible]	346.[illegible]	[illegible].[illegible]2
318	[illegible].3[illegible]1[illegible]7E+0[illegible]	[illegible].36912E+0[illegible]	3[illegible]9.65[illegible]	.[illegible]2
319	.32267E+0[illegible]	[illegible].3[illegible]21E+0[illegible]	366.655	.[illegible]31
320	0.35723E+00	0.30[illegible]21E+0[illegible]	385.1[illegible]9	[illegible]
321	0.39176E+00	0.30021E+0[illegible]	383.255	[illegible]
322	[illegible].426[illegible]7E+0[illegible]	[illegible].30[illegible]21E+0[illegible]	381.257	[illegible]
323	.46135E+0[illegible]	[illegible].30[illegible]21E+0[illegible]	379.266	.[illegible]11
324	0.4968[illegible]E+0[illegible]	0.30021E+0[illegible]	377.511	.[illegible]21
325	.53161E+0[illegible]	0.30[illegible]21E+0[illegible]	375.[illegible]	.[illegible]22
326	[illegible].56[illegible]98E+0[illegible]	.30[illegible]21E+0[illegible]	373.565	.[illegible]18
327	.6[illegible]25[illegible]E+0[illegible]	[illegible].30[illegible]21E+0[illegible]	371.[illegible]	[illegible]
328	[illegible].63816E+0[illegible]	0.30021E+0[illegible]	37[illegible].2[illegible]	[illegible]
329	[illegible].67395E+00	[illegible].30[illegible]21E+0[illegible]	368.769	.[illegible]17
330	.7[illegible]98[illegible]E+0[illegible]	.3[illegible]21E+0[illegible]	367.[illegible]7	.[illegible]23
331	[illegible].7[illegible]58[illegible]E+0[illegible]	[illegible].3[illegible]21E+0[illegible]	366.25	.[illegible]1[illegible]
332	[illegible].782[illegible]E+0[illegible]	0.30[illegible]21E+0[illegible]	365.213	.[illegible]1[illegible]
333	[illegible].8162[illegible]E+00	0.30021E+0[illegible]	364.33[illegible]	.[illegible]11
334	[illegible].85[illegible]7[illegible]E+0[illegible]	[illegible].30[illegible]21E+0[illegible]	363.6[illegible]5	.[illegible]18
335	[illegible].89[illegible]E+ [illegible]	[illegible].30[illegible]21E+0[illegible]	363.[illegible]	.[illegible]1[illegible]
336	[illegible].92718E+00	0.30021E+0[illegible]	362.635	.[illegible]9
337	.96[illegible]58[illegible]E+00	0.30[illegible]21E+0[illegible]	362.394	.[illegible]19
338	[illegible].1[illegible]E+01	[illegible].30[illegible]21E+0[illegible]	362.315	.[illegible]2[illegible]
339	[illegible].12[illegible]E+0[illegible]	[illegible].99136E+0[illegible]	[illegible]	-.1542
340	.14304E+0[illegible]	0.9239[illegible]E+0[illegible]	61.51[illegible]	[illegible]
341	[illegible].164[illegible]E+0[illegible]	0.85644E+0[illegible]	117.[illegible]7	[illegible]
342	[illegible].18496E+ [illegible]	[illegible].78698E+0[illegible]	166.673	-[illegible]
343	[illegible].2[illegible]552E+ [illegible]	[illegible].72152E+0[illegible]	213.939	[illegible]
344	[illegible].226[illegible]9E+0[illegible]	0.654[illegible]6E+0[illegible]	253.874	-[illegible]
345	[illegible].24665E+0[illegible]	0.586[illegible]E+0[illegible]	288.7[illegible]	-[illegible]
346	[illegible].26721E+0[illegible]	[illegible].51914E+0[illegible]	319.[illegible]2[illegible]	-[illegible]
347	[illegible].28777E+0[illegible]	[illegible].45168E+0[illegible]	344.88[illegible]	.[illegible]2
348	[illegible].30833E+0[illegible]	[illegible].38422E+0[illegible]	366.521	.[illegible]2
349	[illegible].32889E+0[illegible]	[illegible].31676E+0[illegible]	384.[illegible]12	[illegible].[illegible]34

350	.36231E+	.31676E+0?	382.217	0.0013
351	.39539E+	.31676E+00	380.365	0.0030
352	.42993E+00	0.31676E+00	378.489	0.0020
353	.46413E+00	0.31676E+00	376.572	0.0028
354	.49857E+	0.31676E+00	374.674	0.0029
355	.53326E+00	0.31676E+00	372.626	0.0012
356	.56618E+00	0.31676E+00	371.056	0.0010
357	.60333E+00	0.31676E+00	369.383	0.0021
358	.63568E+00	0.31676E+00	367.819	0.0024
359	.67422E+00	0.31676E+00	366.378	0.0015
360	.70995E+00	0.31676E+00	365.069	0.0015
361	.74584E+00	0.31676E+00	363.698	0.0013
362	.78137E+00	0.31676E+00	362.674	0.0016
363	.81683E+	0.31676E+00	361.999	0.0008
364	.85429E+00	0.31676E+00	361.279	0.0015
365	.89064E+00	0.31676E+00	360.717	0.0022
366	.92706E+00	0.31676E+00	360.315	0.0010
367	.96352E+00	0.31676E+00	360.074	0.0012
368	.10000E+01	0.31676E+00	359.997	0.0025
369	.13771E+00	0.99369E+00	0.0	-0.1565
370	.15744E+00	0.92768E+00	60.635	0.0000
371	.17717E+00	0.86166E+00	116.561	0.0000
372	.19690E+00	0.79565E+00	166.633	-0.0000
373	.21663E+00	0.72964E+00	211.656	-0.0000
374	.23636E+00	0.66362E+00	251.238	0.0000
375	.25609E+00	0.59761E+00	285.664	-0.0000
376	.27582E+00	0.53159E+00	315.933	-0.0000
377	.29555E+00	0.46558E+00	341.691	-0.0000
378	.31527E+00	0.39956E+00	363.364	0.0003
379	.33510E+00	0.33355E+00	381.063	0.0033
380	.36709E+00	0.33355E+00	379.266	0.0021
381	.40032E+00	0.33355E+00	377.467	0.0005
382	.43349E+00	0.33355E+00	375.654	0.0018
383	.46711E+00	0.33355E+00	373.809	0.0018
384	.50085E+00	0.33355E+00	371.961	0.0016
385	.53501E+00	0.33355E+00	370.196	0.0012
386	.56949E+00	0.33355E+00	368.463	0.0006
387	.60425E+00	0.33355E+00	366.856	0.0023
388	.63929E+00	0.33355E+00	365.330	0.0009
389	.67459E+00	0.33355E+00	363.916	0.0016
390	.71012E+00	0.33355E+00	362.631	0.0014
391	.74587E+00	0.33355E+00	361.477	0.0006
392	.78181E+00	0.33355E+00	360.464	0.0022
393	.81791E+00	0.33355E+00	359.598	0.0019
394	.85416E+00	0.33355E+00	358.884	0.0015
395	.89052E+00	0.33355E+00	358.325	0.0018
396	.92697E+00	0.33355E+00	357.925	0.0015
397	.96347E+00	0.33355E+00	357.687	0.0030
398	.10000E+01	0.33355E+00	357.609	0.0026
399	.15218E+00	0.99630E+00	0.0	-0.1590
400	.17108E+00	0.93173E+00	60.159	0.0
401	.18998E+00	0.86716E+00	115.259	0.0000
402	.20889E+00	0.80258E+00	164.991	-0.0000
403	.22779E+00	0.73801E+00	209.365	-0.0000
404	.24669E+00	0.67344E+00	248.586	0.0000
405	.26559E+00	0.60887E+00	282.959	0.0000
406	.28450E+00	0.54430E+00	312.820	-0.0000
407	.30340E+00	0.47973E+00	338.481	-0.0000
408	.32230E+00	0.41515E+00	360.175	0.0002
409	.34120E+00	0.35056E+00	378.045	0.0033

410	.37276E+00	0.35058E+00	376.307	0.0020
411	.40475E+00	0.35058E+00	374.553	0.0023
412	.43716E+00	0.35058E+00	372.777	0.0011
413	.46999E+00	0.35058E+00	370.997	0.0025
414	.50324E+00	0.35058E+00	369.233	0.0007
415	.53698E+00	0.35058E+00	367.509	0.0014
416	.57090E+00	0.35058E+00	365.846	0.0012
417	.60528E+00	0.35058E+00	364.261	0.0018
418	.64000E+00	0.35058E+00	362.771	0.0015
419	.67514E+00	0.35058E+00	361.386	0.0003
420	.71038E+00	0.35058E+00	360.121	0.0014
421	.74598E+00	0.35058E+00	358.984	0.0026
422	.78181E+00	0.35058E+00	357.983	0.0005
423	.81706E+00	0.35058E+00	357.126	0.0014
424	.85177E+00	0.35058E+00	356.417	0.0021
425	.89043E+00	0.35058E+00	355.862	0.0007
426	.92600E+00	0.35058E+00	355.465	0.0011
427	.96343E+00	0.35058E+00	355.227	0.0020
428	.10000E+01	0.35058E+00	355.15	0.0026
429	.16606E+00	0.99918E+00	0.0	-0.1617
430	.18476E+00	0.93065E+00	59.406	0.0000
431	.20284E+00	.87292E+00	113.963	0.0000
432	.22093E+00	0.80979E+00	163.149	0.0000
433	.23901E+00	0.74666E+00	207.263	-0.0000
434	.25709E+00	0.68352E+00	245.920	0.0000
435	.27517E+00	.62039E+00	280.015	0.0000
436	.29325E+00	0.55726E+00	309.666	-0.0000
437	.31133E+00	.49413E+00	335.248	0.0000
438	.32941E+00	0.43100E+00	356.953	0.0002
439	.34749E+00	0.36786E+00	374.97	0.0041
440	.37813E+00	0.36786E+00	373.281	0.0027
441	.40928E+00	0.36786E+00	371.575	0.0025
442	.44094E+00	0.36786E+00	369.856	0.0020
443	.47309E+00	0.36786E+00	368.134	0.0007
444	.50573E+00	0.36786E+00	366.426	0.0017
445	.53885E+00	0.36786E+00	364.758	0.0013
446	.57241E+00	0.36786E+00	363.142	0.0015
447	.60641E+00	0.36786E+00	361.593	0.0000
448	.64081E+00	0.36786E+00	360.142	0.0032
449	.67559E+00	0.36786E+00	358.784	0.0009
450	.71072E+00	0.36786E+00	357.54	0.0007
451	.74616E+00	0.36786E+00	356.419	0.0015
452	.78189E+00	0.36786E+00	355.429	0.0001
453	.81786E+00	0.36786E+00	354.581	0.0013
454	.85403E+00	0.36786E+00	353.878	0.0016
455	.89038E+00	.36786E+00	353.327	0.0016
456	.92685E+00	0.36786E+00	352.932	0.0011
457	.96340E+00	0.36786E+00	352.696	0.0023
458	.10000E+01	0.36786E+00	352.619	0.0031
459	.18122E+00	0.10023E+01	0.0	-0.1648
460	.19848E+00	0.94065E+00	56.825	0.0
461	.21575E+00	0.87896E+00	112.075	0.0000
462	.23302E+00	0.81726E+00	161.305	0.0000
463	.25028E+00	0.75557E+00	204.760	-0.0000
464	.26755E+00	0.69387E+00	243.240	-0.0000
465	.28481E+00	0.63218E+00	277.052	-0.0000
466	.30208E+00	0.57048E+00	306.530	0.0000
467	.31934E+00	0.50879E+00	331.989	0.0000
468	.33661E+00	0.44709E+00	353.695	-0.0000
469	.35388E+00	0.38540E+00	371.642	0.0034

470	0.38367E+00	0.36540E+00	370.295	0.0020
471	0.41392E+00	0.36540E+00	366.555	0.0019
472	0.44822E+00	0.36540E+00	366.684	0.0013
473	0.47630E+00	0.36540E+00	365.217	0.0020
474	0.50635E+00	0.36540E+00	363.564	0.0016
475	0.54033E+00	0.36540E+00	361.940	0.0014
476	0.57404E+00	0.36540E+00	360.372	0.0019
477	0.60785E+00	0.36540E+00	358.865	0.0012
478	0.64172E+00	0.36540E+00	357.449	0.0017
479	0.67623E+00	0.36540E+00	356.109	0.0019
480	0.71115E+00	0.36540E+00	354.885	0.0015
481	0.74643E+00	0.36540E+00	353.779	0.0011
482	0.78203E+00	0.36540E+00	352.802	0.0021
483	0.81792E+00	0.36540E+00	351.961	0.0017
484	0.85404E+00	0.36540E+00	351.264	[illegible]
485	0.89036E+00	0.36540E+00	350.717	[illegible]
486	0.92683E+00	0.36540E+00	350.324	0.0011
487	0.96339E+00	0.36540E+00	350.089	0.0013
488	0.10000E+01	0.36540E+00	350.013	0.0023
489	0.19576E+00	0.10058E+01	0.0	-0.1680
490	0.21224E+00	0.94553E+00	56.166	[illegible]
491	0.22570E+00	0.88527E+00	111.391	[illegible]
492	0.24513E+00	0.82501E+00	159.467	[illegible]
493	0.26161E+00	0.76475E+00	202.446	[illegible]
494	0.27807E+00	0.70449E+00	240.546	[illegible]
495	0.29452E+00	0.64423E+00	274.070	[illegible]
496	0.31098E+00	0.58397E+00	303.349	[illegible]
497	0.32744E+00	0.52371E+00	326.702	[illegible]
498	0.34389E+00	0.46345E+00	350.401	-0.0000
499	0.36035E+00	0.40319E+00	368.066	0.0026
500	0.38917E+00	0.40319E+00	367.070	0.0036
501	0.41867E+00	0.40319E+00	365.473	0.0024
502	0.44862E+00	0.40319E+00	363.858	0.0022
503	0.47943E+00	0.40319E+00	362.242	0.0021
504	0.51107E+00	0.40319E+00	360.638	0.0006
505	0.54313E+00	0.40319E+00	359.063	0.0013
506	0.57578E+00	0.40319E+00	357.532	0.0010
507	0.60899E+00	0.40319E+00	356.061	0.0015
508	0.64273E+00	0.40319E+00	354.665	0.0012
509	0.67697E+00	0.40319E+00	353.359	0.0020
510	0.71167E+00	0.40319E+00	352.154	0.0009
511	0.74677E+00	0.40319E+00	351.063	0.0013
512	0.78224E+00	0.40319E+00	350.097	0.0015
513	0.81804E+00	0.40319E+00	349.265	0.0009
514	0.85410E+00	0.40319E+00	348.573	-0.0001
515	0.89036E+00	0.40319E+00	348.030	0.0015
516	0.92683E+00	0.40319E+00	347.640	0.0011
517	0.96339E+00	0.40319E+00	347.406	0.0014
518	0.10000E+01	0.40319E+00	347.330	0.0016
519	0.21037E+00	0.10095E+01	0.0	-0.1715
520	0.22603E+00	0.95071E+00	57.514	0.0
521	0.24168E+00	0.89188E+00	110.114	0.0000
522	0.25734E+00	0.83305E+00	157.627	0.0000
523	0.27299E+00	0.77422E+00	200.127	[illegible]
524	0.28865E+00	0.71538E+00	237.639	[illegible]
525	0.30430E+00	0.65655E+00	271.068	0.0000
526	0.31995E+00	0.59772E+00	300.143	0.0000
527	0.33561E+00	0.53889E+00	325.384	0.0000
528	0.35126E+00	0.48006E+00	347.108	-0.0000
529	0.36692E+00	0.42123E+00	365.626	0.0030

530	0.39485E+00	0.42123E+00	363.893	0.0024
531	0.42352E+00	0.42123E+00	362.340	0.0025
532	0.45293E+00	0.42123E+00	360.773	0.0011
533	0.48307E+00	0.42123E+00	359.206	0.0029
534	0.51391E+00	0.42123E+00	357.649	0.0035
535	0.54544E+00	0.42123E+00	356.115	0.0010
536	0.57763E+00	0.42123E+00	354.622	0.0015
537	0.61045E+00	0.42123E+00	353.184	0.0019
538	0.64385E+00	0.42123E+00	351.816	0.0016
539	0.67781E+00	0.42123E+00	350.532	0.0012
540	0.71227E+00	0.42123E+00	349.346	0.0012
541	0.74720E+00	0.42123E+00	348.270	0.0013
542	0.78253E+00	0.42123E+00	347.315	0.0015
543	0.81822E+00	0.42123E+00	346.490	0.0015
544	0.85421E+00	0.42123E+00	345.805	0.0022
545	0.89044E+00	0.42123E+00	345.266	0.0012
546	0.92686E+00	0.42123E+00	344.878	0.0023
547	0.96340E+00	0.42123E+00	344.645	0.0010
548	0.10000E+01	0.42123E+00	344.569	0.0022
549	0.22498E+00	0.10136E+01	0.0	-0.1755
550	0.23984E+00	0.95617E+00	56.870	0.0000
551	0.25470E+00	0.89876E+00	108.844	0.0000
552	0.26956E+00	0.84136E+00	155.790	0.0000
553	0.28442E+00	0.78396E+00	197.803	0.0000
554	0.29928E+00	0.72656E+00	235.119	0.0000
555	0.31414E+00	0.66916E+00	268.045	0.0000
556	0.32900E+00	0.61175E+00	296.910	-0.0000
557	0.34386E+00	0.55435E+00	322.032	-0.0000
558	0.35872E+00	0.49695E+00	343.895	-0.0000
559	0.37358E+00	0.43955E+00	362.134	0.0029
560	0.40062E+00	0.43955E+00	360.652	0.0023
561	0.42849E+00	0.43955E+00	359.147	0.0019
562	0.45716E+00	0.43955E+00	357.629	0.0021
563	0.48663E+00	0.43955E+00	356.120	0.0010
564	0.51688E+00	0.43955E+00	354.591	0.0019
565	0.54788E+00	0.43955E+00	353.098	0.0021
566	0.57960E+00	0.43955E+00	351.640	0.0024
567	0.61202E+00	0.43955E+00	350.232	0.0018
568	0.64510E+00	0.43955E+00	348.990	0.0014
569	0.67875E+00	0.43955E+00	347.628	0.0017
570	0.71298E+00	0.43955E+00	346.459	0.0020
571	0.74771E+00	0.43955E+00	345.396	0.0015
572	0.78289E+00	0.43955E+00	344.452	0.0019
573	0.81846E+00	0.43955E+00	343.636	0.0018
574	0.85437E+00	0.43955E+00	342.956	0.0010
575	0.89058E+00	0.43955E+00	342.420	0.0010
576	0.92631E+00	0.43955E+00	342.035	0.0009
577	0.96342E+00	0.43955E+00	341.803	0.0007
578	0.10000E+01	0.43955E+00	341.729	0.0019
579	0.23961E+00	0.10179E+01	0.0	-0.1797
580	0.25368E+00	0.96193E+00	56.230	-0.0000
581	0.26775E+00	0.90595E+00	107.578	0.0000
582	0.28183E+00	0.84997E+00	153.952	0.0000
583	0.29590E+00	0.79399E+00	195.473	0.0000
584	0.30998E+00	0.73802E+00	232.365	-0.0000
585	0.32405E+00	0.68204E+00	265.001	-0.0000
586	0.33813E+00	0.62606E+00	293.648	-0.0000
587	0.35220E+00	0.57008E+00	318.645	-0.0000
588	0.36627E+00	0.51411E+00	340.270	-0.0000
589	0.38035E+00	0.45813E+00	358.784	0.0027

590	.40551E+00	0.45813E+00	357.359	0.0007
591	0.43356E+00	0.45813E+00	355.893	0.0009
592	.46156E+00	0.45813E+00	354.419	.0030
593	0.49131E+00	0.45813E+00	352.935	.0016
594	0.51965E+00	0.45813E+00	351.464	.0026
595	.55 43E+00	0.45813E+00	350.007	.0013
596	0.58169E+00	0.45813E+00	348.582	.0022
597	0.61377E+00	0.45813E+00	347.203	0.0021
598	.64682E+00	0.45813E+00	345.865	0.0010
599	0.67979E+00	0.45813E+00	344.643	0.0020
600	.71377E+00	0.45813E+00	343.490	.0008
601	0.74851E+00	0.45813E+00	342.441	.0014
602	0.78333E+00	0.45813E+00	341.506	-0.0001
603	0.81877E+00	0.45813E+00	340.698	0.0011
604	0.85458E+00	0.45813E+00	340.024	0.0014
605	0.89 48E+00	0.45813E+00	339.492	.0013
606	0.927 E+00	.45813E+00	339.1 9	0.0013
607	.96346E+00	0.45813E+00	338.879	.0012
608	0.10 E+01	0.45813E+00	338.8 4	0.0026
609	0.25425E+00	0.10225E+01	0.0	-0.1843
610	.26754E+00	0.96796E+00	55.597	0.0000
611	.28 54E+00	0.91343E+00	106.319	-
612	0.29414E+00	0.85887E+00	152.117	
613	.30743E+00	0.80432E+00	193.137	-0.0000
614	.32 73E+00	0.74976E+00	229.639	-0.00
615	.334 2E+00	0.69521E+	261.936	
616	0.34732E+00	0.64065E+00	290.357	-0.00
617	0.36062E+00	0.58609E+00	315.215	-0.000
618	.37391E+00	0.53154E+00	336.8 6	-0.000
619	0.38721E+00	0.47698E+00	355.371	0.0019
620	.41250E+00	0.47698E+00	353.965	.0021
621	0.43876E+00	0.47698E+00	352.573	0.0020
622	.46597E+00	0.47698E+00	351.142	.0012
623	0.49411E+00	0.47698E+00	349.701	0.00
624	0.52317E+00	0.47698E+00	348.264	0.0023
625	.55311E+00	0.47698E+00	346.841	0.0020
626	0.5839 E+00	0.47698E+00	345.440	0.0021
627	.6156 E+00	0.47698E+00	344.094	0.0024
628	.64767E+00	0.47698E+00	342.799	.0006
629	.68094E+00	0.47698E+00	341.576	0.0017
630	0.71467E+00	0.47698E+00	340.439	.0014
631	0.74899E+00	0.47698E+00	339.402	.0011
632	0.78364E+00	0.47698E+00	338.477	0.0011
633	0.81915E+00	0.47698E+00	337.675	0.0010
634	0.85485E+00	0.47698E+00	337.007	0.0015
635	0.89 86E+00	0.47698E+00	336.479	0.0011
636	0.92711E+00	0.47699E+00	336.098	0.0016
637	0.96351E+00	0.47698E+00	335.869	0.0002
638	0.10000E+01	0.47698E+00	335.795	0.0024
639	0.26890E+00	.10275E+01	0.0	-0.1895
640	0.28142E+00	0.97435E+00	54.97	-0.00
641	0.29395E+00	0.92121E+00	105.065	-0.00
642	0.30648E+00	0.86807E+00	150.263	0.0
643	0.3190 1E+00	0.81494E+00	190.797	0.0
644	0.33153E+00	0.76180E+00	226.679	-0.0
645	0.34406E+00	0.70866E+00	258.645	0.00
646	0.35659E+00	0.65553E+00	287.035	0.00
647	0.36912E+00	0.60239E+00	311.752	-0.0
648	0.38165E+00	0.54925E+00	333.289	-0.000
649	0.39417E+00	0.49611E+00	351.892	0.0029

650	0.41861E+00	0.49611E+00	350.552	0.0016
651	0.44437E+00	0.49611E+00	349.183	0.0012
652	0.47055E+00	0.49611E+00	347.793	0.0025
653	0.49874E+00	0.49611E+00	346.39	0.0016
654	0.52651E+00	0.49611E+00	344.988	0.0020
655	0.55591E+00	0.49611E+00	343.596	0.0023
656	0.58624E+00	0.49611E+00	342.230	0.0014
657	0.61742E+00	0.49611E+00	340.902	0.0018
658	0.64943E+00	0.49611E+00	339.629	0.0022
659	0.68219E+00	0.49611E+00	338.424	0.0018
660	0.71566E+00	0.49611E+00	337.302	0.0015
661	0.74976E+00	0.49611E+00	336.276	0.0014
662	0.78443E+00	0.49611E+00	335.360	0.00 3
663	0.81959E+00	0.49611E+00	334.565	0.0011
664	0.85517E+00	0.49611E+00	333.9 2	0.001
665	0.8910 E+00	0.49611E+00	333.378	0.0017
666	0.92724E+00	0.49611E+00	332.999	0.0004
667	0.96356E+00	0.49611E+00	332.772	0.0015
668	0.10 E+01	0.49611E+00	332.698	0.0027
669	0.28355E+00	0.10327E+01	0.0	-0.1949
670	0.29332E+00	0.98102E+00	54.349	-0.0000
671	0.3 79E+00	0.9293 E+00	1 3.816	-0.0000
672	0.31286E+00	0.87758E+00	148.450	0.0
673	0.33 63E+00	0.82586E+00	188.450	0.0000
674	0.34239E+00	0.77414E+00	224.1 4	-0.0000
675	0.35416E+00	0.72241E+00	255.737	-0.00
676	0.36593E+00	0.67069E+00	283.679	0.00
677	0.3777 E+00	0.61897E+00	308.242	-0.00
678	0.38947E+00	0.56725E+00	329.714	-0.00
679	0.4 124E+00	0.51553E+00	346.343	0.0036
680	0.42482E+00	0.51553E+00	347. 48	0.002
681	0.44350E+00	0.51553E+00	345.72	0.0012
682	0.47526E+00	0.51553E+00	344.369	0.0021
683	0.502 9 E+00	0.51553E+00	343. 2	0.00 2
684	0.52996E+00	0.51553E+00	341.633	0.0021
685	0.55834E+00	0.51553E+00	340.271	0.0016
686	0.58869E+00	0.51553E+00	338.931	0.0019
687	0.61947E+00	0.51553E+00	337.626	0.0013
688	0.65111E+00	0.51553E+00	336.373	0.0021
689	0.68356E+00	0.51553E+00	335.184	0.0018
690	0.71675E+00	0.51553E+00	334.076	0.0018
691	0.75 62E+00	0.51553E+00	333. 62	0.0012
692	0.78510E+00	0.51553E+00	332.154	0.0006
693	0.82 1 E+00	0.51553E+00	331.306	0.0008
694	0.85554E+00	0.51553E+00	330.7 7	0.0009
695	0.89134E+00	0.51553E+00	330.186	-0.0003
696	0.92741E+00	0.51553E+00	329.810	0.00 2
697	0.96366E+00	0.51553E+00	329.585	0.0009
698	0.1 E+01	0.51553E+00	329.511	0.0022
699	0.2982 E+00	0.10383E+01	0.0	-0.2007
700	0.30922E+00	0.98801E+00	53.729	-0.0000
701	0.32025E+00	0.93770E+00	102.571	-0.0000
702	0.33127E+00	0.88739E+00	146.616	0.0000
703	0.34229E+00	0.83708E+00	186.096	0.0
704	0.35331E+00	0.78678E+00	221.314	-0.0000
705	0.36433E+00	0.73647E+00	252.0	0.0000
706	0.37535E+00	0.68616E+00	280.267	-0.0000
707	0.38637E+00	0.63585E+00	3 4.685	0.0000
708	0.39739E+00	0.58554E+00	326. 79	-0.0000
709	0.40841E+00	0.53523E+00	344.719	0.0041

710	.43115E+00	0.53523E+00	343.468	0.0029
711	0.455[illegible]5E+00	0.53523E+00	342.16	0.0015
712	0.48017E+00	0.53523E+00	340.866	0.0018
713	0.50628E+00	0.53523E+00	339.533	0.0016
714	.53356E+00	.53523E+00	338.194	0.0014
715	.56191E+00	0.53523E+00	336.867	0.0012
716	0.59128E+00	0.53523E+00	335.545	0.0017
717	0.62163E+00	0.53523E+00	334.262	0.0011
718	0.65290E+00	0.53523E+00	333.027	0.0018
719	0.68513E+00	0.53523E+00	331.855	0.0020
720	0.71795E+00	0.53523E+00	330.76[illegible]	0.0023
721	.75158E+00	.53523E+00	329.755	.0027
722	.78585E+00	.53523E+00	328.855	.[illegible]1
723	.82068E+00	0.53523E+00	328.[illegible]74	.[illegible]13
724	.85597E+00	0.53523E+00	327.42[illegible]	0.0014
725	.89167E+00	.53523E+00	326.9[illegible]2	0.00[illegible]2
726	0.9276[illegible]E+00	0.53523E+00	326.528	0.00[illegible]
727	.96375E+00	0.53523E+00	326.376	.[illegible]31
728	.1[illegible]E+01	0.53523E+00	326.231	[illegible]23
729	0.31285E+00	0.10442E+01	0.0	-0.2172
730	.32314E+00	0.99531E+00	53.115	-0.01[illegible]
731	.33342E+00	0.94642E+00	1[illegible]1.328	-[illegible]
732	0.34370E+00	.89752E+00	144.782	-[illegible]
733	0.35399E+00	0.84862E+00	183.734	[illegible]
734	0.36427E+00	0.79972E+00	218.5[illegible]7	-[illegible]
735	0.37455E+00	0.75[illegible]82E+00	249.437	[illegible]
736	.38484E+00	0.7[illegible]192E+00	276.856	-[illegible]
737	0.39512E+00	0.65302E+00	301.[illegible]77	-[illegible]
738	.4[illegible]5[illegible]E+00	.6[illegible]412E+00	322.38[illegible]	-[illegible]
739	.41569E+00	0.55522E+00	341.015	[illegible]3[illegible]
740	0.43759E+00	0.55522E+00	339.8[illegible]6	.[illegible]2
741	0.46[illegible]72E+00	0.55522E+00	338.558	.0023
742	.485[illegible]6E+00	.55522E+00	337.28[illegible]	0.001[illegible]
743	.51[illegible]59E+00	0.55522E+00	335.95	[illegible]
744	0.53728E+00	0.55522E+00	334.67[illegible]	.[illegible]18
745	.5651[illegible]E+00	0.55522E+00	333.382	[illegible]
746	0.59[illegible]E+00	0.55522E+00	332.[illegible]7[illegible]	0.0017
747	0.62392E+00	0.55522E+00	330.8[illegible]7	[illegible]16
748	0.65482E+00	0.55522E+00	329.589	.[illegible]18
749	0.68662E+00	0.55522E+00	328.431	0.0017
750	0.71925E+00	0.55522E+00	327.345	.[illegible]24
751	.75263E+00	0.55522E+00	326.354	0.001[illegible]
752	0.78669E+00	0.55522E+00	325.462	.[illegible]12
753	0.82133E+00	0.55522E+00	324.687	0.001[illegible]
754	0.85646E+00	0.55522E+00	324.[illegible]37	[illegible]
755	0.89199E+00	0.55522E+00	323.522	[illegible]5
756	0.92783E+00	0.55522E+00	323.151	[illegible]
757	0.96386E+00	0.55522E+00	322.927	[illegible]19
758	0.1[illegible]E+01	0.55522E+00	322.855	0.0024
759	.3275[illegible]E+00	0.10505E+01	0.0	-0.2143
760	0.337[illegible]5E+00	0.10037E+01	52.591	-0.00[illegible]
761	0.34661E+00	0.95546E+00	100.066	-0.00[illegible]
762	0.35617E+00	0.90797E+00	142.943	[illegible]
763	0.36573E+00	0.86046E+00	181.363	[illegible]
764	0.37528E+00	0.81298E+00	215.681	-[illegible]
765	0.38484E+00	0.76549E+00	246.244	-0.0[illegible]
766	0.39440E+00	0.71799E+00	273.386	[illegible]
767	0.40396E+00	0.67050E+00	297.416	-[illegible]
768	0.41351E+00	0.62301E+00	318.614	-0.00[illegible]
769	0.42307E+00	0.57551E+00	337.228	0.0033

770	0.44415E+00	0.57551E+00	336.060	0.0013
771	0.46652E+00	0.57551E+00	334.851	0.0012
772	0.49016E+00	0.57551E+00	333.606	0.0023
773	0.51504E+00	0.57551E+00	332.337	0.0017
774	0.54115E+00	0.57551E+00	331.055	0.0015
775	0.56843E+00	0.57551E+00	329.772	0.0025
776	0.59685E+00	0.57551E+00	328.501	0.0014
777	0.62634E+00	0.57551E+00	327.257	0.0011
778	0.65686E+00	0.57551E+00	326.055	0.0010
779	0.68832E+00	0.57551E+00	324.912	0.0024
780	0.72065E+00	0.57551E+00	323.840	0.0013
781	0.75378E+00	0.57551E+00	322.855	0.0008
782	0.78760E+00	0.57551E+00	321.971	0.0011
783	0.82205E+00	0.57551E+00	321.201	0.0007
784	0.85701E+00	0.57551E+00	320.555	0.0014
785	0.89239E+00	0.57551E+00	320.044	0.0021
786	0.92808E+00	0.57551E+00	319.675	0.0017
787	0.96399E+00	0.57551E+00	319.452	0.0007
788	0.10[illegible]E+01	0.57551E+00	319.379	0.0018
789	0.34212E+00	0.10570E+01	0.0	-0.2220
790	0.35097E+00	0.10109E+01	51.888	-0.0000
791	0.35981E+00	0.96463E+00	98.843	0.0000
792	0.36866E+00	0.91874E+00	141.100	0.0000
793	0.37750E+00	0.87265E+00	178.980	0.0000
794	0.38635E+00	0.82656E+00	212.836	0.0000
795	0.39519E+00	0.78047E+00	243.021	-0.0000
796	0.40403E+00	0.73438E+00	269.872	-0.0000
797	0.41288E+00	0.68829E+00	293.698	-0.0000
798	0.42172E+00	0.64220E+00	314.776	-0.0000
799	0.43057E+00	0.59611E+00	333.351	0.0028
800	0.45064E+00	0.59611E+00	332.224	0.00[illegible]9
801	0.47295E+00	0.59611E+00	331.051	0.0020
802	0.49539E+00	0.59611E+00	329.84[illegible]	0.0015
803	0.51963E+00	0.59611E+00	328.601	0.0014
804	0.54515E+00	0.59611E+00	327.348	0.0012
805	0.57190E+00	0.59611E+00	326.086	0.0016
806	0.59924E+00	0.59611E+00	324.836	0.0016
807	0.6283[illegible]E+00	0.59611E+00	323.6[illegible]9	0.0006
808	0.659[illegible]2E+00	0.59611E+00	322.423	0.0010
809	0.69[illegible]14E+00	0.59611E+00	321.291	0.0010
810	0.72217E+00	0.59611E+00	320.230	0.0017
811	0.755[illegible]2E+00	0.59611E+00	319.254	0.0009
812	0.78861E+00	0.59611E+00	318.377	0.0010
813	0.82284E+00	0.59611E+00	317.613	0.0013
814	0.857[illegible]1E+00	0.59611E+00	316.972	0.0026
815	0.89292E+00	0.59611E+00	316.464	0.0016
816	0.92836E+00	0.59611E+00	316.096	0.0016
817	0.96413E+00	0.59611E+00	315.874	0.0018
818	0.10[illegible]E+01	0.59611E+00	315.802	0.0025
819	0.35673E+00	0.11639E+01	0.0	-0.2304
820	0.36487E+00	0.10192E+01	51.276	-0.0000
821	0.373[illegible]2E+00	0.97454E+00	97.598	-0.0000
822	0.38116E+00	0.92985E+00	139.252	0.0000
823	0.38931E+00	0.88515E+00	176.565	0.0000
824	0.39745E+00	0.84046E+00	209.968	0.0000
825	0.40560E+00	0.79577E+00	239.765	0.0000
826	0.41374E+00	0.75108E+00	266.312	-0.0000
827	0.42189E+00	0.70639E+00	289.92[illegible]	-0.0000
828	0.43003E+00	0.66170E+00	310.862	-0.0000
829	0.43818E+00	0.61701E+00	329.383	0.0029

830	0.45764E+00	0.61701E+00	328.295	0.0021
831	0.47851E+00	0.61701E+00	327.157	0.0013
832	0.50075E+00	0.61701E+00	325.976	0.0014
833	0.52436E+00	0.61701E+00	324.768	0.0021
834	0.54929E+00	0.61701E+00	323.538	0.0019
835	0.57531E+00	0.61701E+00	322.301	0.0022
836	0.60296E+00	0.61701E+00	321.070	0.0022
837	0.63156E+00	0.61701E+00	319.860	0.0013
838	0.66132E+00	0.61701E+00	318.687	0.0010
839	0.69278E+00	0.61701E+00	317.568	0.0008
840	0.72379E+00	0.61701E+00	316.517	0.0008
841	0.75636E+00	0.61701E+00	315.549	0.0009
842	0.78977E+00	0.61701E+00	314.679	0.0014
843	0.82371E+00	0.61701E+00	313.929	0.0009
844	0.85828E+00	0.61701E+00	313.262	0.0005
845	0.89331E+00	0.61701E+00	312.778	0.0016
846	0.92668E+00	0.61701E+00	312.412	0.0013
847	0.96428E+00	0.61701E+00	312.191	0.0010
848	0.10000E+01	0.61701E+00	312.118	0.0014
849	0.37131E+00	0.10712E+01	0.0	-0.2397
850	0.37877E+00	0.10279E+01	50.663	-0.0000
851	0.38623E+00	0.98458E+00	96.349	-0.0000
852	0.39369E+00	0.94128E+00	137.394	0.0000
853	0.40114E+00	0.89799E+00	174.174	0.0000
854	0.40860E+00	0.85469E+00	207.076	0.0000
855	0.41606E+00	0.81140E+00	236.472	-0.0000
856	0.42352E+00	0.76810E+00	262.703	-0.0000
857	0.43098E+00	0.72481E+00	286.677	-0.0000
858	0.43844E+00	0.68152E+00	306.667	-0.0000
859	0.44590E+00	0.63822E+00	325.314	0.0013
860	0.46457E+00	0.63822E+00	324.266	0.0035
861	0.48470E+00	0.63822E+00	323.163	0.0013
862	0.50626E+00	0.63822E+00	322.015	0.0009
863	0.52923E+00	0.63822E+00	320.832	0.0012
864	0.55358E+00	0.63822E+00	319.627	0.0015
865	0.57926E+00	0.63822E+00	318.411	0.0017
866	0.60623E+00	0.63822E+00	317.198	0.0016
867	0.63441E+00	0.63822E+00	316.005	0.0015
868	0.66374E+00	0.63822E+00	314.845	0.0002
869	0.69414E+00	0.63822E+00	313.737	0.0008
870	0.72553E+00	0.63822E+00	312.696	0.0016
871	0.75781E+00	0.63822E+00	311.736	0.0010
872	0.79089E+00	0.63822E+00	310.872	0.0019
873	0.82466E+00	0.63822E+00	310.116	0.0011
874	0.85901E+00	0.63822E+00	309.465	0.0016
875	0.89384E+00	0.63822E+00	308.962	0.0007
876	0.92903E+00	0.63822E+00	308.619	0.0017
877	0.96445E+00	0.63822E+00	308.399	0.0019
878	0.10000E+01	0.63822E+00	308.327	0.0021
879	0.38586E+00	0.10788E+01	0.0	-0.2497
880	0.39264E+00	0.10369E+01	50.344	-0.0000
881	0.39943E+00	0.99496E+00	95.092	-0.0000
882	0.40622E+00	0.95306E+00	135.523	0.0000
883	0.41301E+00	0.91116E+00	171.743	0.0000
884	0.41980E+00	0.86926E+00	204.155	0.0
885	0.42658E+00	0.82736E+00	233.139	-0.0000
886	0.43337E+00	0.78546E+00	259.040	-0.0000
887	0.44016E+00	0.74356E+00	282.166	-0.0000
888	0.44695E+00	0.70166E+00	302.787	-0.0000
889	0.45373E+00	0.65975E+00	321.140	-0.0007

890	0.47163E+00	0.65975E+00	320.131	0.0042
891	0.491 2E+00	0.65975E+00	319.063	0.0016
892	0.51190E+00	0.65975E+00	317.945	0.0015
893	.53425E+00	0.65975E+00	316.789	0.0014
894	.558 1E+00	0.65975E+00	315.607	0.0013
895	0.58316E+00	0.65975E+00	314.411	0.0011
896	0.6 364E+00	0.65975E+00	313.217	0.0016
897	0.63737E+00	0.65975E+00	312.039	0.0013
898	0.66629E+00	0.65975E+00	310.892	0.0009
899	0.69633E+00	0.65975E+00	309.795	0.0003
900	0.72738E+00	0.65975E+00	308.762	0.0000
901	0.75936E+00	0.65975E+00	307.810	0.0012
902	0.79216E+00	0.65975E+00	306.952	0.0002
903	0.82568E+00	0.65975E+00	306.203	0.0007
904	0.85981E+00	0.65975E+00	305.574	0.0011
905	0.89442E+00	0.65975E+00	305.074	0.0005
906	0.92941E+00	0.65975E+00	304.713	0.0019
907	0.96464E+00	0.65975E+00	304.494	0.0012
908	0.10000E+01	0.65975E+00	304.423	0.0027
909	0.40037E+00	0.10867E+01	0.0	-0.2628
910	0.40651E+00	0.10462E+01	49.421	-0.0000
911	0.41263E+00	0.10057E+01	93.827	0.0000
912	0.41876E+00	0.96519E+00	133.638	-0.0000
913	0.42490E+00	0.92467E+00	169.291	-0.0000
914	0.43103E+00	0.88416E+00	201.204	0.0
915	0.43716E+00	0.84365E+00	229.764	0.0000
916	0.44329E+00	0.80314E+00	255.320	0.0000
917	0.44942E+00	0.76263E+00	278.151	-0.0000
918	0.45556E+00	0.72212E+00	298.617	-0.0000
919	0.46169E+00	0.68161E+00	316.858	-0.0022
920	0.47881E+00	0.68161E+00	315.887	0.0034
921	0.49749E+00	0.68161E+00	314.852	0.0025
922	0.51759E+00	0.68161E+00	313.764	0.0015
923	0.53941E+00	0.68161E+00	312.634	0.0019
924	0.56260E+00	0.68161E+00	311.474	0.0011
925	0.58721E+00	0.68161E+00	310.299	0.0020
926	0.61319E+00	0.68161E+00	309.121	0.0007
927	0.64047E+00	0.68161E+00	307.958	0.0019
928	0.66899E+00	0.68161E+00	306.823	0.0011
929	0.69864E+00	0.68161E+00	305.736	0.0006
930	0.72935E+00	0.68161E+00	304.713	0.0010
931	0.76102E+00	0.68161E+00	303.768	0.0012
932	0.79353E+00	0.68161E+00	302.916	0.0005
933	0.82679E+00	0.68161E+00	302.172	0.0013
934	0.86057E+00	0.68161E+00	301.547	0.0017
935	0.895 5E+00	0.68161E+00	301.051	0.0011
936	0.92962E+00	0.68161E+00	300.691	0.0023
937	0.96465E+00	0.68161E+00	300.474	0.0003
938	0.10000E+01	0.68161E+00	300.402	0.0020
939	0.41483E+00	0.10955E+01	[illegible]	-0.2729
940	0.42032E+00	0.10559E+01	48.790	-0.0000
941	0.42582E+00	0.10166E+01	92.547	-0.0000
942	0.43131E+00	0.97766E+00	131.734	-0.0000
943	0.43680E+00	0.93854E+00	166.612	-0.0000
944	0.44230E+00	0.89941E+00	198.216	0.0
945	0.44779E+00	0.86029E+00	226.341	0.0000
946	0.45328E+00	0.82117E+00	251.539	-0.0000
947	0.45878E+00	0.78204E+00	274.119	-0.0000
948	0.46427E+00	0.74292E+00	294.349	-0.0000
949	0.46976E+00	0.70379E+00	312.461	-0.0004

950	0.48613E+00	0.70379E+00	311.526	0.0047
951	0.50409E+00	0.70379E+00	310.523	0.0020
952	0.52363E+00	0.70379E+00	309.464	0.0008
953	0.54472E+00	0.70379E+00	308.360	0.0008
954	0.56733E+00	0.70379E+00	307.223	0.0020
955	0.59141E+00	0.70379E+00	306.067	0.0015
956	0.61690E+00	0.70379E+00	304.906	0.0007
957	0.64372E+00	0.70379E+00	303.756	0.0019
958	0.67182E+00	0.70379E+00	302.634	0.0007
959	0.70109E+00	0.70379E+00	301.557	0.0009
960	0.73144E+00	0.70379E+00	300.542	0.0013
961	0.76278E+00	0.70379E+00	299.604	0.0004
962	0.79500E+00	0.70379E+00	298.760	0.0009
963	0.82797E+00	0.70379E+00	298.020	0.0001
964	0.86159E+00	0.70379E+00	297.400	0.0012
965	0.89574E+00	0.70379E+00	296.907	0.0015
966	0.93027E+00	0.70379E+00	296.549	0.0012
967	0.96507E+00	0.70379E+00	296.333	0.0012
968	0.10000E+01	0.70379E+00	296.261	0.0013
969	0.42924E+00	0.11037E+01	0.0	-0.2863
970	0.43411E+00	0.10660E+01	48.150	-0.0000
971	0.43898E+00	0.10282E+01	91.251	-0.0000
972	0.44386E+00	0.99049E+00	129.807	-0.0000
973	0.44873E+00	0.95275E+00	164.303	-0.0000
974	0.45360E+00	0.91501E+00	195.189	-0.0000
975	0.45847E+00	0.87727E+00	222.866	0.0000
976	0.46334E+00	0.83953E+00	247.691	-0.0000
977	0.46822E+00	0.80179E+00	269.973	-0.0000
978	0.47309E+00	0.76405E+00	289.979	-0.0001
979	0.47796E+00	0.72631E+00	307.940	-0.0023
980	0.49358E+00	0.72631E+00	307.042	0.0054
981	0.51083E+00	0.72631E+00	306.072	0.0023
982	0.52972E+00	0.72631E+00	305.042	0.0032
983	0.55019E+00	0.72631E+00	303.963	0.0013
984	0.57223E+00	0.72631E+00	302.848	0.0025
985	0.59577E+00	0.72631E+00	301.710	0.0014
986	0.62076E+00	0.72631E+00	300.565	0.0015
987	0.64712E+00	0.72631E+00	299.429	0.0020
988	0.67479E+00	0.72631E+00	298.319	0.0011
989	0.70366E+00	0.72631E+00	297.253	0.0014
990	0.73365E+00	0.72631E+00	296.246	-0.0002
991	0.76465E+00	0.72631E+00	295.316	0.0010
992	0.79656E+00	0.72631E+00	294.478	0.0016
993	0.82924E+00	0.72631E+00	293.744	0.0005
994	0.86259E+00	0.72631E+00	293.127	0.0006
995	0.89647E+00	0.72631E+00	292.637	-0.0000
996	0.93075E+00	0.72631E+00	292.282	0.0001
997	0.96531E+00	0.72631E+00	292.068	0.0009
998	0.10000E+01	0.72631E+00	291.998	0.0017
999	0.44359E+00	0.11128E+01	0.0	-0.3010
1000	0.44786E+00	0.10764E+01	47.499	-0.0000
1001	0.45213E+00	0.10400E+01	89.937	-0.0000
1002	0.45640E+00	0.10037E+01	127.654	-0.0000
1003	0.46066E+00	0.96733E+00	161.760	-0.0000
1004	0.46493E+00	0.93097E+00	192.117	-0.0000
1005	0.46920E+00	0.89461E+00	219.335	0.0000
1006	0.47347E+00	0.85825E+00	243.773	-0.0000
1007	0.47774E+00	0.82189E+00	265.740	-0.0000
1008	0.48201E+00	0.78553E+00	285.503	-0.0000
1009	0.48628E+00	0.74917E+00	303.269	-0.0046

1010	0.5[illegible]116E+00	0.74917E+00	302.426	0.0017
1011	0.51773E+00	0.74917E+00	301.490	0.0014
1012	0.53595E+00	0.74917E+00	300.488	0.0011
1013	0.55582E+00	0.74917E+00	299.435	0.0026
1014	0.57726E+00	0.74917E+00	298.341	0.0008
1015	0.60[illegible]E+00	0.74917E+00	297.222	0.0014
1016	0.62477E+00	0.74917E+00	296.094	0.0018
1017	0.65067E+00	0.74917E+00	294.971	0.0009
1018	0.67790E+00	0.74917E+00	293.873	0.0014
1019	0.70637E+00	0.74917E+00	292.817	0.0011
1020	0.73599E+00	0.74917E+00	291.819	0.0004
1021	0.76664E+00	0.74917E+00	290.897	0.0014
1022	0.79822E+00	0.74917E+00	290.065	0.0014
1023	0.83[illegible]59E+00	0.74917E+00	289.337	0.0006
1024	0.86365E+00	0.74917E+00	288.726	0.0014
1025	0.89725E+00	0.74917E+00	288.240	0.0015
1026	0.93127E+00	0.74917E+00	287.868	0.0011
1027	0.96557E+00	0.74917E+00	287.670	0.0005
1028	0.10000E+01	0.74917E+00	287.6[illegible]6	0.0018
1029	0.45787E+00	0.11222E+01	0.0	-0.3172
1030	0.46155E+00	0.10872E+01	46.634	-0.0000
1031	0.46524E+00	0.10522E+01	86.599	-0.0000
1032	0.46892E+00	0.10173E+01	125.869	-0.0000
1033	0.47261E+00	0.98227E+00	159.175	-0.0000
1034	0.47630E+00	0.94729E+00	188.994	-0.0000
1035	0.47998E+00	0.91231E+00	215.740	-0.0000
1036	0.48367E+00	0.87732E+00	239.776	-0.0000
1037	0.48735E+00	0.84234E+00	261.412	-0.0000
1038	0.49104E+00	0.80736E+00	280.913	-0.0000
1039	0.49472E+00	0.77238E+00	298.5[illegible]4	-0.0055
1040	0.50886E+00	0.77238E+00	297.677	0.0027
1041	0.52476E+00	0.77238E+00	296.771	0.0010
1042	0.54235E+00	0.77238E+00	295.799	0.0018
1043	0.56160E+00	0.77238E+00	294.770	0.0011
1044	0.58249E+00	0.77238E+00	293.698	0.0010
1045	0.60495E+00	0.77238E+00	292.598	0.0014
1046	0.62894E+00	0.77238E+00	291.4[illegible]	0.00[illegible]5
1047	0.65437E+00	0.77238E+00	290.376	0.0017
1048	0.68116E+00	0.77238E+00	289.29[illegible]	0.0014
1049	0.70922E+00	0.77238E+00	288.244	0.0012
1050	0.73885E+00	0.77238E+00	287.255	0.0008
1051	0.76874E+00	0.77238E+00	286.342	0.0007
1052	0.79998E+00	0.77238E+00	285.517	0.0002
1053	0.83203E+00	0.77238E+00	284.796	0.0016
1054	0.86478E+00	0.77238E+00	284.190	0.0003
1055	0.89[illegible]9E+00	0.77238E+00	283.709	0.0010
1056	0.93162E+00	0.77238E+00	283.361	[illegible]
1057	0.96584E+00	0.77238E+00	283.151	0.0011
1058	0.10000E+01	0.77238E+00	283.082	0.0019
1059	0.472[illegible]7E+00	0.1132[illegible]E+01	0.0	-0.3352
1060	0.47519E+00	0.10984E+01	46.153	-0.0000
1061	0.47831E+00	0.10648E+01	87.232	-0.0000
1062	0.48144E+00	0.10312E+01	123.846	-0.0000
1063	0.48456E+00	0.99758E+00	156.545	-0.0000
1064	0.48768E+00	0.96397E+00	185.614	-0.0000
1065	0.49081E+00	0.93036E+00	212.077	-0.0000
1066	0.49393E+00	0.89676E+00	235.697	-0.0000
1067	0.497[illegible]5E+00	0.86315E+00	256.984	-0.0000
1068	0.50017E+00	0.82954E+00	276.203	-0.0000
1069	0.50338E+00	0.79593E+00	293.578	-0.0052

1070	0.51675E+00	0.79593E+00	292.764	0.0003
1071	0.53195E+00	0.79593E+00	291.910	-0.0025
1072	0.54889E+00	0.79593E+00	290.966	0.0016
1073	0.56754E+00	0.79593E+00	289.962	0.0013
1074	0.58756E+00	0.79593E+00	288.912	0.0016
1075	0.60979E+00	0.79593E+00	287.830	0.0017
1076	0.63327E+00	0.79593E+00	286.733	0.0019
1077	0.65823E+00	0.79593E+00	285.638	0.0006
1078	0.68457E+00	0.79593E+00	284.564	0.0012
1079	0.71221E+00	0.79593E+00	283.528	0.0002
1080	0.74105E+00	0.79593E+00	282.550	0.0004
1081	0.77096E+00	0.79593E+00	281.645	0.0000
1082	0.80184E+00	0.79593E+00	280.829	0.0013
1083	0.83356E+00	0.79593E+00	280.116	0.0013
1084	0.86599E+00	0.79593E+00	279.516	-0.0000
1085	0.89898E+00	0.79593E+00	279.041	0.0004
1086	0.93241E+00	0.79593E+00	278.697	-0.0002
1087	0.96613E+00	0.79593E+00	278.490	0.0009
1088	0.10000E+01	0.79593E+00	278.421	0.0014
1089	0.48616E+00	0.11422E+01	0.0	-0.3552
1090	0.48876E+00	0.11100E+01	45.453	-0.0000
1091	0.49134E+00	0.10777E+01	85.635	-0.0000
1092	0.49393E+00	0.10455E+01	121.761	-0.0000
1093	0.49651E+00	0.10133E+01	153.861	-0.0000
1094	0.49909E+00	0.98103E+00	182.570	-0.0000
1095	0.50167E+00	0.94879E+00	208.337	-0.0000
1096	0.50425E+00	0.91655E+00	231.526	-0.0000
1097	0.50684E+00	0.88432E+00	252.448	-0.0000
1098	0.50942E+00	0.85208E+00	271.366	-0.0000
1099	0.51200E+00	0.81984E+00	288.501	-0.0059
1100	0.52475E+00	0.81984E+00	287.743	-0.0002
1101	0.53929E+00	0.81984E+00	286.900	-0.0023
1102	0.5556[illegible]E+00	0.81984E+00	285.984	0.0014
1103	0.57365E+00	0.81984E+00	285.004	0.0015
1104	0.59340E+00	0.81984E+00	283.974	0.0015
1105	0.61480E+00	0.81984E+00	282.910	0.0011
1106	0.63777E+00	0.81984E+00	281.829	0.0009
1107	0.66224E+00	0.81984E+00	280.749	[illegible]
1108	0.68813E+00	0.81984E+00	279.688	0.0016
1109	0.71534E+00	0.81984E+00	278.664	0.0006
1110	0.74377E+00	0.81984E+00	277.697	0.0005
1111	0.77330E+00	0.81984E+00	276.802	0.0010
1112	0.80381E+00	0.81984E+00	275.995	0.0009
1113	0.83518E+00	0.81984E+00	275.291	0.0012
1114	0.86728E+00	0.81984E+00	274.699	0.0010
1115	0.89993E+00	0.81984E+00	274.230	0.0003
1116	0.93304E+00	0.81984E+00	273.891	0.0007
1117	0.96645E+00	0.81984E+00	273.687	0.0010
1118	0.10000E+01	0.81984E+00	273.620	0.0022
1119	0.50019E+00	0.11528E+01	0.0	-0.3775
1120	0.50226E+00	0.11219E+01	44.734	-0.0000
1121	0.50432E+00	0.10911E+01	84.402	-0.0000
1122	0.50638E+00	0.10602E+01	119.669	-0.0000
1123	0.50845E+00	0.10293E+01	151.119	-0.0000
1124	0.51051E+00	0.99846E+00	179.256	-0.0000
1125	0.51258E+00	0.96759E+00	204.514	-0.0000
1126	0.51464E+00	0.93672E+00	227.257	-0.0000
1127	0.51671E+00	0.90585E+00	247.796	-0.0000
1128	0.51877E+00	0.87498E+00	266.393	-0.0001
1129	0.52083E+00	0.84411E+00	283.269	-0.0056

1130	0.53290E+00	0.84411E+00	282.545	0.0003
1131	0.54679E+00	0.84411E+00	281.732	-0.0006
1132	0.56248E+00	0.84411E+00	280.843	0.0020
1133	0.57993E+00	0.84411E+00	279.887	0.0016
1134	0.59911E+00	0.84411E+00	278.878	0.0015
1135	0.61997E+00	0.84411E+00	277.833	0.0018
1136	0.64243E+00	0.84411E+00	276.769	0.0017
1137	0.66642E+00	0.84411E+00	275.703	0.0011
1138	0.69165E+00	0.84411E+00	274.655	0.0007
1139	0.71862E+00	0.84411E+00	273.644	0.0006
1140	0.74663E+00	0.84411E+00	272.689	0.0012
1141	0.77576E+00	0.84411E+00	271.805	0.0011
1142	0.80589E+00	0.84411E+00	271.010	0.0007
1143	0.83698E+00	0.84411E+00	270.315	0.0007
1144	0.86861E+00	0.84411E+00	269.733	0.0010
1145	0.90094E+00	0.84411E+00	269.272	0.0002
1146	0.93371E+00	0.84411E+00	268.939	0.0000
1147	0.96678E+00	0.84411E+00	268.739	0.0006
1148	0.10000E+01	0.84411E+00	268.672	0.0017
1149	0.51410E+00	0.11638E+01	0.0	-0.4024
1150	0.51567E+00	0.11343E+01	43.969	-0.0000
1151	0.51724E+00	0.11048E+01	82.927	-0.0000
1152	0.51881E+00	0.10753E+01	117.501	-0.0000
1153	0.52038E+00	0.10458E+01	148.309	-0.0000
1154	0.52195E+00	0.10163E+01	175.863	-0.0000
1155	0.52352E+00	0.98677E+00	200.597	-0.0000
1156	0.52509E+00	0.95726E+00	222.860	-0.0000
1157	0.52666E+00	0.92776E+00	243.019	-0.0000
1158	0.52823E+00	0.89825E+00	261.276	-0.0000
1159	0.52980E+00	0.86875E+00	277.869	-0.0066
1160	0.54120E+00	0.86875E+00	277.178	-0.0008
1161	0.55441E+00	0.86875E+00	276.396	-0.0040
1162	0.56951E+00	0.86875E+00	275.533	-0.0003
1163	0.58638E+00	0.86875E+00	274.602	0.0009
1164	0.60500E+00	0.86875E+00	273.615	0.0015
1165	0.62532E+00	0.86875E+00	272.589	0.0020
1166	0.64726E+00	0.86875E+00	271.542	0.0013
1167	0.67076E+00	0.86875E+00	270.492	0.0012
1168	0.69572E+00	0.86875E+00	269.458	0.0009
1169	0.72204E+00	0.86875E+00	268.461	0.0002
1170	0.74962E+00	0.86875E+00	267.519	0.0004
1171	0.77834E+00	0.86875E+00	266.649	0.0013
1172	0.80807E+00	0.86875E+00	265.866	0.0006
1173	0.83868E+00	0.86875E+00	265.184	0.0005
1174	0.87004E+00	0.86875E+00	264.613	-0.0002
1175	0.90200E+00	0.86875E+00	264.162	0.0008
1176	0.93441E+00	0.86875E+00	263.836	-0.0001
1177	0.96713E+00	0.86875E+00	263.640	0.0002
1178	0.10000E+01	0.86875E+00	263.576	0.0020
1179	0.52788E+00	0.11752E+01	0.0	-0.4305
1180	0.52898E+00	0.11471E+01	43.222	-0.0000
1181	0.53009E+00	0.11189E+01	81.409	-0.0000
1182	0.53119E+00	0.10908E+01	115.274	-0.0000
1183	0.53229E+00	0.10626E+01	145.425	-0.0000
1184	0.53339E+00	0.10345E+01	172.382	-0.0000
1185	0.53449E+00	0.10063E+01	196.580	-0.0000
1186	0.53560E+00	0.97819E+00	218.386	-0.0000
1187	0.53670E+00	0.95004E+00	238.109	-0.0000
1188	0.53780E+00	0.92190E+00	256.005	-0.0000
1189	0.53890E+00	0.89375E+00	272.294	-0.0059

1190	0.5495E+00	0.89375E+00	271.638	0.0013
1191	0.56225E+00	0.89375E+00	270.685	-0.0039
1192	0.57672E+00	0.89375E+00	270.648	-0.0017
1193	0.5930E+00	0.89375E+00	269.141	0.0013
1194	0.611 6E+00	0.89375E+00	268.176	0.0016
1195	0.63 84E+00	0.89375E+00	267.169	0.0009
1196	0.65227E+00	0.89375E+00	266.14	0.0013
1197	0.67527E+00	0.89375E+00	265.10	0.0015
1198	0.69975E+00	0.89375E+00	264.06	0.0006
1199	0.72562E+00	0.89375E+00	263.107	0.0012
1200	0.75276E+00	0.89375E+00	262.161	0.0010
1201	0.78135E+00	0.89375E+00	261.326	0.0005
1202	0.81136E+00	0.89375E+00	260.559	0.0002
1203	0.84058E+00	0.89375E+00	259.652	0.0002
1204	0.87154E+00	0.89375E+00	259.335	0.0010
1205	0.90312E+00	0.89375E+00	258.695	0.0012
1206	0.93515E+00	0.89375E+00	258.578	0.0006
1207	0.9673E+00	0.89375E+00	258.368	0.0012
1208	0.1000E+01	0.89375E+00	258.325	0.0016
1209	0.54154E+00	0.11870E+01	0.0	-0.4622
1210	0.5422E+00	0.11602E+01	42.425	-0.000
1211	0.54286E+00	0.11334E+01	79.839	-0.001
1212	0.54352E+00	0.11066E+01	112.976	-0.000
1213	0.54418E+00	0.10799E+01	142.455	-0.000
1214	0.54484E+00	0.10531E+01	168.684	-0.000
1215	0.5455E+00	0.10263E+01	192.459	-0.00
1216	0.54616E+00	0.99949E+00	213.765	-0.00
1217	0.54682E+00	0.97271E+00	233.058	-0.000
1218	0.5474E+00	0.94592E+00	250.573	0.0001
1219	0.54814E+00	0.91914E+00	266.533	-0.0069
1220	0.55824E+00	0.91914E+00	265.949	-0.0046
1221	0.5723E+00	0.91914E+00	265.167	-0.0035
1222	0.5849E+00	0.91914E+00	264.377	-0.0020
1223	0.5995E+00	0.91914E+00	263.494	-0.0010
1224	0.61730E+00	0.91914E+00	262.551	0.0019
1225	0.63654E+00	0.91914E+00	261.564	0.0009
1226	0.6574E+00	0.91914E+00	260.553	0.0009
1227	0.67995E+00	0.91914E+00	259.538	0.0009
1228	0.70395E+00	0.91914E+00	258.538	0.0015
1229	0.72935E+00	0.91914E+00	257.575	0.0006
1230	0.756 3E+00	0.91914E+00	256.666	0.0008
1231	0.78348E+00	0.91914E+00	255.83	0.0008
1232	0.81277E+00	0.91914E+00	255.081	0.0006
1233	0.84257E+00	0.91914E+00	254.432	0.0012
1234	0.87312E+00	0.91914E+00	253.892	0.0006
1235	0.9043 E+00	0.91914E+00	253.467	0.0012
1236	0.93594E+00	0.91914E+00	253.161	0.0005
1237	0.96789E+00	0.91914E+00	252.978	0.0001
1238	0.1000E+01	0.91914E+00	252.918	0.0024
1239	0.5551 5E+00	0.11992E+01	0.0	-0.4962
1240	0.55529E+00	0.11736E+01	41.594	-0.000
1241	0.55554E+00	0.11483E+01	76.215	-0.00
1242	0.55579E+00	0.11229E+01	110.609	-0.000
1243	0.5560 3E+00	0.10975E+01	139.4 1	-0.00
1244	0.55628E+00	0.10721E+01	165.118	-0.000
1245	0.55653E+00	0.10466E+01	188.197	-0.000
1246	0.55678E+00	0.10212E+01	209.[illegible]3	-0.000
1247	0.55702E+00	0.99576E+00	227.842	0.0001
1248	0.55727E+00	0.97033E+00	244.962	0.0001
1249	0.55752E+00	0.94490E+00	260.576	-0.0056

1250	0.56699E+00	0.94490E+00	259.980	0.0019
1251	0.57837E+00	0.94490E+00	259.292	-0.0033
1252	0.59164E+00	0.94490E+00	258.599	-0.0016
1253	0.60677E+00	0.94490E+00	257.650	[illegible]
1254	0.62371E+00	0.94490E+00	256.729	0.0017
1255	0.64242E+00	0.94490E+00	255.763	0.0015
1256	0.66281E+00	0.94490E+00	254.772	0.0011
1257	0.68486E+00	0.94490E+00	253.776	0.0014
1258	0.70831E+00	0.94490E+00	252.797	0.0010
1259	0.73323E+00	0.94490E+00	251.854	0.0010
1260	0.75945E+00	0.94490E+00	250.967	0.0015
1261	0.78685E+00	0.94490E+00	250.153	0.0006
1262	0.81529E+00	0.94490E+00	249.427	0.0018
1263	0.84465E+00	0.94490E+00	248.80[illegible]	0.0017
1264	0.87479E+00	0.94490E+00	248.28[illegible]	0.0007
1265	0.90554E+00	0.94490E+00	247.873	0.0011
1266	0.93676E+00	0.94490E+00	247.581	0.0007
1267	0.9683[illegible]E+00	0.94490E+00	247.407	0.0012
1268	0.1[illegible]E+01	0.94490E+00	247.349	0.0016
1269	0.56847E+00	0.12116E+01	0.0	-0.5395
1270	0.56826E+00	0.11877E+01	40.737	[illegible]
1271	0.56812E+00	0.11637E+01	76.529	[illegible]
1272	0.56799E+00	0.11396E+01	108.156	[illegible]
1273	0.56785E+00	0.11155E+01	136.243	[illegible]
1274	0.56771E+00	0.10914E+01	161.316	[illegible]
1275	0.5675[illegible]E+00	0.10674E+01	183.611	[illegible]
1276	0.56744E+00	0.10433E+01	204.[illegible]91	[illegible]
1277	0.56731E+00	0.10192E+01	222.459	0.0001
1278	0.56717E+00	0.99512E+00	239.162	0.0001
1279	0.567[illegible]3E+00	0.97104E+00	254.41[illegible]	-0.0014
1280	0.57589E+00	0.97104E+00	253.850	-0.0031
1281	0.58667E+00	0.97104E+00	253.185	-0.0032
1282	0.59936E+00	0.97104E+00	252.43[illegible]	-0.0026
1283	0.61392E+00	0.97104E+00	251.595	-0.0012
1284	0.63032E+00	0.97104E+00	250.697	0.001[illegible]
1285	0.64848E+00	0.97104E+00	249.753	0.0007
1286	0.66835E+00	0.97104E+00	248.78[illegible]	0.0012
1287	0.68983E+00	0.97104E+00	247.811	[illegible]
1288	0.71284E+00	0.97104E+00	246.854	0.0009
1289	0.73727E+00	0.97104E+00	245.935	0.0005
1290	0.763[illegible]2E+00	0.97104E+00	245.074	0.0011
1291	0.78995E+00	0.97104E+00	244.287	0.0006
1292	0.81753E+00	0.97104E+00	243.589	0.0018
1293	0.84584E+00	0.97104E+00	242.989	0.0018
1294	0.87653E+00	0.97104E+00	242.495	0.0005
1295	0.90684E+00	0.97104E+00	242.495	0.0004
1296	0.93763E+00	0.97104E+00	242.11[illegible]	0.0011
1297	0.96573E+00	0.97104E+00	241.835	0.0007
1298	0.1[illegible]E+01	0.97104E+00	241.671	[illegible]
		0.97104E+00	241.618	0.0015
1299	0.58159E+00	0.12249E+01	0.0	-0.5869
1300	0.58109E+00	0.12021E+01	39.53[illegible]	[illegible]
1301	0.5806[illegible]E+00	0.11794E+01	74.776	[illegible]
1302	0.58011E+00	0.11567E+01	105.614	[illegible]
1303	0.57962E+00	0.11339E+01	132.974	[illegible]
1304	0.57913E+00	0.11112E+01	157.363	[illegible]
1305	0.57864E+00	0.10885E+01	179.277	[illegible]
1306	0.57816E+00	0.10658E+01	199.[illegible]14	[illegible]
1307	0.57767E+00	0.10431E+01	216.892	0.0001
1308	0.57718E+00	0.10203E+01	233.158	0.0001
1309	0.57669E+00	0.99757E+00	248.017	[illegible]

1310	.58494E+00	0.99757E+00	247.490	-0.0032
1311	.59514E+00	0.99757E+00	246.856	-0.0030
1312	0.60726E+00	0.99757E+00	246.127	-0.0025
1313	.62120E+00	0.99757E+00	245.318	-0.0024
1314	.63717E+00	0.99757E+00	244.442	-0.00 5
1315	.65473E+00	0.99757E+00	243.523	0.001
1316	.67437E+00	0.99757E+00	242.577	-0.0003
1317	.69524E+00	0.99757E+00	241.629	0.0013
1318	.71754E+00	0.99757E+00	240.699	0.0009
1319	.74107E+00	0.99757E+00	239.810	0.0006
1320	.76673E+00	0.99757E+00	238.979	0.0008
1321	.79318E+00	0.99757E+00	238.228	0.0009
1322	.82 69E+00	0.99757E+00	237.561	0.000
1323	.84913E+00	0.99757E+00	236.996	0.0010
1324	.87835E+00	0.99757E+00	236.533	0.0004
1325	.9 820E+00	0.99757E+00	236.175	0.0001
1326	.93354E+00	0.99757E+00	235.922	0.0004
1327	.96919E+00	0.99757E+00	235.772	0.0006
1328	0.1 E+01	0.99757E+00	235.723	0.0017
1329	.59 57E+00	0.12383E+01	0.0	-0.6420
1330	.59376E+00	0.12169E+01	36.891	-0.00
1331	.59296E+00	0.11955E+01	72.956	-0.00
1332	.59215E+00	0.11742E+01	1 2.973	-0.00
1333	.59134E+00	0.11528E+01	129.584	-0.00
1334	.59 53E+00	.11314E+01	153.309	-0.00
1335	.58972E+00	.111 E+01	174.583	0.0001
1336	.58891E+00	0.10886E+01	193.757	0.0001
1337	.58810E+00	0.10672E+01	211.128	0.0001
1338	.58729E+00	0.10459E+01	226.933	-0.000
1339	.586 9E+00	0.10245E+01	241.383	-0.0007
1340	.59416E+00	0.10245E+01	240.869	-0.0031
1341	.60376E+00	0.10245E+01	240.285	-0.0027
1342	.61533E+00	0.10245E+01	239.583	-0.0038
1343	.62578E+00	0.10245E+01	238.799	-0.0029
1344	0.64408E+00	0.10245E+01	237.951	-0.0013
1345	0.66117E+00	0.10245E+01	237.056	0.0005
1346	.67998E+00	0.1.245E+01	236.138	0.0001
1347	.7 42E+00	0.10245E+01	235.218	0.0011
1348	0.72241E+00	0.10245E+01	234.321	0.0012
1349	.74584E+00	0.10245E+01	233.465	0.001
1350	.77 9E+00	0.10245E+01	232.673	0.0002
1351	.79654E+00	0.1 245E+01	231.959	0.0008
1352	.82357E+00	0.10245E+01	231.337	0.0001
1353	.85152E+00	0.10245E+01	230.813	0.0009
1354	.88 26E+00	.10245E+01	230.391	0.0013
1355	.90963E+00	.10245E+01	230.066	0.0009
1356	.93309E+00	0.10245E+01	229.841	0.0015
1357	0.96966E+00	0.10245E+01	229.7	0.0012
1358	0.1 E+01	0.10245E+01	229.665	0.0016
1359	0.60737E+00	0.12522E+01	0.0	-0.7065
1360	0.60627E+00	0.12321E+01	37.906	-0.000
1361	.60516E+00	0.12121E+01	71.052	-0.00
1362	0.60 8E+00	0.11921E+01	100.224	-0.00
1363	0.60299E+00	0.1172 E+01	126.06	-0.00
1364	0.60169E+00	0.1152 E+01	149.06	0.00
1365	0.60080E+00	0.11319E+01	169.712	0.0001
1366	0.59971E+00	0.11119E+01	188.304	0.0001
1367	.59861E+00	0.10919E+01	2 5.104	0.00
1368	0.59752E+00	0.10718E+01	220.474	0.000
1369	0.59642E+00	0.10518E+01	234.491	-0.0008

1370	0.60353E+00	0.10518E+01	234.029	-0.0039
1371	0.61259E+00	0.10518E+01	233.455	-0.0027
1372	0.62359E+00	0.10518E+01	232.782	-0.0035
1373	0.63609E+00	0.10518E+01	232.025	-0.0024
1374	0.65125E+00	0.10518E+01	231.203	-0.0040
1375	0.66730E+00	0.10518E+01	230.338	-0.0014
1376	0.686[illegible]7E+00	0.10518E+01	229.451	0.0008
1377	0.70599E+00	0.10518E+01	228.564	0.0006
1378	0.72746E+00	0.10518E+01	227.703	0.0003
1379	0.75037E+00	0.10518E+01	226.89[illegible]	0.0009
1380	0.77461E+00	0.10518E+01	226.144	0.0006
1381	0.8[illegible]5E+00	0.10518E+01	225.461	0.0001
1382	0.82656E+00	0.10518E+01	224.911	0.0005
1383	0.85[illegible]1E+00	0.10518E+01	224.44[illegible]	0.0003
1384	0.88225E+00	0.10518E+01	224.[illegible]67	0.0011
1385	0.91112E+00	0.10518E+01	223.788	0.0007
1386	0.94[illegible]E+00	0.10518E+01	223.595	0.0007
1387	0.97[illegible]16[illegible]E+00	0.10518E+01	223.483	0.001[illegible]
1388	0.10[illegible]E+01	0.10518E+01	223.447	0.0014
1389	0.61994E+00	0.12664E+01	0.0	-0.7827
1390	0.6180[illegible]E+0[illegible]	0.12477E+01	36.872	-0.00[illegible]
1391	0.61725E+00	0.12291E+01	69.[illegible]59	-0.000[illegible]
1392	0.61591E+00	0.12104E+01	97.353	[illegible]
1393	0.61457E+00	0.11917E+01	122.380	[illegible]
1394	0.61322E+00	0.1173[illegible]E+01	144.676	0.000[illegible]
1395	0.61138E+00	0.11543E+01	164.643	[illegible]
1396	0.61[illegible]E+00	0.11356E+01	182.632	[illegible]
1397	0.6[illegible]919E+00	0.11169E+01	198.924	[illegible]
1398	0.6[illegible]705E+00	0.1[illegible]982E+01	213.755	0.000[illegible]
1399	0.6[illegible]5[illegible]E+00	0.10795E+01	227.319	-0.0013
1400	0.613[illegible]E+00	0.10795E+01	226.89[illegible]	-0.0031
1401	0.62156E+00	0.10795E+01	226.347	-0.003[illegible]
1402	0.632[illegible]3E+00	0.10795E+01	225.703	-0.0025
1403	0.64[illegible]39E+00	0.10795E+01	224.975	-0.0029
1404	0.65860E+00	0.10795E+01	224.182	-0.0044
1405	0.67402E+00	0.10795E+01	223.343	-0.0023
1406	0.69236E+00	0.10795E+01	222.[illegible]	0.0017
1407	0.71174E+00	0.10795E+01	221.645	0.001[illegible]
1408	0.73269E+00	0.10795E+01	220.832	0.00[illegible]2
1409	0.75[illegible]E+00	0.10795E+01	220.[illegible]09	0.0002
1410	0.77877E+00	0.10795E+01	219.381	0.0006
1411	0.8[illegible]369E+00	0.10795E+01	218.782	0.0012
1412	0.82866E+00	0.10795E+01	218.278	0.0008
1413	0.85[illegible]1E+00	0.10795E+01	217.874	0.0007
1414	0.88139E+00	0.10795E+01	217.563	0.0007
1415	0.91266E+00	0.10795E+01	217.338	0.0008
1416	0.94152E+00	0.10795E+01	217.189	0.0007
1417	0.97[illegible]E+00	0.10795E+01	217.1[illegible]4	0.000[illegible]
1418	0.1[illegible]E+01	0.10795E+01	217.[illegible]77	0.0013
1419	0.63228E+00	0.12811E+01	0.[illegible]	-0.8736
1420	0.63[illegible]72E+00	0.12636E+01	35.780	-0.000[illegible]
1421	0.62917E+00	0.1246[illegible]E+01	68.972	-0.000[illegible]
1422	0.62761E+00	0.12291E+01	94.351	0.000[illegible]
1423	0.62[illegible]6E+00	0.12117E+01	118.551	[illegible]
1424	0.624[illegible]E+00	0.11944E+01	14[illegible].[illegible]83	[illegible]
1425	0.62295E+00	0.1177[illegible]E+01	159.302	[illegible]
1426	0.62139E+00	0.11596E+01	176.723	[illegible]
1427	0.61984E+00	0.11423E+01	192.446	[illegible]
1428	0.61828E+00	0.11249E+01	2[illegible]6.750	[illegible]
1429	0.61673E+00	0.11[illegible]76E+01	219.845	-0.001[illegible]

143.	.62275E+ [illegible]	[illegible].11076E+01	219.448	-0.0029
1431	.63 73E+[illegible]	[illegible].11076E+01	218.936	-0.0025
1432	[illegible].64 65E+00	0.11076E+01	218.322	-[illegible].[illegible]3[illegible]
1433	.[illegible]247E+[illegible]	[illegible].11076E+01	217.625	-0.0027
1434	[illegible].66 15[illegible]+ [illegible]	.11076E+01	216.865	-[illegible].0029
1435	.6[illegible]183E+ [illegible]	[illegible].11076E+01	216.[illegible]65	- .[illegible]015
1436	[illegible].69884E+[illegible]	0.11076E+01	215.252	.[illegible]005
1437	[illegible].71768E+0[illegible]	0.11076E+01	214.451	[illegible].0005
1438	.733[illegible]8E+[illegible]	[illegible].11076E+01	213.69[illegible]	[illegible].0007
1439	[illegible].75992E+ [illegible]	[illegible].11076E+01	212.991	.0007
144[illegible]	.76310E+0[illegible]	0.11076E+01	212.375	[illegible].[illegible]008
1441	.8[illegible]748E+0[illegible]	0.11076E+01	211.855	-[illegible].[illegible]002
1442	[illegible].83293E+[illegible]	[illegible].11076E+01	211.436	.[illegible]006
1443	[illegible].85932E+[illegible]	[illegible].11076E+01	211.115	.0012
1444	[illegible].88649E+0[illegible]	0.11076E+01	21[illegible].885	0.0015
1445	.91430E+0[illegible]	0.11076E+01	210.729	[illegible].[illegible]008
1446	[illegible].94260E+[illegible]	0.11076E+01	21[illegible].633	[illegible].[illegible]003
1447	.97122E+[illegible]	[illegible].11076E+01	21[illegible].583	[illegible].[illegible]008
1448	[illegible].10[illegible]E+01	0.11076E+01	21[illegible].566	0.0015
1449	.64436E+0[illegible]	0.12962E+01	[illegible]	-0.9839
145[illegible]	[illegible].64263E+[illegible]	[illegible].128[illegible]2E+01	34.[illegible]	[illegible]
1451	[illegible].64[illegible]91E+[illegible]	[illegible].12642E+01	60.776	-[illegible]
1452	[illegible].63918E+0[illegible]	0.12482E+01	91.2[illegible]1	[illegible]
1453	[illegible].63745E+00	0.12321E+01	114.533	[illegible]
1454	[illegible].63572E+[illegible]	[illegible].12161E+01	135.278	[illegible]
1455	[illegible].63[illegible]E+ [illegible]	[illegible].12[illegible]1E+01	153.841	[illegible]
1456	.63227E+0[illegible]	0.11841E+01	17[illegible].551	[illegible]
1457	.63[illegible]54E+0[illegible]	0.11681E+01	185.676	[illegible].0001
1458	[illegible].62882E+[illegible]	0.11521E+01	199.446	[illegible]
1459	.627[illegible]9E+[illegible]	[illegible].1136[illegible]E+01	212.[illegible]38	-[illegible].0013
146[illegible]	[illegible].632[illegible]E+0[illegible]	0.11360E+01	211.673	-[illegible].0024
1461	[illegible].64[illegible]E+0[illegible]	0.11360E+01	211.192	-[illegible].0020
1462	[illegible].649[illegible]5E+[illegible]	[illegible].1136[illegible]E+01	21[illegible].[illegible]9	-[illegible].0020
1463	.66[illegible]75E+[illegible]	[illegible].1136[illegible]E+01	2[illegible]9.944	-[illegible].0023
1464	[illegible].67399E+00	[illegible].11360E+01	2[illegible]9.219	-[illegible].[illegible]026
1465	[illegible].68884E+00	0.1136[illegible]E+01	2[illegible]8.459	-[illegible].0029
1466	.7[illegible]E+[illegible]	[illegible].1136[illegible]E+01	2[illegible]7.693	-[illegible].[illegible]9
1467	.72361E+ [illegible]	[illegible].1136[illegible]E+01	2[illegible]6.95[illegible]	[illegible].[illegible]07
1468	[illegible].74366E+0[illegible]	0.1136[illegible]E+01	2[illegible]6.256	[illegible]
1469	[illegible].76495E+0[illegible]	0.1136[illegible]E+01	2[illegible]5.638	[illegible]
147[illegible]	[illegible].78758E+[illegible]	[illegible].1136[illegible]E+01	2[illegible]5.11[illegible]	[illegible].[illegible]005
1471	[illegible].811[illegible]E+0[illegible]	[illegible].1136[illegible]E+01	2[illegible]4.695	-[illegible].[illegible]1
1472	[illegible].83630E+00	0.1136[illegible]E+01	2 4.383	-[illegible].[illegible]1
1473	[illegible].86213E+[illegible]	[illegible].1136[illegible]E+01	2[illegible]4.171	[illegible]3
1474	[illegible].88874E+[illegible]	[illegible].1136[illegible]E+01	2[illegible]4.[illegible]2	[illegible].[illegible]3
1475	[illegible].91599E+ [illegible]	[illegible].1136[illegible]E+01	2[illegible]3.975	[illegible].[illegible]6
1476	[illegible].94373E+00	[illegible].1136[illegible]E+01	2[illegible]3.967	[illegible]
1477	[illegible].97178E+00	[illegible].1136[illegible]E+01	2[illegible]3.9[illegible]	[illegible].[illegible]06
1478	[illegible].1[illegible]E+01	[illegible].1136[illegible]E+01	2[illegible]3.9[illegible]	0.0014
1479	[illegible].65617E+[illegible]	[illegible].13117E+01	[illegible]	-1.1192
148[illegible]	[illegible].65431E+0[illegible]	0.1297[illegible]E+01	33.4[illegible]4	[illegible].000[illegible]
1481	[illegible].65245E+00	0.12823E+01	62.458	[illegible]
1482	[illegible].65[illegible]59E+[illegible]	[illegible].12677E+01	87.661	[illegible]
1483	[illegible].64873E+[illegible]	[illegible].1253[illegible]E+01	11[illegible].3[illegible]9	[illegible]
1484	[illegible].64688E+00	0.12383E+01	13[illegible].231	[illegible]
1485	[illegible].645[illegible]2E+0[illegible]	0.12236E+01	148.[illegible]	[illegible]
1486	0.64316E+[illegible]	[illegible].12[illegible]89E+01	16[illegible]	[illegible]
1487	[illegible].6413[illegible]E+ [illegible]	[illegible].11942E+01	178.387	0.0001
1488	[illegible].63945E+00	0.11796E+01	1[illegible]1.737	-[illegible].0001
1489	[illegible].63759E+00	0.11649E+01	2[illegible]3.658	-0.0015

1490	.64261E+	.11649E+01	203.525	-0.0023
1491	.64355E+	.11649E+01	203.175	-0.0026
1492	.65644E+	.11649E+01	202.525	-0.002
1493	.65921E+	.11649E+01	201.895	-0.0024
1494	.65183E+	.11649E+01	201.21	-0.0034
1495	.69524E+	.11649E+01	200.497	-0.0029
1496	.71236E+	.11649E+01	199.788	-0.0014
1497	.73012E+	.11649E+01	199.116	0.0002
1498	.74942E+	.11649E+01	198.508	0.0006
1499	.77015E+	.11649E+01	197.993	-0.0001
1500	.79221E+	.11649E+01	197.587	0.0007
1501	.81547E+	.11649E+01	197.300	0.0010
1502	.83979E+	.11649E+01	197.127	0.0007
1503	.86504E+	.11649E+01	197.053	.0007
1504	.89106E+	.11649E+01	197.053	.0005
1505	.91775E+	.11649E+01	197.098	0.0002
1506	.94494E+	.11649E+01	197.157	.0006
1507	.97237E+	.11649E+01	197.205	.0005
1508	.10000E+01	.11649E+01	197.223	.0017
1509	.66767E+	0.13276E+01	0.	-1.2981
1510	.66573E+	.13142E+01	32.133	[illegible]
1511	.66378E+	.13009E+01	59.999	[illegible]
1512	.66184E+	0.12875E+01	84.308	[illegible]
1513	.65989E+	0.12742E+01	105.845	[illegible]
1514	.65795E+	.12608E+01	124.911	[illegible]
1515	.65600E+	.12475E+01	141.947	[illegible]
1516	.65406E+	0.12341E+01	157.208	[illegible]
1517	.65211E+	0.12208E+01	171.128	[illegible]
1518	.65016E+	.12074E+01	183.739	[illegible]
1519	.64822E+	.11941E+01	195.259	[illegible]
1520	.65275E+	0.11941E+01	194.957	-0.0027
1521	.65921E+	0.11941E+01	194.539	-0.0020
1522	.66739E+	.11941E+01	194.024	-0.0023
1523	.67786E+	.11941E+01	193.432	-0.0026
1524	.68995E+	0.11941E+01	192.792	-0.0029
1525	.70383E+	0.11941E+01	192.136	-0.0025
1526	.71941E+	.11941E+01	191.495	-0.0025
1527	.73661E+	.11941E+01	191.914	-0.002
1528	.75535E+	.11941E+01	190.914	-0.0012
1529	.77552E+	0.11941E+01	190.416	.0004
1530	.797 E+	.11941E+01	190.038	.0004
1531	.81967E+	.11941E+01	189.786	.0006
1532	.84341E+	0.11941E+01	189.670	.0009
1533	.86806E+	0.11941E+01	189.677	.0008
1534	.89350E+	0.11941E+01	189.782	.0001
1535	.91957E+	.11941E+01	189.949	.0009
1536	.94611E+	0.11941E+01	190.137	-0.000
1537	.97281E+	0.11941E+01	190.305	.000
1538	.10000E+01	.11941E+01	190.422	.0007
1539	.67495E+	.13438E+01	190.468	.0016
1540	.67686E+	0.13318E+01	0.	-1.5028
1541	.67486E+	0.13197E+01	30.756	[illegible]
1542	.67289E+	.13077E+01	57.361	[illegible]
1543	.67091E+	.12957E+01	80.632	[illegible]
1544	.66891E+	0.12837E+01	101.105	[illegible]
1545	.66693E+	0.12717E+01	119.265	[illegible]
1546	.66494E+	.12597E+01	135.481	-0.0001
1547	.66295E+	.12477E+01	150.058	-0.0001
1548	.66096E+	0.12357E+01	163.235	-0.0001
1549	.65898E+	0.12237E+01	175.222	-0.0011
			186.175	-0.0012

1550	0.66365E+00	0.12237E+01	185.904	-0.0012
1551	0.66914E+00	0.12237E+01	185.519	-0.0021
1552	0.67692E+00	0.12237E+01	185.04[illegible]	-0.0026
1553	0.68868E+00	0.12237E+01	184.492	-0.0022
1554	0.69826E+00	0.12237E+01	183.9[illegible]6	-0.0026
1555	0.711[illegible]E+00	0.12237E+01	183.319	-0.0029
1556	0.72664E+00	0.12237E+01	182.771	-0.0032
1557	0.74329E+00	0.12237E+01	182.3[illegible]4	-0.0012
1558	0.76146E+00	0.12237E+01	181.954	0.000[illegible]
1559	0.781[illegible]5E+00	0.12237E+01	181.75[illegible]	-0.0[illegible]
1560	0.80194E+00	0.12237E+01	181.704	0.0009
1561	0.824[illegible]1E+00	0.12237E+01	181.815	0.000[illegible]
1562	0.84714E+00	0.12237E+01	182.056	0.0001
1563	0.87119E+00	0.12237E+01	182.390	0.0015
1564	0.896[illegible]1E+00	0.12237E+01	182.777	-0.0002
1565	0.92145E+00	0.12237E+01	183.146	0.0015
1566	0.94737E+00	0.12237E+01	183.452	0.0004
1567	0.97361E+00	0.12237E+01	183.653	0.00[illegible]0
1568	0.10000E+01	0.12237E+01	183.724	0.0011
1569	0.68967E+00	0.13603E+01	0.0	-1.7815
1570	0.68769E+00	0.13496E+01	29.275	-0.0000
1571	0.68571E+00	0.13389E+01	54.576	0.0000
1572	0.68372E+00	0.13283E+01	76.64[illegible]	0.0000
1573	0.68174E+00	0.13176E+01	96.[illegible]36	-0.0000
1574	0.67976E+00	0.13069E+01	113.235	-0.0000
1575	0.67778E+00	0.12962E+01	128.585	-0.0001
1576	0.67579E+00	0.12856E+01	142.378	-0.0001
1577	0.67381E+00	0.12749E+01	154.84[illegible]	-0.0001
1578	0.67183E+00	0.12642E+01	166.169	-0.0001
1579	0.66985E+00	0.12535E+01	176.517	-0.0019
1580	0.67346E+00	0.12535E+01	176.278	-0.002[illegible]
1581	0.67900E+00	0.12535E+01	175.928	-0.0018
1582	0.68642E+00	0.12535E+01	175.489	-0.0023
1583	0.69568E+00	0.12535E+01	174.991	-0.002[illegible]
1584	0.70674E+00	0.12535E+01	174.471	-0.0029
1585	0.71956E+00	0.12535E+01	173.972	-0.0033
1586	0.734[illegible]5E+00	0.12535E+01	173.54[illegible]	-0.0023
1587	0.75[illegible]E+00	0.12535E+01	173.232	-0.0023
1588	0.76774E+00	0.12535E+01	173.08[illegible]	-0.00[illegible]8
1589	0.78673E+00	0.12535E+01	173.116	0.0001
1590	0.8[illegible]7[illegible]3E+00	0.12535E+01	173.348	0.0003
1591	0.82849E+00	0.12535E+01	173.762	0.0001
1592	0.85100E+00	0.12535E+01	174.316	0.0002
1593	0.87442E+00	0.12535E+01	174.955	0.0004
1594	0.8986[illegible]E+00	0.12535E+01	175.611	0.0002
1595	0.9234[illegible]E+00	0.12535E+01	176.2[illegible]8	0.000[illegible]
1596	0.94867E+00	0.12535E+01	176.684	0.00[illegible]2
1597	0.97426E+00	0.12535E+01	176.99[illegible]	0.0005
1598	0.1[illegible]E+01	0.12535E+01	177.[illegible]96	0.0014
1599	0.7[illegible]E+00	0.13771E+01	0.0	-2.15[illegible]
1600	0.69817E+00	0.13678E+01	27.641	-0.0000
1601	0.69624E+00	0.13584E+01	51.519	0.0000
1602	0.69431E+00	0.13491E+01	72.325	-0.0000
1603	0.69238E+00	0.13397E+01	90.569	-0.0000
1604	0.69046E+00	0.13304E+01	106.751	-0.0000
1605	0.68853E+00	0.13210E+01	121.168	-0.0000
1606	0.6866[illegible]E+00	0.13117E+01	134.116	-0.0001
1607	0.68467E+00	0.13023E+01	145.625	-0.0001
1608	0.68274E+00	0.12930E+01	156.455	-0.0001
1609	0.68082E+00	0.12837E+01	166.166	-0.0028

1610	0.66[illegible]27E+00	0.12837E+01	165.956	-0.0010
1611	0.68311E+00	0.12837E+01	165.642	-0.0024
1612	.69[illegible]52E+00	0.12837E+01	165.249	-0.0019
1613	0.70483E+00	0.12837E+01	164.811	-0.0017
1614	.71539E+00	0.12837E+01	164.374	-0.0024
1615	.727[illegible]E+00	0.12837E+01	163.993	-0.0024
1616	.74162E+00	0.12837E+01	163.727	-0.0029
1617	0.75715E+00	0.12837E+01	163.632	-0.0029
1618	0.77417E+00	0.12837E+01	163.757	-0.0010
1619	.79257E+00	0.12837E+01	164.129	0.0005
1620	0.81225E+00	0.12837E+01	164.745	0.0013
1621	0.83309E+00	0.12837E+01	165.57[illegible]	0.0016
1622	0.85497E+00	0.12837E+01	166.54[illegible]	0.0019
1623	.87774E+00	0.12837E+01	167.569	0.0001
1624	0.90127E+00	0.12837E+01	168.566	0.0000
1625	0.92541E+00	0.12837E+01	169.442	0.0005
1626	.95[illegible]1E+00	0.12837E+01	170.123	0.0001
1627	0.97493E+00	0.12837E+01	170.554	0.0001
1628	.1[illegible]E+01	0.12837E+01	170.7[illegible]2	0.0001
1629	0.71[illegible]7E+00	0.13941E+01	0.0	0.0016
1630	.71425E+00	0.13861E+01	25.6[illegible]2	-2.6563
1631	0.71[illegible]43E+00	0.13781E+01	46.[illegible]67	-0.0000
1632	0.71401E+00	0.13701E+01	67.519	-0.0000
1633	0.71279E+00	0.13620E+01	84.593	-0.00[illegible]
1634	0.71[illegible]96E+00	0.1354[illegible]E+01	99.086	-0.0001
1635	0.69914E+00	0.1346[illegible]E+01	113.113	-0.0001
1636	0.69732E+00	0.1338[illegible]E+01	125.144	-0.0001
1637	0.69550E+00	0.1330[illegible]E+01	136.016	-0.0001
1638	.69367E+00	0.1322[illegible]E+01	145.911	-0.0001
1639	0.69185E+00	0.1314[illegible]E+01	154.932	-0.0001
1640	0.69406E+00	0.1314[illegible]E+01	154.757	-0.0014
1641	0.69931E+00	0.1314[illegible]E+01	154.461	-0.0012
1642	.70531E+00	0.1314[illegible]E+01	154.137	-0.0022
1643	0.71411E+00	0.1314[illegible]E+01	153.774	-0.0022
1644	0.72417E+00	0.1314[illegible]E+01	153.452	-0.0024
1645	.73394E+00	0.1314[illegible]E+01	153.236	-0.0027
1646	0.74[illegible]4E+00	0.1314[illegible]E+01	153.2[illegible]4	-0.0024
1647	.76[illegible]E+00	.1314[illegible]E+01	153.426	-0.002[illegible]
1648	0.78[illegible]73E+00	0.1314[illegible]E+01	153.955	-0.0018
1649	0.79954E+00	0.1314[illegible]E+01	154.61[illegible]	-0.0023
1650	0.8170[illegible]E+00	.1314[illegible]E+01	155.966	-0.0015
1651	.8376[illegible]E+00	.1314[illegible]E+01	157.354	0.00[illegible]3
1652	0.859[illegible]3E+00	0.1314[illegible]E+01	158.87[illegible]	0.00[illegible]9
1653	0.88114E+00	0.1314[illegible]E+01	160.395	0.0017
1654	0.9[illegible]E+00	0.1314[illegible]E+01	161.811	0.00[illegible]4
1655	.92747E+00	.1314[illegible]E+01	163.[illegible]17	0.0007
1656	0.95139E+00	0.1314[illegible]E+01	163.934	0.00[illegible]6
1657	.97562E+00	0.1314[illegible]E+01	164.5[illegible]7	0.00[illegible]6
1658	0.1[illegible]E+01	0.1314[illegible]E+01	164.7[illegible]2	-0.0001
1659	.719[illegible]E+00	0.14111E+01	0.0	0.0017
1660	0.71787E+00	0.14044E+01	23.613	-3.392[illegible]
1661	0.71621E+00	0.13978E+01	44.256	-0.0001
1662	0.71455E+00	0.13911E+01	62.[illegible]61	-0.000[illegible]
1663	.71289E+00	0.13844E+01	77.744	-0.000[illegible]
1664	0.71122E+00	0.13777E+01	91.675	-0.0001
1665	0.70956E+00	0.13711E+01	104.1[illegible]7	-0.0001
1666	.70790E+00	0.13644E+01	115.226	-0.0001
1667	0.70623E+00	0.13577E+01	125.211	-0.0001
1668	0.70457E+00	0.13510E+01	134.241	-0.0001
1669	0.70291E+00	0.13443E+01	142.5[illegible]	-0.0022

1670	0.77533E+00	0.13443E+01	142.388	-0.0010
1671	0.76958E+00	0.13443E+01	142.152	-0.0021
1672	0.71563E+00	0.13443E+01	141.883	-0.0013
1673	0.72347E+00	0.13443E+01	141.628	-0.0018
1674	0.733[illegible]E+00	0.13443E+01	141.4[illegible]	-0.0024
1675	0.74429E+00	0.13443E+01	141.496	-0.0015
1676	0.75716E+00	0.13443E+01	141.626	-0.0022
1677	0.77156E+00	0.13443E+01	142.542	-0.0017
1678	0.787[illegible]E+00	0.13443E+01	143.690	-0.0020
1679	0.80460E+00	0.13443E+01	145.266	-0.0011
1680	0.823[illegible]E+00	0.13443E+01	147.197	0.0006
1681	0.84260E+00	0.13443E+01	149.350	0.0005
1682	0.86317E+00	0.13443E+01	151.566	0.0003
1683	0.88462E+00	0.13443E+01	153.69	0.0011
1684	0.90660E+00	0.13443E+01	155.569	0.0007
1685	0.92957E+00	0.13443E+01	157.161	0.0002
1686	0.95279E+00	0.13443E+01	158.332	0.0002
1687	0.97632E+00	0.13443E+01	159.[illegible]53	0.0004
1688	0.10000E+01	0.13443E+01	159.296	0.0009
1689	0.72837E+00	0.14279E+01	0.0	-4.5103
1690	0.72692E+00	0.14226E+01	21.822	-0.0001
1691	0.72548E+00	0.14173E+01	40.3[illegible]5	[illegible]
1692	0.72403E+00	0.14119E+01	56.211	[illegible]
1693	0.72258E+00	0.14066E+01	70.112	[illegible]
1694	0.72113E+00	0.14012E+01	82.461	-0.0001
1695	0.71968E+00	0.13959E+01	93.569	-0.0001
1696	0.71823E+00	0.13905E+01	103.657	-0.0001
1697	0.71679E+00	0.13852E+01	112.834	-0.0001
1698	0.71534E+00	0.13799E+01	121.135	-0.0001
1699	0.71389E+00	0.13745E+01	126.5[illegible]2	-0.0020
1700	0.71595E+00	0.13745E+01	128.423	[illegible]
1701	0.71981E+00	0.13745E+01	128.260	-0.0020
1702	0.72545E+00	0.13745E+01	128.[illegible]3	-0.0022
1703	0.73233E+00	0.13745E+01	127.916	-0.0018
1704	0.74193E+00	0.13745E+01	128.[illegible]33	-0.0026
1705	0.75267E+00	0.13745E+01	128.595	-0.0027
1706	0.765[illegible]E+00	0.13745E+01	129.446	-0.0023
1707	0.77864E+00	0.13745E+01	130.976	-0.0019
1708	0.79411E+00	0.13745E+01	133.133	-0.0010
1709	0.81070E+00	0.13745E+01	135.625	-0.0008
1710	0.82852E+00	0.13745E+01	138.656	0.0004
1711	0.84744E+00	0.13745E+01	141.997	0.0005
1712	0.86735E+00	0.13745E+01	145.042	0.0002
1713	0.88812E+00	0.13745E+01	147.823	0.0004
1714	0.90951E+00	0.13745E+01	150.222	0.0006
1715	0.93169E+00	0.13745E+01	152.154	0.0001
1716	0.95421E+00	0.13745E+01	153.567	0.0007
1717	0.97703E+00	0.13745E+01	154.427	0.0002
1718	0.10000E+01	0.13745E+01	154.716	0.0011
1719	0.73639E+00	0.14441E+01	0.0	-6.536
1720	0.73521E+00	0.14401E+01	19.533	-0.0001
1721	0.73404E+00	0.14361E+01	36.125	-0.0001
1722	0.73286E+00	0.14321E+01	50.271	-0.0001
1723	0.73168E+00	0.14281E+01	62.4[illegible]	-0.0001
1724	0.73051E+00	0.14240E+01	72.916	-0.0001
1725	0.72933E+00	0.14200E+01	82.155	-0.0001
1726	0.72816E+00	0.14160E+01	90.423	0.0007
1727	0.72698E+00	0.14120E+01	98.018	0.0007
1728	0.72580E+00	0.14080E+01	105.191	0.0011
1729	0.72463E+00	0.14040E+01	112.176	-0.0037

1730	0.72035E+00	0.14040E+01	111.976	0.0210
1731	0.72994E+00	0.14040E+01	111.765	-0.0016
1732	0.73508E+00	0.14040E+01	111.606	-0.0025
1733	0.74203E+00	0.14040E+01	112.116	-0.0028
1734	0.75056E+00	0.14040E+01	112.722	-0.0027
1735	0.76092E+00	0.14040E+01	113.907	-0.0022
1736	0.77273E+00	0.14040E+01	116.076	-0.0023
1737	0.78603E+00	0.14040E+01	119.112	-0.0016
1738	0.80073E+00	0.14040E+01	123.069	-0.0017
1739	0.81673E+00	0.14040E+01	127.344	-0.0005
1740	0.83393E+00	0.14040E+01	131.765	0.0006
1741	0.85222E+00	0.14040E+01	136.001	0.0011
1742	0.87148E+00	0.14040E+01	139.868	0.0011
1743	0.89158E+00	0.14040E+01	143.249	0.0007
1744	0.91240E+00	0.14040E+01	146.073	0.0007
1745	0.93379E+00	0.14040E+01	148.299	0.0002
1746	0.95562E+00	0.14040E+01	149.901	0.000[illegible]
1747	0.97774E+00	0.14040E+01	150.857	0.0005
1748	0.10000E+01	0.14040E+01	151.19[illegible]	0.0015
1749	0.74321E+00	0.14586E+01	0.0	-7.2165
1750	0.74237E+00	0.14559E+01	15.3[illegible]6	-0.0[illegible]
1751	0.74153E+00	0.14532E+01	28.958	-0.0002
1752	0.74068E+00	0.14506E+01	41.[illegible]8[illegible]	0.0003
1753	0.73984E+00	0.14479E+01	51.865	0.0003
1754	0.73899E+00	0.14452E+01	61.218	0.0005
1755	0.73815E+00	0.14426E+01	69.427	0.0005
1756	0.73730E+00	0.14399E+01	76.499	-0.0003
1757	0.73646E+00	0.14372E+01	82.510	-0.0008
1758	0.73561E+00	0.14346E+01	87.519	-0.001[illegible]
1759	0.73477E+00	0.14319E+01	91.563	-0.0032
1760	0.73618E+00	0.14319E+01	92.013	0.0193
1761	0.73932E+00	0.14319E+01	92.52[illegible]	-0.00[illegible]
1762	0.74418E+00	0.14319E+01	92.536	-0.0022
1763	0.75074E+00	0.14319E+01	92.79[illegible]	-0.0019
1764	0.75893E+00	0.14319E+01	94.295	-0.001[illegible]
1765	0.76873E+00	0.14319E+01	97.735	-0.0011
1766	0.78006E+00	0.14319E+01	102.0[illegible]7	-0.0015
1767	0.79284E+00	0.14319E+01	1[illegible]6.911	-0.0017
1768	0.80700E+00	0.14319E+01	115.244	-0.0003
1769	0.82244E+00	0.14319E+01	121.303	0.0007
1770	0.83906E+00	0.14319E+01	127.[illegible]66	0.0006
1771	0.85675E+00	0.14319E+01	132.158	0.0006
1772	0.87540E+00	0.14319E+01	136.596	0.0008
1773	0.89487E+00	0.14319E+01	140.36[illegible]	0.0006
1774	0.91504E+00	0.14319E+01	143.434	0.0005
1775	0.93578E+00	0.14319E+01	145.622	0.0005
1776	0.95695E+00	0.14319E+01	147.524	0.0004
1777	0.97840E+00	0.14319E+01	148.544	0.0010
1778	0.10000E+01	0.14319E+01	148.884	0.0014
1779	0.74813E+00	0.14695E+01	0.0	-5.5626
1780	0.74768E+00	0.14681E+01	7.727	[illegible]
1781	0.74723E+00	0.14668E+01	15.178	-0.00[illegible]2
1782	0.74677E+00	0.14655E+01	22.377	-0.00[illegible]5
1783	0.74632E+00	0.14642E+01	29.354	-0.00[illegible]5
1784	0.74587E+00	0.14628E+01	36.1[illegible]	-0.00[illegible]3
1785	0.74542E+00	0.14615E+01	42.678	-0.0005
1786	0.74497E+00	0.14602E+01	49.059	-0.0007
1787	0.74451E+00	0.14588E+01	55.268	-0.0005
1788	0.74406E+00	0.14575E+01	61.293	-0.0007
1789	0.74361E+00	0.14562E+01	67.125	0.0118

1790	.74473E+0[illegible]	.14562E+01	65.312	0.0146
1791	0.74756E+0[illegible]	.14562E+01	62.749	-0.0011
1792	.75278E+00	0.14562E+01	63.[illegible]61	-0.0011
1793	.75627E+00	0.14562E+01	67.652	-0.0011
1794	.76[illegible] 92+[illegible]	.14562E+01	76.[illegible]57	-0.0012
1795	.775[illegible]7E+0[illegible]	.14562E+01	85.673	-0.0012
1796	.78637E+00	.14562E+01	95.244	-0.0003
1797	0.79871E+00	0.14562E+01	1[illegible]4.112	0.0006
1798	.8124[illegible]E+[illegible]	.14562E+01	112.09[illegible]	0.0009
1799	.62735E+0[illegible]	.14562E+01	119.104	.0007
1800	.64347E+00	0.14562E+01	125.372	.0001
1801	.86065E+00	0.14562E+01	13[illegible].755	0.000[illegible]
1802	0.87876E+[illegible]	.14562E+01	135.352	[illegible]
1803	.89789E+0	.14562E+01	139.195	.0001
1804	.91731E+0[illegible]	0.14562E+01	142.3[illegible]9	.0007
1805	.93749E+0[illegible]	0.14562E+01	144.71[illegible]	0.0011
1806	.958[illegible]9E+[illegible]	.14562E+01	146.42[illegible]	0.001[illegible]
1807	0.97897E+0[illegible]	0.14562E+01	147.441	0.0[illegible]4
1808	.10[illegible]0E+01	0.14562E+01	147.761	0.0013
1809	.75[illegible]0E+0[illegible]	0.14737E+01	0.[illegible]	-49.9620
1810	.75[illegible]85E+[illegible]	0.14737E+01	6.472	0.000[illegible]
1811	.75341E+[illegible]	.14737E+01	22.[illegible]99	-0.0005
1812	.75765E+00	0.14737E+01	41.[illegible]13	0.0[illegible]2
1813	.76355E+00	0.14737E+01	56.[illegible]1	0.0005
1814	.771[illegible]6E+0[illegible]	.14737E+01	73.299	0.00[illegible]6
1815	.76[illegible]13E+[illegible]	.14737E+01	85.462	0.0008
1816	.79071E+00	0.14737E+01	95.61[illegible]	0.0007
1817	.80271E+00	0.14737E+01	1[illegible]4.614	0.0006
1818	.81697E+00	.14737E+01	112.716	0.00[illegible]9
1819	.83[illegible]68E+0[illegible]	.14737E+01	119.651	.0009
1820	0.84645E+00	0.14737E+01	125.796	0.0[illegible]9
1821	.86326E+00	0.14737E+01	13[illegible].952	0.0009
1822	0.881[illegible]1E+[illegible]	.14737E+01	135.429	0.0009
1823	0.89958E+0[illegible]	.14737E+01	139.172	0.0012
1824	.91682E+00	0.14737E+01	142.2[illegible]5	0.0011
1825	.93663E+0[illegible]	0.14737E+01	144.548	0.0012
1826	0.95885E+0[illegible]	0.14737E+01	146.213	0.0009
1827	.97935E+00	0.14737E+01	147.2[illegible]6	0.0001
1828	0.10[illegible]E+01	0.14737E+01	147.539	-[illegible]

SUMMARY

SUM OF NODAL FLOWS = -[illegible].551[illegible]1 BTU/HR

VALUE OF FUNCTIONAL = -[illegible].2136[illegible]E+ 5

AVG. SURFACE TEMP. = [illegible]25.[illegible] DEG FAHR

TOTAL HEAT FLOW = 1[illegible].[illegible] BTU/HR

TOTAL RESISTANCE = 4.2555 DEG F/BTU/HR

EQUIV. NUSSELT.NO. = [illegible]1.634 BTU/(HR-SQ.FT-F)

(EQ. NO.) * (KF/KM) = [illegible].[illegible]613 BTU/(HR-SQ.FT-F)

Appendix F

Linear Quadrilateral Isoparametric Finite Element

F.1 Introduction

In this appendix, the element 'shape functions' are determined for a linear quadrilateral isoparametric finite element. The word 'isoparametric' is used to describe the element since the approximation for the dependent variable, in this case the temperature, is taken to the same degree of polynomial as is the coordinate description. The element is linear since the geometric discription of the local coordinate values between any two nodes is a linear function of the global coordinate values. The element under consideration is a general quadrilateral, a four-sided geometric configuration for which there is no a priori fixed relationship between the four sides. That is, the opposite sides are not required to be parallel or have any prescribed orientation and adjacent sides need not meet at any specific angle.

F.2 Geometric Description

The general quadrilateral element is illustrated in figure F-1. A 'natural' or 'local' coordinate system is established with the origin located at the center of the quadrilateral. This coordinate system, in general non-orthogonal, is characterized by the coordinate pairs (t,s) with the coordinates t and s as shown in the figure. The element nodes are numbered consecutively in the local system as nodes 1 through 4, in a clockwise sense. The natural coordinate system also is defined to have the property that $s = -1$ and $+1$ over the surfaces

4-1 and 2-3 respectively and that $t = -1$ and $+1$ over the surfaces 1-2 and 3-4 respectively.

The global coordinates throughout the element can be related to the natural coordinates through the transformation equations, expressed in parametric form as

$$u_1(t,s) = \frac{1}{4}[(1-s)(1-t),(1+s)(1-t),(1+s)(1+t),(1-s)(1+t)]\begin{bmatrix} u_{1_1} \\ u_{1_2} \\ u_{1_3} \\ u_{1_4} \end{bmatrix} \qquad (-1)$$

$$u_2(t,s) = \frac{1}{4}[(1-s)(1-t),(1+s)(1-t),(1+s)(1+t),(1-s)(1+t)]\begin{bmatrix} u_{2_1} \\ u_{2_2} \\ u_{2_3} \\ u_{2_4} \end{bmatrix} \qquad (F-2)$$

From these relations it can be easily verified that for the appropriate combinations of $t=\pm 1$ and $s=\pm 1$, that both x and y take on their respective nodal point values and that the coordinate description is continuous within the element, the variation of both u_1 and u_2 being linear in both t and s. The equations (F-1) and (F-2), can be written in abbreviated functions by the definitions

$$\left.\begin{aligned} u_1(t,s) &= \{N_n\}^T \{u_{1_n}\} \\ u_2(t,s) &= \{N_n\}^T \{u_{2_n}\} \end{aligned}\right\} \qquad (F-3)$$

where the elements of the transpose vector, $\{N_n\}^T$, are called the element shape functions.

F.3 Field Description

In a manner directly analogous to the above geometric description, the temperature field can be approximated within each element by a linear interpolation. Thus we have for the temperature field approximation the relation

$$T(t,s) = \frac{1}{4}[(1-s)(1-t),(1+s)(1-t),(1+s)(1+t),(1-s)(1+t)]\begin{bmatrix} T_1 \\ T_2 \\ T_3 \\ T_4 \end{bmatrix} \quad \text{(F-4)}$$

which can be also written more compactly as

$$T(t,s) = \{N_n\}^T \{T_n\} \quad \text{(F-5)}$$

where the N_n are the identical shape functions (for isoparametric elements) to those used in the coordinate description.

The above defining equation (F-5), then, completes, the description of the temperature field throughout the element. However, in order to utilize this description, the 'effective curvilinear field vector' defined in Chapter 5 and Appendix C of this report must be determined.

The derivative operators with respect to the local coordinates can be expressed by

$$\begin{bmatrix} \frac{\partial}{\partial s} \\ \frac{\partial}{\partial t} \end{bmatrix} = \begin{bmatrix} \frac{\partial u_1}{\partial s} & \frac{\partial u_2}{\partial s} \\ \frac{\partial u_1}{\partial t} & \frac{\partial u_2}{\partial t} \end{bmatrix} \begin{bmatrix} \frac{\partial}{\partial u_1} \\ \frac{\partial}{\partial u_2} \end{bmatrix} \quad \text{(F-6)}$$

Inverting (F-6) to solve for the global derivatives yields

$$\begin{bmatrix} \dfrac{\partial}{\partial u_1} \\ \\ \dfrac{\partial}{\partial u_2} \end{bmatrix} = \frac{1}{|J|} \begin{bmatrix} \dfrac{\partial u_2}{\partial t} & -\dfrac{\partial u_2}{\partial s} \\ \\ -\dfrac{\partial u_1}{\partial t} & \dfrac{\partial u_1}{\partial s} \end{bmatrix} \begin{bmatrix} \dfrac{\partial}{\partial s} \\ \\ \dfrac{\partial}{\partial t} \end{bmatrix} \tag{F-7}$$

where the determinant of the Jacobian transformation is given by

$$|J| = \left| \left(\frac{\partial u_1}{\partial s} \frac{\partial u_2}{\partial t} - \frac{\partial u_2}{\partial s} \frac{\partial u_1}{\partial t} \right) \right| \tag{F-8}$$

and where the derivatives with respect to the natural coordinates, of say the element shape functions, can readily be found. Global derivatives are then found from

$$\begin{bmatrix} \dfrac{\partial T}{\partial u_1} \\ \\ \dfrac{\partial T}{\partial u_2} \end{bmatrix} = \frac{1}{|J|} \begin{bmatrix} \dfrac{\partial u_2}{\partial t} & \dfrac{-\partial u_2}{\partial s} & \dfrac{\partial \{N_n\}^T}{\partial s} \\ \\ \dfrac{-\partial u_1}{\partial t} & \dfrac{-\partial u_1}{\partial s} & \dfrac{\partial \{N_n\}^T}{\partial t} \end{bmatrix} \begin{bmatrix} T_1 \\ T_2 \\ T_3 \\ T_4 \end{bmatrix} \tag{F-9}$$

Performing the indicated operations, and after excessive tedious algebraic manipulation, equation (F-9) can be written as

$$\begin{bmatrix} \dfrac{\partial T}{\partial u_1} \\ \\ \dfrac{\partial T}{\partial u_2} \end{bmatrix} = \begin{bmatrix} u_{2_1} & u_{2_2} & u_{2_3} & u_{2_4} \\ u_{1_1} & u_{1_2} & u_{1_3} & u_{1_4} \end{bmatrix} \begin{bmatrix} T_1 \\ T_2 \\ T_3 \\ T_4 \end{bmatrix} \tag{F-10}$$

where

$$\begin{bmatrix} U_{2_1} \\ U_{2_2} \\ U_{2_3} \\ U_{2_4} \end{bmatrix} = \frac{1}{8|J|} \begin{bmatrix} u_{2_{24}} - u_{2_{34}} S - u_{2_{23}} t \\ -u_{2_{13}} + u_{2_{34}} S + u_{2_{14}} t \\ -u_{2_{24}} + u_{2_{12}} S - u_{2_{14}} t \\ u_{2_{13}} - u_{2_{12}} S + u_{2_{23}} t \end{bmatrix} \qquad \text{(F-11)}$$

$$\begin{bmatrix} U_{1_1} \\ U_{1_2} \\ U_{1_3} \\ U_{1_4} \end{bmatrix} = \frac{1}{8|J|} \begin{bmatrix} -u_{1_{24}} + u_{1_{34}} S + u_{1_{23}} t \\ u_{1_{13}} - u_{1_{34}} S - u_{1_{14}} t \\ u_{1_{24}} - u_{1_{12}} S + u_{1_{14}} t \\ -u_{1_{13}} + u_{1_{12}} S - u_{1_{23}} t \end{bmatrix} \qquad \text{(F-12)}$$

with the factor $8|J|$ given by

$$\begin{aligned} 8|J| = {} & (u_{1_{13}} u_{2_{24}} - u_{2_{13}} u_{1_{34}}) \\ & + (u_{1_{34}} u_{2_{12}} - u_{2_{34}} u_{1_{12}}) S \\ & + (u_{1_{23}} u_{2_{14}} - u_{2_{23}} u_{1_{14}}) t \end{aligned} \qquad \text{(F-13)}$$

In the above the differencing notation has been used, for example for u_1, that

$$u_{1_{ij}} \equiv u_{1_i} - u_{1_j} \qquad \text{(F-14)}$$

In the case of a cartesian global coordinate system, as is used for the problem under examination in this report, the u_1-direction is identified with x and y the u_2 - direction is identified with y.

It can also be shown, in conclusion of this appendix, that by forming the necessary cross-products for the integration, $\vec{du_1} \times \vec{du_2}$, an area element in the $u_1 - u_2$ plane, that

$$\vec{du_1} \times \vec{du_2} = |J| \, ds \, dt \qquad \text{(F-15)}$$

which is the final relation necessary to perform the integrations of Chapter 5.

It is due to the complex algebraic form of the resulting integrand that, orthogonal local coordinate systems excepted, numerical integration procedures are generally required for evaluation of the elements of the stiffness matrix [K] of chapter 5. The solution program of Appendix D uses a four point Chebyshev quadrature numerical integration procedure for this purpose. Higher order formulae did not detectibly alter the results obtained for the linear quadrilateral element when applied to the groove problem, or to either of the two example problems cited in Appendix C of this report.

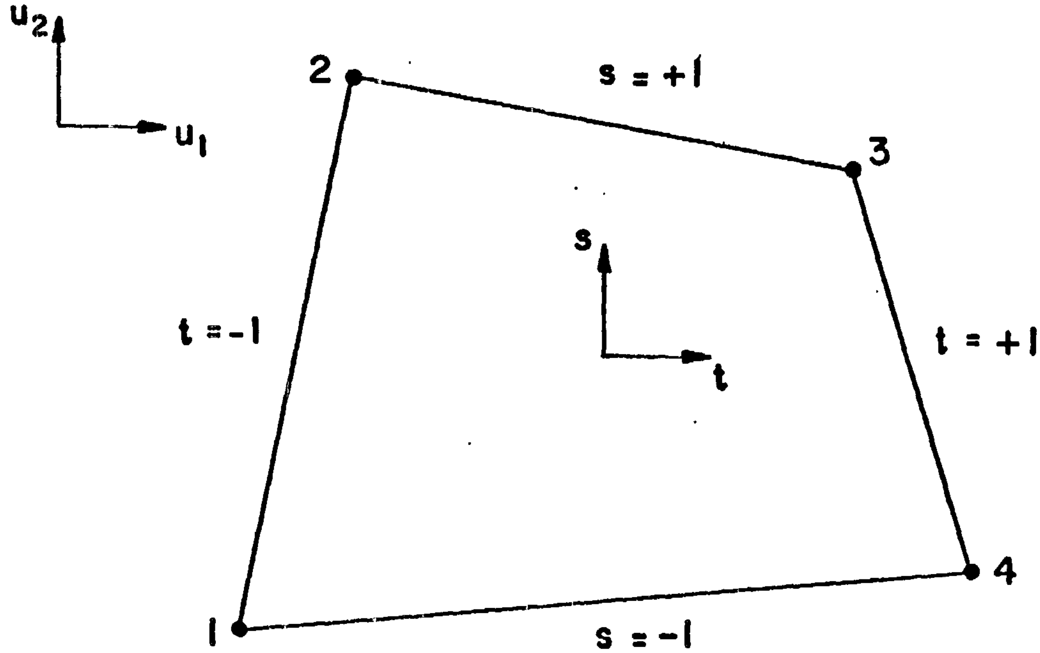

Figure F-1